Integrating Genomics, Phenomics, and Quantitative Genetic Models to Accelerate Genetic Gain in Intercrop and Monoculture Breeding Systems

by

Oluwaseye Gideon Oyebode

A dissertation submitted to the Graduate Faculty of
Auburn University
in partial fulfillment of the
requirements for the Degree of
Doctor of Philosophy

Auburn, Alabama
August 08, 2026

Keywords: Genomic prediction, UAV-Phenomics, Mixing ability, GWAS, Root system architecture, Ecosystem services

Approved by

Marnin D. Wolfe, Chair, Assistant Professor of Crop, Soil and Environmental Science
Alvaro S. Jauregui, Associate Professor of Crop, Soil and Environmental Science
Jenny Koebernick, Associate Professor of Crop, Soil and Environmental Science
Tanzeel Ur Rehman, Assistant Professor of Biosystems Engineering
Esteban Rios, Associate Professor of Forage Breeding, University of Florida

Abstract

Sustainable intensification of agriculture requires breeding systems that simultaneously improve productivity, resilience, and ecosystem services. However, most breeding programs remain optimized for monoculture yield, despite growing interest in intercrops and cover crops. Breeding directly for these systems is constrained by the combinatorial burden of testing genotype combinations across species, species-specific phenotyping in mixed canopies, limited quantitative genetic characterization of tropical intercrops, and the difficulty of measuring root traits. This dissertation evaluated genomic prediction (GP), unmanned aerial vehicle (UAV) phenomics, root phenotyping, and quantitative genetic approaches across crimson clover–oat mixtures, dual-purpose white lupin, and cassava–cowpea intercropping systems.

In crimson clover–oat mixtures, UAV-derived vegetation indices predicted species-specific biomass in mixed canopies with accuracies of r = 0.70–0.87, and calibration analyses showed that harvesting only 25–50% of plots preserved over 90% of expected response to selection, enabling a 50–75% reduction in destructive sampling. In cassava–cowpea intercropping, 120 cassava clones showed moderate-to-high intercrop heritability (H^2 = 0.50–0.75), and genetic correlations between monoculture and intercrop performance were near-unity (rg = 0.92–0.97), yet realized selection efficiency was only 26–44%, showing that high genetic correlation does not ensure effective indirect selection. General mixing ability dominated specific mixing ability, which was negligible, with producer effects explaining 20–47% of intercrop variance. In white lupin, root traits linked to phosphorus mobilization revealed a trade-off with grain yield, motivating the Alabama Ecosystem Service Index for dual-purpose

selection, which shows potential for GP (r = 0.18). Integrating genomic and phenomic kernels improved prediction for high-heritability traits such as alkaloid status (r = 0.55–0.59, exceeding genomic-only prediction by 0.16–0.17), whereas structural root traits remained poorly predicted across all data sources.

Collectively, these studies demonstrate that GP, UAV phenomics, quantitative genetic analysis, and direct root phenotyping can improve phenotyping efficiency and selection accuracy in breeding programs targeting multispecies cropping systems and ecosystem services. Belowground architectural traits remain difficult to predict indirectly, supporting continued integration of direct root phenotyping with UAV measurements and the use of selection indices when ecosystem service and yield objectives are negatively correlated.

Artificial Intelligence (AI) Use Disclosure Statement

In the preparation of this dissertation, the following Artificial Intelligence (AI) tools were used: Grammarly and Claude AI. These tools were used primarily to check grammar, spelling, punctuation, and language clarity during manuscript preparation, and to troubleshoot, debug, and refine R and Python code for SNP data processing and statistical analyses. The author acknowledges full responsibility for the intellectual content of this work and has ensured that all AI-assisted sections have been reviewed and revised for accuracy and appropriate academic style. All AI-generated content was reviewed and validated for relevance, appropriateness, and accuracy before incorporation into the final document to maintain the scholarly integrity of this research.

Digital Accessibility Disclosure Statement

In the preparation of this dissertation, the following digital accessibility tools were used to ensure this document complies with federal requirements: Microsoft Word Accessibility Checker, built-in Microsoft Word accessibility features (including heading styles, alternative text for figures where appropriate, accessible table formatting, and descriptive hyperlinks), and Adobe Acrobat accessibility verification tools where applicable. The author acknowledges full responsibility for the intellectual content of this work and has made a good faith effort to comply with digital accessibility requirements in publishing, wherein the nature of the content does not significantly change in order to do so. Furthermore, all content has been reviewed and revised to meet these requirements prior to final publication.

Acknowledgements

“O give thanks unto the LORD, for he is good: for his mercy endureth for ever.”

Psalm 107:1 (KJV)

First and foremost, I give thanks to God Almighty, whose grace, mercy, strength, and faithfulness have sustained me throughout this journey.

I express my deepest gratitude to my advisor, Dr. Marnin D. Wolfe, for his exceptional support, kindness, generosity, and mentorship throughout my doctoral training. I am especially grateful for his patience in teaching me new concepts and guiding me through analytical approaches, statistical models, and computational pipelines. I am sincerely grateful to my committee members, Dr. Alvaro Sanz Saez de Jauregui, Dr. Jenny Koebernick, Dr. Tanzeel Ur Rehman, Dr. Esteban Rios, and University reader Dr. Chen Ding. I also acknowledge the Wolfe Lab, the Tanzeel Lab, and the Alvaro Sanz Lab at Auburn University, the Rios Lab at the University of Florida, and Dr. Ismail Rabbi and the cassava breeding program at the International Institute of Tropical Agriculture, Ibadan, Nigeria, for their support and collaboration.

I am deeply indebted to my mentors who helped shape my academic and professional path. I thank Prof. A. M. Hassan, who has supported and encouraged me since my undergraduate years in 2011. I am grateful to Dr. Peter Kulakow for his guidance, training, and support. I honor the memory of Late Prof. Malachy Oghenovo Akoroda, my M.S. advisor. I remember with gratitude Late Prof. Elijah E. Omizegba, who was both a mentor and pastor to me since 2011. I also honor Late Pastor Dr. Obed Uzodinma of Glory Tabernacle, Ibadan, Nigeria. May their souls continue to rest in peace.

I thank my father, Engr. Ademola Solomon Oyebode and my mother, Matron Emily Motunrayo Oyebode, for their prayers, love, sacrifice, and unwavering belief in education. They gave beyond their convenience and held nothing back so that I could have the best opportunities available to me. Their faith, discipline, and sacrifices remain foundational to everything I have achieved. I am also grateful to my siblings, Peter Oyebode, Timothy Oyebode, Emmanuel Oyebode, Michael Oyebode, and Olabisi Tosin, for their love, prayers, encouragement, and support. I thank my in-laws, the Amos and Olabisi family, for their prayers, kindness, encouragement, and support. I am thankful for the friends and communities: Dr. Ogwuche Oche ThankGod, Dr. Paul Adunola, Dr. Muyideen Yusuf, Dr Afolabi Agbona, and Dr Mashood Bakare for their friendship. I am also deeply grateful to Grace Auburn Church and Pastor Matt Dean for their love, prayers, and care. I thank Pastor Hoffman and Courtney Ryhne, Jeff and Becky Kitchens, Jeremy and Rachel Pekins, Alex Hostetter, Mr. Joe Carpenter, Caden and Rachel Merrill, and the Christ Our Redeemer Seminary, Auburn, AL.

Finally, I give my deepest appreciation to my beloved wife, Huldah Ndridin Oyebode, and to our children, Daniel Adeshina Chongbami Oyebode and Divine-Favor Mayowa Chongmanyar Oyebode. My wife carried an enormous burden with courage, strength, wisdom, and sacrifice while I was away pursuing this degree. For four years, she cared for our children and held our family together with grace and resilience. Daniel and Divine were only two and one years old when I left, and they, too, paid the price of their father’s absence. This accomplishment also belongs to them.

I dedicate this dissertation to my parents, Huldah, Daniel, Divine-Favor, and my siblings.

Table of Contents

List of Tables

List of Figures

List of Abbreviations

ADMIXTURE	Software for estimating individual ancestries from SNP data
AESI	Alabama Ecosystem Service Index
ATER	Area-Time Equivalent Ratio
AU	Auburn University (Alabama)
AYT	Advanced Yield Trial
BGLR	Bayesian Generalized Linear Regression (R package)
BLINK	Bayesian-information and Linkage-disequilibrium Iteratively Nested Keyway (GWAS model)
BLUE	Best Linear Unbiased Estimate
BLUP	Best Linear Unbiased Prediction
BRR	Bayesian Ridge Regression
cGDD	Cumulative Growing Degree Days
CV	Cross-Validation
DAP	Days After Planting
DMC	Dry Matter Content (cassava)
DMSPG	Dry Matter Specific Gravity
ENET / EN	Elastic Net
FAC	Favorable Allele Count
FDR	False Discovery Rate
FarmCPU	Fixed and random model Circulating Probability Unification (GWAS model)

FRWT	Fresh Root Weight
GAPIT3	Genome Association and Prediction Integrated Tool version 3
GBLUP	Genomic Best Linear Unbiased Prediction (linear kernel)
GMA	General Mixing Ability
GRM	Genomic Relationship Matrix
GS	Genomic Selection
GWAS	Genome-Wide Association Study
H^2	Broad-sense heritability
H^2C	Cullis heritability estimator
IID	Independent and Identically Distributed (identity covariance model)
IITA	International Institute of Tropical Agriculture
LER	Land Equivalent Ratio
LRT	Likelihood Ratio Test
MAF	Minor Allele Frequency
MAP	Months After Planting
MET	Multi-Environment Trial
Ne	Effective Population Size
NPGS	National Plant Germplasm System (USDA)
PBU	Plant Breeding Unit (Auburn University)
PCA	Principal Component Analysis
PLER	Partial Land Equivalent Ratio (cassava or cowpea component)
Pr	Producer effect
As	Associate effect

p-rep	Partially Replicated (experimental design)
REML	Residual Maximum Likelihood
RF	Random Forest
RKHS	Reproducing Kernel Hilbert Space regression
RKHS-G	RKHS with Gaussian kernel
RKHS-L	RKHS with linear kernel
RVE	RhizoVision Explorer
RCT	Root Crown Trait
Se%	Selection efficiency percentage (Hamblin-Zimmermann metric)
SEM	Structural Equation Modelling
SMA	Specific Mixing Ability
SNP	Single Nucleotide Polymorphism
SSA	Sub-Saharan Africa
UAV	Unmanned Aerial Vehicle
UF	University of Florida
VI	Vegetation Index
W	Phenomic kernel prediction model
WL	White lupin (Lupinus albus L.)

Chapter 1 General Introduction

1.1 The sustainability challenge in modern agriculture

Producing sufficient food and fiber for a growing human population while maintaining environmental sustainability is among the central challenges of twenty-first-century agriculture (Moore et al., 2022; Manono, 2026). Although the prevalent monoculture cropping systems are highly productive, they have contributed substantially to soil degradation, biodiversity loss, nutrient runoff, and they continue to depend on synthetic inputs (Wolfe et al., 2021; Bourke et al., 2021; Moore et al., 2022). In the southeastern United States, these challenges are amplified by the predominance of highly weathered Ultisols, which are aluminum and iron-saturated, strongly phosphorus fixing, and frequently enriched with legacy phosphorus from decades of poultry-litter use (Waldrip et al., 2023). These edaphic conditions increase the risk of nutrient losses and contribute to the persistent water-quality challenges across the region, making agriculture a source of non-point-source pollution. In Alabama, approximately 40% of assessed rivers and streams do not fully support their designated uses because of water-quality impairments (ADEM, 2024). This level of impairment has remained largely unchanged for more than two decades (USEPA, 2012; Jordan and Rogers, 2024), highlighting the need for agricultural systems that maintain productivity while reducing environmental impacts.

Two cropping strategies are repeatedly identified as scalable and sustainable solutions: species mixtures (intercropping), in which two or more species are grown together, and cover cropping, in which a non-cash species occupies the field during the fallow season to protect the soil, build organic matter, and improve soil structure and

nutrient availability (Annicchiarico et al., 2019; Bourke et al., 2021; Scavo et al., 2022; Moore et al., 2022; Myers and Wilson, 2023).

Cover crops are widely promoted as the most practical conservation intervention for row-crop systems; reducing tile-drain phosphorus losses by 7–58% and nitrate-nitrogen losses by 27–72% in multi-year field studies (Speir et al., 2021). However, adoption of cover cropping remains low: in 2022, cover crops were planted on only 4.7% and 7.6% of cropland in the United States and Alabama, respectively, leaving more than 90% of Alabama's cropland without cover (Myers and Wilson, 2023; USDA-NASS, 2024; Sawadgo and Okonkwo, 2024). Profitability has been consistently listed among the leading barriers to adoption (Myers and Wilson, 2023).

Intercropping, the simultaneous cultivation of two or more species in the same field, accounts for 30–50% of global crop production and delivers documented yield advantages of 22–30% over sole cropping, along with improvements in yield stability, resource capture, and land-use efficiency (Himmelstein et al., 2017; Martin-Guay et al., 2018; Maitra et al., 2021; Moore et al., 2022; Adam et al., 2025). In sub-Saharan Africa, 70–83% of smallholder farmers intercrop, and root–legume systems such as cassava–cowpea dominate climate-resilient production landscapes (Anderson et al., 2013; Adam et al., 2025). Despite these well-documented system-level benefits, cultivar development has historically focused almost exclusively on monoculture conditions, leaving a structural mismatch between the breeding evaluation environment and the production systems where most cultivars will be deployed (Annicchiarico et al., 2019; Bourke et al., 2021; Moore et al., 2022).

To address this mismatch, this work uses five integrated research chapters to ask how genomic, phenomic, and joint genomic-plus-phenomic approaches can be deployed to support breeding for sustainability in three cropping contexts: cool-season cover-crop and forage mixtures of crimson clover (Trifolium incarnatum L.) and oat (Avena sativa L.) in the southeastern United States; the tropical cassava (Manihot esculenta Crantz) and cowpea (Vigna unguiculata L. Walp.) intercrop in sub-Saharan Africa; and dual-purpose white lupin (Lupinus albus L.) grown as a monoculture cash cover crop on Alabama Ultisols. Clover, cassava, and white lupin are the focal breeding targets, whereas oat and cowpea serve as companion testers used to reveal the mixing ability of the focal crop rather than as objects of selection.

Across these systems, three common methodological approaches were applied. The first is genetic decomposition of mixing ability into general (GMA) and specific (SMA) mixing-ability components, and into their producer (Pr) and associate (As) effects (Wright, 1985; Haug et al., 2021). The second is unmanned aerial vehicle (UAV) multispectral and hyperspectral phenomics as a scalable, non-destructive phenotyping strategy for both intercrop and monoculture systems. The third is genomic prediction, and the fourth is the integration of these data sources within joint genomic-plus-phenomic kernel models, and within genomic models that include top vegetation indices as fixed covariates.

1.2 Quantitative genetics of breeding in mixtures

Genetic gain per unit time in any breeding program is governed by the breeder's equation,

$$\Delta G = (i \cdot r \cdot \sigma_A) / L \qquad (1.1)$$

where i is the selection intensity, r the accuracy of selection (the correlation between true and estimated breeding value), σ_A the additive genetic standard deviation, and L the cycle length (Falconer and Mackay, 1996). The obstacles discussed in Sections 1.3 to 1.5 act directly on this equation. For instance, phenotyping bottlenecks limit i, sparse combinatorial trials and low-heritability traits reduce r, and traits that cannot be measured at scale prevent σ_A from being captured in detail. The methodological tools developed in this work, namely phenomic prediction, genomic prediction, and their integration, are interventions that attempt to raise i or r, or that make σ_A accessible.

The quantitative genetics foundation of intercrop breeding was described by Wright (1985), who partitioned mixture performance into general mixing ability (GMA) and specific mixing ability (SMA), in direct similarity with general and specific combining ability in hybrid breeding (Sprague and Tatum, 1942; Sampoux et al., 2020). The GMA captures the additive component of a genotype's effect that is broadly compatible across partners; SMA captures the non-additive interaction effect specific to a particular combination of genotypes. The GMA can be further decomposed into a producer effect (Pr; the direct genetic effect of a genotype on its own species' yield in mixture) and an associate effect (As; its indirect effect on the companion species' yield) (Wright, 1985; Bourke et al., 2021; Haug et al., 2021, 2023). The relative magnitudes of GMA and SMA variance, the sign and magnitude of the Pr/As genetic correlation, and the structure of the SMA × environment interaction together determine the optimal selection strategy in any given mixture breeding program (Sampoux et al., 2020). When GMA dominates over SMA and the Pr/As correlation is positive, selection on GMA, or equivalently on a phenotype highly correlated with Pr, can simultaneously improve mixture performance

and reduce the combinatorial burden of evaluating all pairwise combinations. When the Pr/As correlation is negative or SMA × environment interactions are substantial, more complex breeding designs are required, including partial factorial mixture trials and the use of testers analogous to those used in hybrid breeding (Annicchiarico et al., 2019; Haug et al., 2021; Moore et al., 2022). Empirical studies in temperate legume–cereal mixtures, particularly pea–barley, have shown that GMA typically dominates SMA, that Pr effects are the primary driver of GMA, and that breeding programs can therefore base selection on traits correlated with Pr while remaining uncorrelated with As (Annicchiarico et al., 2019, 2021; Forst et al., 2019; Haug et al., 2021, 2023; Sampoux et al., 2020). However, these mixing-ability foundations had been tested in only a small number of genotypes (Rowe and Brink, 1993; Holland and Brummer, 1999) or in simulation studies (Bančič et al., 2021). As a result, mixing ability had not been partitioned into GMA and SMA, or into producer and associate effects, for cool-season crimson clover–oat cover-crop mixtures in the southeastern United States or for tropical cassava-based intercrop systems (Wolfe et al., 2021).

1.3 Project area I: temperate mixture breeding (crimson clover–oat)

Crimson clover (Trifolium incarnatum) and oat (Avena sativa) mixtures are well-known and adapted for cool-season annual cover cropping where they provide soil protection, nutrient retention, biological nitrogen fixation, winter forage suitable for livestock consumption, and diversified income streams (Chapagain et al., 2020, Franzluebbers et al., 2008). When managed as a cool-season forage mixture, they can extend the grazing season in the southeastern USA. In this system, clover is typically the weaker competitor, so realized mixture value depends on improving the contribution

of the less competitive partner (Blanco-Canqui et al., 2015; Chapagain et al., 2020), and imbalanced competition between legume/grass species included in the mixture can lead to a significant reduction in the productivity of the system (Høgh-Jensen et al., 2006, Holland and Brummer, 1999). To make cover crop mixtures reach their potential, they can be subjected to breeding.

Breeding clover for mixture performance therefore requires species-specific evaluation, and this is where the system becomes intractable. For example, pairing 500 clover maternal half-sib families with 28 oat lines would generate 14,000 possible clover–oat mixtures, a scale that rapidly exceeds what can be phenotyped under realistic budget constraints. This combinatorial problem is especially limiting in early-generation populations, where direct selection requires evaluating large numbers of candidates each cycle (Bančič et al., 2021; Wolfe et al., 2021). Compounding this, species-specific biomass evaluation requires destructive harvest followed by hand-separation of the two species, an effort so labor-intensive that it directly caps population size, measurement frequency, and ultimately the selection intensity i achievable in the program (Rincent et al., 2018; Krause et al., 2019; Biswas et al., 2021; Wolfe et al., 2021).

Two information sources could in principle reduce these constraints, but each is compromised at the early stage where it is most needed. Genomic selection can be applied to predict the genomic estimated breeding values (GEBVs) of unobserved combinations through genomic marker-based relationship matrices, including a Kronecker product of species-specific matrices for the SMA term, and a simulation study showed that genomic selection can outpace phenotypic selection even under

constrained budgets (Bančič et al., 2021; Dubey et al., 2024). UAV phenomics offers a complementary, non-destructive data through vegetation indices that track canopy growth, species composition, and stress and are heritable (Rincent et al., 2018; Krause et al., 2019; Biswas et al., 2021; Lane et al., 2023). In a mixed-species canopy, the spectral signal contains both species, complicating inference of species-specific performance (Bretas et al., 2026; Pranga et al., 2024; Li et al., 2021; Sun et al., 2021).

Chapter 2 addresses these obstacles in a clover–oat breeding population evaluated at the Plant Breeding Unit (PBU) in Tallassee and at the University of Florida (Citra) under a sparse incomplete-factorial mixture design. Chapter 2 reframes destructive phenotyping as a resource-allocation problem, asking not merely how accurately UAV vegetation indices predict species-specific biomass, but how few destructively phenotyped plots are required to calibrate a phenomic model while preserving expected response to selection.

1.4 Project area II: tropical intercrop breeding (cassava–cowpea)

Intercropping accounts for 30–50% of global crop production and, in sub-Saharan Africa, is practiced by 70–83% of smallholder farmers, with root–legume systems such as cassava–cowpea dominating climate-resilient production landscapes (Anderson et al., 2013; Himmelstein et al., 2017; Adam et al., 2025). Cassava, the most important tropical root crop, is rarely grown alone, yet cassava breeding programs have evaluated and selected genotypes almost exclusively under monoculture. This raises a fundamental and untested question for a tropical root crop: does monoculture selection adequately capture genetic merit for intercrop performance, or does intercrop adaptation demand a different cassava ideotype entirely?

This question cannot be answered from the genetic correlation between monoculture and intercrop performance alone. A high correlation may suggest that the same genotypes perform well in both systems, but it does not guarantee that the same genotypes would be selected. Studies in temperate intercrops have shown that monoculture selection can recover only about half of the gain achieved by direct selection in mixture, and that substantial genotype re-ranking can occur even when genetic correlations are moderate to high (Zimmermann, 1996; Annicchiarico et al., 2019, 2021). Variance-based parameters and realized selection overlap must therefore be evaluated jointly. Cassava cowpea systems add a further complication absent from temperate cereal-legume literature: pronounced yield-scale asymmetry, because cassava root yield per plot is orders of magnitude larger than cowpea grain yield. As a result, naive aggregation can collapse the mixing ability analysis into effective single-species selection and bias estimates of GMA, SMA, and producer effects (Wright, 1985). The operational scale of intercrop evaluation is also constrained by the intractable number of genotype × partner combinations, which the use of a limited tester set can relax only if focal-crop rankings are stable across testers: an assumption untested in cassava-based systems (Annicchiarico et al., 2019, 2021; Haug et al., 2023).

Chapter 3 evaluates 120 cassava clones under monoculture and under intercropping with two contrasting cowpea testers across two years at the International Institute of Tropical Agriculture (IITA), Ibadan, Nigeria. It quantifies genetic variation and genotype × cropping-system interaction; estimates genetic correlation, genotype re-ranking, and realized selection efficiency between systems; partitions intercrop performance into

GMA, SMA, and producer–associate components using a z-score standardization framework that addresses the yield-scale asymmetry; tests whether cassava yield-formation pathways are invariant between systems via multi-group structural equation modelling; and assesses whether using two cowpea testers with different growth habit and phenology is sufficient for field evaluation.

1.5 Project area III: dual-purpose cover-crop breeding (white lupin)

As noted earlier, cover crops are among the most scalable conservation interventions for row crop systems (Speir et al., 2021), yet adoption remains limited, with profitability consistently identified as a leading barrier among nonadopters (Myers and Wilson, 2023; USDA-NASS, 2024; Sawadgo and Okonkwo, 2024). A dual-purpose cash cover crop that provides ecosystem services while also generating harvestable income could directly address this economic barrier. White lupin is uniquely suited to this role on Alabama Ultisols: it occupies the fallow winter season without competing with summer row crops, produces a 32–51% crude-protein grain comparable to soybean, contributes approximately 143 kg N ha^{-1} to subsequent crops, and, distinctively among grain legumes, forms cluster (proteoid) roots that exude citrate and malate to mobilize phosphorus from forms otherwise inaccessible in weathered, phosphorus-fixing soils (Lambers et al., 2006, 2013; Damon et al., 2014). The breeding problem is that no white lupin cultivar has been selected for these ecosystem-service functions, and building a dual-purpose breeding program requires solving two coupled problems that monoculture yield breeding never confronts.

First, the ecosystem services themselves (phosphorus mobilization, erosion control, soil organic matter contribution) cannot be measured directly at breeding scale; rather, root architectural traits serve as the practical proxies, but the heritability, genetic correlations with yield, and genomic architecture of root traits in white lupin are currently uncharacterized, and root systems cannot be phenotyped non-destructively at field scale, since conventional excavation is incompatible with population-level breeding (Freschet et al., 2021; Lynch, 2022; Bagale et al., 2025). The shovelomics protocol combined with the RhizoVision Explorer image-analysis platform now makes field-scale root phenotyping feasible (Trachsel et al., 2011; Burridge et al., 2016; Seethepalli et al., 2020, 2021), but its integration with genomic prediction had not been attempted in this species. Second, ecosystem-service traits and grain yield are frequently antagonistic, so a defensible dual-purpose program needs a selection index that integrates the two into a single criterion (Céron-Rojas and Crossa, 2022). Even with an established phenotyping pipeline, root traits are often low in heritability and strongly influenced by genotype-by-environment interaction (de Dorlodot et al., 2007; Griffiths et al., 2022; Středa et al., 2024; Griffin et al., 2025). As a result, genomic prediction alone, which depends on additive genetic variance and selection accuracy, may struggle to support effective selection, thereby motivating the search for complementary information sources.

Chapters 4 and 5 develop the breeding framework for dual-purpose white lupin in 232 accessions evaluated over two seasons at the E.V. Smith Research Center, Auburn, Alabama. Chapter 5 characterizes the genetic architecture of root traits, estimates their heritability and genetic correlations with yield, maps them by genome-

wide association, and develops and validates the Alabama Ecosystem Service Index (AESI), a selection index that weights heritable, non-redundant root traits and grain yield by their relative importance for phosphorus mobilization, erosion control, and soil organic matter contribution. Chapter 6 then tests whether UAV multispectral phenomics, as an additional information layer, can improve genomic prediction for root and agronomic traits, evaluating genomic, phenomic, and joint genomic-plus-phenomic kernel models within and across seasons and clarifying for which traits phenomic information rescues prediction and for which it does not.

A recent caution from Wang et al. (2025) shapes how genomic and phenomic prediction accuracies are interpreted in this work. The cross-validation accuracy of phenomic prediction can be inflated relative to genomic prediction, because the phenomic kernel absorbs non-genetic plot-to-plot covariance that the genomic kernel does not. The cross-validation statistic from phenomic prediction is therefore not a direct estimate of the accuracy term in the breeder's equation (Falconer and Mackay, 1996; Runcie and Cheng, 2019). Furthermore, phenomic and genomic selection affect selection intensity, cycle length, and the additive genetic variance of the selected population in different ways, so accuracy alone is an incomplete basis for advocating one tool over the other. The analyses reported here therefore do not benchmark phenomic prediction against genomic prediction as competing tools. The question throughout is operational: when is phenomic information necessary, when is it complementary, and when is the joint genomic-plus-phenomic kernel the best framework to carry both information sources forward?

1.6 Research objectives

This work pursues four interrelated objectives across the four research chapters:

(1) To quantify genetic variation for mixing ability in cassava × cowpea systems by decomposing mixture performance into GMA, SMA, and producer and associate components, and to evaluate the implications of these decompositions for selection strategy.

(2) To evaluate whether UAV phenomics can replace, or substantially reduce reliance on, destructive phenotyping in mixture breeding and root phenotyping in monoculture cover-crop breeding.

(3) To assess the value of integrating genomic and phenomic information in joint kernel models for prediction in white lupin across multiple breeding scenarios.

(4) To develop and validate a quantitative selection framework (the Alabama Ecosystem Service Index) that integrates root architectural traits and grain yield for dual-purpose cover-crop breeding, supported by both phenotypic and genomic evaluation.

1.7 Structure of the dissertation

The dissertation comprises six chapters organized around the three project areas introduced above. Chapter 2 reframes destructive mixture phenotyping in clover and oat as a resource-allocation problem, quantifying how far UAV multispectral prediction can reduce destructive sampling. Chapter 3 provides the first empirical decomposition of mixing ability (GMA, SMA, and producer and associate effects) in tropical cassava and cowpea intercrop, estimating genetic correlation and indirect-selection efficiency between monoculture and intercrop. Chapter 4 characterized the genetic architecture of white lupin root traits and developed the Alabama Ecosystem Service Index for dual-purpose breeding. Chapter 5 integrates UAV phenomics with genomic prediction in

white lupin through joint genomic-plus-phenomic kernel models, within and across seasons. Chapter 6 synthesizes the findings across all four research chapters and sets out future directions.

References

Adam, A. M., Giller, K. E., Rusinamhodzi, L., Rasche, F., Koomson, E., Marohn, C., and Cadisch, G. (2025). Enhancing the resilience of intercropping systems to changing moisture conditions in Africa through the integration of grain legumes: A meta-analysis. Field Crops Research, 321, 109663. https://doi.org/10.1016/j.fcr.2024.109663

Alabama Department of Environmental Management (ADEM). (2024). 2024 Integrated Water Quality Monitoring and Assessment Report: Water Quality in Alabama 2022–2024. Montgomery, AL: ADEM Water Division, Water Quality Branch.

Anderson, S., Gündel, S., Pound, B., and Triomphe, B. (2013). Cropping systems and soil resources in sub-Saharan Africa: A review. Cahiers Agricultures, 22(6), 519–528. https://doi.org/10.1684/agr.2013.0664

Annicchiarico, P., Nazzicari, N., Notario, T., Monterrubio Martin, C., Romani, M., Ferrari, B., and Pecetti, L. (2021). Pea breeding for intercropping with cereals: Variation for competitive ability and associated traits, and assessment of phenotypic and genomic selection strategies. Frontiers in Plant Science, 12, 731949. https://doi.org/10.3389/fpls.2021.731949

Annicchiarico, P., Collins, R. P., De Ron, A. M., Firmat, C., Litrico, I., and Hauggaard-Nielsen, H. (2019). Do we need specific breeding for legume-based mixtures? Advances in Agronomy, 157, 141–215. https://doi.org/10.1016/bs.agron.2019.04.001

Bagale, M., Acharya, J. P., Andrade, M. H. M. L., Cervantes Arango, K. A., Castillo, S. L., Frantz, R. S., Kannan, B., Nuñez, J. D., de Souza, C. L., Vaughn, J. N., Vermerris, W., Sanz-Saez, A., and Rios, E. F. (2025). Root genetic variation and architecture in forages and bioenergy grasses. Crop Science, 65(2), e21456. https://doi.org/10.1002/csc2.21456

Bančič, J., Werner, C. R., Gaynor, R. C., Gorjanc, G., Odeny, D. A., Ojulong, H. F., Dawson, I. K., Hoad, S. P., and Hickey, J. M. (2021). Modeling illustrates that genomic selection provides new opportunities for intercrop breeding. Frontiers in Plant Science, 12, 605172. https://doi.org/10.3389/fpls.2021.605172

Biswas, A., Andrade, M. H. M. L., Acharya, J. P., de Souza, C. L., Lopez, Y., de Assis, G., Shirbhate, S., Singh, A., Munoz, P., and Rios, E. F. (2021). Phenomics-assisted selection for herbage accumulation in alfalfa (Medicago sativa L.). Frontiers in Plant Science, 12, 756768. https://doi.org/10.3389/fpls.2021.756768

Blanco-Canqui, H., Shaver, T. M., Lindquist, J. L., Shapiro, C. A., Elmore, R. W., Francis, C. A., and Hergert, G. W. (2015). Cover crops and ecosystem services: Insights from studies in temperate soils. Agronomy Journal, 107(6), 2449–2474. https://doi.org/10.2134/agronj15.0086

Bourke, P. M., Evers, J. B., Bijma, P., van Apeldoorn, D. F., Smulders, M. J. M., Kuyper, T. W., Mommer, L., and Bonnema, G. (2021). Breeding beyond monoculture: Putting the “intercrop” into crops. Frontiers in Plant Science, 12, 734167. https://doi.org/10.3389/fpls.2021.734167

Bretas, I. L., Zhao, C., Dubeux, J. C. B., Xin, Y., Tang, Z., Trumpp, K. R., Acuna, J. P., Small, I. M., and de Souza, C. H. L. (2026). Estimating the botanical composition of bahiagrass–rhizoma peanut pastures using aerial multispectral imagery and deep learning. Crop Science, 66, e70253. https://doi.org/10.1002/csc2.70253

Burridge, J., Jochua, C. N., Bucksch, A., and Lynch, J. P. (2016). Legume shovelomics: high-throughput phenotyping of common bean and cowpea root architecture in the field. Field Crops Research, 192, 21–32. https://doi.org/10.1016/j.fcr.2016.04.008

Céron-Rojas, J. J., and Crossa, J. (2022). Linear selection indices in modern plant breeding (2nd ed.). Springer. https://doi.org/10.1007/978-3-030-77103-1

Chapagain, T., Lee, E. A., and Raizada, M. N. (2020). The potential of multi-species mixtures to diversify cover crop benefits. Sustainability, 12(5), 2058. https://doi.org/10.3390/su12052058

Damon, P. M., Bowden, B., Rose, T., and Rengel, Z. (2014). Crop residue contributions to phosphorus pools in agricultural soils: a review. Soil Biology and Biochemistry, 74, 127–137. https://doi.org/10.1016/j.soilbio.2014.03.003

de Dorlodot, S., Forster, B., Pagès, L., Price, A., Tuberosa, R., and Draye, X. (2007). Root system architecture: Opportunities and constraints for genetic improvement of crops. Trends in Plant Science, 12(10), 474–481. https://doi.org/10.1016/j.tplants.2007.08.012

Dubey, R., Zustovi, R., Landschoot, S., Dewitte, K., Verlinden, G., Haesaert, G., and Maenhout, S. (2024). Harnessing monocrop breeding strategies for intercrops. Front. Plant Sci. 15, 1394413. doi: 10.3389/fpls.2024.1394413

Falconer, D. S., and Mackay, T. F. C. (1996). Introduction to quantitative genetics (4th ed.). Longman.

Forst, E., Enjalbert, J., Allard, V., Ambroise, C., Krissaane, I., Mary-Huard, T., Robin, S., and Goldringer, I. (2019). A generalized statistical framework to assess mixing ability from incomplete mixing designs using binary or higher order variety mixtures and application to wheat. Field Crops Research, 242, 107571. https://doi.org/10.1016/j.fcr.2019.107571

Franzluebbers, A. J., and Stuedemann, J. A. (2008). Soil physical responses to cattle grazing cover crops under conventional and no tillage in the Southern Piedmont USA. Soil and Tillage Research, 100(1–2), 141–153. https://doi.org/10.1016/j.still.2008.05.011

Freschet, G. T., Roumet, C., Comas, L. H., Weemstra, M., Bengough, A. G., Rewald, B., … Stokes, A. (2021). Root traits as drivers of plant and ecosystem functioning: current understanding, pitfalls and future research needs. New Phytologist, 232(3), 1123–1158. https://doi.org/10.1111/nph.17072

Griffin, A., Jungers, J. M., and Bajgain, P. (2025). Root phenotyping and plant breeding of crops for enhanced ecosystem services. Crop Science, 65, e21315. https://doi.org/10.1002/csc2.21315

Griffiths, M., Delory, B. M., Jawahir, V., Wong, K. M., Bagnall, G. C., Dowd, T. G., Chamberlain, A., Meldrum, K., Schaefer, A. L., Kaeppler, H. F., Lynch, J. P., Kaeppler, S. M., and York, L. M. (2022). Optimization of root traits to provide enhanced ecosystem services in agricultural systems: a focus on cover crops. Plant, Cell and Environment, 45(3), 751–770. https://doi.org/10.1111/pce.14247

Haug, B., Messmer, M. M., Enjalbert, J., Goldringer, I., Forst, E., Flutre, T., Mary-Huard, T., and Hohmann, P. (2021). Advances in breeding for mixed cropping: Incomplete factorials and the producer/associate concept. Frontiers in Plant Science, 11, 620400. https://doi.org/10.3389/fpls.2020.620400

Haug, B., Messmer, M. M., Enjalbert, J., Goldringer, I., Flutre, T., Mary-Huard, T., and Hohmann, P. (2023). New insights towards breeding for mixed cropping of spring pea and barley to increase yield and yield stability. Field Crops Research, 297, 108923. https://doi.org/10.1016/j.fcr.2023.108923

Himmelstein, J., Ares, A., Gallagher, D., and Myers, J. (2017). A meta-analysis of intercropping in Africa: Impacts on crop yield, farmer income, and integrated pest management. International Journal of Agricultural Sustainability, 15(1), 1–10. https://doi.org/10.1080/14735903.2016.1242332

Høgh-Jensen, H., Nielsen, B., and Thamsborg, S. M. (2006). Productivity and quality, competition and facilitation of chicory in ryegrass/legume-based pastures under various nitrogen supply levels. European Journal of Agronomy, 24(3), 247-256. https://doi.org/10.1016/j.eja.2005.10.007

Holland, J. B., and Brummer, E. C. (1999). Cultivar effects on oat–berseem clover intercrops. Agronomy Journal, 91(2), 321–329. https://doi.org/10.2134/agronj1999.00021962009100020023x

Jordan, M. A., and Rogers, S. R. (2024). A new perspective on water quality: Exploring spatial and temporal patterns of impaired waters. Journal of Environmental Management, 359, 120983. https://doi.org/10.1016/j.jenvman.2024.120983

Krause, M. R., González-Pérez, L., Crossa, J., Pérez-Rodríguez, P., Montesinos-López, O., Singh, R. and P., Mondal, S. (2019). Hyperspectral reflectance-derived relationship matrices for genomic prediction of grain yield in wheat. G3: Genes, Genomes, Genetics, 9(4), 1231–1247. https://doi.org/10.1534/g3.118.200856

Lambers, H., Shane, M. W., Cramer, M. D., Pearse, S. J., and Veneklaas, E. J. (2006). Root structure and functioning for efficient acquisition of phosphorus: Matching morphological and physiological traits. Annals of Botany, 98(4), 693–713. https://doi.org/10.1093/aob/mcl114

Lambers, H., Clements, J. C., and Nelson, M. N. (2013). How a phosphorus-acquisition strategy based on carboxylate exudation powers the success and agronomic potential of lupines (Lupinus, Fabaceae). American Journal of Botany, 100(2), 263–288. https://doi.org/10.3732/ajb.1200474

Lane, H. M., Murray, S. C., Montesinos-López, O. A., Montesinos-López, A., Crossa, J., Rooney, D. K., et al., (2023). Temporal phenomic predictions from unoccupied aerial systems can outperform genomic predictions. G3: Genes, Genomes, Genetics, 13(1), jkac294. https://doi.org/10.1093/g3journal/jkac294

Li, K.-Y., Burnside, N. G., Sampaio de Lima, R., Villoslada Peciña, M., Sepp, K., et al. (2021). The application of an unmanned aerial system and machine learning techniques for red clover–grass mixture yield estimation under variety performance trials. Remote Sensing, 13, 1994. https://doi.org/10.3390/rs13101994

Lynch, J. P. (2022). Harnessing root architecture to address global challenges. The Plant Journal, 109(2), 415–431. https://doi.org/10.1111/tpj.15560

Maitra, S., Hossain, A., Brestic, M., Skalicky, M., Ondrisik, P., Gitari, H., et al., (2021). Intercropping: A low input agricultural strategy for food and environmental security. Agronomy, 11(2), 343. https://doi.org/10.3390/agronomy11020343

Manono, B. O. (2026). Beyond monoculture: Exploring the benefits, challenges, and potential of intercropping systems. Agronomy Journal, 118, e70401. https://doi.org/10.1002/agj2.70401

Martin-Guay, M.-O., Paquette, A., Dupras, J., and Rivest, D. (2018). The new green revolution: Sustainable intensification of agriculture by intercropping. Science of the Total Environment, 615, 767–772. https://doi.org/10.1016/j.scitotenv.2017.10.024

Moore, V. M., Schlautman, B., Fei, S.-Z., Roberts, L. M., Wolfe, M., Ryan, M. R., Wells, S., and Lorenz, A. J. (2022). Plant breeding for intercropping in temperate field crop systems: A review. Frontiers in Plant Science, 13, 843065. https://doi.org/10.3389/fpls.2022.843065

Myers RL and Wilson KR (2023) Farmer perspectives about cover crops by non-adopters. Front. Sustain. Food Syst. 7:1011201. doi: 10.3389/fsufs.2023.1011201

Pranga, J., Borra-Serrano, I., Quataert, P., De Swaef, T., Vanden Nest, T., Willekens, K., et al., (2024). Quantification of species composition in grass–clover swards using RGB and multispectral UAV imagery and machine learning. Frontiers in Plant Science, 15, 1414181. https://doi.org/10.3389/fpls.2024.1414181

Rincent, R., Charpentier, J.-P., Faivre-Rampant, P., Paux, E., Le Gouis, J., Bastien, C., and Segura, V. (2018). Phenomic selection is a low-cost and high-throughput method based on indirect predictions: Proof of concept on wheat and poplar. G3:

Genes, Genomes, Genetics, 8(12), 3961–3972. https://doi.org/10.1534/g3.118.200760

Rowe, D. E., and Brink, G. E. (1993). Heritabilities and genetic correlations of white clover clones grown in three environments. Crop Science, 33(6), 1149–1152. https://doi.org/10.2135/cropsci1993.0011183X003300060008x

Runcie, D., and Cheng, H. (2019). Pitfalls and remedies for cross validation with multi-trait genomic prediction methods. G3: Genes, Genomes, Genetics, 9(11), 3727–3741. https://doi.org/10.1534/g3.119.400598

Sampoux, J.-P., Giraud, H., and Litrico, I. (2020). Which recurrent selection scheme to improve mixtures of crop species? Theoretical expectations. G3: Genes, Genomes, Genetics, 10(1), 89–107. https://doi.org/10.1534/g3.119.400809

Sawadgo, W., and Okonkwo, E. (2024). Where were cover crops and no-till used in Alabama in 2022? Alabama Cooperative Extension System. https://www.aces.edu/blog/topics/crop-production/where-were-cover-crops-and-no-till-used-in-alabama-in-2022/

Scavo, A., Fontanazza, S., Restuccia, A., Pesce, G. R., Abbate, C., and Mauromicale, G. (2022). The role of cover crops in improving soil fertility and plant nutritional status in temperate climates. A review. Agronomy for Sustainable Development, 42, Article 93. https://doi.org/10.1007/s13593-022-00825-0

Seethepalli, A., Guo, H., Liu, X., Griffiths, M., Almtarfi, H., Li, Z., et al., (2020). RhizoVision Crown: An integrated hardware and software platform for root crown

phenotyping. Plant Phenomics, 2020, 3074916. https://doi.org/10.34133/2020/3074916

Seethepalli, A., Dhakal, K., Griffiths, M., Guo, H., Freschet, G. T., and York, L. M. (2021). RhizoVision Explorer: Open-source software for root image analysis and measurement standardization. AoB PLANTS, 13(6), plab056. https://doi.org/10.1093/aobpla/plab056

Speir, S. L., Tank, J. L., Bieroza, M., Mahl, U. H., and Royer, T. V. (2021). Catchment-scale differences in nutrient losses driven by agricultural management. Journal of Environmental Quality, 50(4), 921–933. https://doi.org/10.1002/jeq2.20255

Sprague, G. F., and Tatum, L. A. (1942). General vs. specific combining ability in single crosses of corn. Journal of the American Society of Agronomy, 34(10), 923–932. https://doi.org/10.2134/agronj1942.00021962003400100008x

Středa, T., Hajzlerová, J., Alba-Mejía, J., Jovanović, I., Frantová, N., and Středová, H. (2024). Quo vadis, breeding for an efficient root system, in the era of climate change? Czech Journal of Genetics and Plant Breeding, 60(4), 181–211. https://doi.org/10.17221/57/2024-CJGPB

Sun, S., Liang, N., Zuo, Z., Parsons, D., Morel, J., Shi, J., et al., (2021). Estimation of botanical composition in mixed clover–grass fields using machine learning-based image analysis. Frontiers in Plant Science, 12, 622429. https://doi.org/10.3389/fpls.2021.622429

Trachsel, S., Kaeppler, S. M., Brown, K. M., and Lynch, J. P. (2011). Shovelomics: High throughput phenotyping of maize (Zea mays L.) root architecture in the field. Plant and Soil, 341(1–2), 75–87. https://doi.org/10.1007/s11104-010-0623-8

USDA National Agricultural Statistics Service (USDA-NASS). (2024). 2022 Census of Agriculture (Volume 1, U.S. and State Data). United States Department of Agriculture. https://www.nass.usda.gov/AgCensus

USEPA. (2012). National summary of state information: Water quality assessment and total maximum daily loads report. United States Environmental Protection Agency.

Waldrip, H. M., He, Z., Mele, G., Senwo, Z. N., and Brantley, E. (2023). Legacy phosphorus in Alabama Hartsells soil after long-term amendment with broiler litter. Journal of Environmental Quality, 52(3), 534–547. https://doi.org/10.1002/jeq2.20462

Wang, F., Feldmann, M. J., and Runcie, D. E. (2025). Do not benchmark phenomic prediction against genomic prediction accuracy. The Plant Phenome Journal, 8(1), e70029. https://doi.org/10.1002/ppj2.70029

Wolfe, M. D., Jannink, J.-L., Kantar, M. B., and Santantonio, N. (2021). Multi-species genomics-enabled selection for improving agroecosystems across space and time. Frontiers in Plant Science, 12, 665349. https://doi.org/10.3389/fpls.2021.665349

Wright, A. J. (1985). Selection for improved yield in inter-specific mixtures or intercrops. Theoretical and Applied Genetics, 69(4), 399–407. https://doi.org/10.1007/BF00263967

Zimmermann, M. J. O. (1996). Breeding for yield in mixtures of common bean (Phaseolus vulgaris L.) and maize (Zea mays L.). Euphytica, 92(1–2), 129–134. https://doi.org/10.1007/BF00022837

Chapter 2 UAV-Based Phenomics Supports Early-Stage Breeding of Clover–Oat Mixtures by Reducing Destructive Phenotyping

Abstract

Crimson clover (Trifolium incarnatum L.), a widely used annual legume cover crop, is commonly grown with oat (Avena sativa L.) in winter mixtures to protect the soil, fix nitrogen, retain nutrients, and extend the grazing season in the southeastern United States. These mixtures frequently produce greater biomass and ecosystem services than monocultures, but realizing these benefits depends on the contribution of clover, which is typically the weaker competitor. Most cultivars grown in mixtures, however, were selected under monoculture conditions. Because mixture conditions constitute a different target environment in which cultivar choice influences performance, genetic improvement requires direct selection for mixture performance. This selection requires destructive harvesting and manual species separation to quantify species-specific biomass, creating a phenotyping bottleneck that restricts population size, measurement frequency, and genetic gain.

This study evaluated whether unmanned aerial vehicle (UAV) based phenomic prediction could reduce the destructive phenotyping required to evaluate clover–oat mixtures. Across four site-year environments, 600 clover–oat mixture plots per environment were evaluated for clover biomass, oat biomass, total biomass, and clover proportion. Thirty-three vegetation indices were derived from multispectral and harmonized hyperspectral UAV images. These indices were used to train Elastic Net, Random Forest, Bayesian Ridge Regression, and linear and Gaussian kernel models under within-environment, cross-location, and cross-year cross-validation. Within-

environment predictive abilities reached r = 0.70–0.87 for biomass traits at optimal flight timings. Elastic Net, Bayesian Ridge Regression, and Random Forest consistently outperformed Gaussian-kernel and ensemble models. Calibration analysis showed that predictive ability for total biomass reached 95% of the full-dataset baseline when only 25% of the plots, 150 of 600, were destructively harvested. Because destructive harvest is the binding constraint on how many entries a program can evaluate each cycle, this reduction releases capacity that can be redirected toward evaluating more families. These findings establish UAV phenomics as a practical resource-allocation tool for mixture breeding programs.

2.1 Introduction

Intercropping, defined as the simultaneous cultivation of two or more species, is a key strategy for sustainable intensification, improving productivity, resource-use efficiency, and ecosystem services such as nutrient retention, nitrogen fixation, carbon sequestration, and soil protection (Brooker et al., 2015; Moore et al., 2022). These benefits arise from ecological processes including complementarity and facilitation among component species (Eric et al., 2019). Grass–legume mixtures, particularly crimson clover and oat, are widely used in temperate agroecosystems as both forage and cover crops, supporting livestock production while delivering ecosystem services (Blanco-Canqui et al., 2015; Chapagain et al., 2020). In these systems, biomass production is a central driver of productivity, forage value, and ecological function (Blanco-Canqui et al., 2015; Poeplau & Don, 2015; MacLaren et al., 2019). However, system performance depends not only on total biomass but also on the balance between species contributions. In grass–legume mixtures, legumes are often less competitive than companion grasses, leading to reduced persistence and functional contribution, thereby limiting system performance (Høgh-Jensen et al., 2006; Hollard & Brummer, 1999). This imbalance highlights the need for breeding strategies that improve mixture performance, particularly by enhancing the contribution of the less competitive species.

Despite the advantages of mixtures, breeding programs have historically focused on monocultures, limiting the ability to fully exploit system-level benefits (Haug et al., 2021; Wolfe et al., 2021). Mixture breeding introduces additional complexity, requiring evaluation of genotype combinations across species and estimation of species-specific performance metrics such as general and specific mixing ability (Moore et al., 2022).

These requirements substantially increase phenotyping demands, especially in early-stage breeding. A major bottleneck is the reliance on destructive phenotyping, where plots must be harvested, species separated, and biomass measured individually. This process is labor-intensive and constrains both population size and measurement frequency, ultimately limiting selection intensity and genetic gain, particularly in open-pollinated species such as clover.

UAV-based phenomics provides a scalable alternative by enabling high-throughput, non-destructive measurement of canopy reflectance across large field experiments (Bretas et al., 2026; Biswas et al., 2021). However, in mixed-species canopies, spectral signals represent integrated responses of multiple interacting species, complicating inference of species-specific performance (Bretas et al., 2026; Pranga et al., 2024; Sun et al., 2021; Li et al., 2021). Breeding programs are increasingly distributed across locations, institutions, and states, and each partner acquires imagery with the platform it already owns, hence, UAV-based phenomic data are rarely collected with a single sensor and device. Also, sensors change over time, due to upgrades, replacements, or discontinued between breeding cycles. Sensors nonetheless differ in spectral resolution, bandwidth, and spectral response function, and these differences introduce systematic inconsistencies that alter vegetation index behavior and limit model transferability (Schaepman-Strub et al., 2006; Adam et al., 2010; Thenkabail et al., 2002, 2004). Without harmonization, phenomic predictions may reflect sensor-specific artifacts rather than biologically meaningful variation (Haboudane et al., 2004), biasing multi-environment inference. A phenomics workflow intended to serve a breeding program across many cycles must therefore be flexible across platforms, and able to combine data from different sensors into a common scale.

Spectral resampling provides this: hyperspectral reflectance is aggregated to match the band-pass functions of a multispectral sensor, following established sensor alignment frameworks (Chander et al., 2009; Thenkabail et al., 2000, 2004), so that vegetation indices can be derived consistently across platforms and compared across environments.

In this study, a supervised phenomic prediction framework is used to infer species-specific performance from non-destructively phenotyped plots. Considering that a phenomic model is trained on multi-dimensional UAV-based reflectance data over a plot to obtain an estimate of the biomass in that plot. What it estimates is therefore a measurement, containing both genetic and environmental contributions, and not the breeding value of the maternal half-sib family growing there (Feldmann et al., 2026). Therefore, in this study prediction was evaluated at two levels. First was at the plot level, vegetation indices from individual plots were used to predict the biomass of those same plots, substituting for the destructive harvest that would otherwise supply the measurement. Second was at the family-mean level, indices and biomass were first summarized as best linear unbiased predictions (BLUPS) for each clover maternal half-sib family, so that prediction targeted the family means on which selection acts.

Predictive accuracy alone is insufficient for breeding applications. The key question is whether phenomic prediction can reduce destructive phenotyping without compromising selection response. This question was addressed in this study using a calibration framework that evaluates how reducing the number of destructively phenotyped plots used for model training affects prediction accuracy and selection outcomes. By quantifying trade-offs between phenotyping effort and breeding efficiency, this study reframes phenomic prediction as a resource allocation problem. Specifically,

the objectives of this study were to (i) estimate variance components and heritability for species-specific and total biomass traits, (ii) evaluate prediction within and across environments, (iii) determine the minimum calibration required to sustain predictive ability and selection response, and (iv) assess multi-flight integration and identify vegetation indices consistently associated with biomass. This provides a practical framework for integrating UAV phenomics into mixture breeding.

2.2 Materials and Methods

2.2.1 Genetic Material and Breeding Scheme

Crimson clover germplasm was developed through a cyclic, pedigree-based recurrent selection scheme alternating between (i) individual plant selection in spaced-plant nurseries and (ii) family-level evaluation in mixture trials. Oat entries consisted of advanced breeding lines and cultivars from the University of Florida and Louisiana State University. Clover germplasm originated from a spaced-plant nursery established in Fall 2022, where individual plants were evaluated for vigor, phenology and seed production. Based on these data, superior plants were selected as parents for the 2023-2024 growing season. Seeds from each selected plant are considered maternal half-sib families. For the 2023–2024 growing season (Year 1), the half-sib families were used to establish both mixture trials and spaced-plant nurseries in 2023-2024. Crimson clover seed harvested from spaced-plants in 2024 were subsequently used as entries for 2024-2026 growing season trials (Year 2).

2.2.2 Experimental Design and Field Establishment

Field experiments were conducted across four site-year environments spanning two locations and two growing seasons. Trials were established at Auburn University (E.V. Smith Research and Extension Center's (Plant Breeding Unit in Tallassee, AL) and the University of Florida Citra Research Unit (FL). One environment at Citra (2024–2025) provided biomass data without UAV spectral acquisition. Detailed site characteristics, coordinates, and planting and harvest dates are provided in Table 2.1.

The clover component consisted of 162 half-sib families in Year 1 and 206 entries (177 half-sib families plus 29 advanced bulk entries from the Cover Crop Breeding Network) in Year 2. An incomplete factorial design was employed following (Haug et al. (2021), wherein a subset of clover families was combined with a subset of oat lines rather than evaluating all possible combinations (Table 2.2). Each environment comprised 600 clover–oat mixture plots. In Year 1, 560 unique clover–oat entry combinations were evaluated (40 replicated); in Year 2, 562 unique combinations (38 replicated). The oat component consisted of 26 advanced lines in Year 1, one line was dropped due to limited seed for 25 oats in Year 2.

Trials were arranged in partially replicated (p-rep) row–column designs (30 columns × 20 rows in 2023; 40 columns × 15 rows in 2024). Each experimental unit consisted of a single-row plot (1.83 m in 2023; 3.66 m in 2024). Clover seed was inoculated with Rhizobium leguminosarum biovar trifolii prior to planting. Seeding rates were approximately 10 lb acre−1 for clover and 30 lb acre−1 for oat. Each experimental unit represented a specific combination of one clover half-sib family and one oat genotype (Table 2.2).

2.2.3 Biomass Evaluation

Aboveground biomass was harvested from the mixture trials and separated by species, dried, and weighed to obtain clover biomass, oat biomass, and total biomass. Clover proportion was calculated as the ratio of clover biomass to total biomass. In 2023, the entire available plot area was harvested and the harvested length recorded, which varied among plots; harvested plot length was therefore fitted as a fixed covariate to account for the resulting variation in harvested area in 2023. For 2024, longer plots allowed a fixed length to be harvested from a uniform section of each plot, so harvested length did not vary within an environment and no covariate was required.

2.2.4 UAV Imagery Acquisition

UAV flights were conducted at Tallassee using a DJI Mavic 3M, which is equipped with a multispectral sensor capturing reflectance in four bands: green (560 ± 16 nm), red (650 ± 16 nm), red-edge (730 ± 16 nm), and near-infrared (NIR; 840 ± 26 nm). Seven flights were conducted per year between 29–166 days after planting (DAP). At Citra, a Headwall Photonics Nano hyperspectral pushbroom sensor captured contiguous reflectance across 273 bands (~400–1000 nm) at four time points in 2023–2024 (DAP ≈ 85–139). Plot-level mean reflectance was extracted from orthorectified imagery using zonal statistics. A suite of 33 vegetation indices (VIs) was computed from the four multispectral bands for all environments.

2.2.5 Sensor Harmonization

Because the Tallassee (multispectral) and Citra (hyperspectral) sensors differ fundamentally in spectral resolution, direct cross-sensor use of VIs requires harmonization. For each of the four DJI bands, the subset of hyperspectral channels whose center wavelengths fell within the corresponding spectral window (green: 544–576

nm; red: 634–666 nm; red-edge: 714–746 nm; NIR: 814–866 nm) was identified, and the harmonized band value was computed as:

$$\hat{\rho}_b^{plot} = \frac{1}{|S_b|}\sum_{k\in S_b} \quad \rho_k^{plot} \tag{2.1}$$

where ρkplot is the reflectance of hyperspectral band k for a given plot, Sb is the set of hyperspectral bands within DJI band window b, and |Sb| is the number of such bands.

Multispectral sensors do not respond equally to all wavelengths within a band. As a result, sensitivity is always highest near the band center and declines toward the edges, and differences in how hyperspectral sensors function are a principal cause of vegetation index values differing across sensors (Cundill et al., 2015). The arithmetic mean in Eq. 2.1 ignores this and gives every hyperspectral channel inside the band window the same weight. To test whether that simplification mattered, a Gaussian-weighted alternative was evaluated, in which channels near the band center contribute more than those at the edges:

$$w_k = \frac{expexp\left(-\frac{(\lambda_k-\lambda_b)^2}{2\sigma^2}\right)}{\sum_{j\in S_b} \quad exp\left(-\frac{(\lambda_j-\lambda_b)^2}{2\sigma^2}\right)} \tag{2.2}$$

where λb is the nominal center wavelength of DJI band b, λk is the center wavelength of hyperspectral band k, and σ = 12 nm controls the rate of weight decay, approximating a Gaussian spectral response function consistent with documented DJI filter properties. Functional equivalence between methods was assessed via Pearson correlation, mean absolute VI differences, and comparison of VI–biomass relationships. Because the two methods were functionally equivalent (mean r = 0.99 across 132 comparisons), the simpler arithmetic mean was retained.

2.2.6 Cross-Sensor VI Stability Classification

Having different sensors from the two locations can make a vegetation index differ between the locations because of the sensor rather than the canopy of the mixture plots. The purpose of this section was to identify which of the 33 VI behaved consistently across the two instruments. This enables the determination of VI that can be carried into cross-environment prediction, and also identifies unstable VI to drop.

To achieve this goal, consistency was assessed at four growth-stage-matched flight pairs identified by cumulative growing degree days (cGDD see section 2.2.5). Each VI was evaluated against four data-driven instability criteria: (i) scale divergence, flagged when mean |đ_AU − đ_UF| exceeded the median plus 1.5×IQR; (ii) direction inconsistency, flagged when the sign of (AU mean − UF mean) was not consistent across all four pairs; (iii) leverage outlier behavior, flagged when the maximum absolute z-score exceeded 3.0 in either environment; and (iv) high cross-pair variability, flagged when the standard deviation of AU–UF differences exceeded the median plus 1.5×IQR. VIs with zero flags were classified as STABLE, one flag as MARGINAL, and two or more flags as UNSTABLE. UNSTABLE VIs were excluded from cross-environment prediction.

2.2.7 Growing Degree Days and Flight Staging

Cumulative growing degree days (cGDD) were calculated from planting to each flight date using daily temperatures from the NASA POWER API (Sparks et al., 2018) via the EnvRtype package (Costa-Neto et al., 2021):

$$GDD_d = max(0,\ min(\ T_{base2}) - T_{base1}) \quad (2.3)$$

where Tbase1 = 4.4°C is the base temperature for crimson clover in the southeastern USA (Ball et al., 2004; Holliday, 1960), and Tbase2 = 35°C is a conservative thermal ceiling for

the oat–clover mixture. Flight pairs across locations were matched by minimizing cGDD differences at time of acquisition.

2.2.8 Variance Components, Heritability, and BLUPs

To partition phenotypic variation, separate mixed models were fitted for each trait–environment combination using ASReml-R v4 (Butler et al., 2017). All biomass traits were log-transformed [log(x + 1)] prior to analysis. The within-environment model was:

$$y_{ijk} = \mu + Cov + \alpha_i + \beta_j + \gamma_{ij} + \varepsilon_{ijk} \quad (2.4)$$

where yijk is the observed phenotype for the kth replicate of clover family i combined with oat line j; μ is the overall mean; Cov is the fixed effect of harvested plot length (2023 environments only); αi ~ N(0, σ2CC) is the random clover family effect; βj ~ N(0, σ2Oat) is the random oat line effect; γij ~ N(0, σ2Comb) is the random combination (clover × oat interaction) effect; and εijk is the residual. Spatial field variation was modeled via a separable first-order autoregressive process, AR1(row) ⊗ AR1(column), fitted on a complete spatial grid with missing cells included as missing data (Gilmour et al., 1997).

For the multi-environment analysis, the model was extended as:

$$y_{ijkl} = \mu + Env_l + \alpha_i + \beta_j + \gamma_{ij} + (\alpha_i \times Env_l) + (\beta_j \times Env_l) + (\gamma_{ij} \times Env_l) + e_{ijkl} \quad (2.5)$$

where Envl is the fixed effect of environment l, and the interaction terms (αi × Envl), (βj × Envl), and (γij × Envl) capture genotype-by-environment interactions. Residual variation was modelled independently within each environment as a direct sum of environment-specific separable first-order autoregressive structures, AR1(row) ⊗ AR1(column), each with its own residual variance and autocorrelation parameters (fitted using the dsum() residual specification in ASReml-R; Butler et al., 2017).

Significance of each random term was assessed by likelihood ratio tests (LRT), with p-values computed as 0.5 × P(χ21 > Λ) following Self and Liang (1987) for boundary testing. Broad-sense heritability was estimated using both the Falconer method (H2F = σ2G / σ2P) and the Cullis method (H2C = 1 − ūBLUP / 2σ2G; Cullis et al., 2006), the latter being more appropriate under unbalanced designs. BLUPs for clover families, oat lines, and their combinations, as well as for VIs and band reflectance, were extracted for downstream prediction.

2.2.9 Feature matrix

For each environment–flight combination, plot-level means of 33 VIs served as predictors. For UF 2023, hyperspectral reflectance was harmonized to equivalent multispectral bands as described above. Predictor matrices were standardized to zero mean and unit variance using training-set parameters only; zero-variance columns were removed before scaling.

2.2.10 Prediction models

Five base models were evaluated. Elastic Net (Zou and Hastie, 2005) performed simultaneous variable selection and shrinkage, with the mixing parameter α tuned over [0, 1] in steps of 0.1 via family-grouped inner cross-validation. Random Forest (RF; Breiman, 2001) was included as a nonlinear ensemble learner with 2,000 trees and a minimum node size of five; mtry was tuned over 4, 6, 11, and 17 predictors by minimizing out-of-bag prediction error within each training set. Bayesian Ridge Regression (BRR; Pérez and de los Campos, 2014) provided a full-Bayesian linear benchmark fitted via BGLR (20,000 iterations, 5,000 burn-in, thinning = 5).

Reproducing Kernel Hilbert Space (RKHS) was fitted with two kernels. First is the linear kernel, $K_L = XX^T / p$, where X is the n × p matrix of standardized VIs and p the number of indices. Second is the Gaussian kernel, which was constructed as $K_G(i,j) = \exp(-d^2_{ij} / h)$, where d^2_{ij} is the squared Euclidean distance between the standardized index vectors of plots i and j, allowing nonlinear relationships between indices and biomass. Instead of fixing the bandwidth h a priori, it was set by the median heuristic, $h = \text{median}(d^2)$, computed separately within each training set, so that the kernel is scaled to the observed spread of the data in each analysis, with the resulting kernel scaled using the mean of its diagonal. The two models were fitted using BGLR with model option set to "RKHS" (Pérez and de los Campos, 2014), this setting treats the kernel as the covariance of a random effect in the Bayesian mixed model. To get the predictions for plots used in validation, a kernel was constructed over the training and validation plots together, with the validation phenotypes set to missing, and then finally extracting the posterior mean of the linear predictor for those plots.

Two ensemble predictors were constructed: Ensemble_Best2 (equal-weight average of the two models with highest training-set Pearson correlation) and Ensemble_All (equal-weight average of all five base models).

2.2.11 Cross-validation

Three cross-validation (CV) schemes were used to assess prediction performance under different breeding-relevant applications. CV1 evaluated within-environment prediction using fivefold cross-validation repeated 15 times. For plot-level analyses, folds were grouped by clover family so that all plots containing the same clover family remained within the same fold. At the BLUP level, the corresponding genetic-effect units were

assigned to folds. CV2 evaluated reciprocal cross-location prediction between Tallassee 2023 and Citra 2023, whereas CV3 evaluated reciprocal cross-year prediction between Tallassee 2023 and Tallassee 2024. Flights across locations and years were paired by minimizing differences in cumulative growing degree days (Eq. 3).

Each scheme was run at two data levels. At the plot level, responses were the observed plot values for clover biomass, oat biomass, total biomass, and clover proportion, and predictors were the vegetation indices extracted from those same plots. At the BLUP level, responses and predictors were the corresponding genetic effects: clover-family BLUPs for clover biomass and clover proportion, oat-line BLUPs for oat biomass, and clover–oat combination BLUPs for total biomass. Predictive ability was reported as the Pearson correlation (r) between observed and predicted values.

Because CV2 and CV3 train on one environment and validate on another, each direction yields a single accuracy estimate. To characterize variability in that estimate, the rows of the training dataset were sampled with replacement to the original training-set size, the model was refitted to each bootstrap sample, and predictions were generated for the full, unchanged validation environment. This was repeated 20 times for plot-level analyses and 40 times for BLUP-level analyses. Variation among bootstrap estimates therefore reflects sensitivity to the composition of the training environment rather than sampling variability in the validation environment.

To test whether combining imagery from multiple flights improved prediction, VIs from individual flights were pivoted to wide format (for example, Flight1_NDVI and Flight2_NDVI), creating one row per observational unit with flight-specific VIs as separate predictors. Three temporal groupings were evaluated within each environment: all flights,

early flights, and late flights. This analysis was conducted under CV1 using both plot-level observations and the corresponding BLUP-level data.

2.2.12 Calibration Requirement

To quantify the minimum destructive phenotyping requirement, calibration subsets of $N \in \{25, 50, 150, 300, 600\}$ plots were randomly sampled per environment x flight x trait combination and used to train Elastic Net, RF, and RKHS-G models (20 iterations per calibration level; 5-fold CV for N = 600). BRR and RKHS-L were excluded from this analysis due to redundancy with Elastic Net and negligible differences in preliminary analyses. Predictive ability at each calibration size was expressed relative to that obtained with the full set of 600 plots, within each environment, flight, trait, and model.

2.3 Results

2.3.1 Weather, Phenotypic variation, variance components, and heritability of biomass traits

Thermal environments varied substantially across site-years (Fig. 2.1). Cumulative growing degree days at harvest ranged from approximately 1,000°C·d (Tallassee 2023–24) to over 2,000°C·d (Tallassee 2024–25 and Citra 2024–25), representing a near twofold difference in seasonal heat accumulation. Precipitation was unevenly distributed, with Tallassee 2023–24 receiving frequent high-intensity events exceeding 60 mm d^{-1} while Citra 2023–24 received markedly less rainfall overall.

Biomass traits varied substantially across environments (Table 2.3; Fig. 2.2). Clover biomass ranged from 26.9 g (Citra 2024–25) to 144.0 g (Tallassee 2024–25), while clover proportion spanned 0.00–0.99, with means from 0.17 to 0.41. Oat biomass

exceeded clover biomass in all environments. Variability was high for clover biomass (CV 65–85%) and oat biomass (CV 29–73%), whereas total biomass was less variable (CV 21–57%).

Clover biomass exhibited low–moderate Cullis heritability (H^2 = 0.01–0.60), with combination effects contributing substantially to variance (Table 2.4; Fig. 2.3). Clover proportion showed higher H^2 (0.52–0.75) and significant genotype × environment interaction. Oat biomass had consistently high H^2 (0.59–0.85), while total biomass showed moderate heritability (H^2 = 0.63–0.73). In the MET, clover variance was low relative to residual variance, with significant clover × environment and combination × environment effects (Table 2.4; Fig. 2.3).

2.3.2 Sensor harmonization and cross-environment VI stability

The two locations were imaged with different instruments, so a vegetation index could differ between them for reasons unrelated to the mixture canopy. To address this, two checks were applied before any index was carried into cross-environment prediction: whether the harmonization method itself altered the derived indices, and whether each index behaved comparably on the two platforms.

The choice of harmonization method had negligible effect. Arithmetic-mean and Gaussian-weighted (σ = 12 nm) resampling of hyperspectral reflectance to DJI-equivalent bands produced near-identical indices (mean r = 0.99 across 33 VIs; Fig. 2.4a), so the simpler arithmetic mean was retained. Across cGDD-matched flight pairs, the mean values of the 33 indices at Tallassee and Citra agreed closely (r = 0.815; Fig. 2.4b), indicating that after harmonization the two platforms placed the indices on a common scale rather than on systematically offset ones.

Individual indices nonetheless differed in how consistently they behaved across platforms. The four instability criteria classified 24 VIs as STABLE (no criterion flagged), 4 as MARGINAL (one flagged), and 5 as UNSTABLE (two or more flagged; Fig. 2.4c, d), with MNDVI failing all four. STABLE here denotes an index whose values at the two locations differed by no more than the typical difference among indices, did so in a consistent direction, showed no leverage outliers, and behaved consistently across the four flight pairs. It does not imply that an index took the same value at both locations, which would not be expected, since different plots were grown at each. The five UNSTABLE indices were excluded from cross-environment modelling, leaving 28.

Among the retained indices, the direction and strength of the index–biomass correlation was largely consistent between locations, so an index that tracked biomass at Tallassee generally tracked it at Citra. Total biomass correlations reached r = 0.57 at Tallassee and r = 0.46 at Citra, while the oat biomass signal was weaker at Citra ($|r| \leq 0.22$).

2.3.3 Within-Environment Phenomic Prediction (CV1) and effect of cumulative flight

Predictive ability varies by trait, flight timing, and environment (Fig. 2.5). At the plot level (Fig. 2.5a), clover proportion and clover biomass peaked at late-season flights ($r \approx 0.70–0.79$), whereas early flights were substantially lower ($r \leq 0.42$). Oat biomass peaked mid-season ($r \approx 0.87$ at AU_2023) and declined thereafter. Total biomass was the most predictable and temporally stable trait, exceeding r = 0.84 across mid-season flights. ElasticNet, BRR, and RF consistently outperformed kernel-based methods, and ensembles did not improve performance. Predictive ability at UF_2023 was generally lower, particularly for oat biomass ($r \leq 0.46$), reflecting reduced temporal coverage.

At the BLUP level (Fig. 2.5b), similar patterns were observed, with lower peak accuracies ($r \approx 0.49–0.66$) and higher variability for oat biomass ($sd\_r > 0.30$). Model ranking and temporal trends were consistent across both data levels. Pooling all flights (Fig. 2.6) did not improve prediction over the best single-flight models and generally reduced accuracy.

Sequential cumulative flight integration was evaluated using raw plot-level data under CV1 (Fig. 2.7). Predictive ability increased rapidly with the inclusion of early flights and plateaued thereafter across all traits and environments. Most gains were achieved by the first 2–3 flights, particularly for total biomass and clover proportion. Additional flights provided marginal improvement, with diminishing returns beyond mid-season. Model rankings remained consistent, with ElasticNet and RF outperforming RKHS_Gaussian across traits.

2.3.4 Cross-Location Prediction

Cross-location prediction between Tallassee and Citra revealed strong directional asymmetry (Figure 2.8). Because the two locations were flown on different dates and with different numbers of flights, flight numbers do not correspond to comparable growth stages; flights were therefore paired by cumulative growing degree days (Section 2.2.5), therefore, each result below refers to a cGDD-matched pair of flights, one at each location. At the plot level (Figure 2.8a), total biomass was the only trait with r above 0.50 in both directions, reaching $r = 0.69$ when trained at Tallassee flight 3 and validated at Citra flight 2 (Ensemble_All and RKHS_Linear), and $r = 0.77$ when trained at Citra flight 4 and validated at Tallassee flight 5 (RF). Clover biomass transferred only when trained at Tallassee flight 4 and validated at Citra flight 3 ($r = 0.68$), while oat biomass

transferred only in the opposite direction when trained at Citra flight 4 and validated at Tallassee flight 5 (RF, r = 0.67). Clover proportion showed the weakest transferability, reaching r = 0.44 (ElasticNet) only when trained at Tallassee and validated at Citra. Later flight pairs consistently outperformed early pairs for clover traits.

At the BLUP level (Figure 2.8b), most predictions fell below r = 0.30. Clover proportion was the most balanced trait, with RKHS_Linear reaching r = 0.33 (AU predicting UF F4 to F3) and r = 0.38 (UF predicting AU F4 to F5). Total biomass, the strongest plot-level trait, dropped to r ≤ 0.27 at the BLUP level. Oat predictions were erratic with frequent negative values, reflecting only 26 genotypes. Genotype-level spectral signals did not generalize reliably across locations.

To test if combining all flights into a single feature matrix improves cross-location transferability over cGDD matched paired-flight predictions, the study evaluated pooled-flight CV2 at both data levels: at the plot level (Figure 2.9), pooling did not exceed the best paired-flight result, reaching r = 0.61–0.70 only for total biomass at AU_2023 (RKHS_Linear, Ensemble_All) and total or oat biomass at UF_2023 (RF), while clover traits remained near zero with wide spread across models; at the BLUP level, pooling further collapsed predictive ability across nearly every trait–model combination, with median r below 0.30 in all panels and oat biomass at UF_2023 reaching r ≈ −0.50 (ElasticNet, Ensemble_Best2, Ensemble_All)

2.3.5 Cross-Year Prediction

Cross-year prediction between AU_2023 and AU_2024 was strongly direction-dependent (Figure 2.10). At the plot level (Figure 2.10a), clover proportion did not transfer across years in either direction. Clover biomass transferred only when AU_2023

predicted AU_2024 at late flights (r = 0.66, RKHS_Linear F5 to F6). Total biomass was the most robust trait, reaching r = 0.84 (AU_2024 predicting AU_2023) and r = 0.65 in the reverse direction. At the BLUP level (Figure 2.10b), clover biomass and clover proportion achieved moderate accuracy only when AU_2024 predicted AU_2023 at late flights (r = 0.60 and r = 0.58, respectively; RKHS_Linear F6 to F5), while total biomass reached r = 0.52 (AU_2023 predicting AU_2024 F5 to F6). Later flight pairs consistently outperformed early pairs for clover traits at both data levels.

2.3.6 Effect of calibration set size on phenomic prediction accuracy

This study evaluated how reducing destructive phenotyping through calibration set subsampling affected predictive ability across traits, environments, and models (Fig. 2.11). Predictive ability increased with calibration proportion and approached full-dataset performance by 50–75% across all traits. For total biomass, predictive ability exceeded 95% of baseline at 25% calibration and reached ~100% by 50%. Clover biomass and clover proportion showed the largest gains between 10% and 25%, with diminishing returns thereafter. In contrast, oat biomass was more sensitive to calibration size, particularly in UF_2023 and AU_2024, where low calibration levels reduced performance. Model differences were minor, with ElasticNet and RF generally outperforming RKHS.

2.3.7 Trait- and environment-specific vegetation index importance derived from Random Forest models

Variable importance derived from Random Forest models revealed trait- and environment-specific patterns of vegetation index contributions (Fig. 2.12). Across environments, ExGR and VARI frequently ranked among the most important indices for

clover biomass and clover proportion, although their relative importance varied by environment. MCARI was the top-ranked predictor for total and oat biomass in AU_2023 but showed reduced importance in UF_2023 and AU_2024. Total biomass prediction relied on environment-specific VI sets, with MCARI and NDRE dominating in AU_2023, DVI and NRI in UF_2023, and NRI and SRI in AU_2024. Clover-related traits exhibited greater variability in their top-ranked predictors, with no single index consistently dominating across environments.

2.4. Discussion

Results from this study showed that UAV-based phenomic prediction can substantially reduce destructive phenotyping in clover–oat mixture breeding while preserving selection response, providing a practical framework for integrating remote sensing into early-stage intercrop improvement programs. The results address a central bottleneck in mixture breeding: the labor-intensive requirement to harvest, separate, and weigh species-specific biomass from every experimental plot (Haug et al., 2021; Moore et al., 2022). By quantifying the trade-offs between calibration effort, predictive accuracy, and expected genetic gain across environments, traits, and prediction scenarios, our findings reframe phenomic prediction as a resource allocation tool rather than merely a prediction exercise.

2.4.1 Phenomic prediction captures species-specific biomass signals in mixed canopies

A key finding is that UAV-derived vegetation indices can predict species-specific biomass from spectrally mixed canopies, despite the integrated spectral response of two co-occurring species. Total biomass was the most predictable trait, consistent with the

expectation that aggregate canopy reflectance most directly indexes total vegetation cover (Grüner et al., 2020; Grüner et al., 2021). Clover biomass and clover proportion were also well predicted at late-season flights (r = 0.70–0.79), indicating that spectral features capture species-specific signatures as canopy composition differentiates over the growing season. This temporal dependence aligns with Pranga et al. (2024), who reported that classification accuracy of grass versus clover in mixed swards improved at later growth stages when species morphological and spectral differences become more pronounced. The lower prediction accuracy for oat biomass at UF_2023 (r ≤ 0.46) likely reflects both the reduced temporal coverage (four flights versus seven at Tallassee) and the dominance of oat in the canopy, which may compress the spectral variance available for distinguishing oat-specific biomass differences among plots.

The distinct timing of peak predictive ability for each trait, during the middle of the season for oat and late in the season for clover, has direct implications for flight scheduling in operational breeding programs. Rather than acquiring imagery at a single time point, breeders should target flights to match the phenological stage at which the trait of interest is most spectrally informative. This finding extends the single-species temporal optimization reported by Sakurai et al. (2022) in soybean and Sangjan et al. (2022) in forage crops to the more complex multi-species context.

2.4.2 Model performance and the limited advantage of nonlinear and ensemble methods

ElasticNet, BRR, and RF consistently outperformed kernel-based methods (RKHS_Gaussian, RKHS_Linear), and ensemble predictors did not exceed the best individual model. This pattern suggests that, for 33 vegetation indices derived from four

spectral bands, the relationship between spectral features and biomass is predominantly linear or mildly nonlinear, and the signal-to-noise ratio does not benefit from the added flexibility of Gaussian kernels. Similar conclusions have been reported in UAV-based biomass prediction of oat monocultures, where RF and linear models performed comparably (Hu et al., 2021). The lack of ensemble improvement is consistent with the high correlation among base model predictions when models agree, averaging provides no additional gain. Hence, for operational deployment, this finding simplifies implementation: a regularized linear model (ElasticNet) can offer near-optimal accuracy with lower computational cost and greater interpretability than kernel or ensemble approaches.

2.4.3 Cross-environment transferability: directional asymmetry and implications for multi-environment breeding

Cross-location (CV2) and cross-year (CV3) prediction revealed strong directional asymmetry. For total biomass, cross-location prediction achieved r = 0.77 (UF to AU) and r = 0.69 (AU to UF), but for clover proportion, transferability was weak and unidirectional. This asymmetry likely arises from differences in the spectral feature space between environments, driven by variation in soil background, canopy architecture, and growth stage alignment despite cGDD matching (Fig. S1). Genotype-by-environment interaction for clover traits—reflected in the significant clover × environment variance component further limits the generalizability of spectral–phenotype relationships across locations. These findings are consistent with the broader genomic and phenomic prediction literature, which shows that prediction accuracy decays with increasing genetic and environmental distance between training and target populations

(Burgueño et al., 2012; Würschum et al., 2022). The implication for mixture breeding is that cross-environment phenomic models are most useful for traits with high genetic correlation across environments (e.g., total biomass) and should be applied cautiously for traits with large G × E (e.g., clover proportion).

While the goal is not to compare BLUP-level and plot-level predictions, the BLUP-level predictions were consistently 0.10–0.35 lower than plot-level estimates, reflecting the reduced sample size at the genotype level and the loss of spatial information when plot-level variation is averaged into family means. However, BLUP-level prediction is more relevant for breeding decisions because it targets genetic rather than phenotypic ranking. The substantial drop in cross-environment BLUP accuracy (most estimates below r = 0.30) indicates that genotype-level spectral signatures do not generalize well across locations, reinforcing the need for environment-specific calibration in operational programs.

2.4.4 Sensor harmonization enables cross-platform comparability

A methodological contribution of this study is the validation of arithmetic-mean spectral resampling for harmonizing hyperspectral (Headwall) and multispectral (DJI) sensor data. The functional equivalence between arithmetic-mean and Gaussian-weighted resampling (r = 0.99) confirms that, within the narrow DJI band windows (±16–26 nm), the spectral response function shape has negligible impact on derived vegetation indices. This finding extends the sensor alignment frameworks described by Chander et al. (2009) and Schaepman-Strub et al. (2006) to the specific context of UAV-based crop phenotyping across sensor platforms. The subsequent stability classification of VIs identified 23 of 33 indices as stable across platforms; providing breeders with a

curated set of cross-environment features and excluding indices (e.g., MNDVI) whose instability would introduce sensor-specific artifacts into prediction models (Haboudane et al., 2004; Thenkabail et al., 2002). This harmonization approach is directly applicable to other multi-location breeding programs where sensor standardization is not feasible.

2.4.5 Calibration framework: reducing destructive phenotyping while preserving genetic gain

The calibration analysis provides the most operationally relevant finding: predictive ability for total biomass reached 95% of the full-dataset baseline at 25% calibration (150 of 600 plots). This means that a breeder could harvest only 150 plots, train a phenomic model, and predict the remaining 450 plots with minimal loss in selection response; saving 75% of the destructive phenotyping effort. This result aligns with the broader phenomic selection literature. Zhu et al. (2021) showed that phenomic prediction in wheat required smaller training sets than genomic prediction to achieve comparable accuracy for complex traits, and Würschum et al. (2022) demonstrated that phenomic predictive ability for grain yield was robust to training set reduction. In the forage breeding context, Biswas et al. (2021) demonstrated that UAV-derived NDVI could substitute for destructive biomass assessment in alfalfa, achieving selection gains comparable to conventional phenotyping.

Calibration results extend these findings to the multi-species mixture context, where the phenotyping bottleneck is compounded by the need for species separation. This reframes the phenomic prediction problem from "how accurately can we predict biomass?" to "how few plots do we need to harvest to maintain selection response?" or

“how many more plots can be established without incurring undue biomass harvest burden”; a question of direct relevance to resource-limited breeding programs.

2.4.6 Vegetation index importance and biological interpretation

Random Forest variable importance analysis revealed trait-specific and environment-specific VI contributions. ExGR and VARI indices sensitive to visible-range greenness contrasts were consistently important for clover biomass and clover proportion, consistent with the distinct green color saturation of clover foliage relative to oat. MCARI, which targets chlorophyll absorption, was the dominant predictor for oat and total biomass at AU_2023 but showed reduced importance at other environments, suggesting that its predictive contribution depends on local canopy structure and growth stage. The lack of a single universally dominant VI across traits and environments underscores the advantage of multivariate prediction models over single-index approaches (Thenkabail et al., 2000, 2002).

2.4.7 Limitations

Several limitations should be considered. First, the study used four spectral bands (green, red, red-edge, NIR); additional bands in the shortwave infrared or blue regions may improve species discrimination in mixed canopies. Second, the cross-location comparison involved only two locations with different sensors, confounding sensor and location effects despite harmonization. Finally, UF_2024 lacked UAV spectral data, preventing full reciprocal cross-year validation across locations. Future work should incorporate genomic data to enable joint genomic–phenomic prediction (Wolfe et al., 2021; Bančič et al., 2021), which may improve cross-environment transferability by capturing the additive genetic component that phenomic models alone cannot isolate.

2.5.Conclusions

This study establishes that UAV-based phenomic prediction is operationally viable for reducing destructive phenotyping in clover–oat mixture breeding. Within-environment prediction accuracies of r = 0.70–0.87 for biomass traits, combined with calibration results showing that 75% of plots can be spared from harvest with minimal loss in selection response, provide a strong basis for integration into applied breeding pipelines. Cross-environment prediction, while promising for total biomass, remains limited for species-specific traits with large G × E, highlighting the need for environment-specific calibration and, potentially, the integration of genomic information to improve model performance.

References

Adam, E., Mutanga, O., & Rugege, D. (2010). Multispectral and hyperspectral remote sensing for identification and mapping of wetland vegetation: A review. Wetlands Ecology and Management, 18, 281–296. https://doi.org/10.1007/s11273-009-9169-z

Annicchiarico, P., Collins, R. P., De Ron, A. M., Firmat, C., Litrico, I., & Hauggaard-Nielsen, H. (2019). Do we need specific breeding for legume-based mixtures? Advances in Agronomy, 157, 141–215. https://doi.org/10.1016/bs.agron.2019.04.001

Bančič, J., Werner, C. R., Gaynor, R. C., Gorjanc, G., Odeny, D. A., Ojulong, H. F., Dawson, I. K., Hoad, S. P., & Hickey, J. M. (2021). Modeling illustrates that genomic selection provides new opportunities for intercrop breeding. Frontiers in Plant Science, 12, 605172. https://doi.org/10.3389/fpls.2021.605172

Biswas, A., Andrade, M. H. M. L., Acharya, J. P., de Souza, C. L., Lopez, Y., de Assis, G., Shirbhate, S., Singh, A., Munoz, P., & Rios, E. F. (2021). Phenomics-assisted selection for herbage accumulation in alfalfa (Medicago sativa L.). Frontiers in Plant Science, 12, 756768. https://doi.org/10.3389/fpls.2021.756768

Blanco-Canqui, H., Shaver, T. M., Lindquist, J. L., Shapiro, C. A., Elmore, R. W., Francis, C. A., & Hergert, G. W. (2015). Cover crops and ecosystem services: Insights from studies in temperate soils. Agronomy Journal, 107, 2449–2474.

Breiman, L. (2001). Random forests. Machine Learning, 45(1), 5–32. https://doi.org/10.1023/A:1010933404324

Bretas, I. L., Zhao, C., Dubeux, J. C. B., Xin, Y., Tang, Z., Trumpp, K. R., Acuna, J. P., Small, I. M., & de Souza, C. H. L. (2026). Estimating the botanical composition of bahiagrass–rhizoma peanut pastures using aerial multispectral imagery and deep learning. Crop Science, 66, e70253. https://doi.org/10.1002/csc2.70253

Brooker, R. W., Bennett, A. E., Cong, W. F., Daniell, T. J., George, T. S., Hallett, P. D., et al. (2015). Improving intercropping: A synthesis of research in agronomy, plant physiology and ecology. New Phytologist, 206(1), 107–117. https://doi.org/10.1111/nph.13132

Burgueño, J., de los Campos, G., Weigel, K., & Crossa, J. (2012). Genomic prediction of breeding values when modeling genotype × environment interaction using pedigree and dense molecular markers. Crop Science, 52(2), 707–719. https://doi.org/10.2135/cropsci2011.06.0299

Butler, D. G., Cullis, B. R., Gilmour, A. R., Gogel, B. J., & Thompson, R. (2017). ASReml-R reference manual version 4. VSN International Ltd.

Chander, G., Markham, B. L., & Helder, D. L. (2009). Summary of current radiometric calibration coefficients for Landsat MSS, TM, ETM+, and EO-1 ALI sensors. Remote Sensing of Environment, 113(5), 893–903. https://doi.org/10.1016/j.rse.2009.01.007

Chapagain, T., Lee, E. A., & Raizada, M. N. (2020). The potential of multi-species mixtures to diversify cover crop benefits. Sustainability, 12(5), 2058. https://doi.org/10.3390/su12052058

Cundill, S. L., Van der Werff, H. M. A., & Van der Meijde, M. (2015). Adjusting Spectral Indices for Spectral Response Function Differences of Very High Spatial

Resolution Sensors Simulated from Field Spectra. Sensors, 15(3), 6221-6240. https://doi.org/10.3390/s150306221

Cullis, B. R., Smith, A. B., & Coombes, N. E. (2006). On the design of early generation variety trials with correlated data. Journal of Agricultural, Biological, and Environmental Statistics, 11(4), 381–393. https://doi.org/10.1198/108571106X154443

Falconer, D. S., & Mackay, T. F. C. (1996). Introduction to quantitative genetics (4th ed.). Longman.

Feldmann, M. J., Wang, F., & Runcie, D. E. (2026). Philosophy of phenomic prediction and its incompatibility with causal inference. The Plant Phenome Journal, 9, e70091. https://doi.org/10.1002/ppj2.70091

Grüner, E., Astor, T., & Wachendorf, M. (2020). The potential of UAV-borne spectral and textural information for predicting aboveground biomass and N fixation in legume-grass mixtures. PLOS ONE, 15(6), e0234703. https://doi.org/10.1371/journal.pone.0234703

Grüner, E., Astor, T., & Wachendorf, M. (2021). Prediction of biomass and N fixation of legume–grass mixtures using sensor fusion. Frontiers in Plant Science, 11, 603921. https://doi.org/10.3389/fpls.2020.603921

Haboudane, D., Miller, J. R., Pattey, E., Zarco-Tejada, P. J., & Strachan, I. B. (2004). Hyperspectral vegetation indices and novel algorithms for predicting green LAI of crop canopies: Modeling and validation in the context of precision agriculture. Remote Sensing of Environment, 90(3), 337–352. https://doi.org/10.1016/j.rse.2003.12.013

Haug, B., Messmer, M. M., Enjalbert, J., Goldringer, I., Forst, E., Flutre, T., Mary-Huard, T., & Hohmann, P. (2021). Advances in breeding for mixed cropping—Incomplete factorials and the producer/associate concept. Frontiers in Plant Science, 11, 620400. https://doi.org/10.3389/fpls.2020.620400

Holland, J. B., & Brummer, E. C. (1999). Cultivar effects on oat–berseem clover intercrops. Agronomy Journal, 91, 321–329.

Høgh-Jensen, H., Nielsen, B., & Thamsborg, S. M. (2006). Productivity and quality, competition and facilitation of chicory in ryegrass/legume-based pastures under various nitrogen supply levels. European Journal of Agronomy, 24(3), 247–256. https://doi.org/10.1016/j.eja.2005.10.007

Hu, P., Chapman, S. C., Wang, X., Potgieter, A., Duan, T., Jordan, D., Guo, Y., & Zheng, B. (2018). Estimation of plant height using a high throughput phenotyping platform based on unmanned aerial vehicle and self-calibration: Example for sorghum breeding. European Journal of Agronomy, 95, 24–32. https://doi.org/10.1016/j.eja.2018.02.004

Justes, E., Bedoussac, L., Dordas, C., Frak, E., Louarn, G., Boudsocq, S., et al. (2021). The 4C approach as a way to understand species interactions determining intercropping productivity. Frontiers of Agricultural Science and Engineering, 8(3), 387–399. https://doi.org/10.15302/J-FASE-2021414

Li, K.-Y., Burnside, N. G., Sampaio de Lima, R., Villoslada Peciña, M., Sepp, K., et al. (2021). The application of an unmanned aerial system and machine learning techniques for red clover-grass mixture yield estimation under variety

performance trials. Remote Sensing, 13, 1994. https://doi.org/10.3390/rs13101994

Moore, V. M., Schlautman, B., Fei, S., Roberts, L. M., Wolfe, M., Ryan, M. R., Wells, S., & Lorenz, A. J. (2022). Plant breeding for intercropping in temperate field crop systems: A review. Frontiers in Plant Science, 13, 843065. https://doi.org/10.3389/fpls.2022.843065

Poeplau, C., & Don, A. (2015). Carbon sequestration in agricultural soils via cultivation of cover crops—A meta-analysis. Agriculture, Ecosystems & Environment, 200, 33–41. https://doi.org/10.1016/j.agee.2014.10.024

Pranga, J., Borra-Serrano, I., Quataert, P., De Swaef, T., Vanden Nest, T., Willekens, K., Ruysschaert, G., Janssens, I. A., Roldán-Ruiz, I., & Lootens, P. (2024). Quantification of species composition in grass-clover swards using RGB and multispectral UAV imagery and machine learning. Frontiers in Plant Science, 15, 1414181. https://doi.org/10.3389/fpls.2024.1414181

Pérez, P., & de los Campos, G. (2014). Genome-wide regression and prediction with the BGLR statistical package. Genetics, 198(2), 483–495. https://doi.org/10.1534/genetics.114.164442

Sakurai, K., Toda, Y., Kajiya-Kanegae, H., Ohmori, Y., Yamasaki, Y., Takahashi, H., Takanashi, H., Tsuda, M., Tsujimoto, H., Kaga, A., Anai, T., Iseki, K., Nakazono, M., & Iwata, H. (2022). Time-series multispectral imaging in soybean for improving biomass and genomic prediction accuracy. The Plant Genome, 15(4), e20244. https://doi.org/10.1002/tpg2.20244

Sangjan, W., McGee, R. J., & Sankaran, S. (2022). Optimization of UAV-based imaging and image processing orthomosaic and point cloud approaches for estimating biomass in a forage crop. Remote Sensing, 14(10), 2396. https://doi.org/10.3390/rs14102396

Schaepman-Strub, G., Schaepman, M. E., Painter, T. H., Dangel, S., & Martonchik, J. V. (2006). Reflectance quantities in optical remote sensing—Definitions and case studies. Remote Sensing of Environment, 103(1), 27–42. https://doi.org/10.1016/j.rse.2006.03.002

Self, S. G., & Liang, K.-Y. (1987). Asymptotic properties of maximum likelihood estimators and likelihood ratio tests under nonstandard conditions. Journal of the American Statistical Association, 82(398), 605–610. https://doi.org/10.1080/01621459.1987.10478472

Sun, S., Liang, N., Zuo, Z., Parsons, D., Morel, J., Shi, J., Wang, Z., Luo, L., Zhao, L., Fang, H., He, Y., & Zhou, Z. (2021). Estimation of botanical composition in mixed clover–grass fields using machine learning-based image analysis. Frontiers in Plant Science, 12, 622429. https://doi.org/10.3389/fpls.2021.622429

Thenkabail, P. S., Smith, R. B., & De Pauw, E. (2000). Hyperspectral vegetation indices and their relationships with agricultural crop characteristics. Remote Sensing of Environment, 71(2), 158–182. https://doi.org/10.1016/S0034-4257(99)00067-X

Thenkabail, P. S., Smith, R. B., & De Pauw, E. (2002). Evaluation of narrowband and broadband vegetation indices for determining optimal hyperspectral wavebands for agricultural crop characterization. Photogrammetric Engineering & Remote Sensing, 68(6), 607–621.

Thenkabail, P. S., Enclona, E. A., Ashton, M. S., & Van Der Meer, B. (2004). Accuracy assessments of hyperspectral waveband performance for vegetation analysis. Remote Sensing of Environment, 91(3–4), 354–376. https://doi.org/10.1016/j.rse.2004.03.013

Wolfe, M. D., Jannink, J.-L., Kantar, M. B., & Santantonio, N. (2021). Multi-species genomics-enabled selection for improving agroecosystems across space and time. Frontiers in Plant Science, 12, 665349. https://doi.org/10.3389/fpls.2021.665349

Würschum, T., Langer, S. M., Longin, C. F. H., Tucker, M. R., & Leiser, W. L. (2022). The performance of phenomic selection depends on the genetic architecture of the target trait. Theoretical and Applied Genetics, 135, 653–665. https://doi.org/10.1007/s00122-021-03997-7

Zou, H., & Hastie, T. (2005). Regularization and variable selection via the elastic net. Journal of the Royal Statistical Society: Series B (Statistical Methodology), 67(2), 301–320. https://doi.org/10.1111/j.1467-9868.2005.00503.x

Zhu, X., Leiser, W. L., Hahn, V., & Würschum, T. (2021). Phenomic selection is competitive with genomic selection for breeding of complex traits. The Plant Phenome Journal, 4(1), e20027. https://doi.org/10.1002/ppj2.20027

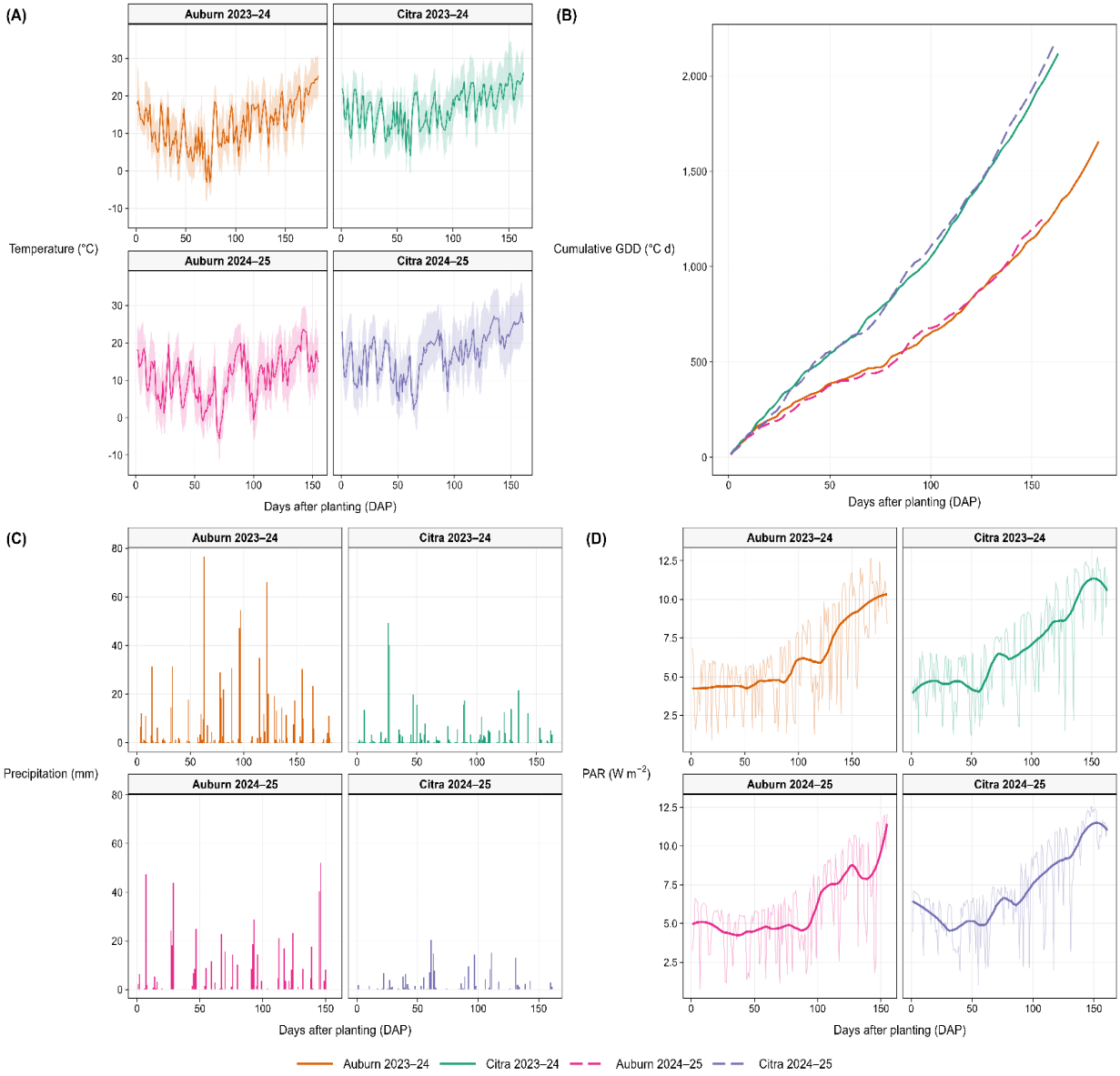

Figure 2.1. Weather data during field experiment seasons at Auburn and Citra.

Panels show (A) daily mean temperature, (B) cumulative growing degree days (CGDD), (C) daily precipitation, and (D) photosynthetically active radiation (PAR) across days after planting (DAP). Smoothed curves represent seasonal trajectories, and shaded regions represent daily variability. These environmental profiles were used to evaluate climatic similarity between environments and to facilitate temporal harmonization of UAV-derived phenomic measurements across locations.

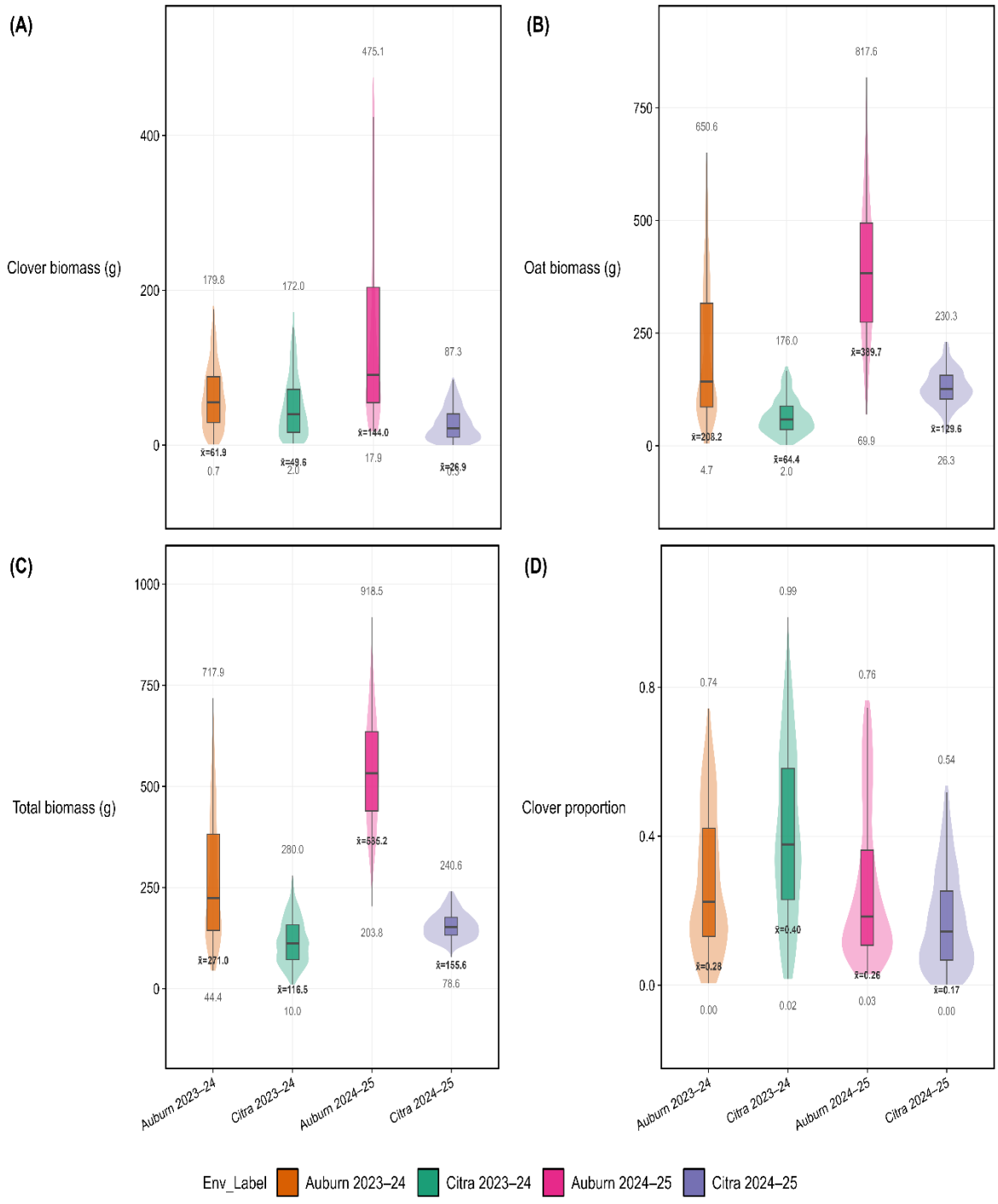

Figure 2.2. Phenotypic distributions of clover, oat, and total biomass, and clover proportion across four clover–oat intercrop environments.

(A) clover biomass, (B) oat biomass, (C) Total biomass, and (D) clover proportion.

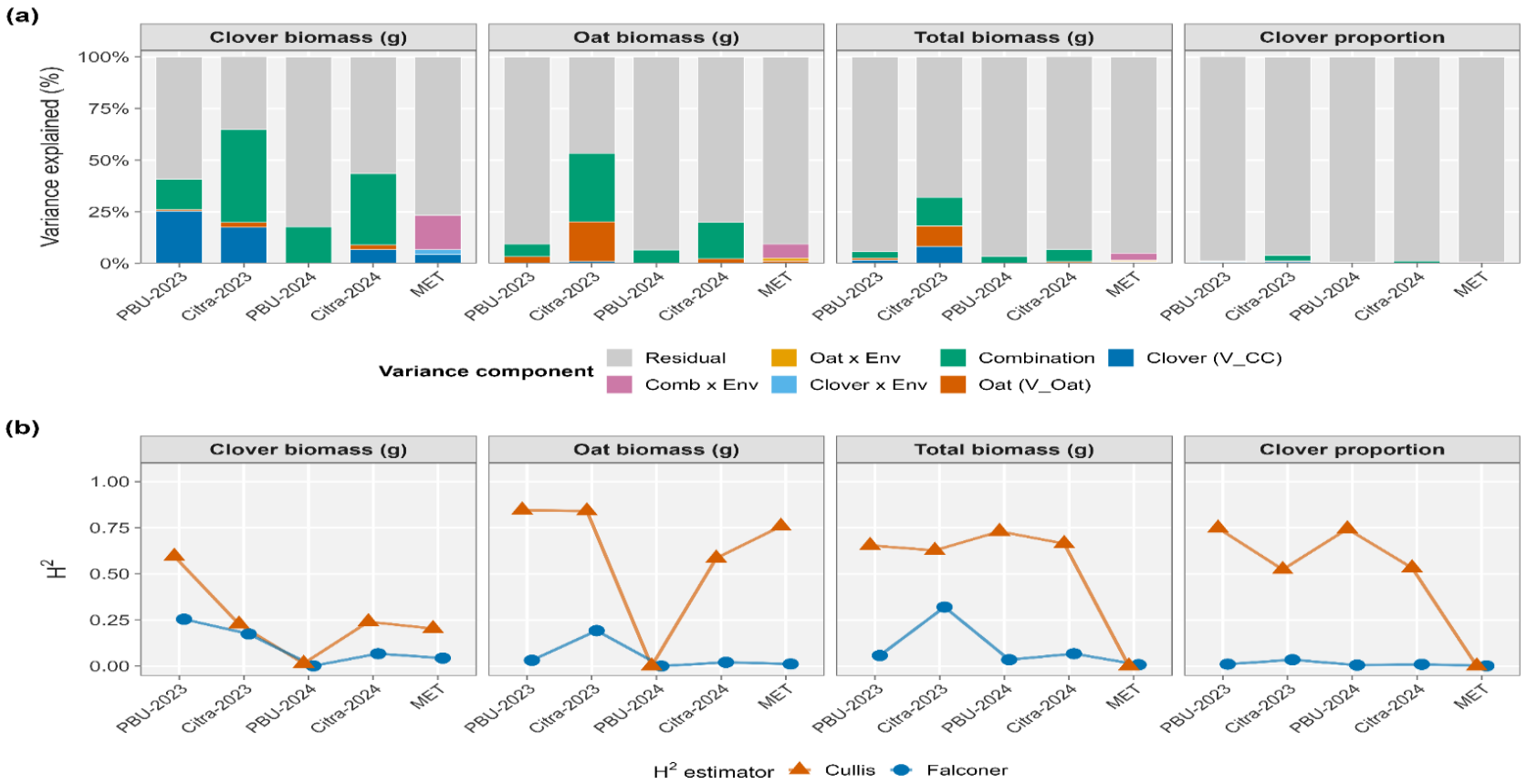

Figure 2.3. Variance component decomposition and broad-sense heritability estimates for clover biomass, oat biomass, total biomass, and clover proportion across environments and the multi-environment trial (MET).

(a) Proportion of phenotypic variance explained by clover, oat, combination, genotype × environment interaction, and residual effects from mixed-model analyses. (b) Broad-sense heritability (H^2) estimated using Falconer- and Cullis-based approaches across environments. Results highlight substantial environmental variation in genetic control and mixture interaction effects across traits and environment.

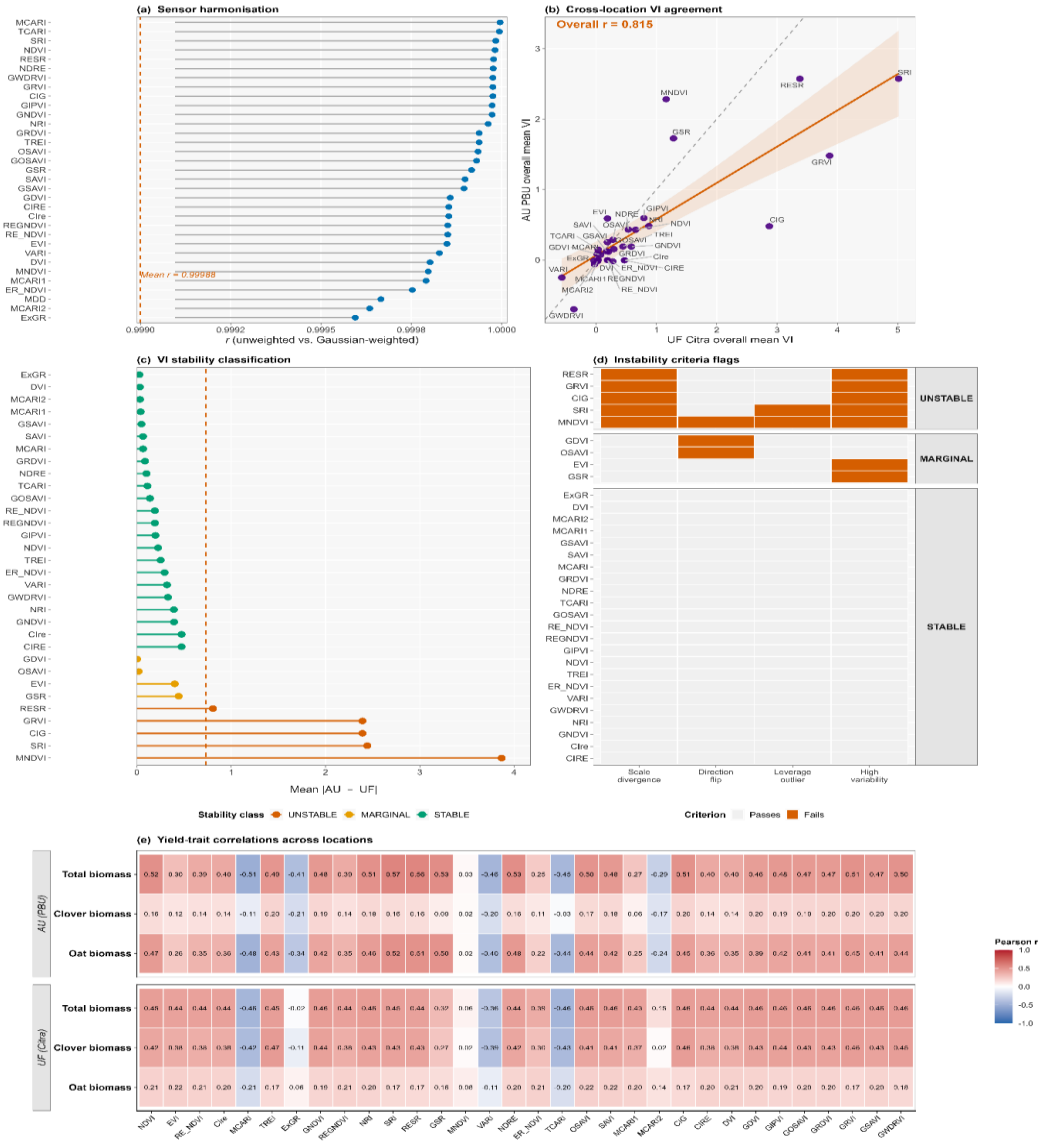

Figure 2.4. Evaluation of cross-platform vegetation index (VI) harmonization and stability between Auburn multispectral and UF-Citra hyperspectral UAV systems.

(a) Agreement between unweighted and Gaussian-weighted spectral resampling approaches for VI derivation. (b) Cross-location agreement of overall VI means between environments. (c) Classification of VI stability based on mean absolute differences between locations. (d) VI instability diagnostics based on scale divergence, direction reversal, leverage outliers, and variability criteria. (e) Pearson correlations between VIs and biomass traits across locations, including total biomass, clover biomass, and oat biomass. Results were used to identify stable and transferable phenomic predictors for downstream genomic–phenomic prediction analyses.

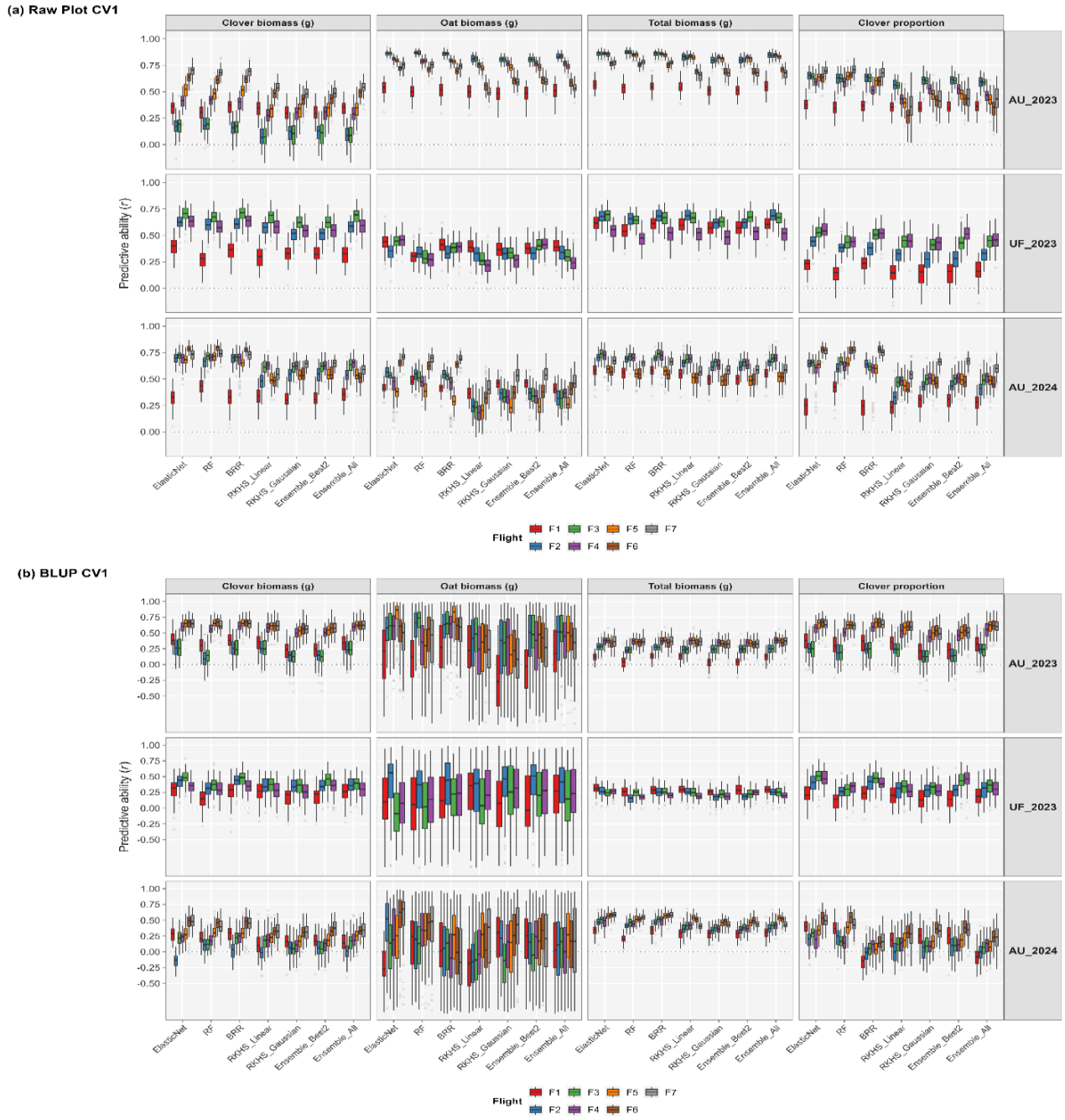

Figure 2.5. Prediction accuracies from within-environment cross-validation (CV1) using plot-level and BLUP-level phenomic prediction models across UAV flights.

Panels represent (a) plot-level CV1 predictions and (b) BLUP-level CV1 predictions for clover biomass, oat biomass, total biomass, and clover proportion across AU_2023, UF_2023, and AU_2024 environments. Colored boxplots correspond to individual UAV flights, while prediction models include Elastic Net, Random Forest (RF), Bayesian Ridge Regression (BRR), Partial Least Squares (PLS), RKHS-linear, RKHS-Gaussian, and ensemble approaches. Predictive ability was measured as the Pearson correlation between observed and predicted values across repeated cross-validation iterations.

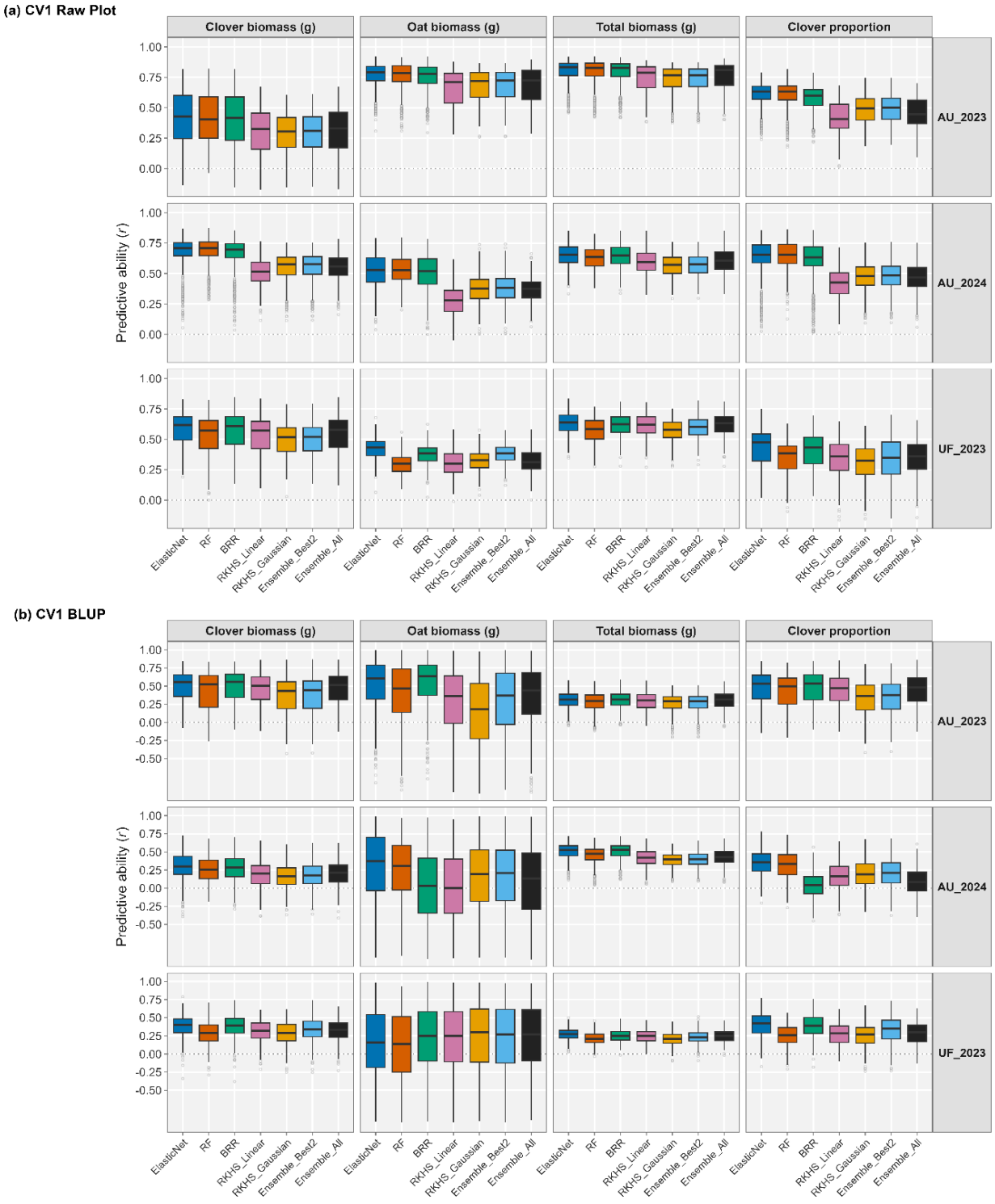

Figure 2.6. Predictive ability of machine learning and kernel-based phenomic prediction models under within-environment cross-validation

(a) raw plot-level data and (b) genotype BLUPs. Raw plots predictions were generally stable and higher.

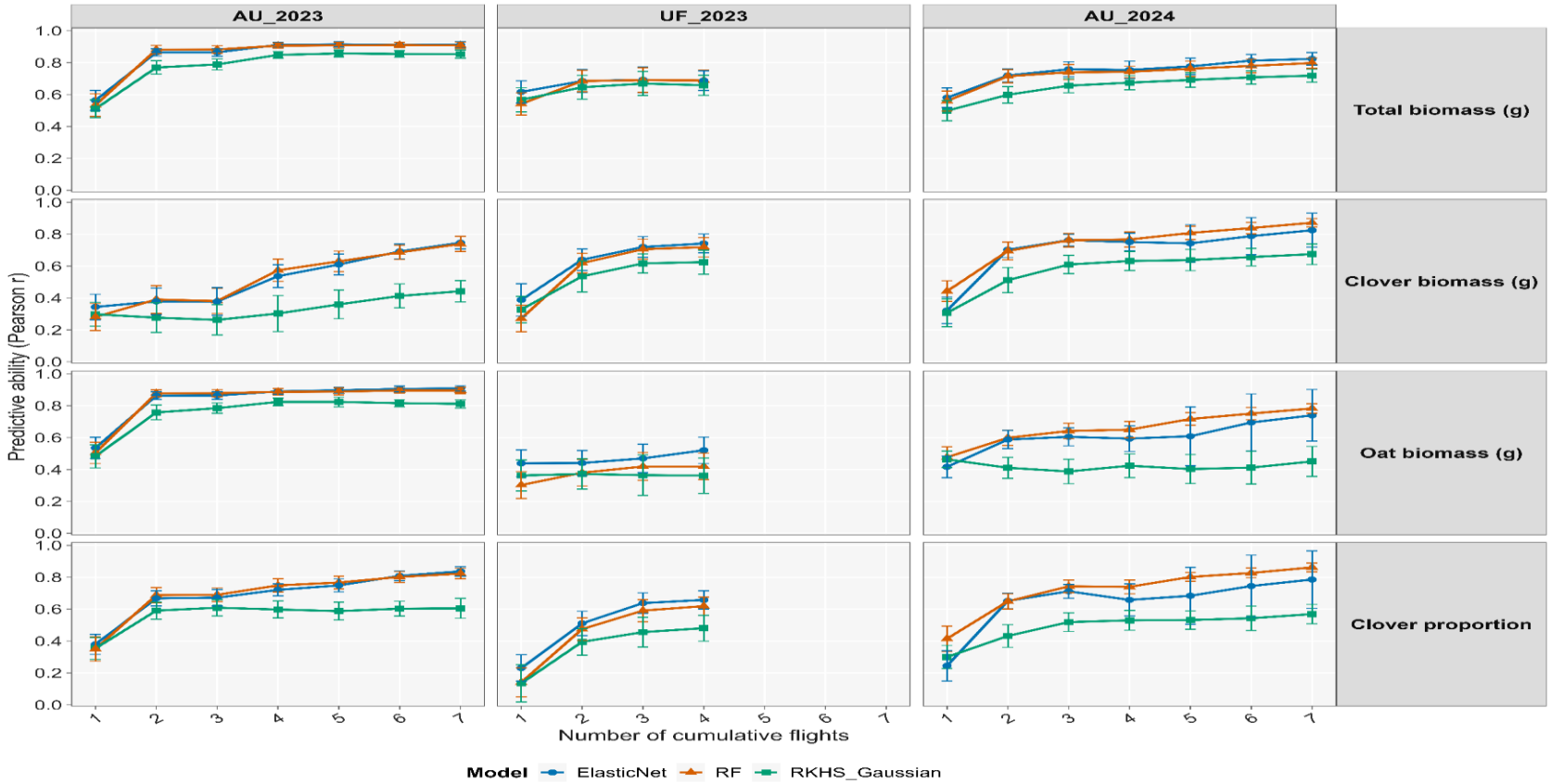

Figure 2.7. Effect of cumulative UAV flight integration on phenomic prediction accuracy across environments and traits.

Prediction accuracy generally improved as information from additional UAV flights was combined, although the magnitude of improvement differed among traits and environments.

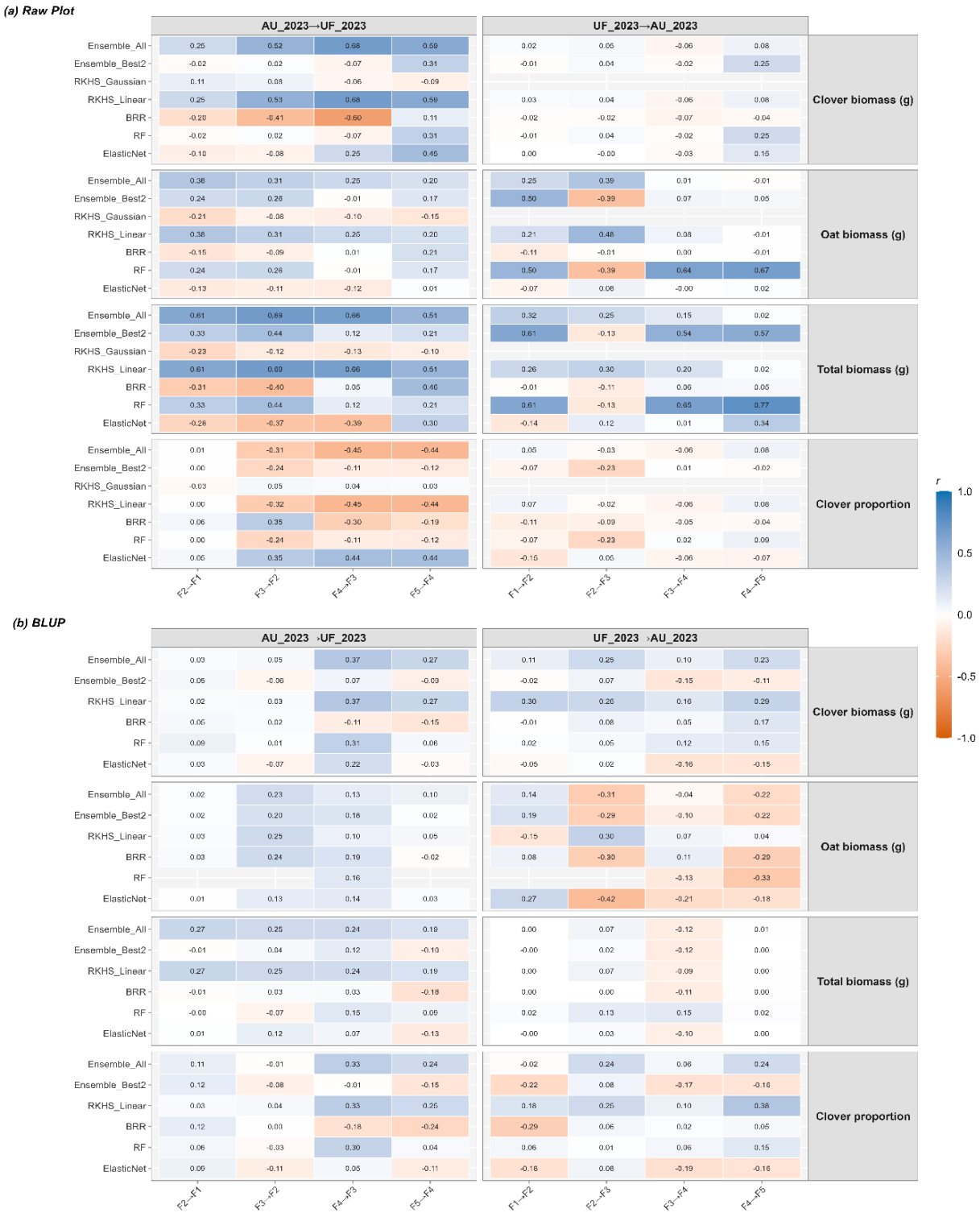

Figure 2.8. Cross-environment transferability of phenomic prediction models between AU_2023 and UF_2023 under reciprocal prediction scenarios.

Cross-location prediction depended strongly on prediction direction, trait, model, and flight pairing.

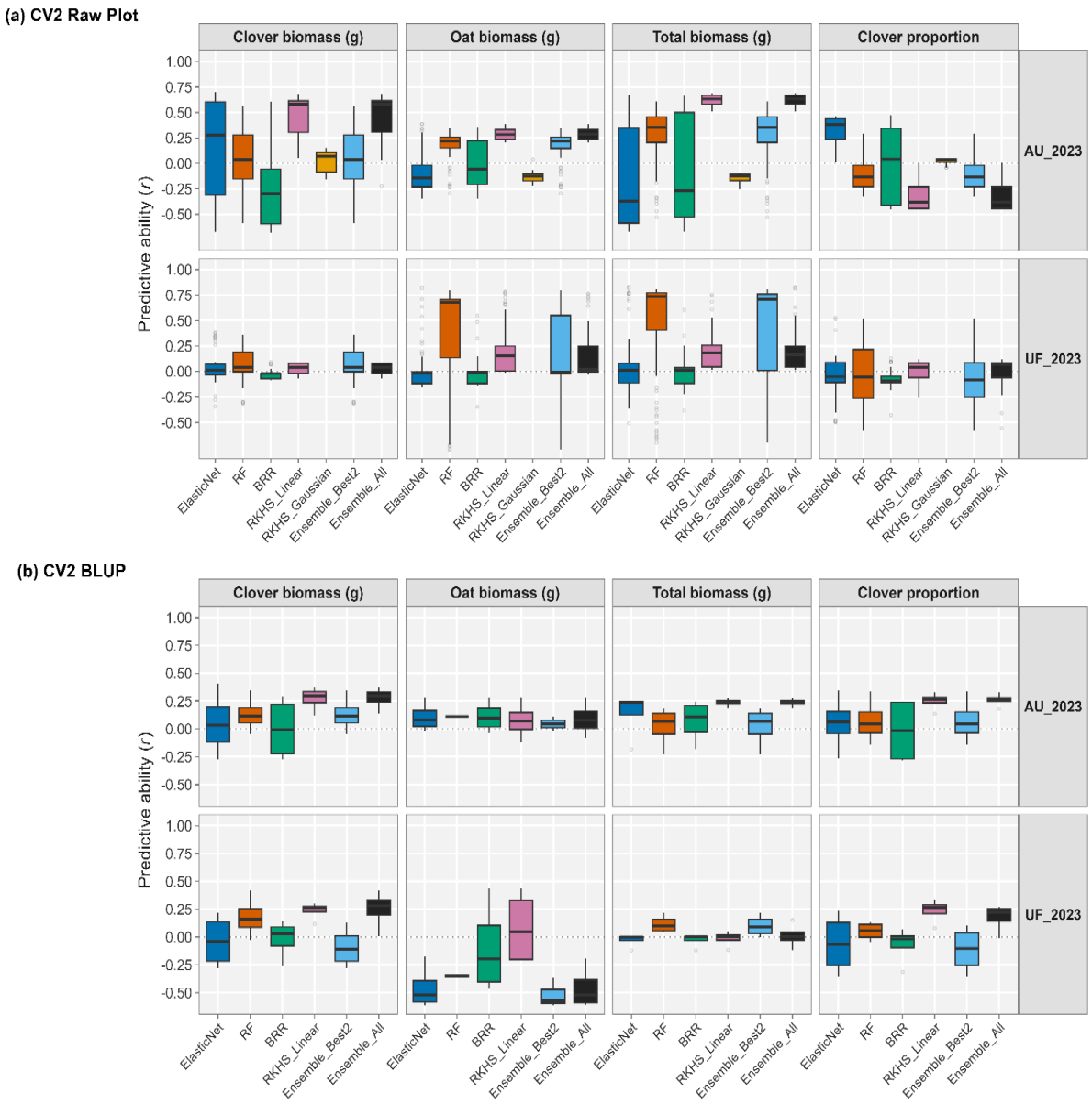

Figure 2.9. Effect of Combined Flight on prediction accuracy for RawPlot and BLUP prediction

(a) raw plot-level data and (b) genotype BLUPs. Predictive ability (r) was evaluated for clover biomass, oat biomass, total biomass, and clover proportion across AU_2023 and UF_2023 environments. Boxplots summarize predictive performance across repeated validation iterations, illustrating differences in model robustness and cross-environment transferability between traits and data level

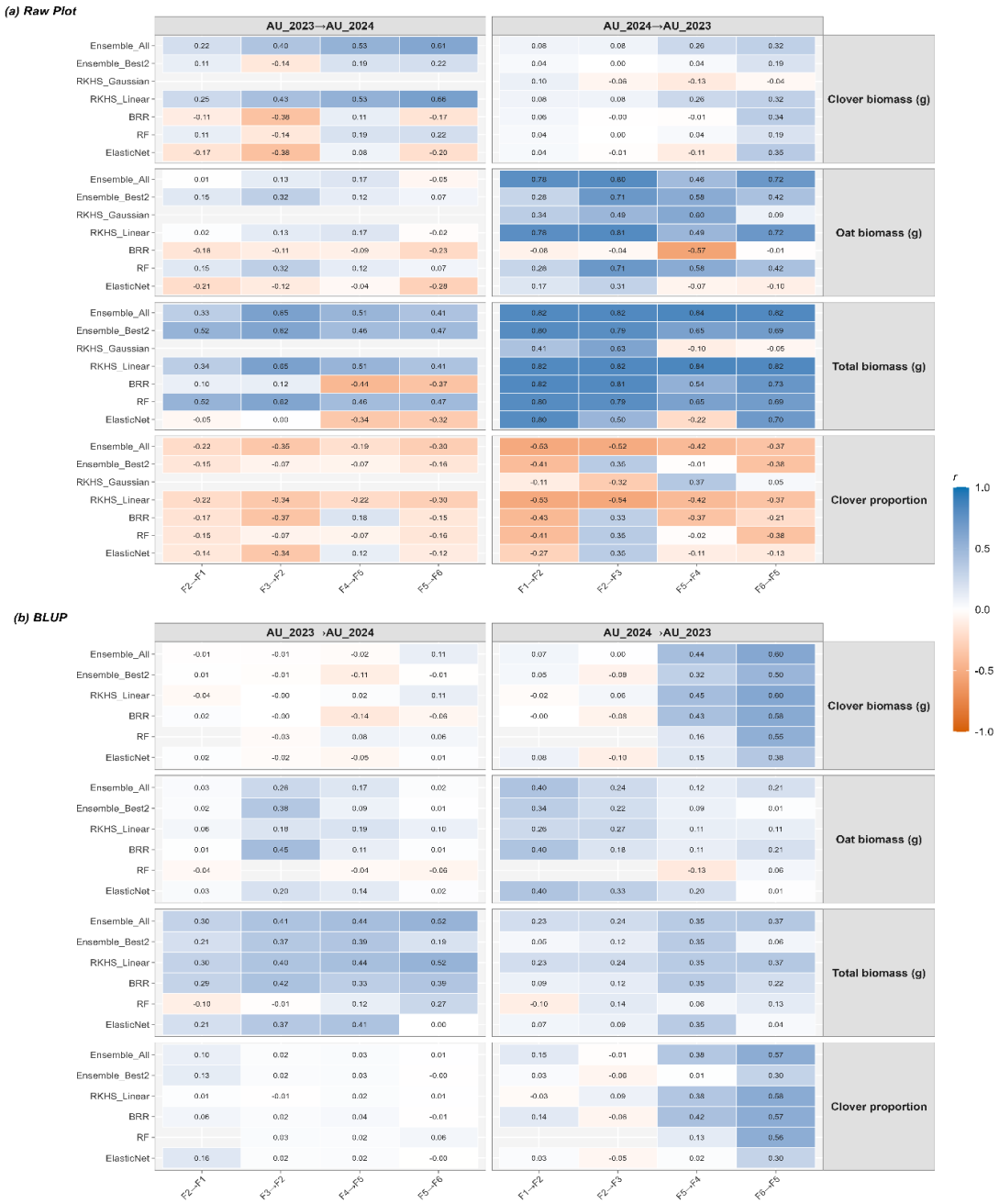

Figure 2.10. Prediction accuracy heatmap for CV3 across years for Auburn-PBU

Heatmaps show predictive ability (r) for (a) raw plot-level and (b) BLUP-level predictions across clover biomass, oat biomass, total biomass, and clover proportion. Prediction models included Elastic Net, Random Forest (RF), Bayesian Ridge Regression (BRR), RKHS-linear, RKHS-Gaussian, and ensemble approaches. Columns represent UAV flight transfer combinations between training and testing years. Positive values indicate successful temporal transferability of phenomic models across years, whereas negative values indicate reduced model stability across growing seasons.

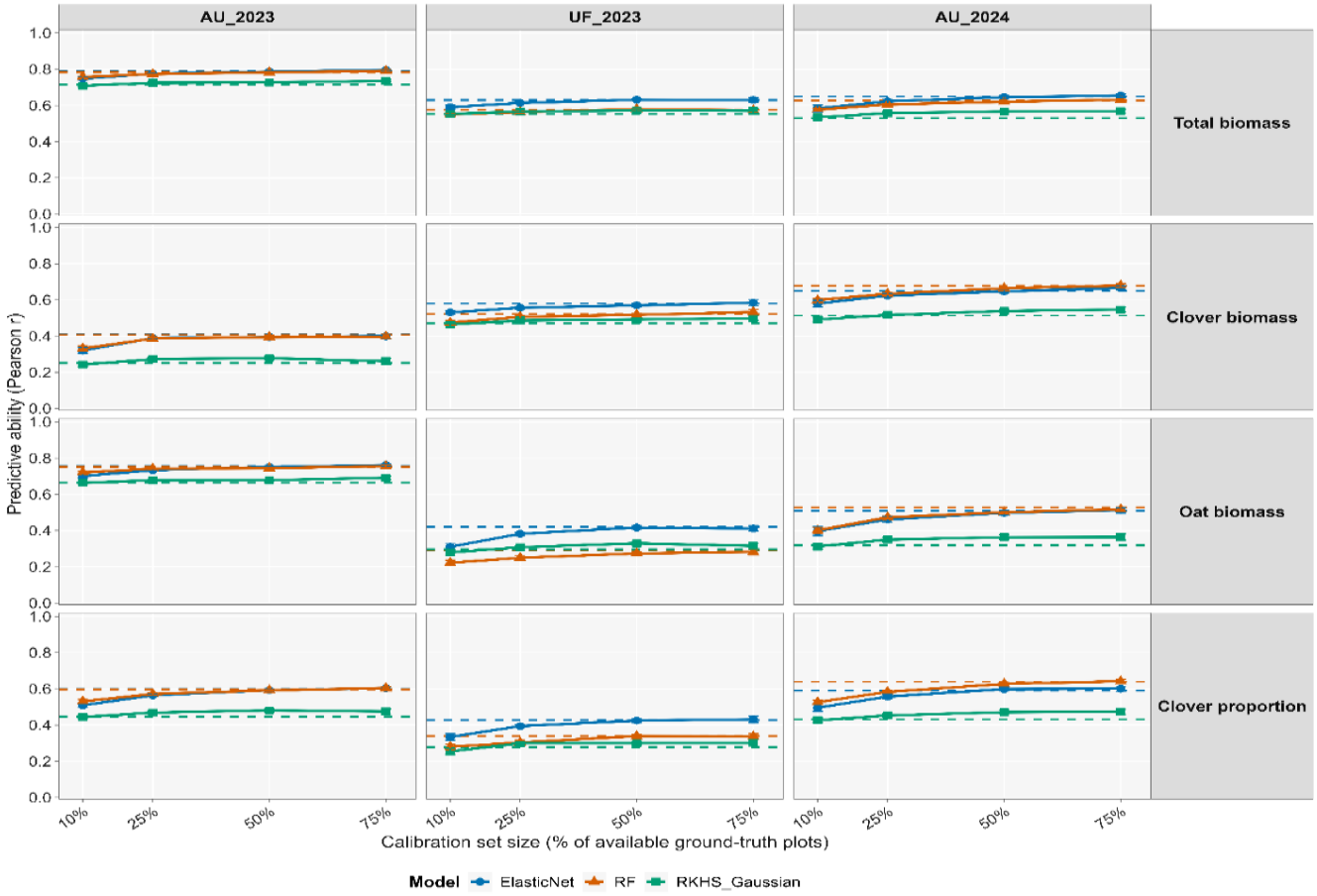

Figure 2.11. Effect of calibration set size on phenomic prediction accuracy across environments and traits.

Predictive ability (r) for total biomass, clover biomass, oat biomass, and clover proportion was evaluated using increasing calibration set proportions (10%, 25%, 50%, and 75% of available ground-truth plots) across AU_2023, UF_2023, and AU_2024 environments. Models included Elastic Net, Random Forest (RF), and Gaussian RKHS. Dashed horizontal lines represent predictive ability obtained using the full calibration dataset. Results illustrate the relationship between training population size and prediction performance for UAV-based phenomic prediction.

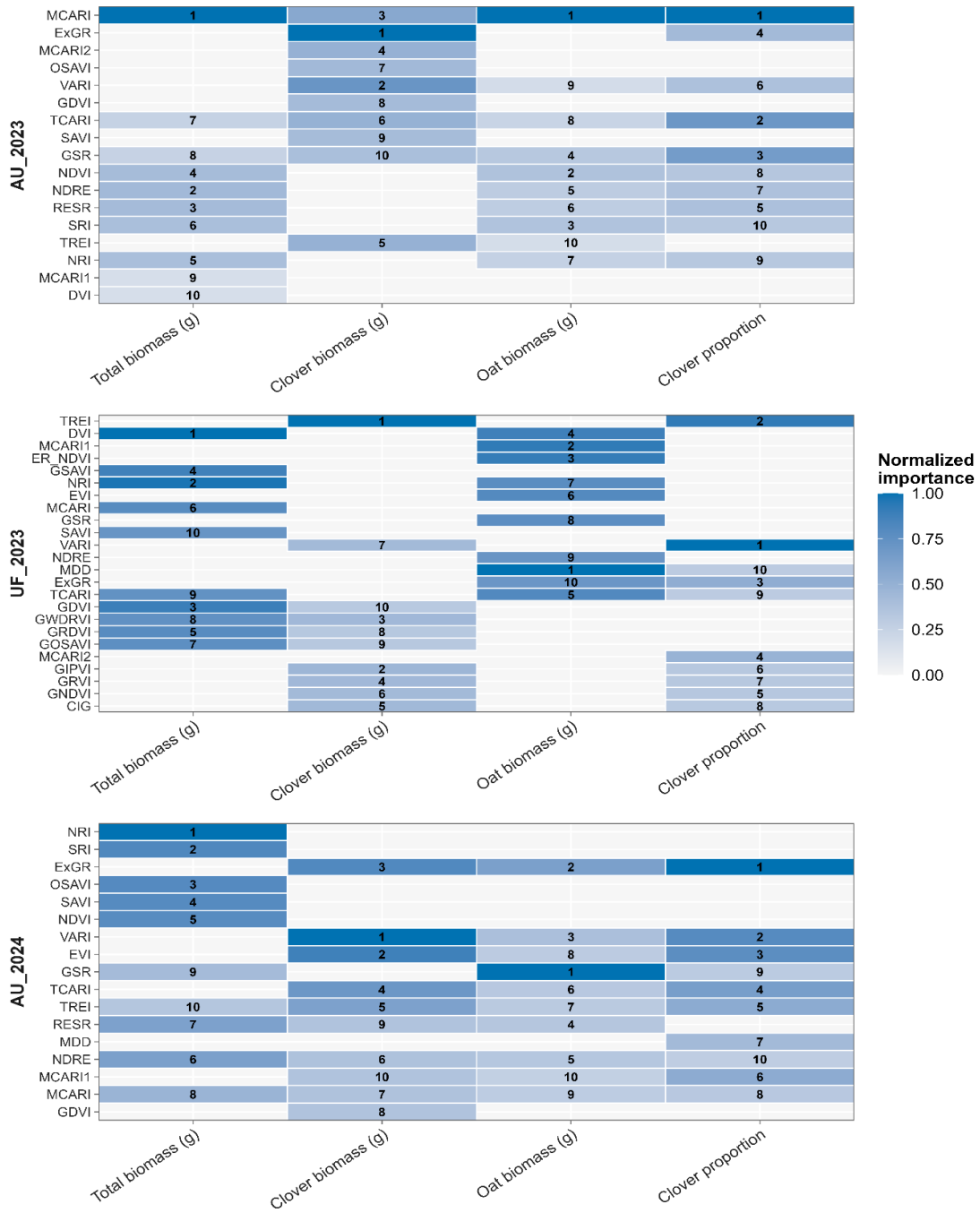

Figure 2.12. Ranked vegetation index (VI) importance across traits and environments based on normalized feature importance from phenomic prediction analyses.

Heatmaps show the top-ranked VIs associated with total biomass, clover biomass, oat biomass, and clover proportion in AU_2023, UF_2023, and AU_2024 environments. Numbers within cells indicate relative VI ranking, while color intensity represents normalized importance values. Results highlight substantial temporal and environmental variation in VI relevance, while also identifying consistently informative spectral indices associated with biomass productivity and mixture composition

Table 2.1. Site-year environments, locations, and data collection details

Environment	Location	Lat (°N)	Lon (°W)	Planting Date	Harvest Date	UAV Spectral Data
AU_2023	Tallassee (PBU)	32.54	85.89	8-Nov-23	8-May-24	Yes
AU_2024	Tallassee (PBU)	32.54	85.89	13-Nov-24	16-Apr-25	Yes
UF_2023	UF Citra Research Unit	29.4	82.17	21-Nov-23	1-May-24	Yes
UF_2024	UF Citra Research Unit	29.4	82.17	20-Nov-24	29-Apr-25	No

AU = Auburn University; UF = University of Florida; PBU = Plant Breeding Unit; UAV = Unmanned Aerial Vehicle; Lat = Latitude; Lon = Longitude. Site-year environments used in this study, including geographic location, planting and harvest dates, and availability of UAV-derived spectral data. Environments are identified by location and year (e.g., AU_2023 = Auburn University, 2023 growing season; UF_2023 = University of Florida Citra, 2023 growing season). UAV spectral data were not collected for UF_2024.

Table 2.2. Summary of experimental design across four site-year environments, including number of clover half-sib families, oat lines, and their factorial combinations.

Location	Year	No. plots	Cc HS families	Oat lines	Unique comb.	Rep. comb.	N Unrep.	% Rep.
Citra	2023-24	600	162	26	560	40	520	6.7
PBU	2023-24	600	177	26	570	30	540	5
Citra	2024-25	600	206	25	562	38	524	6.3
PBU	2024-25	600	206	25	570	30	540	5

Cc HS families = crimson clover half-sib maternal families; Unique comb. = total number of unique clover–oat genotype combinations evaluated; Rep comb. = number of replicated combinations; N unrep. = number of unreplicated combinations; % Rep. = percentage of combinations with replication. An incomplete factorial design s following Haug et al. (2021), in which a subset of clover families was combined with a subset of oat lines.

Table 2.3. Descriptive statistics of yield traits across four environments.

Trait	Environment	Mean	Median	SD	CV (%)	Min	Max
Clover biomass (g)	PBU-2023	61.91	55.50	40.54	65.5	0.70	179.80
Clover biomass (g)	Citra-2023	49.62	40.00	39.31	79.2	2.00	172.00
Clover biomass (g)	PBU-2024	144.00	90.85	122.45	85.0	17.85	475.05
Clover biomass (g)	Citra-2024	26.89	21.79	20.55	76.4	0.28	87.30
Clover proportion	PBU-2023	0.28	0.24	0.19	67.3	0.00	0.77
Clover proportion	Citra-2023	0.41	0.38	0.23	57.0	0.02	0.99
Clover proportion	PBU-2024	0.28	0.20	0.21	77.8	0.03	0.84
Clover proportion	Citra-2024	0.17	0.15	0.13	76.5	0.00	0.57
Oat biomass (g)	PBU-2023	208.24	142.10	150.92	72.5	4.70	650.60
Oat biomass (g)	Citra-2023	64.38	58.00	38.43	59.7	2.00	176.00
Oat biomass (g)	PBU-2024	389.66	383.05	150.84	38.7	69.90	817.65
Oat biomass (g)	Citra-2024	129.61	126.28	38.03	29.3	26.28	230.28
Total biomass (g)	PBU-2023	277.61	232.00	159.30	57.4	44.40	729.30
Total biomass (g)	Citra-2023	125.19	116.00	63.35	50.6	10.00	308.00
Total biomass (g)	PBU-2024	544.25	536.85	141.10	25.9	203.75	942.45
Total biomass (g)	Citra-2024	156.25	152.60	32.62	20.9	78.56	246.56

Table 2.4. Variance component partitioning, broad-sense heritability, and likelihood ratio test significance for clover-oat mixture traits across four environments and the multi-environment trial (MET).

		Variance explained (%)			GxE variance (%)				Heritability	LRT significance				
Environment	Trait	% Clover	% Oat	% Combination	% Clover x Env	% Oat x Env	% Comb x Env	% Residual	H2 (Cullis)	Clover	Oat	Combination	Clover x Env	Oat x Env	Comb x Env
PBU-23	Clover (g)	25.4	0.7	14.7	--	--	--	59.2	0.595	***	ns	***			
Citra-23	Clover (g)	17.4	2.5	45	--	--	--	35.2	0.227	**	ns	ns			
PBU-24	Clover (g)	0.1	0	17.6	--	--	--	82.3	0.014	ns	ns	***			
Citra-24	Clover (g)	6.7	2.2	34.5	--	--	--	56.6	0.240	*	*	***			
MET	Clover (g)	4.3	0	0	2.3	0	16.6	76.8	0.203	***	ns	ns	*	ns	***
PBU-23	Clover proportion	0.7	0.2	0.4	--	--	--	98.8	0.748	***	***	***			
Citra-23	Clover proportion	0.8	0.5	2.6	--	--	--	96	0.523	***	***	***			
PBU-24	Clover proportion	0	0	0.5	--	--	--	99.5	0.744	ns	ns	***			
Citra-24	Clover proportion	0.2	0.1	0.8	--	--	--	98.9	0.532	*	***	***			
MET	Clover proportion	0.1	0	0	0.1	0	0.5	99.2	0.000	**	*	ns	**	**	***

		Variance explained (%)			GxE variance (%)				Heritability	LRT significance					
Environment	Trait	% Clover	% Oat	% Combination	% Clover x Env	% Oat x Env	% Comb x Env	% Residual	H2 (Cullis)	Clover	Oat	Combination	Clover x Env	Oat x Env	Comb x Env
PBU-23	Oat (g)	0.2	3.1	6	--	--	--	90.7	0.846	ns	***	***			
Citra-23	Oat (g)	1	19.2	33	--	--	--	46.8	0.841	ns	***	***			
PBU-24	Oat (g)	0	0	6.5	--	--	--	93.5	0.000	ns	ns	***			
Citra-24	Oat (g)	0.3	2	17.6	--	--	--	80.1	0.585	ns	***	***			
MET	Oat (g)	0	1.1	0	0.1	1.5	6.6	90.6	0.758	ns	**	ns	ns	***	***
PBU-23	Total biomass (g)	1.6	1	3.1	--	--	--	94.3	0.654	***	***	***			
Citra-23	Total biomass (g)	8.2	9.9	13.9	--	--	--	68	0.627	**	***	ns			
PBU-24	Total biomass (g)	0.1	0	3.3	--	--	--	96.6	0.730	ns	ns	***			
Citra-24	Total biomass (g)	0	0.8	6	--	--	--	93.3	0.664	ns	***	***			

		Variance explained (%)			GxE variance (%)				Heritability	LRT significance					
Environment	Trait	% Clover	% Oat	% Combination	% Clover x Env	% Oat x Env	% Comb x Env	% Residual	H2 (Cullis)	Clover	Oat	Combination	Clover x Env	Oat x Env	Comb x Env
MET	Total biomass (g)	0.5	0.3	0	0.3	0.4	3.5	95	0.000	*	*	ns	ns	***	***

Chapter 3 Breeding Cassava for Intercropping: Mixing Ability and the Efficiency of Indirect Selection in a Cassava–Cowpea System

Abstract

Intercropping dominates smallholder cassava production in sub-Saharan Africa, yet breeding programs evaluate genotypes exclusively under monoculture. Despite consistent system-level yield advantages, cassava yield is reduced 17–51% under intercropping, indicating that genetic selection will be needed to reduce this competitive disadvantage. The quantitative genetic foundations for intercrop breeding remain uncharacterized for tropical root crop systems. 120 cassava clones were evaluated under monoculture and intercropping with two contrasting cowpea testers across two years at IITA Ibadan, Nigeria. Significant genetic variance was detected for fresh root weight, harvest index, and dry matter content under both systems, with moderate-to-high intercrop heritability (H^2 = 0.50–0.75). Genotype × management interaction was non-significant and genetic correlations between systems were near-unity (rg = 0.92-0.97) yet realized BLUP correlations were lower and selection efficiency was 26–44% at 10% intensity, confirming that high genetic correlation does not guarantee effective indirect selection. General mixing ability dominated over specific mixing ability, which was negligible, with producer effects explaining 20–47% of intercrop variance. Two contrasting cowpea testers produced interchangeable cassava rankings. Multi-group structural equation modelling showed no detectable difference in yield-formation pathways between systems (p = 0.910), with root size and root number the dominant determinants in both. A z-score standardization framework was developed to address yield-scale asymmetry between component crops. These results support a staged

breeding strategy: monoculture selection at early stages complemented by single-tester intercrop evaluation at advanced stages, a practical and minimal adaptation of existing cassava breeding pipelines.

3.1 Introduction

Intercropping, the cultivation of two or more crops with spatial or temporal overlap, accounts for 30–50% of global crop production (Anderson et al., 2013; Weerarathne et al., 2016; Parmar et al., 2017) and has re-emerged as a strategy for sustainable intensification. Meta-analyses report 22–30% yield advantages over sole cropping, with improved yield stability, resource capture, and land-use efficiency (Himmelstein et al., 2017; Martin-Guay et al., 2018; Maitra et al., 2021; Moore et al., 2022; Gmakouba et al., 2024; Adam et al., 2025).

In sub-Saharan Africa (SSA), where most production is rainfed and 70–83% of smallholder farmers intercrop, the practice is both the dominant production system and a climate-resilient strategy (Anderson et al., 2013; Weerarathne et al., 2016; Parmar et al., 2017; Gmakouba et al., 2024). In SSA, meta-analyses report an average land equivalent ratio (LER; the relative land area required under monocropping to produce the same yield as intercropping) of approximately 1.45, with root–legume systems often outperforming cereal intercrops under moisture variability and other stresses (Himmelstein et al., 2017; Adam et al., 2025). Cassava (Manihot esculenta Crantz), the most important tropical root crop, is often grown in association with other crops, and cassava–legume systems represent one of the most promising climate-resilient intercrops in SSA (Adam et al., 2025).

However, despite the system-level advantages, cassava yield is frequently reduced by 17–51% when intercropped with legumes (Dapaah et al., 2003; Nyi et al., 2014; Hidoto and Loha, 2013; Mwebaze et al., 2024). This contrast between high system productivity and reduced cassava yield suggests that improving intercrop performance may require breeding to reduce cassava's competitive disadvantage (Annicchiarico et al., 2021). However, cassava breeding programs have historically evaluated and selected genotypes almost exclusively under monoculture conditions. This structural mismatch between the breeding evaluation environment and the farmer production system raises a fundamental question: does monoculture selection adequately capture genetic merit for intercrop performance?

The quantitative genetic foundations of breeding in mixtures were formalized by Wright (1985), who partitioned mixture yield into direct (producer, Pr) and interaction (associate, As) effects. In this framework, a genotype's performance in a mixture reflects both its intrinsic yield potential and its influence on its companion species (Haug et al., 2021, 2023). The sum of Pr and As effects corresponds to a genotype's general mixing ability (GMA); the additive genetic effects governing broad compatibility across partners, while specific mixing ability (SMA), captures the non-additive interaction effects specific to particular genotype combinations (Wright, 1985; Forst, 2018; Sampoux et al., 2020). The relative magnitude of GMA and SMA variance therefore has direct implications for breeding strategy: when GMA predominates and SMA is negligible, broadly compatible genotypes can be improved through parallel selection schemes, whereas substantial SMA variance requires partner-specific testing and more complex breeding designs (Wright, 1985; Sampoux et al., 2020).

Results from temperate intercrops (Sampoux et al. 2020; Hauggaard-Nielsen et al., 2021; Annicchiarico et al., 2021; Moore et al., 2022; Haug et al., 2023) suggests that the efficiency of selection in pure stands depends critically on the correlation structure between direct and associate effects in mixtures. Selection under monoculture conditions can produce a correlated response in mixture performance only when pure stand performance is positively correlated with both direct and associate effects. When direct and associate effects are negatively correlated, an interaction frequently observed in competitive crop mixtures, selection in pure stands becomes substantially less efficient than selection schemes explicitly targeting mixture performance, such as GMA. Therefore, breeding strategies based solely on monoculture evaluation may fail to capture key genetic determinants of intercrop performance. In temperate pea–barley intercrops, GMA explained a larger proportion of variation in mixture yield than SMA, indicating that additive general compatibility can drive genetic gain (Hauggaard-Nielsen et al., 2021; Haug et al., 2023). Similarly, Annicchiarico et al. (2021) reported that indirect selection based on monoculture performance achieved 50–60% of the efficiency of direct selection in mixtures, depending on the genetic correlation between monoculture and intercrop performance. However, high genetic correlation does not necessarily guarantee effective indirect selection. In common bean–maize systems, Zimmermann (1996) observed moderate to high correlations between sole and intercrop yield, yet selection coincidence frequently fell below 50%, reflecting genotype re-ranking and genotype × cropping system interaction. These findings indicate that variance-based parameters and realized selection overlap must be evaluated jointly to determine

whether monoculture breeding reliably predicts intercrop performance and whether intercrop adaptation demands a different cassava ideotype completely.

Notwithstanding these advances, quantitative genetic analyses of intercropping have focused primarily on temperate systems, while tropical intercrops particularly cassava-based systems remain uncharacterized from a breeding perspective. This gap is consequential because cassava differs fundamentally in growth habit, phenology, and biomass allocation, and is typically intercropped with short-duration crops such as cowpea (Vigna unguiculata). Cassava–cowpea systems also exhibit pronounced yield-scale asymmetry: cassava root yield per plot is typically orders of magnitude larger than cowpea grain yield, even when expressed in the same units. Such magnitude differences create strong imbalances between component crops, where naïve aggregation or unit conversion can distort variance partitioning and bias inference of mixing ability and producer effects. Wright (1985) cautioned that simple aggregation of component yields may obscure underlying biological interactions. In scale-asymmetric intercrops, inappropriate definition of the response variable may therefore collapse mixture analysis into effective single-species selection, inflating the contribution of one species while suppressing the other and altering genotype rankings. Careful specification of the genetic response variable is thus essential for meaningful estimation of GMA, SMA, and producer–associate effects in cassava–cowpea systems. Also, it remains unknown whether cassava yield formation pathways are structurally invariant between monoculture and intercrop systems, which determines whether trait yield relationships inferred under monoculture remain valid under intercropping.

A major operational constraint in intercrop breeding is the intractable number of species combinations (Annicchiarico and Piano 1994; Annicchiarico et al., 2019; Haug et al., 2021, 2023). To reduce this, a limited set of companion genotypes termed testers, by analogy to hybrid breeding can be used to reveal the mixing ability of the focal crop, assuming that genotype rankings remain stable across testers (Moutier et al., 2022; Haug et al., 2023). This approach is further supported by evidence that general combining ability often exceeds specific combining ability in legume intercrops (Holland and Brummer, 1999; Annicchiarico and Piano 1994; Annicchiarico et al., 2019; Annicchiarico et al., 2021). From a breeding perspective, the influence of tester choice on selection decisions remains untested in cassava-based systems.

Intercrop breeding requires evidence that genetic improvement is achievable under mixed cropping. This depends on the presence of exploitable genetic variation under intercropping, the extent of genotype × management interactions causing genotype re-ranking between monoculture and intercrop systems, and the ability of monoculture selection to predict mixture performance (Moore et al., 2022). For cassava-based intercrops, these questions remain largely unexplored.

The objectives of this study were: (1) quantify genetic variation for cassava performance under monoculture and intercrop conditions and assess genotype × cropping system interaction; (2) evaluate the extent to which monoculture performance predicts intercrop performance by estimating genetic correlations, genotype re-ranking, and realized selection efficiency between systems; (3) partition intercrop performance into genetic components of mixing ability by estimating producer and associate effects and evaluating the relative contributions of general mixing ability (GMA) and specific

mixing ability (SMA); and (4) examine whether cassava yield-formation pathways differ between monoculture and intercrop systems using multi-group structural equation modelling.

3.2 Materials and methods

3.2.1 Field trial, planting arrangement and experimental design

Cassava–cowpea intercropping trials were conducted over two consecutive years at the International Institute of Tropical Agriculture (IITA), Ibadan, Nigeria (7°24′N, 3°54′E), from September 2023 to September 2025. The experiment followed a row–column spatial design with two replicates per year, with monoculture and intercrop treatments randomized within replicates. Plots measured 5 × 3 m (15 m²) with two rows. Cassava was planted at a spacing of 1.0 × 0.8 m. In intercrops, cowpea was interplanted within cassava rows at 0.25 m spacing, whereas cowpea monocultures were planted at 1.0 × 0.25 m spacing. The trial followed an additive intercropping design in which cassava was maintained at monoculture density, and cowpea was introduced within cassava rows, a configuration commonly used to evaluate intercrop productivity under farmer-relevant conditions. Each year, 362 treatments were evaluated with two replicates, resulting in a total of 1,448 plots across the two years. Standard agronomic practices for cowpea and cassava management were followed as described in Popoola et al. (2024) and Rabbi et al. (2022), respectively.

3.2.2 Cassava genotypes and Cowpea tester selection

120 cassava genotypes were selected from the IITA breeding population archived in Cassavabase (www.cassavabase.org). These genotypes originated from

Advanced Yield Trials (Rabbi et al., 2022). Multi-environment mixed-model analyses followed by k-means clustering were used to select representative clones capturing the genetic diversity of the breeding population. Two farmer-preferred cowpea varieties with contrasting maturity and architecture traits linked to competitive ability (Annicchiarico and Piano 1994; Wang et al., 2004; 2006) were selected: Oloyin, a late-maturing spreading growth habit, and IT08K-150-12 (SAMPEA 19), an elite IITA line characterized by early maturity and an erect growth habit (Omoigui et al., 2018).

3.2.3 Trait measurement

All cassava plots were harvested 12 months after planting, while the cowpea plots were harvested at maturity for each plot tester. For cassava, fresh root yield (kg plot^{-1}), root dry matter content (DMC), harvest index (HI), and the number of harvested plants were recorded. For cowpea, grain yield (g plot^{-1}) and the number of harvested plants per plot were recorded. Additional cassava traits were measured for structural equation modelling of yield formation, including sprout count (1 MAP), seedling vigor (3 MAP), shoot weight, root number, root rot incidence, root size, and root shape.

3.2.4 Statistical analysis

All statistical analyses were conducted in R using ASReml-R v4.2.0.392 for fitting linear mixed models, with variance components estimated by residual maximum likelihood (REML) (Butler et al., 2018). Analyses were performed both across years and within individual years. Field heterogeneity was modeled using a separable first-order autoregressive (AR1 × AR1) residual structure for row and column positions. Monoculture and intercrop datasets were initially analyzed separately to estimate system-specific genetic parameters.

3.2.5 Mixed models for monoculture and intercrop

For monoculture plots across years, the following linear mixed model was fitted:

$$y_{ijk} = \mu + Y_i + \beta_1 C_{ijk} + g_j + (gY)_{ij} + r_{k(i)} + \varepsilon_{ijk} \quad (3.1)$$

where $y_{ijk}$is the plot observation, μ the overall mean, $Y_i$the fixed effect of year, $C_{ijk}$the number of harvested cassava plants (centered within year), $g_j$the random clone effect $\left(g_j \sim N(0, \sigma_G^2)\right)$, $(gY)_{ij}$the clone × year interaction $(\sim N(0, \sigma_{GY}^2))$, $r_{k(i)}$the random replication within year, and $\varepsilon_{ijk}$the spatially correlated residual $(\sim N(0, \sigma_e^2))$. For intercrop analyses, the model included both cassava and cowpea plant density covariates:

$$y_{ijk} = \mu + Y_i + \beta_1 C_{ijk} + \beta_2 P_{ijk} + g_j + (gY)_{ij} + r_{k(i)} + \varepsilon_{ijk} \quad (3.2)$$

where P_{ijk}represents the number of harvested cowpea plants (centered within year), other parameters are similar to model 1. Within-year analyses excluded year and clone × year terms.

Entry-mean broad-sense heritability across years was estimated from the variance of Model 1 and 2 as: $H^2 = \frac{\sigma_G^2}{\sigma_G^2 + \frac{\sigma_{GY}^2}{n_Y} + \frac{\sigma_e^2}{r n_Y}}$ (3.3)

where $n_Y$is the number of years (2) and $r$is the number of replications per year (2). Variance components were estimated separately from monoculture and intercrop models to obtain system-specific heritabilities.

3.2.6 Cassava genotype × management interaction

To test whether clone performance differed between monoculture and intercrop systems, a combined mixed model was fitted to the full dataset across years:

$$y_{ijkl} = \mu + Y_i + M_j + (YM)_{ij} + \beta_1 C_{ijkl} + \beta_2 P_{ijkl} + g_k + (gY)_{ik} + (gM)_{jk} + (gYM)_{ijk} + r_{l(ij)} + \varepsilon_{ijkl} \quad (3.4)$$

where $y_{ijkl}$is the observation for the k-th clone in the l-th replication of the i-th year under the j-th management system; $\mu$is the overall mean; $Y_i$is the fixed year effect; $M_j$is the fixed management effect (monoculture or intercrop); and $(YM)_{ij}$is the year × management interaction. Covariates $C_{ijkl}$and P_{ijkl}represent the number of harvested cassava and cowpea plants per plot (centered within year). Random effects included clone $g_k \sim N(0, \sigma_G^2)$, clone × year $(gY)_{ik} \sim N(0, \sigma_{GY}^2)$, clone × management $(gM)_{jk} \sim N(0, \sigma_{GM}^2)$, and clone × year × management $(gYM)_{ijk} \sim N(0, \sigma_{GYM}^2)$. Replication was fitted as a random effect nested within year and management $r_{l(ij)}$, and ε_{ijkl}represents the spatially correlated residual. For within-year analyses, year-related terms (Y_i, gY_{ik}, and gYM_{ijk}) were omitted. Variance components σ_{GM}^2, σ_{GY}^2, and σ_{GYM}^2were tested using likelihood ratio tests comparing the full model with reduced models excluding each term.

3.2.7 Genetic correlation between monoculture and intercrop

Genetic correlation between monoculture and intercrop performance was estimated using a bivariate mixed model in which plot-level observations from both systems were stacked into a single response vector, with system (monoculture vs intercrop) treated as a two-level trait factor.

The model was: $y = X\beta + Z_1 g + Z_2 gY + Z_3 r + \varepsilon$ (3.5)

where fixed effects (Xβ) included system, system×year, system×cowpea partner, and system×stand count covariate (nohav, centred within system×year). Random effects comprised: clone main effects across systems modelled with a heterogeneous correlation structure, g ~ N(0, Σ_g ⊗ I), where Σ_g = diag(σ²_M, σ²_I) with bounded correlation parameter r_g ∈ (−1, 1); clone×year interaction within system, gY ~ N(0, D_gY ⊗ I), where D_gY is diagonal; and replicate within system×year, r. Residual spatial variation was modelled separately for each system×year combination using independent first-order autoregressive processes in both row and column directions (AR1×AR1), with field coordinates offset between systems to prevent aliasing. The model was fitted in ASReml-R v4.2 (Butler et al., 2023) using the corgh() variance structure. The genetic correlation between systems was defined as:

$$r_g = \frac{\sigma_{g(M,I)}}{\sqrt{\sigma^2_{g(M)}\sigma^2_{g(I)}}} \qquad (3.6)$$

and estimated directly as the bounded correlation parameter. The hypothesis H0: r_g = 1 (no genetic differentiation between systems) was tested using a likelihood ratio test comparing the corh model against a constrained model with r_g fixed at unity via corgh(), with the test statistic asymptotically distributed as χ²(df=1) (Self and Liang, 1987).

In addition to the bivariate genetic correlation, Pearson and Spearman correlations between clone BLUPs from monoculture and intercrop models 1 and 2 were also calculated. Selection overlap among top-ranked clones (5%, 10%, and 20%) was quantified to evaluate agreement in selection decisions.

3.2.8 Tester comparison

For tester-specific analyses, the intercrop dataset was partitioned by cowpea tester, and the following linear mixed model was fitted:

$$y_{ijkl} = \mu + Y_i + \beta C_{ijkl} + g_k + (gY)_{ik} + r_{l(i)} + \varepsilon_{ijkl} \qquad (7)$$

where C_{ijkl} is the number of harvested cassava plants (NOHAV), centered within year; $g_k \sim N(0, \sigma_G^2)$, $(gY)_{ik} \sim N(0, \sigma_{GY}^2)$, and $r_{l(i)}$ is the replication effect within a year. Residuals were modeled using a spatial AR1 × AR1 structure within each year.

Tester mean differences were assessed using Wald F-tests, and genotype × tester interaction was tested by comparing models with and without the clone × tester term using likelihood ratio tests with a 0.5χ² boundary correction. Genetic correlations between testers were estimated using bivariate mixed models, and clone BLUPs were compared using Pearson and Spearman correlations and Jaccard overlap among top-ranked clones. Broad-sense heritability and expected selection gain were estimated separately for each tester.

3.2.9 Selection efficiency

Selection efficiency between systems was evaluated following Zimmermann (1996):

$$Se\% = \frac{Y-A}{X-A} \times 100 \qquad (3.8)$$

where X is the number of selected clones at a given selection intensity, Y is the number of clones common to both systems, and A is the expected overlap by chance.

3.2.10 Structural equation modelling

Structural equation models (SEM) were fitted to standardized clone BLUPs derived from the spatial mixed models using the lavaan package in R (Rosseel, 2012). Multi-group SEM was used to quantify direct and indirect relationships among cassava yield components and to test whether yield-formation pathways differed between monoculture and intercrop systems. Model fit was evaluated using the comparative fit index (CFI), standardized root mean square residual (SRMR), and root mean square error of approximation (RMSEA).

3.2.11 Yield metric evaluation and GMA stability

Because cassava fresh root yield (kg) and cowpea grain yield (g) differ in scale and economic value, six alternative metrics were used to quantify intercrop productivity: raw yield sums, unit-consistent sums, economic weighting, standardized z-scores, principal component scores, and partial land equivalent ratios (pLER). Z-scores were computed within a year (mean = 0, SD = 1) and summed to obtain a unit-free total yield. Principal component scores were derived from the first component of the standardized traits within a year. Economic yield was calculated using market prices (Ibadan, 20 January 2026), with cassava fresh root yield valued at ₦300 kg^{-1} and cowpea grain yield at ₦2550 kg^{-1}. pLER was computed as the sum of crop-specific intercrop yields relative to their monoculture means. For each metric, general mixing ability (GMA) models were fitted, variance contributions and broad-sense heritability were estimated, and selection overlap among top-ranked clones was evaluated using Jaccard similarity indices.

3.2.12 Genetic effects in intercrop: GMA, SMA, producer and associate effects

General and specific mixing ability were estimated following Haug et al. (2023):

$$y_{ijkl} = \mu + Year_i + \beta_1 C_{ijkl} + \beta_2 P_{ijkl} + g_j + t_k + (gt)_{jk} + gY_{ij} + tY_{ik} + (gtY)_{ijk} + r_{il} + \varepsilon_{ijkl}$$

(3.9)

where: g_j= cassava clone effect (GMA), t_k= cowpea tester effect, $(gt)_{jk}$= specific mixing ability (SMA), $gY_{ij}, tY_{ik}, (gtY)_{ijk}$= interactions with year, C, P= centered harvested cassava and cowpea plant numbers, r_{il}= replicate $l$within Year i and ε_{ijkl}= spatially structured residual. Variance components were interpreted as: σ_g^2= GMA variance and σ_{gt}^2= SMA variance.

For all GMA/SMA models, the response variable was the combined intercrop merit index computed as the sum of standardized (Z-score) cassava trait value and standardized cowpea grain yield within each environment, following the Z-score framework described in Section 2.8.

3.2.13 Producer Effect (Cassava Fraction Yield)

Producer ability (Pr) was estimated using the same model structure, replacing the response with standardized cassava intercrop yield:$y_{ijkl} = rtwt_z$. Under this formulation:σ_g^2= Producer variance (Pr) of cassava, σ_t^2= Associate variance (As) of cowpea on cassava yield, and σ_{gt}^2= interaction variance on cassava fraction yield.

3.2.14 Associate Effect (Cowpea Fraction Yield)

Associate ability (As) was estimated using: $y_{ijkl} = GrainYld_z$. Here:σ_g^2= Associate variance (As) of cassava, σ_t^2= Producer variance (Pr) of cowpea and σ_{gt}^2= interaction variance on cowpea fraction yield.

3.2.15 Agronomic efficiency

Land equivalent ratio (LER) and area–time equivalent ratio (ATER) were calculated to assess intercrop productivity relative to monoculture systems (Mead and Willey, 1980; Hiebsch, 1978). LER was computed as:

$$LER = \frac{Y_{c,i}}{Y_{c,m}} + \frac{Y_{p,i}}{Y_{p,m}} \qquad (3.10)$$

where $Y_{c,i}$ and $Y_{p,i}$ are cassava fresh root yield and cowpea grain yield in intercrop, respectively, and $Y_{c,m}$ and $Y_{p,m}$ are the corresponding monoculture yields.

To account for differences in crop duration, ATER was calculated as:

$$ATER = \frac{1}{t_i}\left(t_c \frac{Y_{c,i}}{Y_{c,m}} + t_p \frac{Y_{p,i}}{Y_{p,m}}\right) \qquad (3.11)$$

where t_c and t_p are the growth durations (days) of cassava and cowpea in monoculture, respectively, and t_i is the total duration of the intercrop system. Partial LER values for cassava and cowpea were calculated using clone BLUEs from monoculture and intercrop trials, and total LER and ATER were derived to assess productivity advantages of the intercropping system.

3.3 Results

3.3.1 Environmental variables and cassava performance under monoculture and intercrop systems

Both seasons accumulated similar thermal time (2023: ~14,600 °Cd; 2024: ~13,800 °Cd) and total rainfall (~1,750 mm; Figure 3.1) but differed in rainfall timing: Year 1 (2023-2024) had only 3 mm during December 2023 – January 2024 alongside elevated vapor pressure deficit (up to 1.2 kPa), whereas Year 2 (2024-2025) experienced a shorter low-rainfall period.

Fresh root weight varied consistently between cropping systems across both trial years (Figure 3.2). When pooled across years, monoculture yielded 30.52 kg plot^{-1} compared with 24.69 kg plot^{-1} under intercrop, representing an average reduction of approximately 5.8 kg plot^{-1} (19%) in intercrop. This pattern was consistent within individual years. Within the intercrop system, differences between cowpea testers were smaller than the overall monoculture–intercrop contrast. Across years, mean fresh root weight was 25.04 kg plot^{-1} with IT08K-150-12 and 24.34 kg plot^{-1} with Oloyin. Tester differences were modest in both 2023 (23.82 vs. 22.61 kg plot^{-1}) and 2024 (26.28 vs. 26.05 kg plot^{-1}). Harvest index (HI) and root dry matter content (DMC) showed smaller system contrasts than fresh root weight (Figure 3.3). Across years, HI averaged 0.56 under monoculture and 0.53 under intercrop, while DMC averaged 32.54% and 32.53%, respectively. Year effects were more pronounced for DMC, which declined from ~35% in 2023 to ~30% in 2024 across systems.

3.3.2 Is there exploitable genetic variation for cassava performance under intercropping?

Significant genetic variance among cassava clones was detected for all three traits under both monoculture and intercrop systems across years (Table 3.1). For fresh root weight, genetic variance among cassava clones in the combined analysis was

23.21 under monoculture and 15.49 under intercrop, with moderate broad-sense heritability estimates of 0.55 and 0.50, respectively ($P < 0.001$). Year-specific estimates varied, with substantially higher genetic variance and heritability observed in 2024 (H^2 = 0.72 monoculture; 0.64 intercrop) compared with 2023 (H^2 = 0.32 monoculture; 0.36 intercrop). Harvest Index also exhibited substantial heritable variation among cassava clones, with high heritability across systems in the combined analysis (H^2 = 0.81 monoculture; 0.73 intercrop; $P < 0.001$) and consistent clone significance in both years. Root dry matter content showed moderate to high heritability (H^2 = 0.68 monoculture; 0.75 intercrop), with significant genetic variance detected among clones in both systems and both years ($P < 0.001$).

In the combined model including both management systems and years, genotype × management interaction (G×M) variance among cassava clones was small and not significant for all traits. Genotype × year interaction (G×Y) was significant for fresh root weight (σ^2(G×Y) = 9.69; $P < 0.001$) and harvest index (σ^2(G×Y) = 0.0004; $P = 0.011$). No significant three-way interaction (G×M×Y) was detected for any trait.

3.3.3 Correlation, Selection efficiency and realized gain transfer between monoculture and intercrop systems

Two distinct correlation estimates are reported in this section (Table 3.2): the bivariate genetic correlation (r_g) is the bounded correlation parameter obtained via a joint heterogenous-correlation (corgh) bivariate model, in which monoculture and intercrop observations are modelled as correlated traits sharing a genetic covariance structure (Model 5). The univariate BLUP correlation (r_{BLUP}) is the Pearson and Spearman correlation between clone BLUPS extracted separately from the monoculture

(Model 1) and intercrop model (Model 2), each fitted independently. These two quantities estimate fundamentally different things: r_g aims to reveal the latent genetic correlation between systems, while r_BLUP shows the realized agreement between shrunken predictions from models that do not share information across systems.

Bivariate genetic correlations (r_g) between monoculture and intercrop performance were high across traits (Table 3.2). For fresh root weight, the combined-year r_g was near unity (0.996). Year-specific correlations were similarly high (0.99 in 2023; 0.92 in 2024). Harvest index and root dry matter content also had high r_g (≥ 0.95) in all analyses.

Pearson and Spearman univariate correlation (r_BLUP) for fresh root weight were moderate (Pearson r=0.65; Spearman ρ = 0.63 in combined year analysis), with 50% selection overlap at 5-10% selection intensity. Visualization of rank shifts further illustrates this pattern (Figure 3.4). Although genetic correlations were near unity, several cassava clones exhibited substantial re-ranking between systems, with the largest shifts exceeding 50 rank positions in the combined analysis. Harvest index and dry matter content showed stronger BLUP correlations (r ≥ 0.83 and r ≥ 0.84, respectively) and higher selection overlap, particularly at moderate selection intensities (Table 3.2). While the primary analysis focused on fresh root weight, harvest index, and dry matter content, the near-unity genetic correlations observed prompted further investigation across four additional traits to assess robustness (Table 3.3). Root number and shoot weight showed slightly lower genetic correlations in 2023 (r_g = 0.90 and 0.78), with shoot weight being the only trait × period where the profile CI excluded unity (0.62, 0.95). Root rot and root size showed the widest CIs, reflecting lower heritability.

Nevertheless, likelihood ratio tests failed to reject H0: $r_g = 1$ across all traits and periods (all $P > 0.90$), confirming that genetic rankings are conserved across cropping systems.

Across traits, bivariate genetic correlations between monoculture and intercrop performance were high ($r_g = 0.92–0.99$), Table 3.2. However, univariate BLUP correlation (r_{BLUP}) was consistently lower, particularly for fresh root weight ($r_{BLUP} = 0.45–0.66$). For fresh root weight, chance-corrected selection efficiency (Se%) at 10% intensity was moderate (44.4% combined; 25.9% in both individual years) Table 3.2. Realized gain from selecting in monoculture and testing in intercrop was 68.8% of the direct intercrop selection gain in the combined analysis, with year-specific efficiencies of 31.9% (2023) and 50.5% (2024). Reciprocal selection (intercrop predicting monoculture) showed similar magnitudes (60–70%). In contrast, selection based on the mean performance across systems captured 87–92% of the direct gain in both systems. Harvest index exhibited higher cross-system predictability. Combined Se% at 10% intensity reached 72.2%, and realized gain transfer from monoculture to intercrop was 89.2% of direct selection gain. Similar patterns were observed in individual years. Root dry matter content showed intermediate behavior, with Se% ranging from 25.9% to 44.3% at 10% intensity and realized gain transfer of 68–74%, increasing substantially at moderate selection intensities (Se33% up to 70.0%). Overall, although genetic correlations were near unity for all traits, realized selection efficiency and gain transfer were trait-dependent. Fresh root weight showed incomplete transferability between systems, whereas harvest index and dry matter content displayed stronger cross-system stability.

Diagnostic analyses were conducted to investigate further the consistently near-unity (r_g) estimates observed in this study, with comprehensive model diagnostics presented for each trait in Figures 3.5 to 3.7. The diagnostic plate for each trait shows six panels: (a) clone BLUPs from separate univariate models; r_{BLUP} with Pearson and Spearman correlations; (b) clone BLUPs from the bivariate corgh model, showing the near-perfect co-linearity that arises when the model imposes the estimated covariance structure (r_g); (c) the estimated genetic variance–covariance matrix; (d) a direct comparison of the off-diagonal genetic covariance with the geometric mean $\sqrt{(\sigma^2M \cdot \sigma^2I)}$, diagnosing whether the correlation has reached the parameter boundary; (e) a summary of variance components and likelihood ratio tests; and (f) selection overlap at varying intensities from univariate BLUPs. For fresh root weight, the genetic covariance (21.22) was nearly identical to $\sqrt{(\sigma^2M \cdot \sigma^2I)} = 21.25$ (Figure 3.5), confirming that the estimated $r_g = 0.999$ lies at the parameter boundary. The profile likelihood surface was flat across a wide range of starting values (Figure 3.5e), indicating that the data cannot distinguish $r_g = 0.90$ from $r_g = 0.99$; the likelihood is uninformative in this region. Similar boundary conditions were observed for harvest index (Figure 3.6) and dry matter content (Figure 3.7). Crucially, while the bivariate BLUPs showed near-perfect alignment (panel b, r = 1.00), the univariate BLUPs showed substantial scatter (panel a, r = 0.652 for FRWT), and selection overlap at 10% intensity was only 50%.

3.3.4 Cowpea tester interchangeability within intercrop

Cassava performance was broadly consistent across the two cowpea testers (IT08K-150-12 and Oloyin). Tester effects were not significant for fresh root weight (FRWT) or harvest index in the combined analysis ($P > 0.05$), with nearly identical

predicted means (FRWT: 24.72 vs 24.45 kg plot^{-1}; HI: 0.53 vs 0.52; Table 3.4). Heritability and expected selection gains were comparable between testers for all traits. For root dry matter content (DMC), a small but significant tester difference was detected in the combined analysis (32.33% vs 32.60%; p = 0.021), although variance parameters and selection gains remained similar. Clone × tester interaction was not significant for any trait in the combined analysis, with the exception of FRWT in 2024. Genetic correlations between testers were high (r_g = 0.99–0.99), and selection overlap among the top 20% clones was moderate (Jaccard ≈ 0.46–0.55; Table 3.5).

3.3.5 Yield-scale asymmetry and consequences for intercrop productivity metrics

Cassava and cowpea differed markedly in yield magnitude (Figure 3.8A). Cassava fresh root weight ranged from 5–58 kg plot^{-1} (mean 23.6 kg), whereas cowpea grain yield ranged from 100–899 g plot^{-1} (mean 366.7 g). When expressed in the same units, cassava yield was 64.3× larger than cowpea (Figure 3.8B). Variance decomposition of composite metrics showed contrasting crop contributions (Figure 3.8C). Raw and Kg metrics were strongly dominated by the cassava component (>100% relative contribution), whereas Z-score, PC1 and PLER distributed variance between the two crops. Composite–component correlations reflected this pattern (Figure 3.8D): Raw and Kg were strongly correlated with cassava FRWT (r ≈ 1.00) but weakly or negatively associated with cowpea yield (r = −0.16 to −0.29). Metric choice also altered genotype rankings, with substantial shifts among top clones across metrics (Figure 3.9). Consistent with these differences, genetic parameter estimates varied across metrics, with heritability ranging from 0.04 to 0.79 and GMA contributions from 0–41.48%, while SMA remained negligible (Table 3.6).

3.3.6 Variance partitioning of intercrop performance and heritability

In the combined analysis, significant genetic variation among cassava clones was detected for all three traits under all model frameworks. For the combined intercrop merit index derived from fresh root weight (FRWT-index = Z-score cassava FRWT + Z-score cowpea grain yield; Table 3.7), clone general mixing ability (GMA) was significant (LRT = 7.83, P = 0.003). Similarly, GMA was significant for the harvest-index-based (HI-index; LRT = 7.83, P = 0.003) and dry-matter-content-based (DMC-index; LRT = 5.99, P = 0.007) combined merit indices (Table 3.7). When the response was restricted to the cassava fraction only (producer model, response = Z-score cassava trait), clone effects were substantially larger FRWT producer LRT = 16.12 (P < 0.001), HI producer LRT = 55.06 (P < 0.001), DMC producer LRT = 74.59 (P < 0.001).

Broad-sense heritability (Table 3.8) of the general mixing ability (H^2_GMA) component ranged from 0.31 to 0.34, while heritability for producer effects (H^2_Pr) ranged from 0.47 to 0.75. In contrast, associate-effect heritability (H^2_As) was consistently low (0.04–0.05). Variance decomposition showed that genetic contributions differed among models (Figure 3.10). In the combined GMA model, clone effects explained 10.4–11.8% of total variance across traits. In the producer model, clone contributions were substantially larger, accounting for 20.4% (FRWT), 41.9% (HI), and 46.7% (DMC) of the total variance. By contrast, clone contributions in the associate model were small (1.2–1.4%). Year-specific analyses revealed stronger genetic signals in 2024. Clone effects were significant under both GMA and producer models for all traits (Table 3.7), and clone variance contributions increased substantially in 2024, reaching 27.5% in the GMA model and 38.0% in the producer model for FRWT, 27.5% and 36.9% for HI, and 24.7% and

54.3% for DMC (Figure 3.10). Correspondingly, GMA heritability increased in 2024 (0.48 for FRWT, 0.48 for HI, and 0.40 for DMC) compared with 2023 (Table 3.8).

3.3.7. Correlations among GMA, producer, associate, and pure stand performance

Correlation patterns differed among traits (Figure 3.11). For fresh root weight (FRWT), GMA showed significant positive correlations with producer effects (r = 0.79), associate effects (r = 0.52), and pure stand performance (r = 0.57). Producer effects were also strongly correlated with pure stand yield (r = 0.68), whereas correlations involving associate effects and pure stand were not significant. For harvest index (HI), significant correlations were observed between GMA and producer (r = 0.44), GMA and associate (r = 0.52), and GMA and pure stand (r = 0.36). The strongest relationship was between producer effects and pure stand performance (r = 0.85). For dry matter content (DMC), GMA correlated significantly only with associate effects (r = 0.49), while producer effects showed a strong correlation with pure stand performance (r = 0.82).

3.3.8 Quadrant Distribution of Producer and Associate Effects

Producer (Pr) and associate (As) BLUPs were plotted following the framework of Haug et al. (2021), classifying clones into four quadrants based on the sign of Pr and As, with the dashed diagonal (slope = −1) indicating the Pr + As = 0 boundary (Figure 3.12). For fresh root weight, clones were broadly distributed across quadrants, with 27 in Pr+, As+, 34 in Pr+, As−, 25 in Pr−, As+, and 34 in Pr−, As−. A similar pattern was observed for the harvest index, where 32 clones occurred in Pr+, As+, 29 in Pr+, As−, 20 in Pr−, As+, and 39 in Pr−, As−. For dry matter content, quadrant counts were also balanced, with 31 clones in Pr+, As+, 35 in Pr+, As−, 23 in Pr−, As+, and 31 in Pr−, As−.

3.3.9 Yield-formation pathways of cassava fresh root weight

Multi-group SEM revealed no detectable difference in fresh root weight (FRW) pathway structure between monoculture and intercrop systems ($\Delta\chi^2 = 7.58$, df = 14, $p = 0.91$; Table 3.9, Figures 3.13 and 3.14), with consistent year-specific results (2023: $p = 0.65$; 2024: $p = 0.25$). In both systems, FRW was governed primarily by root size ($\beta = 0.56$ monoculture; 0.63 intercrop) and, secondarily, root number ($\beta \approx 0.19$–0.21), while shoot weight acted indirectly through harvest index, to which it was strongly negatively related ($\beta \approx -0.82$ to -0.88) and which was in turn positively related to root number ($\beta \approx 0.45$–0.51). Pathway shifts under intercropping were modest and left the overall network unchanged (Figure 3.13), and cowpea grain yield and remaining traits had negligible direct effects.

3.3.10 Cassava-cowpea intercropping efficiency metrics

Total LER values were consistently above 1.0 for all clones, ranging approximately from 1.4 to above 3.0 under both cowpea testers. In contrast, intercropping efficiency for cassava varied substantially among clones but showed consistent system-level advantage across both cowpea testers (Figure 3.15). For fresh root weight, cassava partial land equivalent ratio (PLER) values were generally below 1.0 across clones (Figure 15), indicating reduced cassava yield in intercrop relative to monoculture. However, PLER increased progressively with clone ranking and approached or exceeded 1.0 among the highest-performing entries. Similar patterns were observed for area–time equivalent ratio (ATER), where lower-ranked clones were near or slightly below 1.0 while higher-ranked clones exceeded this threshold and reached values above 2.0.

3.4 Discussion

3.4.1 Cassava performance under monoculture and intercrop systems

This study provides the first empirical estimates of the genetic parameters identified by Dubey et al. (2024) and Moore et al. (2022) as critical for intercrop breeding scheme design. Intercropping was clearly beneficial, as evidenced by consistently >1 total LER estimates. Nevertheless, there is a 19% reduction in cassava fresh root weight under intercropping, which is consistent with earlier reports (Dapaah et al., 2003; Nyi et al., 2014; Hidoto and Loha, 2013; Mwebaze et al., 2024) and was stable across years, indicating interspecific competition as the primary driver. The yield penalty was more pronounced for fresh root weight than for harvest index or dry matter content, suggesting that cowpea competition operated through reduced biomass accumulation rather than altered assimilate partitioning; a trait-specific pattern consistent with asymmetric exploitation competition in intercropping systems (Moore et al., 2022). This highlights the need for breeding strategies to reduce cassava's competitive disadvantage when intercropped (Annicchiarico et al., 2021). Tester differences in cassava yield were modestly smaller than the monoculture–intercrop contrast, suggesting that the presence of a cowpea companion was more consequential than which variety was used. The erect, early-maturing IT08K-150-12 was marginally less suppressive, consistent with reduced canopy overlap during the cassava establishment phase.

3.4.2 Genetic variation, genotype × management interaction, and the case for intercrop breeding

Following the breeding decision frameworks of Moore et al. (2022), Annicchiarico et al. (2019), Haug et al. (2021), and Dubey et al. (2024), significant genetic variance under intercropping satisfies the first prerequisite for intercrop breeding, while non-significant G×M for all traits supports monoculture-based selection as the default strategy. However, significant G×Y for fresh root weight and harvest index indicates that multi-environment testing remains essential, and the absence of G×M should not be conflated with the absence of re-ranking, as the BLUP Pearson and Spearman correlations demonstrate. These results support the conclusion of Dubey et al. (2024) that minor adaptations to existing monoculture pipelines may represent a practical first step toward intercrop improvement.

Intercrop heritability was comparable to the total mixture yield heritability of 0.59 reported by Haug et al. (2023) for pea–barley. The significant genetic variance under all three models (GMA, Producer, Associate) confirms the foundational requirement of Sampoux et al.'s (2020) selection theory: exploitable variation exists for both direct and associate components. De Oliveira Zimmermann (1996) reported that G×M in bean–maize was environment-dependent. Consistently non-significant G×M may reflect the temporal niche separation between cassava (12 months) and cowpea (3–4 months), though multi-environment validation is needed before generalizing.

3.4.3 Selection efficiency and the relationship between monoculture and intercrop performance

This study evaluated the monoculture–intercrop relationship using genetic correlations from bivariate models and univariate r_BLUP correlations from separate system models. Genetic correlations were near-unity, indicating shared genetic control

(Falconer and Mackay, 1996), yet BLUP correlations were substantially lower for fresh root weight, demonstrating that high genetic correlation does not guarantee identical rankings (Henderson, 1975; Piepho et al., 2008; Annicchiarico et al., 2021). Using the metric of Hamblin and Zimmermann (1986), Se% for FRWT confirmed moderate transferability, consistent with their findings in bean–maize.

The wide gap between bivariate genetic correlations and univariate BLUP correlations warrants mechanistic explanation, as it bears directly on breeding recommendations. The observed boundary r_g estimate accompanied by moderate univariate BLUP concordance is consistent with the well-known behavior of bivariate models when genetic variance is moderate relative to residual variance, and when the data contain insufficient information to resolve the correlation away from the boundary (Lynch and Walsh, 1998), also observed in animal breeding and genetics literature (Schaeffer, 2018). Three statistically linked factors could account for this gap across all three traits.

First, the bivariate model targets the latent genetic correlation and borrows information across systems. When the estimated r_g approaches unity, bivariate BLUPs for monoculture and intercrop become algebraically constrained toward co-linearity, which is a reported property of Henderson's mixed model equations and does not serve as evidence that genotype rankings are identical in practice (Henderson, 1975; Mrode, 2014). Profile likelihood analysis confirmed that the likelihood surface was flat near r_g = 1 for all three traits, meaning the data lack statistical power to resolve the true correlation away from the boundary. This could be partly attributed to the limited size of the dataset, which had 2 replications.

Second, univariate BLUPs are subject to differential shrinkage between systems. Under moderate heritability, BLUPs are regressed toward the population mean, and the degree of shrinkage depends on the ratio of genetic to residual variance in each system (Piepho et al., 2008). Because intercrop heritability for FRWT was lower than monoculture heritability, intercrop BLUPs were shrunk more aggressively, compressing the intercrop ranking scale and reducing the rank correlation with monoculture. This asymmetric shrinkage is operationally relevant: it reflects the actual precision with which a breeder can distinguish genotypes in each system.

Third, significant genotype × year interaction for FRWT introduces temporal instability in clone rankings that is absorbed into the residual of single-year analyses but partially accommodated in the combined bivariate model. The G×Y variance, while not formally a G×M interaction, contributes to rank re-ordering between any two independent evaluations, including monoculture vs. intercrop BLUPs estimated from separate models. Zimmermann (1996) reported a similar trend in bean–maize, in which moderate-to-high genetic correlations coexisted with selection coincidence below 50%, driven by differential environmental sensitivity across systems. Francis et al. (1978) likewise showed that genotype × cropping system interactions in bush beans, while sometimes non-significant in variance terms, produced significant rank changes among the top-performing entries; this conclusion is relevant to the result and selection decisions in general.

Therefore, for breeding practice, the univariate BLUP correlation and realized selection efficiency are more informative than the bivariate r_g, because they reflect what a breeder would actually observe when making independent selection decisions in

each system (Piepho et al., 2008). The moderate Se% for FRWT thus represents the operationally relevant parameter, while the near-unity r_g confirms shared genetic architecture without guaranteeing rank preservation.

Overall, the observed correlations from this pilot study places cassava in the regime where Dubey et al. (2024) propose that monoculture selection can be maintained through advanced trials. However, monoculture heritability exceeding intercrop heritability formally satisfies indirect selection conditions (Holland and Brummer, 1999; Brummer, 2006; Moore et al., 2022), yet the 44% Se at 10% intensity reveals that theoretical conditions do not guarantee operational effectiveness. Selection based on the mean across systems captured 87–92% of direct gain, suggesting a combined strategy optimizes gain transfer. BLUP correlations comparable to the PS–MS correlation of r = 0.52 in pea–barley (Haug et al., 2023) confirm that pure stand performance provides useful but incomplete predictive power. Sampoux et al. (2020) demonstrated theoretically that pure stand selection efficiency depends on the genetic correlation with mixture direct effects; for fresh root weight, estimation noise in BLUPs may cause the Sampoux framework to overpredict pure stand selection value.

3.4.4 Variance partitioning: GMA, SMA, and the producer–associate decomposition

The GMA/SMA ratio is essential for determining intercrop breeding strategy (Annicchiarico et al., 2019; Haug et al., 2023). SMA was negligible across all traits and periods, confirming that cassava mixing ability is general rather than partner-specific, while producer effects dominated. This aligns with Moore et al.'s (2022) recommendation that when GMA dominates, a narrow tester set suffices. In pea–barley, Haug et al. (2023) similarly found GMA driven by producer effects with no associate

contribution; in cassava–cowpea, the GMA–Producer correlation was r = 0.79 for FRWT, confirming that GMA reflects a genotype's own yield capacity under competition.

The variance structure where producer variance is 15–40× larger than associate variance, with SMA absent or close to zero maps onto the scenario where Sampoux et al. (2020) predict that parallel GMA selection is as efficient as reciprocal selection. However, the two-tester design has reduced power for SMA detection (Haug et al., 2021), and this finding should be interpreted with appropriate caution.

3.4.5 Cowpea tester interchangeability

Two cowpea testers with contrasting architecture and maturity produced interchangeable cassava rankings (rg > 0.99) with negligible clone × tester interaction, placing cassava–cowpea in the GMA-dominant regime where a single tester suffices (Moore et al., 2022). While Dubey et al. (2024) note that tester choice is a critical decision, results indicate it is operationally inconsequential for cassava–cowpea. The near-perfect interchangeability empirically validates Wright's (1985) random-partner assumption.

3.4.6 Yield-scale asymmetry and composite metrics

The 64-fold yield asymmetry between cassava and cowpea introduces a challenge not addressed by current frameworks (Dubey et al., 2024; Moore et al., 2022; Haug et al., 2021, 2023, Annicchiarico et al., 2019, 2021). The composite response variable itself determines which genotypes are selected. The z-score standardization is equivalent to Wright's index with weights $\alpha_1 = 1/SD_1$ and $\alpha_2 = 1/SD_2$, and operationally equivalent to the Sampoux et al. (2020) index framework ($I = \alpha_1 x_1 + \alpha_2 x_2$) with variance-equalizing weights. While Haug et al. (2023) managed asymmetry through separated

fraction yields and pLER, cassava–cowpea requires explicit standardization because the scale difference is far more extreme.

3.4.7 Relationships among General Mixing Ability, Producer, Associate, and Pure-Stand Performance

Wright (1985) and Sampoux et al., 2020 demonstrated that negative direct–associate correlations favor selection on total mixture yield. The moderately negative Pr–As correlation for FRWT (r = −0.31) is weaker than in pea–barley (r = −0.65; Haug et al., 2023) and the simulated values of Sampoux et al. (2020) (−0.61 to −0.81) suggest that selecting for high producer effects will not severely erode associate effects, a favorable condition for GMA-based breeding.

Strong Pr–PS correlations for HI (r = 0.85) and DMC (r = 0.82) validate the trait-informed approach (Moore et al., 2022), while the absence of As–PS correlations confirms that pure stand selection captures only the direct-effect component (Sampoux et al., 2020) and that associate effects require direct intercrop evaluation (Moore et al., 2022; Barot et al., 2017).

3.4.8 Quadrant analysis of producer and associate effects

The producer–associate quadrant framework quantifies intercrop performance in terms of ecological interactions (Li et al., 2014; Litrico and Violle, 2015; Moore et al., 2022). Clones were distributed across all quadrants, with 22–27% in Pr+, As+; the mutualistic ideotype that Wright (1985) identified as optimal for maximizing economic yield. This frequency indicates favorable allele combinations already segregate at appreciable rates. The Pr–As trade-off was weaker than in pea–barley (r = −0.31 vs −0.65; Haug et al., 2023), likely reflecting temporal niche separation. For cassava-

prioritized systems, clones in Pr+, As+ sector (Haug et al., 2021) are primary selection targets.

3.4.9 Yield-formation pathways and the cassava intercrop ideotype

Path analysis in cassava has identified root size and root number as primary monoculture yield determinants (Mulualem and Ayenew, 2012; Edet et al., 2020; Andrade et al., 2021), but no study has tested whether these pathways are conserved under intercropping. The multi-group SEM demonstrates structural invariance, with root size and root number dominant in both systems. This provides mechanistic justification for the trait-informed approach (Moore et al., 2022; Barot et al., 2017; Holland and Brummer, 1999), selection for these traits in monoculture should translate to intercrop improvement.

Despite proposals that intercropping requires distinct ideotypes (Nelson and Robichaux, 1997; Litrico and Violle, 2015; Bourke et al., 2021; Moore et al., 2022), results indicate that a fundamentally new cassava ideotype is not required. This extends the trait-informed approach of Haug et al. (2023), who identified aboveground traits for pea GMA selection, to belowground yield components in cassava.

Yield-formation pathways were structurally invariant between systems, with root size and root number as primary determinants in both, consistent with the finding that early canopy vigor and final root yield are genetically decoupled in cassava (Kawano and Thung, 1982; Davis and Woolley, 1993). Producer effects dominated associate effects, SMA was negligible, and genetic correlations were near-unity, collectively confirming that intercrop performance is driven by a clone's intrinsic yield capacity rather than partner-specific adaptation. Davis and Woolley (1993) noted that genotype ×

cropping system interactions are typically less pronounced in dominant crops such as cassava, and non-significant G×M variance supports this. The temporal niche separation inherent in cassava–cowpea (12- vs 3–4-month growth (cowpea) cycles) further limits direct interspecific competition, explaining the small associate effects observed.

Furthermore, Davis and Woolley (1993) proposed that intercrop-adapted dominant crops should combine high harvest index with canopy architecture permitting light penetration, and recommended late-branching, less-vigorous cassava types for legume intercrops (Thung and Cock, 1979; Cenpukdee and Fukai, 1992a,b and c). Integrating their framework with quantitative genetic results, the cassava intercrop ideotype comprises: (i) high root yield potential through large root size and adequate root number; (ii) efficient partitioning reflected in high harvest index, the trait with strongest cross-system transferability (Se% = 72.2%); (iii) moderate early canopy vigor that does not suppress the companion legume; (iv) yield stability across years, since G×Y rather than G×M drove ranking instability; and (v) no requirement for positive associate effects. This profile represents the existing monoculture selection target with a confirmatory filter for yield maintenance under competition, consistent with the minimal pipeline adaptation recommended by Dubey et al. (2024) and with Davis and Woolley's (1993) conclusion that selecting efficient plant types for intercropping is compatible with sole-crop breeding objectives.

3.4.10 Placing the cassava breeding program within the intercrop breeding framework

A simulation study by Dubey et al. (2024) showed that the genetic correlation between monocrop and intercrop performance drives the optimal stage for introducing intercrop testing more than heritability. At correlation of R = 0.9 between monoculture and intercrop, phenotyping can be delayed to the advanced (AYT) or elite yield trial, whereas at R = 0.3 it should begin at the preliminary yield trial (Dubey et al., 2024). Genetic correlations (0.92–0.99) place cassava–cowpea firmly in this high-correlation, late-switching regime, while the non-significant G×M, negligible SMA, and the absence of detectable pathway differences independently confirm that monoculture selection captures most intercrop merit. The genotypes used here came from IITA NextGen AYT, material already selected under monoculture, yet significant intercrop variation persisted, indicating monoculture selection has not purged intercrop-relevant variation. However, the moderate Se% for fresh root yield (25.9–44.4%) calls for caution: a confirmatory single-tester, pooled-tester (Annicchiarico et al., 2021), or incomplete-factorial (Haug et al., 2021) intercrop evaluation at the AYT stage would sharpen yield selection. Therefore, the monoculture pipeline should be preserved, with an incomplete-factorial intercrop evaluation added at the AYT stage as a minimal adaptation consistent with Dubey et al. (2024).

3.5 Conclusion

This study provides the first quantitative genetic characterization of mixing ability in a cassava–cowpea intercropping system and establishes an evidence base for integrating intercrop evaluation into the IITA cassava breeding program. Cassava clones can be selected for improved mixture productivity primarily through high GMA, driven largely by producer effects, while SMA and clone × tester interactions were negligible.

Consequently, a cowpea tester approach may be adequate for operational screening of cassava mixing ability, substantially reducing phenotyping requirements. Producer effects were strongly associated with pure-stand performance, confirming monoculture evaluation as an efficient early-stage selection environment. However, realized selection efficiency for fresh root yield was moderate, suggesting that exclusive pure-stand evaluation may forfeit approximately 30% of achievable gain. Therefore, monoculture-based selection should be retained at the early stages and complemented by single-tester intercrop evaluation in advanced yield trials. The z-score standardization framework used here addresses the pronounced yield-scale asymmetry between cassava and cowpea. Some limitations to this study are that these conclusions are based on a single location over two years with two cowpea testers, which limit inference about genotype × environment × management interactions and constrain statistical power for SMA detection (Haug et al., 2021). The multi-group path analysis fitted acceptably in 2023 but only modestly in the combined and 2024 models, so the conserved yield-formation architecture it indicates should be treated as provisional pending validation in larger clone panels. Transitioning to an incomplete factorial design with more diverse cowpea genotypes would enable estimation of both species' GMA and SMA variances while maintaining feasible experimental plots. Multi-environment validation and integration of genomic prediction are needed to operationalize these findings across diverse agroecological zones.

References

Adam, A. M., Giller, K. E., Rusinamhodzi, L., Rasche, F., Koomson, E., Marohn, C., et al. (2025). Enhancing the resilience of intercropping systems to changing moisture conditions in Africa through the integration of grain legumes: A meta-analysis. Field Crops Res. 321, 109663. doi: 10.1016/j.fcr.2024.109663

Anderson, C. L., Gugerty, M. K., Golenko, A., Kpaka, C., and McKee, C. (2013). LSMS-Integrated Surveys on Agriculture: Intercropping. EPAR Brief No. 216. Seattle, WA: Evans School Policy Analysis and Research, University of Washington.

Annicchiarico, P., and Piano, E. (1994). Interference effects in white clover genotypes grown as pure stands and binary mixtures with different grass species and varieties. Theor. Appl. Genet. 88, 153–158. doi: 10.1007/BF00225891

Annicchiarico, P., Collins, R. P., De Ron, A. M., Firmat, C., Litrico, I., and Hauggaard-Nielsen, H. (2019). Do we need specific breeding for legume-based mixtures? Adv. Agron. 157, 141–215. doi: 10.1016/bs.agron.2019.04.001

Annicchiarico, P., Nazzicari, N., Notario, T., Monterrubio Martin, C., Romani, M., Ferrari, B., and Pecetti, L. (2021). Pea breeding for intercropping with cereals: variation for competitive ability and associated traits, and assessment of phenotypic and genomic selection strategies. Front. Plant Sci. 12, 731949. doi: 10.3389/fpls.2021.731949

Aye, T. M., and Howeler, R. (2012). "Cassava agronomy: intercropping systems," in The Cassava Handbook, ed. R. H. Howeler (Cali, Colombia: CIAT), 613–625.

Bančič, J., Werner, C. R., Gaynor, R. C., Gorjanc, G., Odeny, D. A., Ojulong, H. F., et al. (2021). Modeling illustrates that genomic selection provides new opportunities

for intercrop breeding. Front. Plant Sci. 12, 605172. doi: 10.3389/fpls.2021.605172

Bänziger, M., and Cooper, M. (2001). Breeding for low input conditions and consequences for participatory plant breeding examples from tropical maize and wheat. Euphytica 122, 503–519. doi: 10.1023/A:1017510928038

Barot, S., Allard, V., Cantarel, A., Enjalbert, J., Gauffreteau, A., Goldringer, I., et al. (2017). Designing mixtures of varieties for multifunctional agriculture with the help of ecology. Agron. Sustain. Dev. 37, 13. doi: 10.1007/s13593-017-0418-x

Bourke, P. M., Evers, J. B., Bijma, P., van Apeldoorn, D. F., Smulders, M. J. M., Kuyper, T. W., et al. (2021). Breeding beyond monoculture: putting the "intercrop" into crops. Front. Plant Sci. 12, 734167. doi: 10.3389/fpls.2021.734167

Brummer, E. C. (2006). "Breeding for cropping systems," in Plant Breeding: The Arnel R. Hallauer International Symposium (Ames, Iowa, USA: Blackwell Publishing), 97–106.

Butler, D. G., Cullis, B. R., Gilmour, A. R., Gogel, B. J., and Thompson, R. (2018). ASReml-R Reference Manual Version 4. Hemel Hempstead, UK: VSN International Ltd.

Cenpukdee, U. and Fukai, S., 1992a. Cassava/legume intercropping with contrasting cassava cultivars. 1. Competition between component crops under three intercropping conditions. Field Crops Res., 29:113-133.

Cenpukdee, U. and Fukai, S., 1992b. Cassava/legume intercropping with contrasting cassava cultivars. 2. Selection criteria for cassava genotypes in intercropping with two contrasting legume crops. Field Crops Res., 29:135-149.

Cenpukdee, U. and Fukai, S., 1992c. Agronomic modification of competition between cassava and pigeonpea in intercropping. Field Crops Res., 30:13 l- 146.

Davis, J. H. C., & Woolley, J. N. (1993). Genotypic requirement for intercropping. Field Crops Research, 34(3–4), 407–430. https://doi.org/10.1016/0378-4290(93)90124-6

Dapaah, H. K., Asafu-Agyei, J. N., Ennin, S. A., and Yamoah, C. (2003). Yield stability of cassava, maize, soya bean and cowpea intercrops. J. Agric. Sci. 140, 73–82. doi: 10.1017/S0021859602002770

Dubey, R., Zustovi, R., Landschoot, S., Dewitte, K., Verlinden, G., Haesaert, G., and Maenhout, S. (2024). Harnessing monocrop breeding strategies for intercrops. Front. Plant Sci. 15, 1394413. doi: 10.3389/fpls.2024.1394413

Edet, M. A., Tijani-Eniola, H., Lagoke, S. T. O., and Tarawali, G. (2020). Assessment of yield components of some cassava genotypes using multivariate analysis such as path coefficients. Open Agric. 5, 537–546. doi: 10.1515/opag-2020-0051

Falconer, D. S. (1989). Introduction to Quantitative Genetics. 3rd Edn. Harlow: Longman Scientific and Technical.

Forst, E., Enjalbert, J., Allard, V., Ambroise, C., Krissaane, I., Mary-Huard, T., et al. (2019). A generalized statistical framework to assess mixing ability from incomplete mixing designs using binary or higher order variety mixtures and application to wheat. Field Crops Res. 242, 107571. doi: 10.1016/j.fcr.2019.107571

Francis, C.A., Prager, M., Laing, D.R. and Flor, C.A. (1978), Genotype × Environment Interactions in Bush Bean Cultivars in Monoculture and Associated with

Maize1. Crop Science, 18: 237-242 cropsci1978.0011183X001800020011x. https://doi.org/10.2135/cropsci1978.0011183X001800020011x

Gmakouba, T., Dzidzienyo, D. K., Koussao, S., et al. (2024). Identifying cassava production constraints, farmers preferences, and cassava mosaic disease perceptions in Togo: insights for a participatory breeding approach. Agric. Food Secur. 13, 63. doi: 10.1186/s40066-024-00518-9

Hamblin, J., and Zimmermann, M. J. O. (1986). "Breeding common bean for yield in mixtures," in Plant Breeding Reviews, Vol. 4, ed. J. Janick (Westport, CT: AVI Publishing Company), 245–272.

Haug, B., Messmer, M. M., Enjalbert, J., Goldringer, I., Forst, E., Flutre, T., et al. (2021). Advances in breeding for mixed cropping – incomplete factorials and the producer/associate concept. Front. Plant Sci. 11, 620400. doi: 10.3389/fpls.2020.620400

Haug, B., Messmer, M. M., Enjalbert, J., Goldringer, I., Flutre, T., Mary-Huard, T., et al. (2023). New insights towards breeding for mixed cropping of spring pea and barley to increase yield and yield stability. Field Crops Res. 297, 108923. doi: 10.1016/j.fcr.2023.108923

Hauggaard-Nielsen, H., and Jensen, E. S. (2001). Evaluating pea and barley cultivars for complementarity in intercropping at different levels of soil N availability. Field Crops Res. 72, 185–196.

Henderson, C. R. (1975). Best linear unbiased prediction under a selection model. Biometrics 31, 423–447.

Hiebsch, C. 1978. Comparing intercrops with monoculture. In: Agronomic and Economic Research on Soils in the Tropics. Annual Report 1976-1977. Soil Science Dept., North Carolina State University, Raleigh, North Carolina, USA. pp. 187-200.

Hidoto, L., and Loha, G. (2013). Identification of suitable legumes in cassava (Manihot esculenta Crantz)-legumes intercropping. Afr. J. Agric. Res. 8, 2559–2562. doi: 10.5897/AJAR12.1976

Himmelstein, J., Ares, A., Gallagher, D., and Myers, J. (2017). A meta-analysis of intercropping in Africa: impacts on crop yield, farmer income, and integrated pest management effects. Int. J. Agric. Sustain. 15, 1–10. doi: 10.1080/14735903.2016.1242332

Holland, J., and Brummer, E. (1999). Cultivar effects on oat–berseem clover intercrops. Agron. J. 91, 321–329. doi: 10.2134/agronj1999.00021962009100020023x

Kawano, K. and Thung, M.D., 1982. Intergenotypic competition and competition with associated crops in cassava. Crop Sci., 22: 59-63.

Li, L., Tilman, D., Lambers, H., and Zhang, F.-S. (2014). Plant diversity and overyielding: insights from belowground facilitation of intercropping in agriculture. New Phytol. 203, 63–69. doi: 10.1111/nph.12778

Litrico, I., and Violle, C. (2015). Diversity in plant breeding: a new conceptual framework. Trends Plant Sci. 20, 604–613. doi: 10.1016/j.tplants.2015.07.007

Lynch, M., and Walsh, B. (1998). Genetics and Analysis of Quantitative Traits. Sunderland, MA: Sinauer.

Maitra, S., Hossain, A., Brestic, M., Skalicky, M., Ondrisik, P., Gitari, H., et al. (2021). Intercropping—a low input agricultural strategy for food and environmental security. Agronomy 11, 343. doi: 10.3390/agronomy11020343

Martin-Guay, M.-O., Paquette, A., Dupras, J., and Rivest, D. (2018). The new Green Revolution: sustainable intensification of agriculture by intercropping. Sci. Total Environ. 615, 767–772. doi: 10.1016/j.scitotenv.2017.10.024

Mead, R. and Willey, R.W. 1980. The concept of a “land equivalent ratio” and advantages in yield of intercropping. Experimental Agriculture 16: 217-228

Moore, V. M., Schlautman, B., Fei, S.-z., Roberts, L. M., Wolfe, M., Ryan, M. R., Wells, S., and Lorenz, A. J. (2022). Plant breeding for intercropping in temperate field crop systems: a review. Front. Plant Sci. 13, 843065. doi: 10.3389/fpls.2022.843065

Mrode, R. A. (2014). Linear models for the prediction of animal breeding values (3rd ed.). CABI.

Mulualem, T., and Ayenew, B. (2012). Correlation and path coefficient analysis of cassava (Manihot esculenta Crantz) at Jimma, Southwestern Ethiopia. J. Nat. Sci. Res. 2, 1–7.

Mwebaze, P., Macfadyen, S., De Barro, P., Bua, A., Kalyebi, A., Bayiyana, I., Tairo, F., and Colvin, J. (2024). Adoption determinants of improved cassava varieties and intercropping among East and Central African smallholder farmers. J. Agric. Appl. Econ. Assoc. 3, 292–310.

Nelson, S. C., and Robichaux, R. H. (1997). Identifying plant architectural traits associated with yield under intercropping: implications of genotype–cropping

system interactions. Plant Breed. 116, 163–170. doi: 10.1111/j.1439-0523.1997.tb02172.x

Nyi, T., Mucheru-Muna, M., Shisanya, C., Lama, J. L., Mutuo, P. K., Pypers, P., and Vanlauwe, B. (2014). Effect of delayed cassava planting on yields and economic returns of a cassava-groundnut intercrop in the Democratic Republic of Congo. World J. Agric. Res. 2, 101–108.

Oliveira, C. R. S., Borel, J. C., Pereira, D. A., Carvalho, B. P., Medrado, E. S., Ishikawa, F. H., and Oliveira, E. J. (2021). Genetic parameters and path analysis for root yield of cassava under drought and early harvest. Crop Breed. Appl. Biotechnol. 21, e36162137.

Omoigui, L. O., Kamara, A. Y., Batieno, J., Iorlamen, T., Kouyate, Z., Yirzagla, J., et al. (2018). Guide to Cowpea Production in West Africa. Ibadan, Nigeria: IITA.

Parmar, A., Sturm, B., and Hensel, O. (2017). Crops that feed the world: production and improvement of cassava for food, feed, and industrial uses. Food Secur. 9, 907–927. doi: 10.1007/s12571-017-0717-8

Piepho, H. P., Möhring, J., Melchinger, A. E., and Büchse, A. (2008). BLUP for phenotypic selection in plant breeding and variety testing. Euphytica 161, 209–228. doi: 10.1007/s10681-007-9449-8

Popoola, B. O., Ongom, P. O., Mohammed, S. B., Togola, A., Ishaya, D. J., Bala, G., Fatokun, C., and Boukar, O. (2024). Assessing the impact of genotype-by-environment interactions on agronomic traits in elite cowpea lines across agro-ecologies in Nigeria. Agronomy 14, 263. doi: 10.3390/agronomy14020263

Rabbi, I. Y., Kayondo, S. I., Bauchet, G., Yusuf, M., Aghogho, C. I., Ogunpaimo, K., et al. (2022). Genome-wide association analysis reveals new insights into the genetic architecture of defensive, agro-morphological and quality-related traits in cassava. Plant Mol. Biol. 109, 195–213. doi: 10.1007/s11103-020-01038-3

Rosseel, Y. (2012). lavaan: an R package for structural equation modeling. J. Stat. Softw. 48, 1–36. doi: 10.18637/jss.v048.i02

Sampoux, J.-P., Giraud, H., and Litrico, I. (2020). Which recurrent selection scheme to improve mixtures of crop species? Theoretical expectations. G3 Genes Genomes Genet. 10, 89–107. doi: 10.1534/g3.119.400809

Schaeffer LR. (2018). Necessary changes to improve animal models. J Anim Breed Genet. 2018;135:124–131. https://doi.org/10.1111/jbg.12321

Self SG, Liang KY (1987). Asymptotic properties of maximum likelihood estimators and likelihood ratio tests under nonstandard conditions. Journal of the American Statistical Association 82(398):605–610. https://doi.org/10.2307/2289471

Thung, M. and Cock, J.H., 1979. Multiple cropping cassava and filed beans: status of present work at the International Centre of Tropical Agriculture (CIAT). In: E. Weber, B. Nestel and M. Campbell (editors), Intercropping with Cassava, Proc. Int. Workshop, Trivandrum, India, 27 November- 1 December 1978. Series IDRC- 142e, pp. 7-16.

Wang, G., Ehlers, J., Ogbuchiekwe, E., Yang, S., and McGiffen, M. (2004). Competitiveness of erect, semierect, and prostrate cowpea genotypes with sunflower (Helianthus annuus) and purslane (Portulaca oleracea). Weed Sci. 52, 815–820. doi: 10.1614/WS-03-148R

Wang, G., McGiffen, M., Ehlers, J., and Marchi, E. (2006). Competitive ability of cowpea genotypes with different growth habit. Weed Sci. 54, 775–782. doi: 10.1614/WS-06-011R.1

Weerarathne, L. V. Y., Marambe, B., and Chauhan, B. S. (2016). Does intercropping play a role in alleviating weeds in cassava as a non-chemical tool of weed management? – A review. Crop Prot. 95, 81–88. doi: 10.1016/j.cropro.2016.08.028

Wright, A. J. (1985). Selection for improved yield in inter-specific mixtures or intercrops. Theor. Appl. Genet. 69, 399–407. doi: 10.1007/BF00270871

Zimmermann, M. J. O. (1996). Breeding for yield in mixtures of common beans (Phaseolus vulgaris L.) and maize (Zea mays L.). Euphytica 92, 129–134. doi: 10.1007/BF00022837.

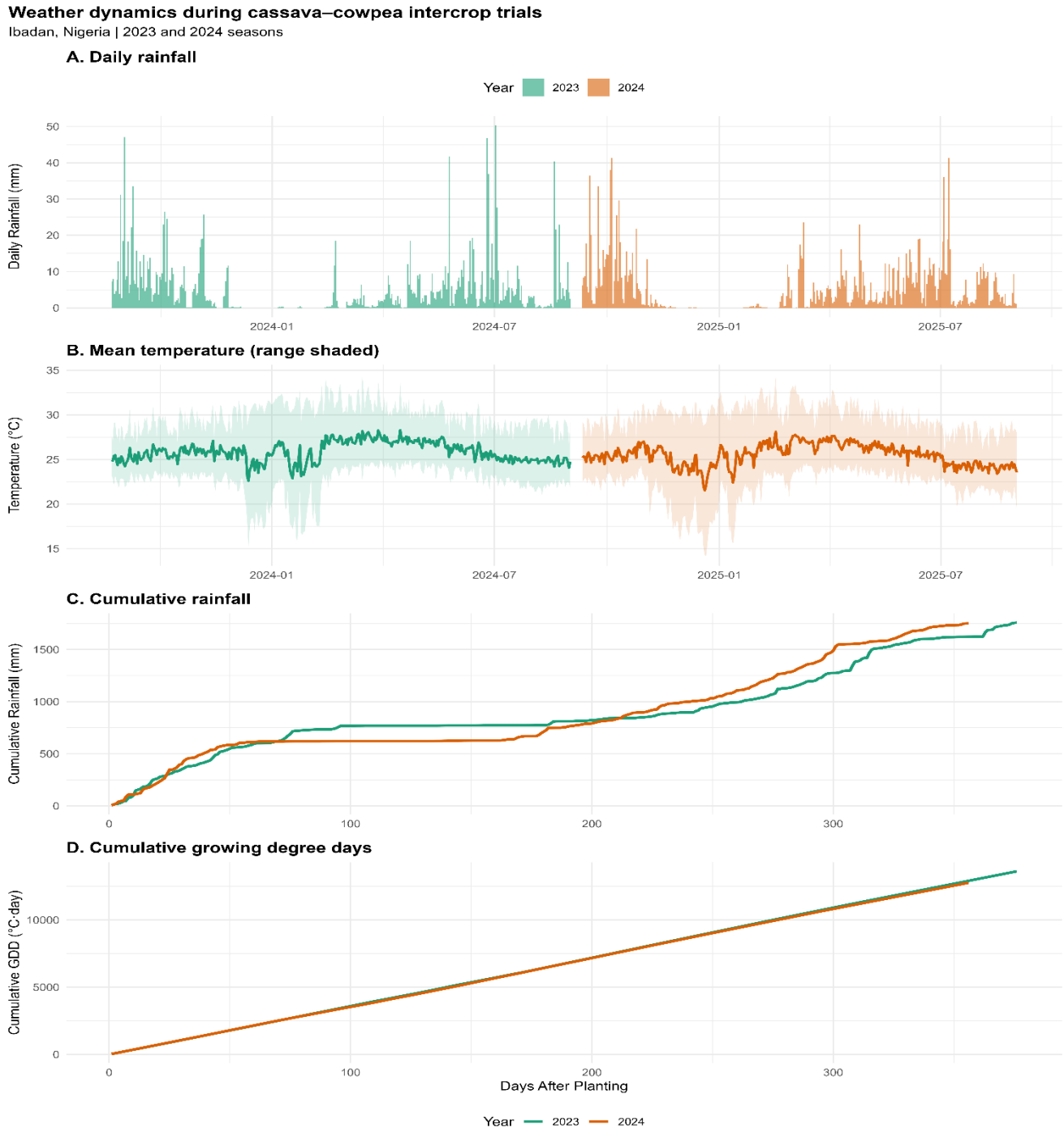

Figure 3.1. Weather conditions during the 2023 and 2024 cassava–cowpea intercrop trials in Ibadan, Nigeria

Daily and cumulative environmental conditions during the two field seasons are shown relative to days after planting (DAP). (A) Daily rainfall (mm). (B) Mean daily temperature (°C), with shaded areas indicating daily range. (C) Cumulative rainfall (mm). (D) Cumulative growing degree days (GDD; °C·day).

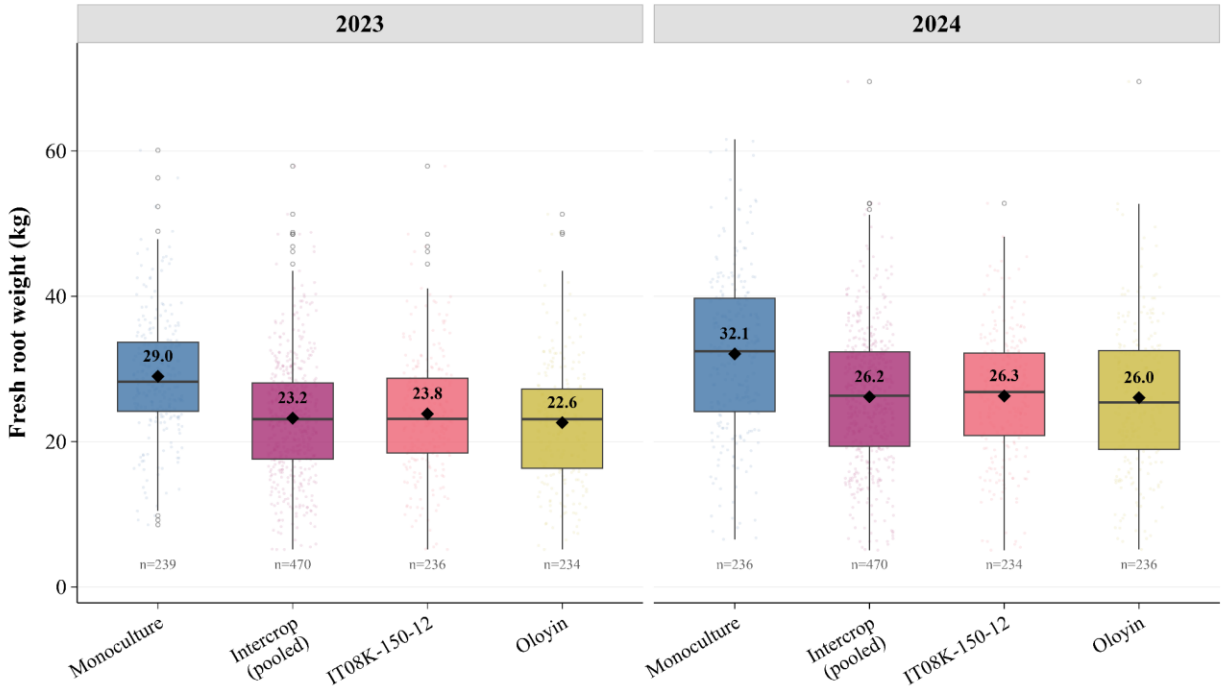

Figure 3.2. Fresh root weight of cassava under monoculture and intercrop systems across two trial years.

Fresh root weight (kg plot^{-1}) measured at harvest in 2023 and 2024 at IITA, Ibadan, Nigeria. Treatments include monoculture, intercrop (pooled across cowpea testers), and intercrops with individual cowpea testers (IT08K-150-12 and Oloyin). Boxplots display the median and interquartile range (IQR); whiskers extend to 1.5 × IQR. Points represent individual plot-level observations. Black diamonds indicate treatment means (μ). Sample sizes (n) are shown below each box.

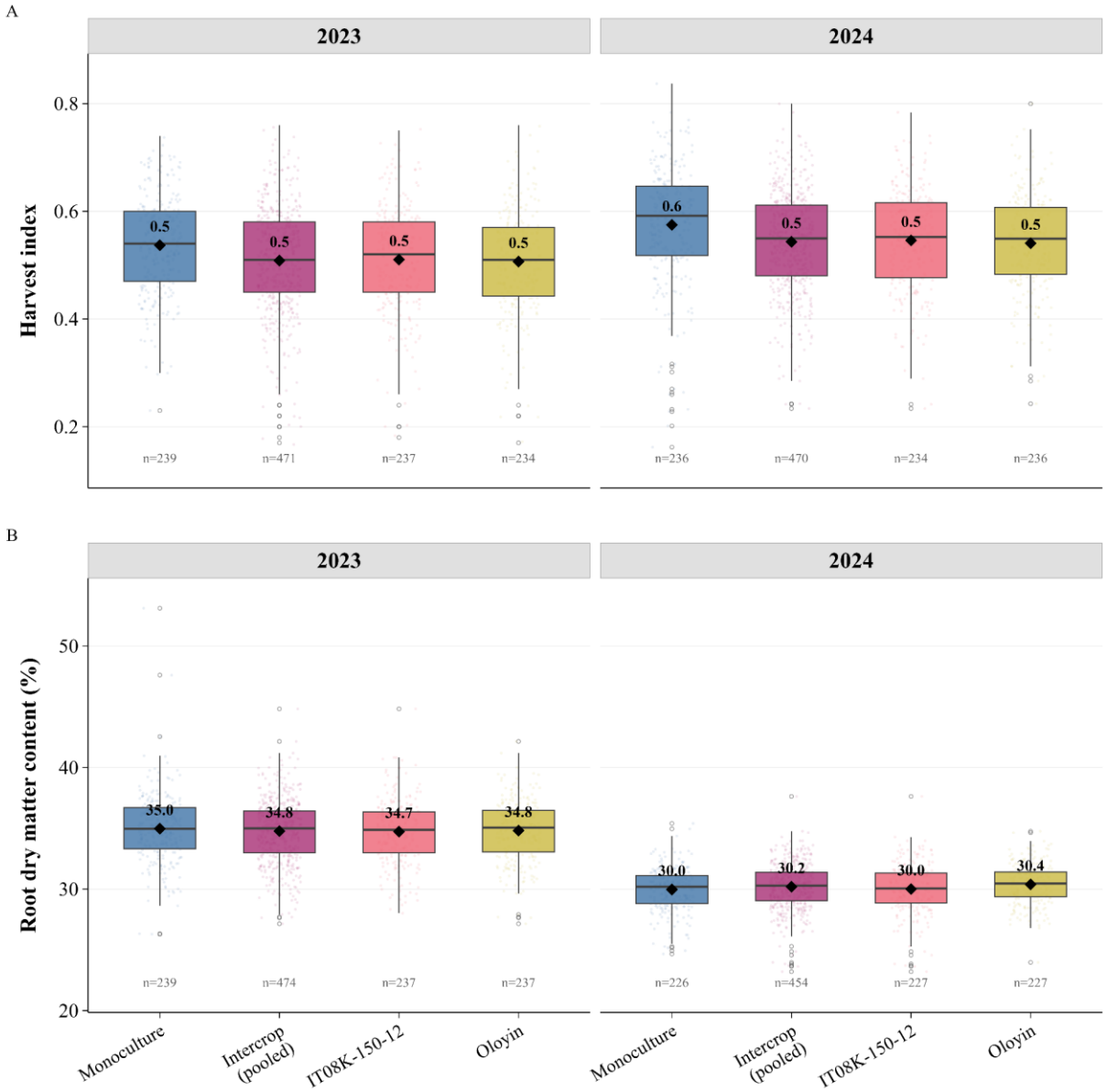

Figure 3.3. Distribution of cassava yield and quality traits under monoculture and intercrop systems across two trial years.

(A) Fresh root weight (kg plot⁻¹), (B) harvest index (HI), and (C) root dry matter content (DMC, %) measured at harvest in 2023 and 2024 at IITA, Ibadan, Nigeria. Treatments include monoculture, intercrop (pooled across cowpea testers), and intercrop with individual cowpea testers (IT08K-150-12 and Oloyin). Boxplots display the median and interquartile range (IQR); whiskers extend to 1.5 × IQR. Points represent individual plot-level observations. Black diamonds indicate treatment means (μ). Minimum and maximum values are annotated for each treatment. Sample sizes (n) are shown below each box.

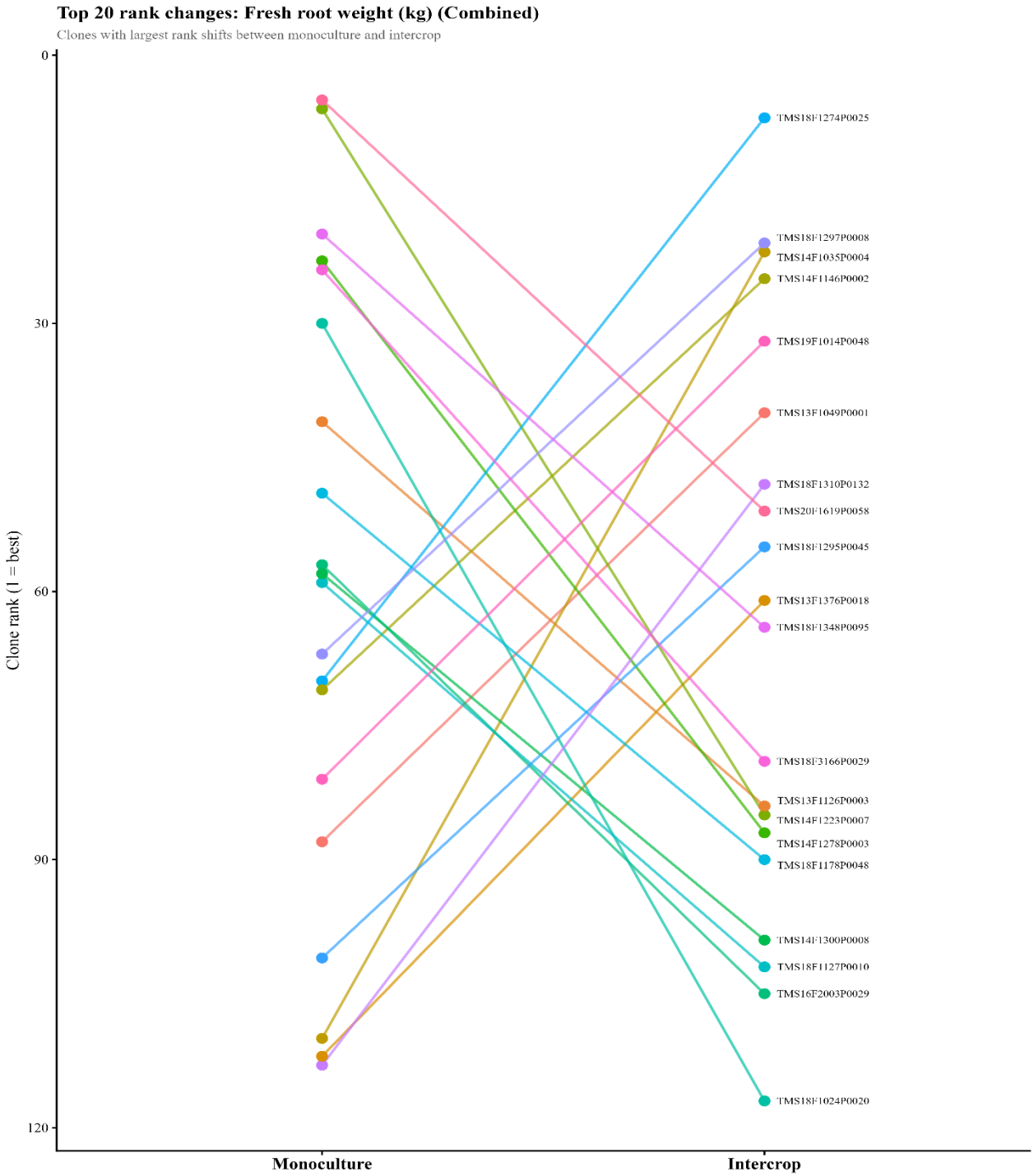

Figure 3.4. Largest cross-system rank shifts for cassava clones in fresh root weight (combined year).

Slope chart shows the 20 cassava clones with the largest changes in fresh root weight rank between monoculture and intercropping. Several clones improved markedly under intercropping while others declined, demonstrating substantial re-ranking across management systems.

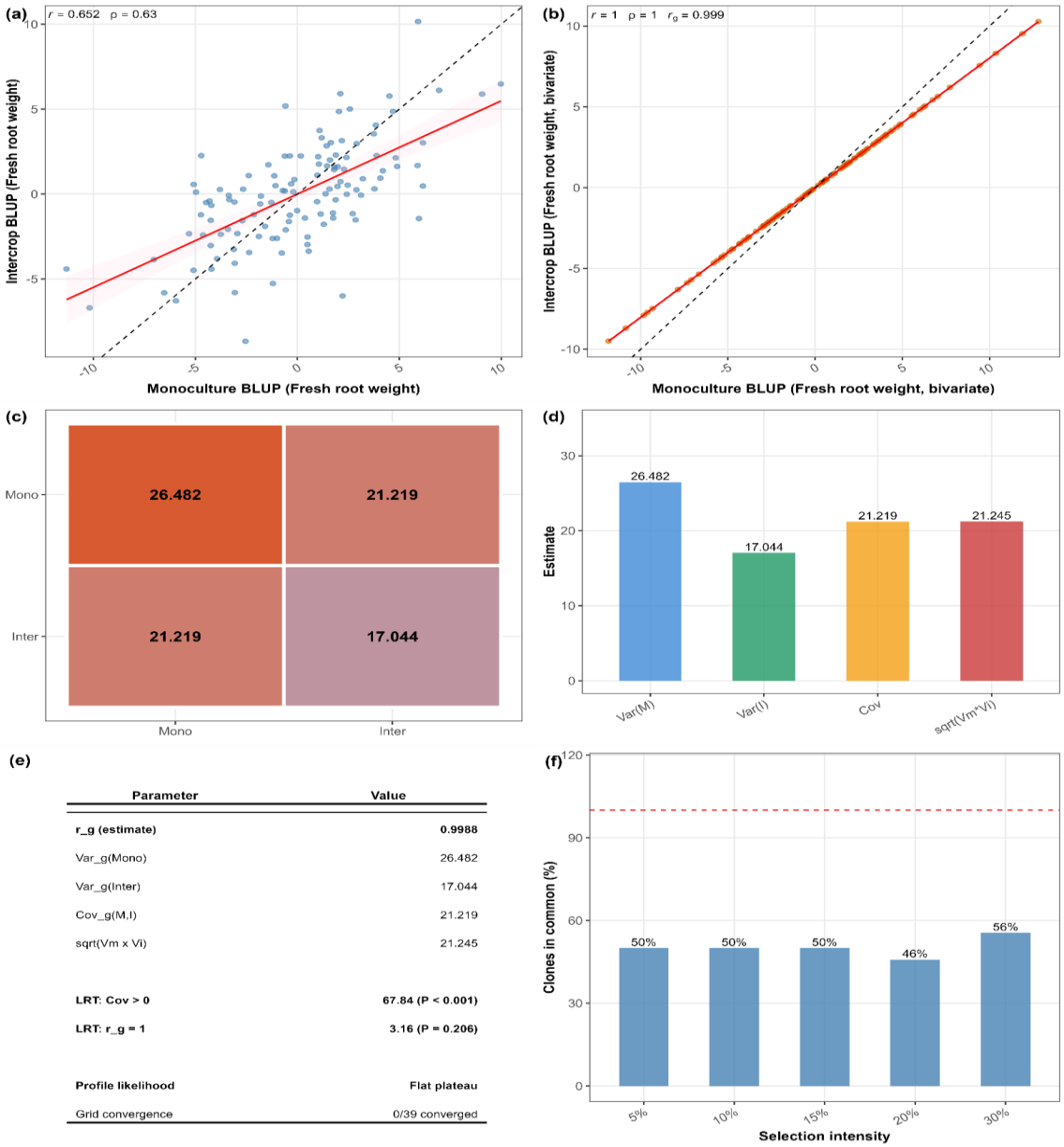

Figure 3.5. Bivariate genetic correlation diagnostic for Fresh root weight (combined years, 120 clones).

(a) Clone BLUPs from separate univariate models; r and rho are Pearson and Spearman correlations. (b) Clone BLUPs from the bivariate corh model. (c) Genetic variance-covariance matrix; off-diagonal covariance approaches the geometric mean of the diagonal variances, placing the correlation at the parameter boundary. (d) Variance component comparison (e) Model summary: variance components, likelihood ratio tests for genetic covariance significance (diag vs corh) and genetic identity (corh vs single Clone), and profile likelihood outcome. (f) Selection overlap at varying intensities; overlap below 100% indicates genotype re-ranking between systems despite the near-unity model-estimated r_g.

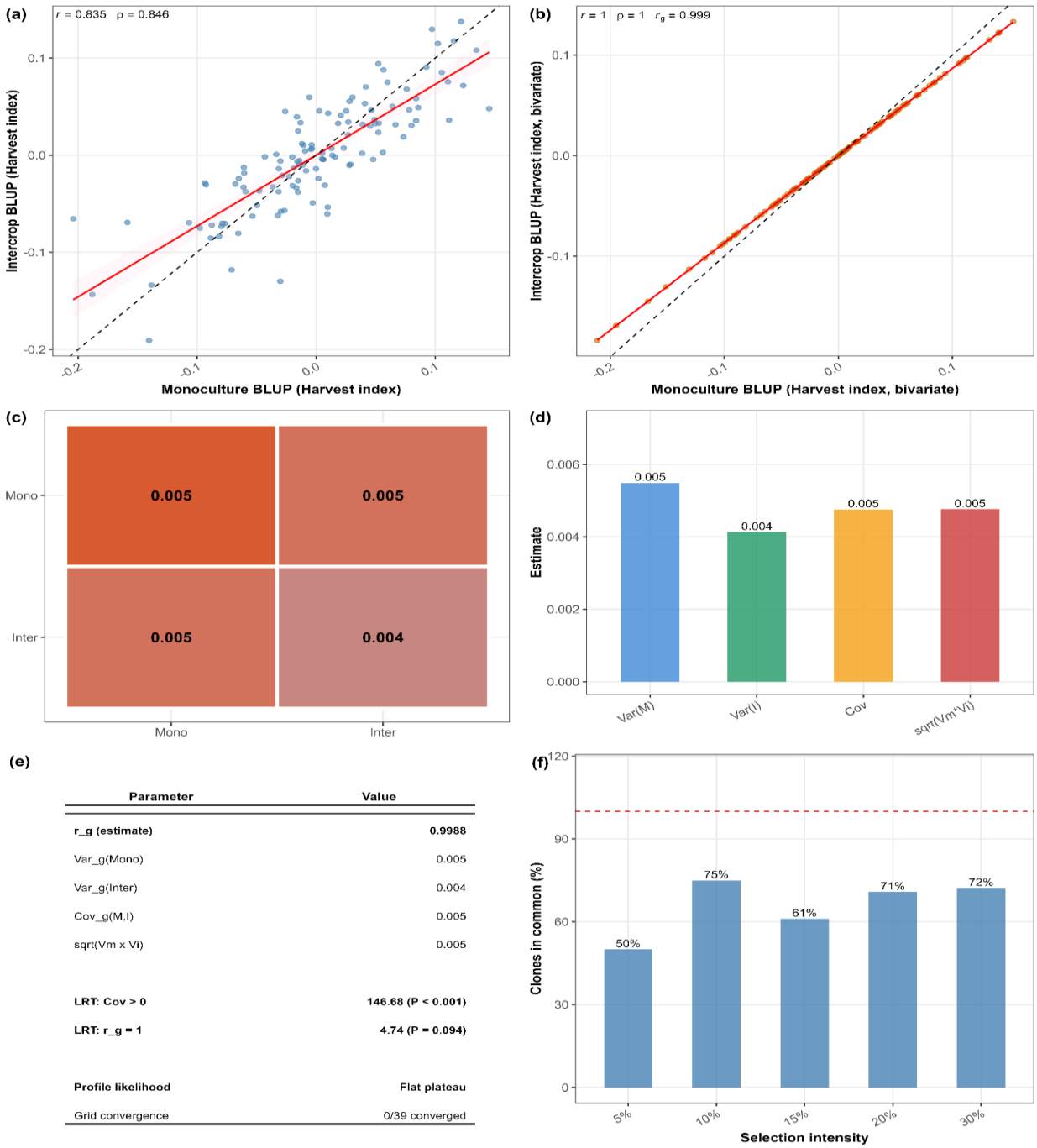

Figure 3.6. Bivariate genetic correlation diagnostic for Harvest index (combined years, 120 clones).

(a) Clone BLUPs from separate univariate models; r and rho are Pearson and Spearman correlations. (b) Clone BLUPs from the bivariate corh model (c) Genetic variance-covariance matrix (d) Variance component comparison (e) Model summary. (f) Selection overlap at varying intensities

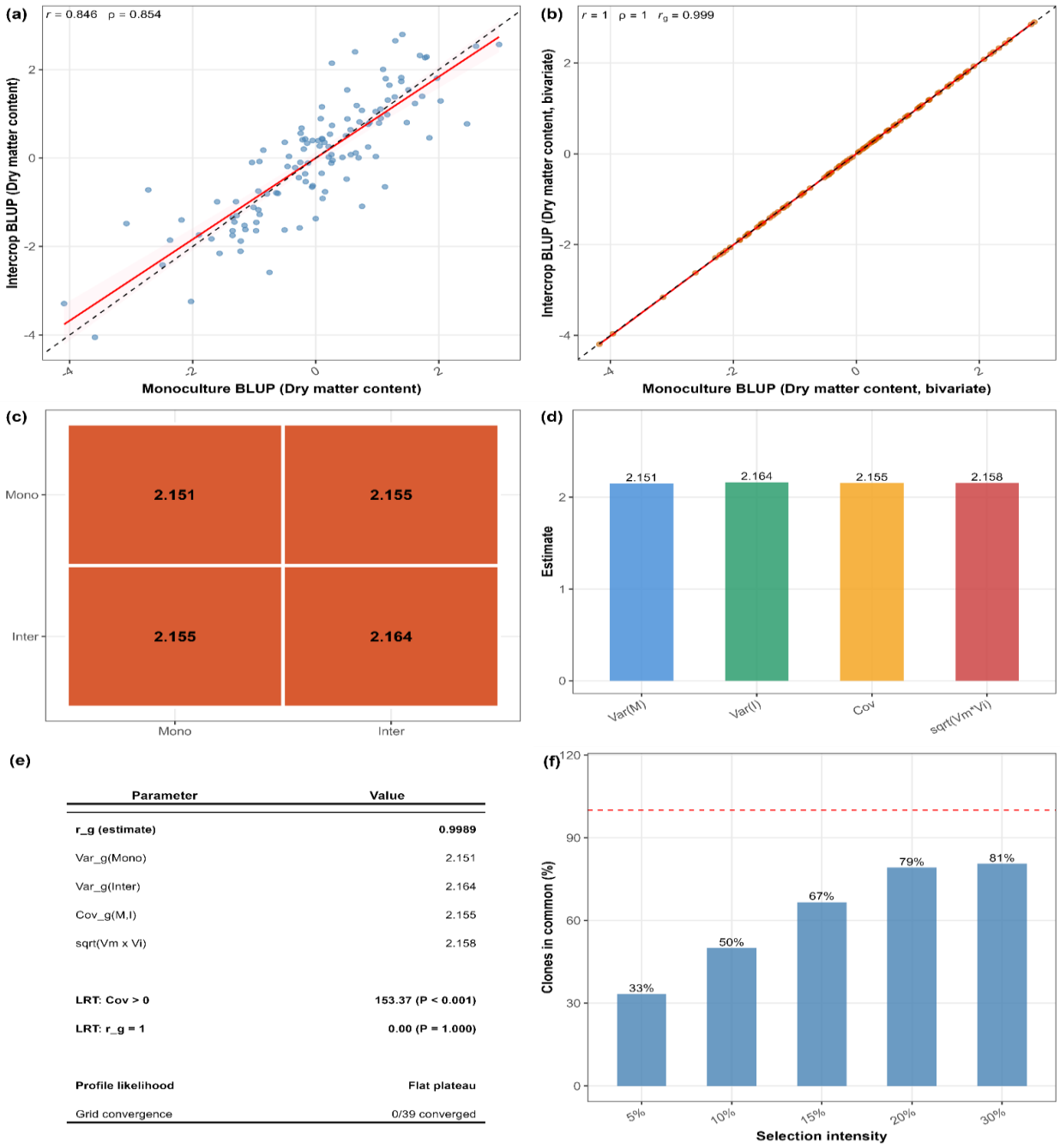

Figure 3.7. Bivariate genetic correlation diagnostic for Dry matter content (combined years, 120 clones).

(a) Clone BLUPs from separate univariate models; r and rho are Pearson and Spearman correlations. (b) Clone BLUPs from the bivariate corh model (c) Genetic variance-covariance matrix (d) Variance component comparison (e) Model summary (f) Selection overlap at varying intensities

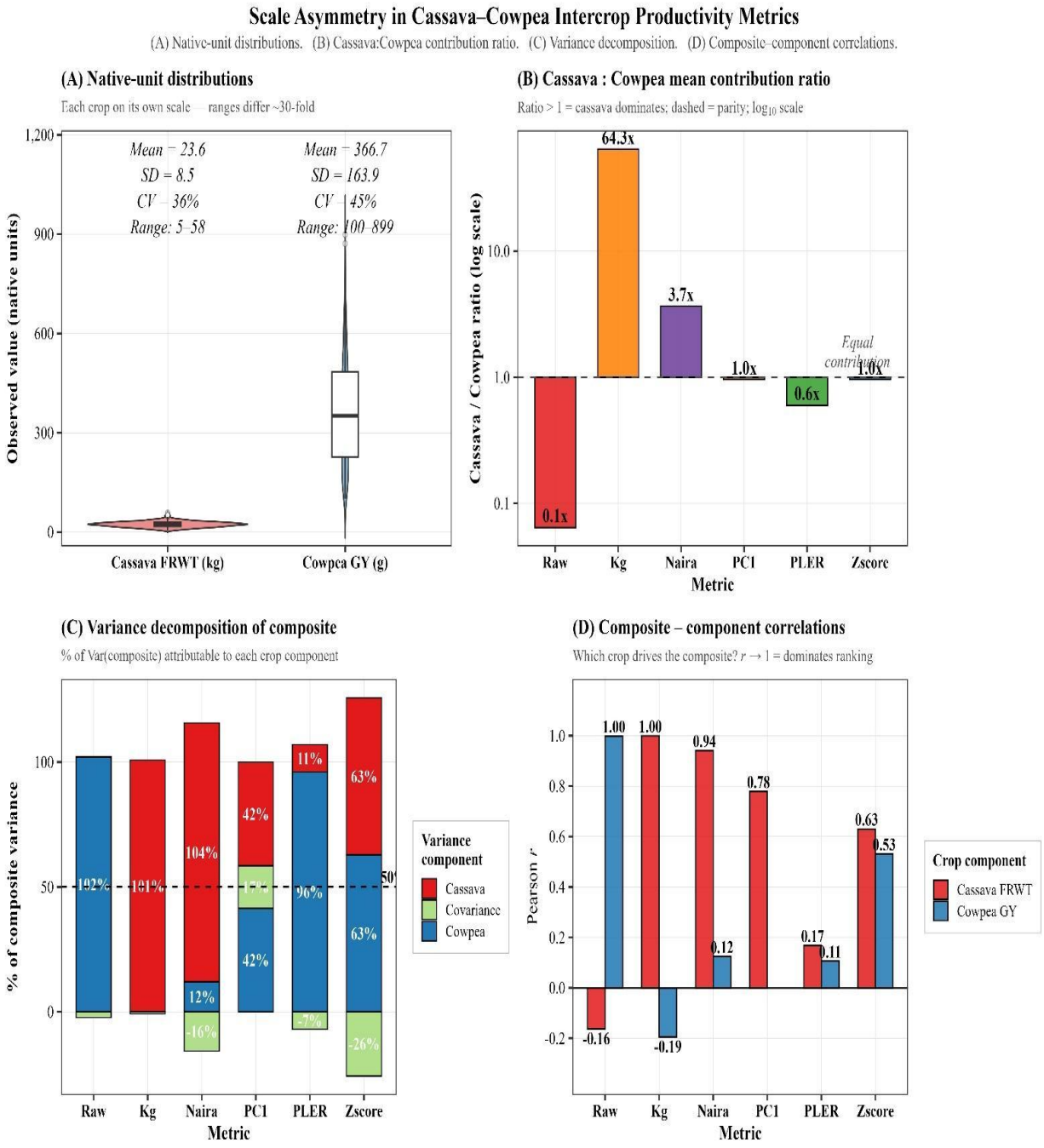

Figure 3.8. Diagnostic decomposition of six total-yield metrics for cassava–cowpea intercrop across four analytical dimensions.

(A) Native-unit distributions of cassava fresh root weight and cowpea grain yield. (B) Cassava-to-cowpea mean contribution ratio (log_{10} scale) per metric; dashed line = equal contribution (1.0×). (C) Variance decomposition showing the percentage of composite metric variance attributable to cassava (red), cowpea (blue), and their covariance (green). (D) Pearson correlations between each composite metric and its two component yields. FRWT = fresh root weight; GY = grain yield; PLER = partial land equivalent ratio; PC1 = first principal component.

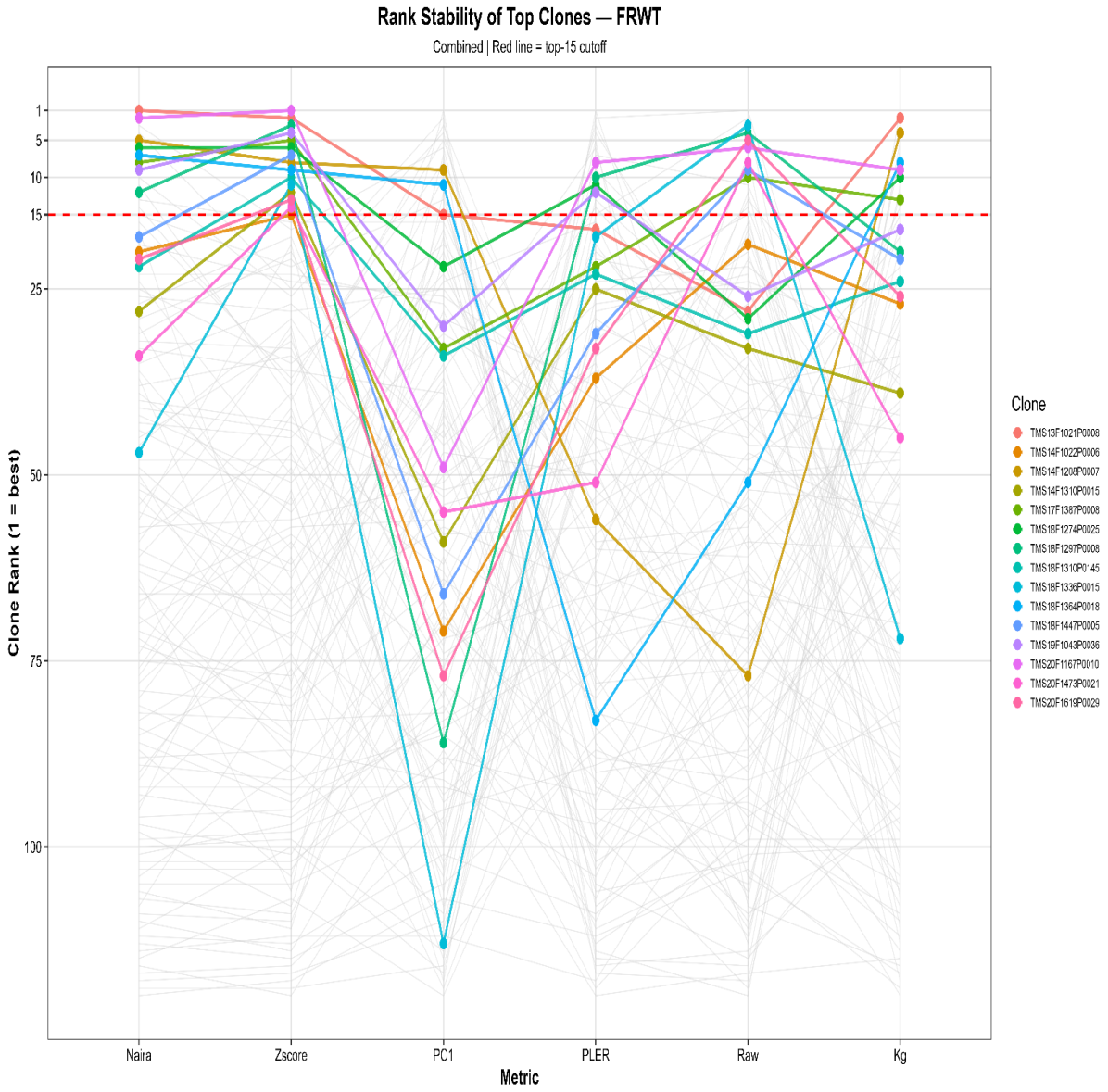

Figure 3.9. Rank shifts of cassava clone GMA across six total-yield metrics for fresh root weight (FRWT) in the combined-year analysis.

Each colored point represents a single cassava clone, and grey lines trace its rank across the six candidate metrics: Naira (using market price of region where experiment was conducted), Z-score, PC1, PLER (partial land equivalent ratio), Raw summation, and Kg (conversion of grain yield from grams to kilograms). The red dashed line marks the top 15 selection threshold.

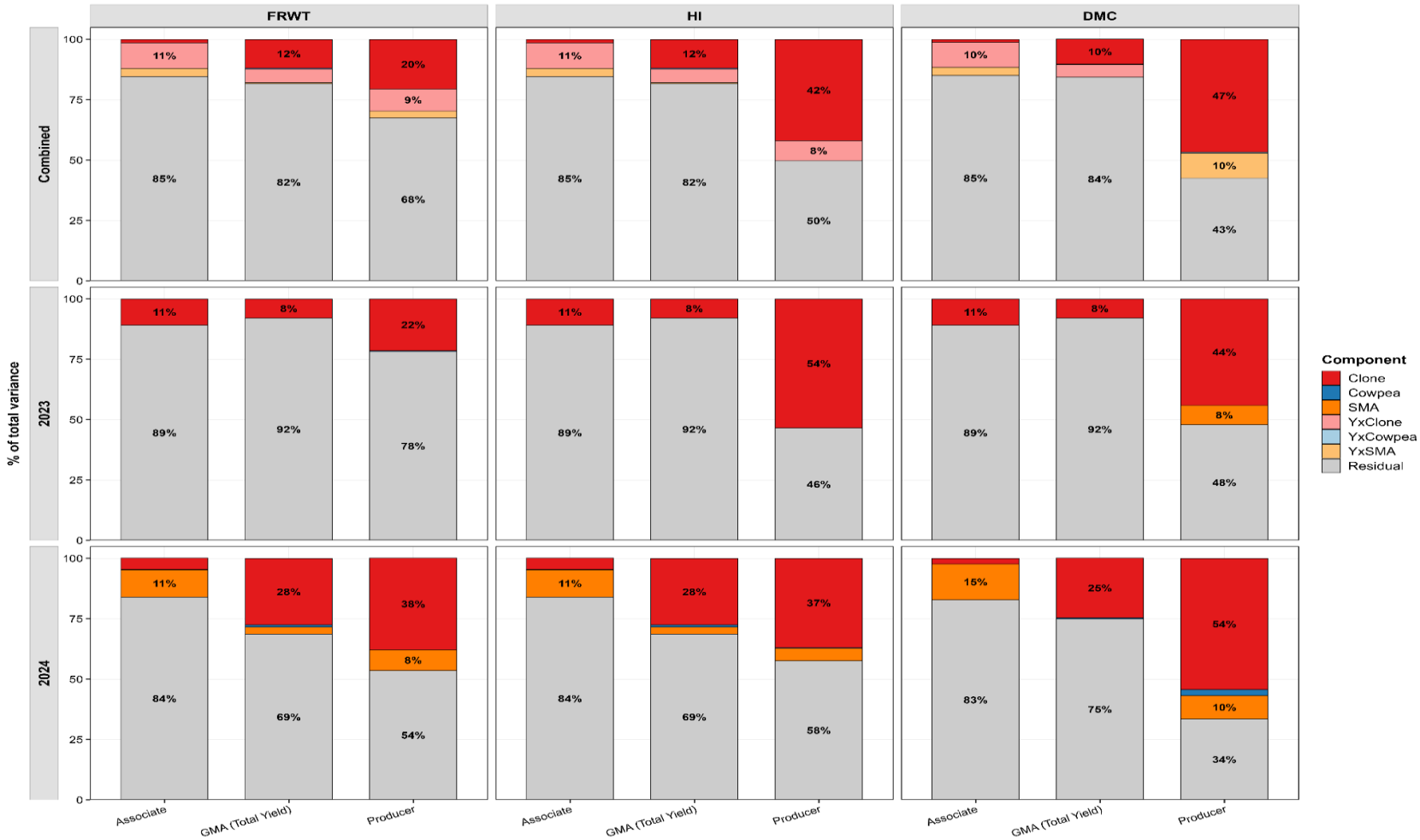

Figure 3.10. Variance component partitioning for cassava–cowpea intercrop models using within-year z-scored traits.

Stacked bars show variance components from mixed models fitted to (i) cassava producer effect (ii) cowpea associate effect (iii) total intercrop yield (Total_Yield_z; GMA/SMA model). Variance components include clone (GMA), cowpea main effect, clone × cowpea interaction (SMA), year interactions, replication within year, and residual variance.

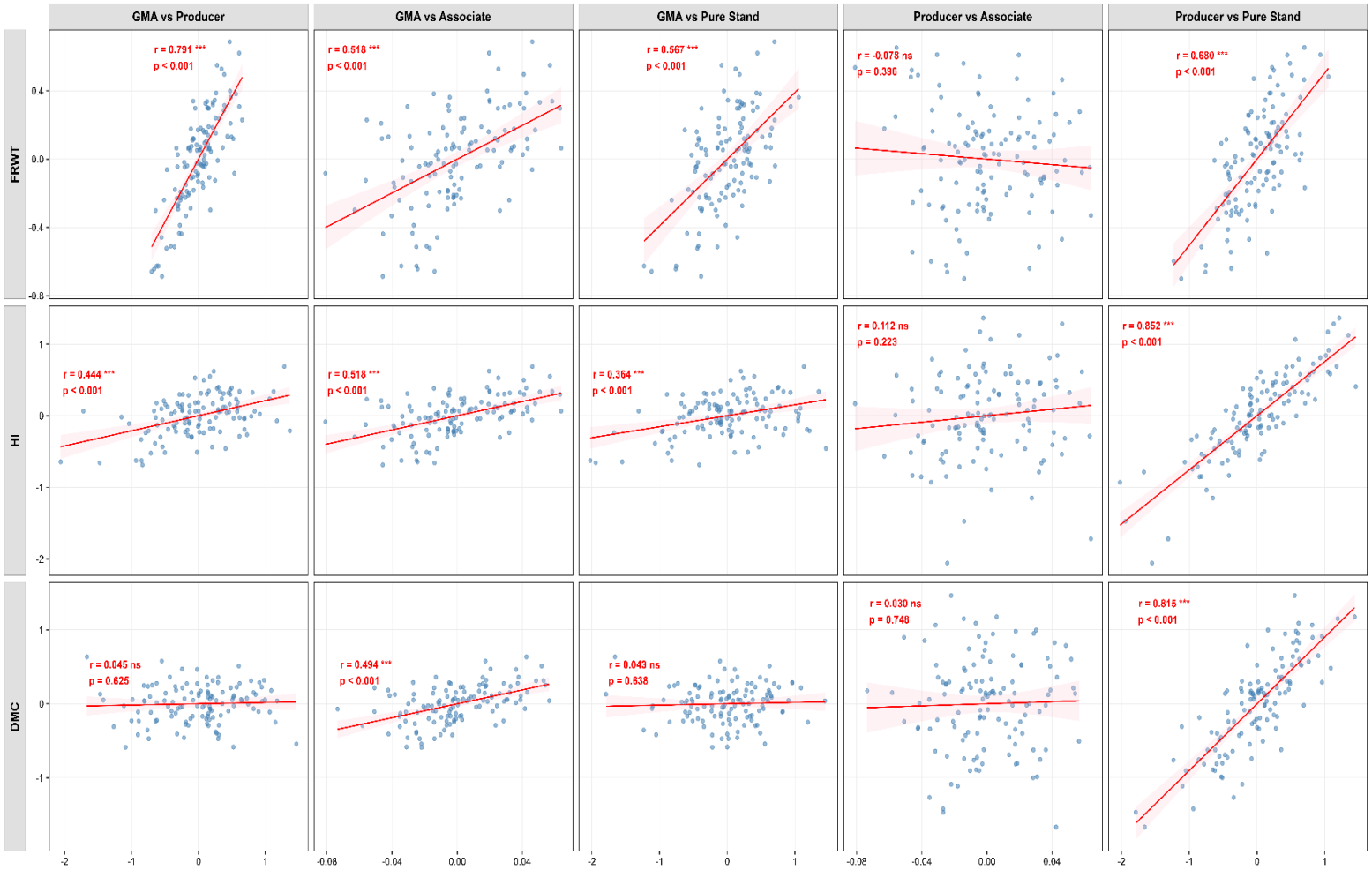

Figure 3.11. Relationships among general mixing ability (GMA), producer and associate effects, and pure stand performance in cassava–cowpea intercrop (z-scored scale) from Combined Years analysis.

Pairwise correlations among clone BLUPs derived from mixed models fitted to total intercrop yield (GMA; Total_Yield_z, HI and DMC), cassava producer effect (rtwt_z, HI and DMC), cowpea associate effect (GrainYld_z), and cassava pure stand yield (rtwt_z, HI and DMC).

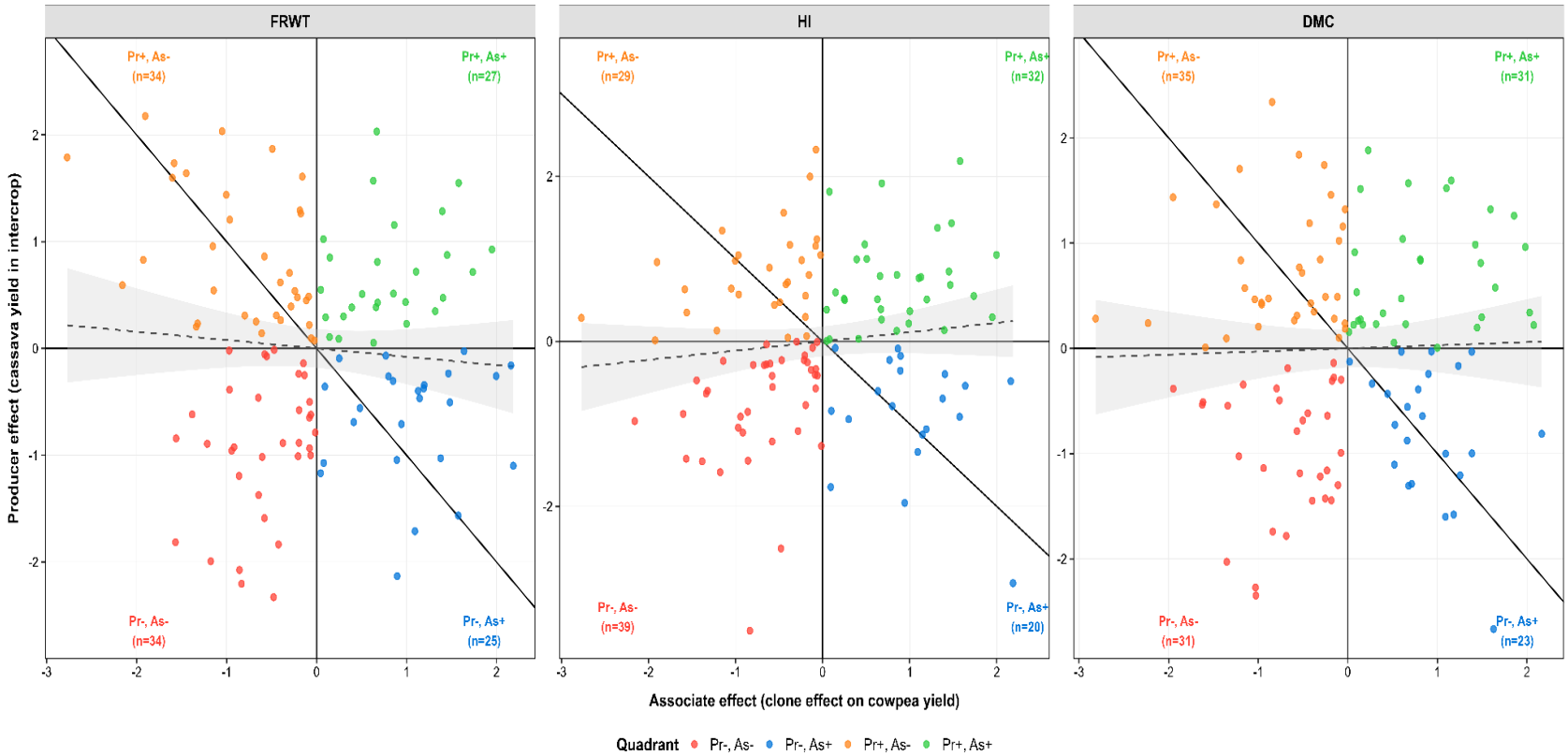

Figure 3.12. Producer and associate effects of 120 cassava clones for fresh root weight (FRWT), harvest index (HI), and root dry matter content (DMC) from the combined-year analysis.

Producer and associate effects are expressed as deviations from the population mean; zero corresponds to average performance. A negative associate effect indicates below-average, not detrimental, influence on cowpea yield. Points are colored by quadrants: green (Pr+, As+), orange (Pr+, As−), blue (Pr−, As+), red (Pr−, As−), with counts shown in each corner. The solid diagonal line represents the GMA = 0 boundary (Pr + As = 0); clones above this line have positive general mixing ability.

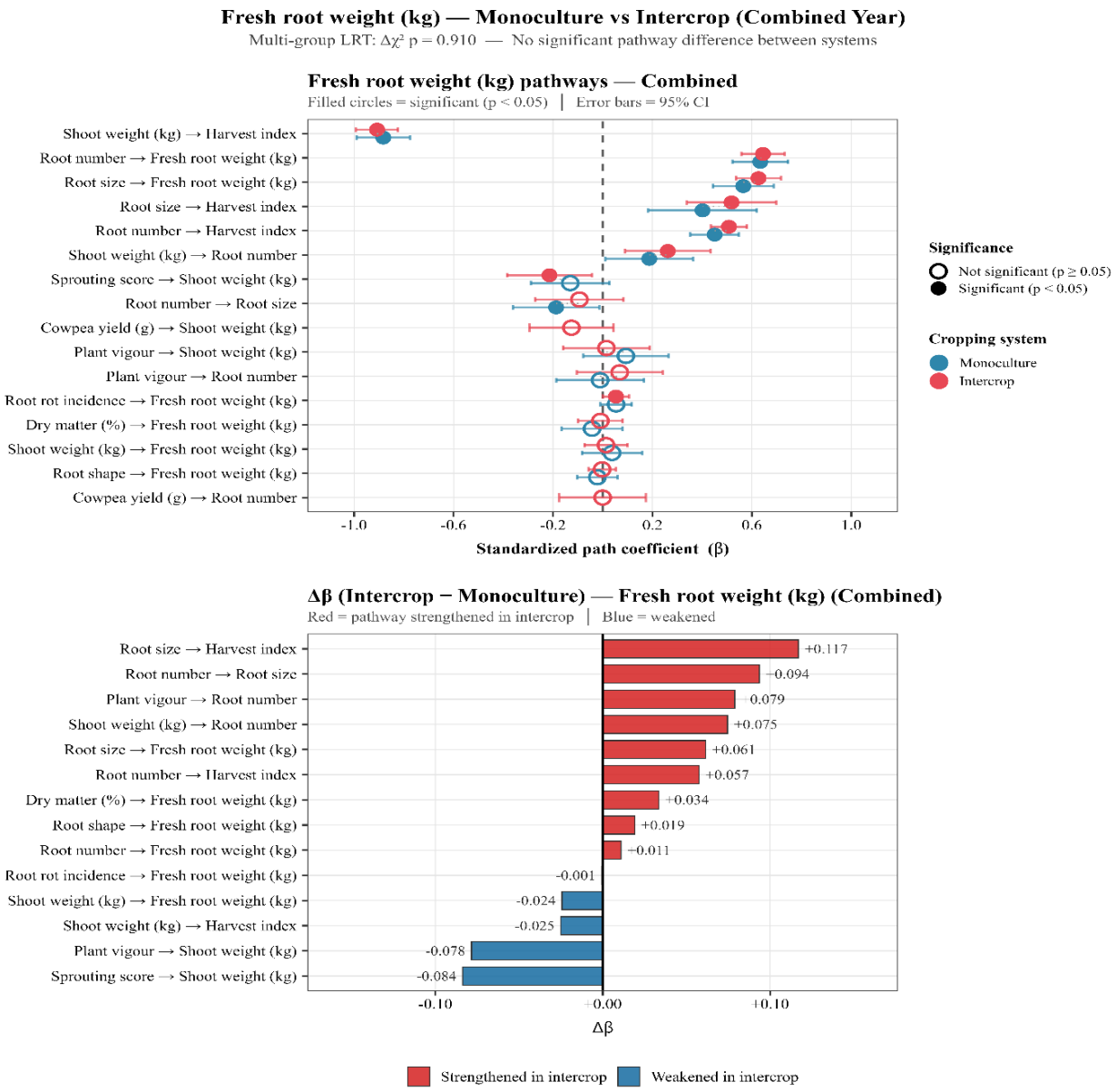

Figure 3.13. Standardized path coefficients and pathway differences between monoculture and cassava–cowpea intercrop systems for cassava fresh root weight (combined-year).

Standardized path coefficients for cassava fresh root weight under monoculture and intercropping are compared across combined years. Points and 95% confidence intervals show the strength and significance of each pathway, while the lower panel shows how pathway effects changed under intercropping. Root number and root size were the strongest direct determinants of fresh root weight, and overall pathway structure did not differ significantly between cropping systems.

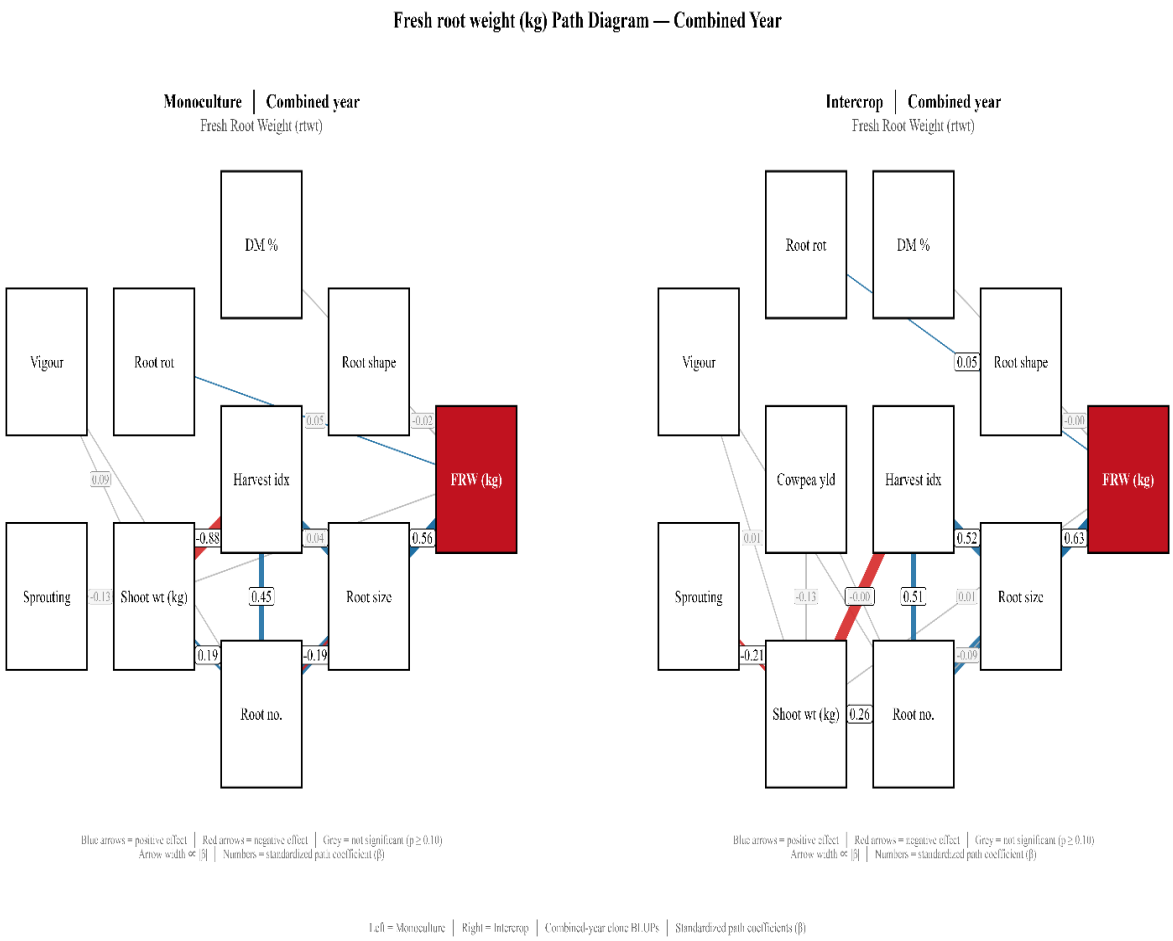

Figure 3.14. Structural equation model of cassava fresh root weight under monoculture and cassava–cowpea intercropping systems (combined-year analysis).

Structural equation models compare cassava growth and yield pathways under monoculture and cassava–cowpea intercropping across combined years. Rectangles represent measured traits, and numbered arrows show standardized path coefficients; blue indicates positive effects and red negative effects. Fresh root weight is the response variable. Root number and root size were the main yield drivers, and pathway structure was broadly similar between cropping systems.

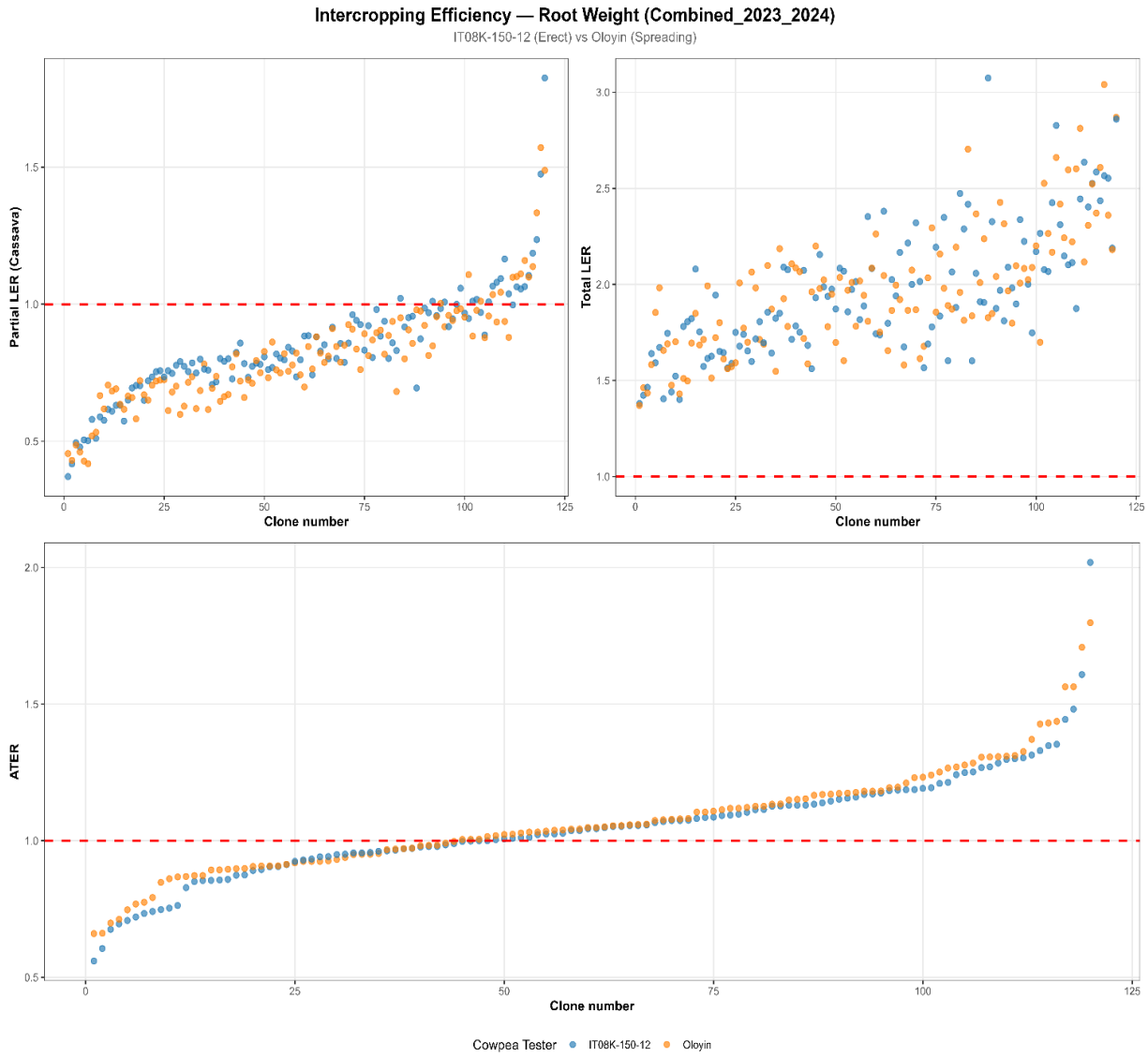

Figure 3.15. Intercropping efficiency metrics of cassava root weight across 120 clones under two cowpea testers (combined 2023–2024).

Partial land equivalent ratio (PLER; cassava component), total land equivalent ratio (LER), and area-time equivalent ratio (ATER) are shown for 120 cassava clones intercropped with two cowpea testers: IT08K-150-12 (erect) and Oloyin (spreading). Clones are ordered by increasing efficiency within panel. Red dashed lines indicate the threshold of unity (1.0), representing equivalence to monoculture performance. PLER values below 1 indicate cassava yield reduction in intercrop relative to monoculture. Total LER values above 1 indicate overall land-use advantage of the intercrop system. ATER accounts for crop duration and provides a time-adjusted measure of intercropping efficiency.

Table 3.1. Genetic variance, broad-sense heritability, and genotype × management interaction.

		Monoculture			Intercrop			G × M		G × Y		G × M × Y	
Trait	Period	Vg	H^2	Clone (Mono)	Vg	H^2	Clone (Inter)	σ^2(G×M)	P (G×M)	σ^2(G×Y)	P (G×Y)	σ^2(G×M×Y)	P (G×M×Y)
FRWT (kg)	Comb.	23.21	0.55	<0.001 ***	15.48	0.50	<0.001 ***	1.59	0.14ns	9.70	<0.001 ***	0.00	0.500 ns
	2023	13.29	0.32	0.010 **	14.39	0.36	<0.001 ***	0.04	0.48ns	0.00	NA	0.00	NA
	2024	71.26	0.72	<0.001 ***	31.71	0.64	<0.001 ***	0.00	0.45ns	0.00	NA	0.00	NA
HI	Comb.	0.01	0.81	<0.001 ***	0.04	0.73	<0.001 ***	0.00	0.36ns	0.00	0.01 *	0.001	0.34 ns
	2023	0.04	0.67	<0.001 ***	0.01	0.68	<0.001 ***	0.00	0.26ns	0.00	NA	0.00	NA
	2024	0.01	0.75	<0.001 ***	0.00	0.61	<0.001 ***	0.00	0.50ns	0.00	NA	0.00	NA
DMC (%)	Comb.	2.05	0.68	<0.001 ***	2.16	0.75	<0.001 ***	0.00	0.50ns	0.06	0.23ns	0.08	0.13 ns
	2023	3.44	0.57	<0.001 ***	3.25	0.64	<0.001 ***	0.08	0.38ns	0.00	NA	0.00	NA
	2024	2.19	0.80	<0.001 ***	1.81	0.69	<0.001 ***	0.09	0.11ns	0.00	NA	0.00	NA

* P < 0.05; ** P < 0.01; *** P < 0.001; ns, not significant. Comb. = combined years, Genetic variance (σ^2G), broad-sense heritability (H^2), G×M = genotype by management, G×Y = genotype x year, G×M×Y = genotype x management x year. Showing there is significant genetic variance for intercropping ability in cassava

Table 3.2. Cross-system genetic correlation, selection efficiency (Se%), and realized gain transfer for cassava clones evaluated under monoculture and cassava–cowpea intercropping (2023–2024).

		Heritability		Genetic cor	BLUP correlations		Se%		Realized gain (10%)			
Trait	Period	H²(M)	H²(I)	r_g	r	ρ	(10)	(33)	RG(M to I)	RG(I to M)	RG(Mn to M)	RG(Mn to I)
FRWT (kg)	Comb.	0.59	0.59	0.99	0.652 ***	0.63***	44.4	43.8	68.8	69.6	87.3	91.9
	2023	0.32	0.36	0.99	0.446 ***	0.42 ***	25.9	21.3	31.9	60.1	74.7	97.4
	2024	0.72	0.64	0.92	0.661 ***	0.63 ***	25.9	32.5	50.5	57.1	90.6	87.1
HI	Comb.	0.81	0.77	0.99	0.834 ***	0.85 ***	72.2	66.2	89.2	87.1	97.5	93.2
	2023	0.67	0.68	0.97	0.713 ***	0.72 ***	44.4	58.8	75.6	58.0	91.1	90.4
	2024	0.75	0.61	0.99	0.771 ***	0.76 ***	53.7	55.0	75.8	80.7	93.5	95.2
DMC (%)	Comb.	0.70	0.76	0.99	0.845 ***	0.85 ***	35.2	70.0	73.9	75.3	94.9	89.7
	2023	0.57	0.64	0.96	0.620 ***	0.61 ***	25.9	43.8	68.3	53.7	91.5	89.3
	2024	0.80	0.69	0.95	0.772 ***	0.80 ***	44.3	57.9	72.6	67.8	95.2	89.3

Comb. = combined year analysis, Pearson = r, Spearman = ρ, Bivariate r_g, BLUP correlations, Hamblin & Zimmermann (1986) Se%, and realized gain (RG%) at 10% and 33% selection intensities. RG(M to I) = realized gain from selecting in monoculture, testing in intercrop, as % of direct intercrop selection gain. RG(Mn) = gain from selecting on system mean.

Table 3.3. Bivariate genetic correlations (rg) between monoculture and intercrop cassava performance across four traits and three analysis periods (combined-year, 2023, 2024) to verify high rg.

Trait	Period	rg	LRT χ^2 (P)	r	ρ	Overlap 10%
shwt	Combined	1.00	−0.003‡ (1.000)	0.763	0.792	17%
	2023	0.78	0.000 (0.988)	0.537	0.599	17%
	2024	0.96	0.000 (0.993)	0.706	0.702	42%
rtno	Combined	1.00	0.003 (0.954)	0.653	0.654	42%
	2023	0.90	0.001 (0.977)	0.519	0.528	33%
	2024	0.85	0.000 (1.000)	0.581	0.556	17%
rtsz	Combined	0.88	0.000 (0.990)	0.484	0.506	33%
	2023	1.00	0.000 (0.983)	0.413	0.311	25%
	2024	0.96	0.000 (1.000)	0.464	0.438	25%
rtrot	Combined	1.00	0.002 (0.961)	0.602	0.526	58%
	2023	1.00	0.000 (0.983)	0.312	0.282	11%
	2024	0.80	0.000 (1.000)	0.373	0.393	27%

Shwt = shoot weight (kg), rtno = number of roots , rtsz = root size, rtrt = number of rotten roots, rg = genetic correlation, ‡ Negative LRT statistic: constrained model (rg = 1) marginally outperformed unconstrained model at convergence; treated as LRT = 0, Pearson = r, Spearman = ρ

Table 3.4. Evaluation of cowpea tester effects on cassava performance in the intercrop system.

		Mean		Tester diff	Heritability H^2		Exp. gain (i=1.4)		Clone×Tester	
Trait	Period	IT08K	Oloyin	P-value	IT08K	Oloyin	IT08K	Oloyin	σ^2(G×T)	P
FRWT	Combined	24.72	24.45	0.56 ns	0.45	0.487	2.31	2.72	1.50	0.18ns
	2023	23.72	22.73	0.15 ns	0.22	0.45	0.89	2.71	0.00	0.49ns
	2024	25.91	26.09	0.78 ns	0.63	0.74	4.69	6.78	7.92	0.01**
HI	Combined	0.53	0.52	0.32 ns	0.65	0.70	0.05	0.06	0.00	0.50ns
	2023	0.51	0.50	0.45 ns	0.66	0.63	0.07	0.05	0.00	0.50ns
	2024	0.55	0.54	0.42 ns	0.64	0.58	0.06	0.05	0.04	0.10ns
DMC	Combined	32.33	32.60	0.02 *	0.67	0.67	1.44	1.32	0.00	0.49 ns
	2023	34.76	34.81	0.78 ns	0.68	0.69	1.86	1.77	0.41	0.09ns
	2024	29.99	30.34	0.02 *	0.66	0.76	1.27	1.47	0.00	0.49ns

cassava means under two cowpea testers (IT08K = IT08K-150-12 and Oloyin), Wald F-tests for tester effects, broad-sense heritability (H^2), expected selection gain ($R = i \cdot H^2 \cdot \sigma g$; selection intensity i = 1.4 ≈ top 10%), and clone × tester interaction for fresh root weight (FRWT, kg plot^{-1}), harvest index, and root dry matter content (DMC, %). Results are presented for combined years (2023–2024) and individual years. Clone × tester interaction was tested using likelihood ratio tests (LRT) with the $0.5 \times \chi^2(1)$ boundary correction appropriate for variance components. Predicted means represent model-adjusted estimates from mixed models fitted with AR1×AR1 spatial residual structure and plant stand covariates. Significance codes: ns = not significant; * P < 0.05; ** P < 0.01; *** P < 0.001.

Table 3.5. Summary of tester performance and validation metrics for cassava evaluation across two years.

		Tester performance						System validation	
Trait	Tester	Mean	σ²g	CVg (%)	Exp. gain	rg(mn)	rg(yr)	rg(testers)	Jaccard(20%)
FRWT	IT08K-150-12	24.72	13.63	14.7	2.30	0.93	0.74	0.99	0.45
	Oloyin	24.45	16.68	16.8	2.72	0.97	0.57	0.99	0.45
HI	IT08K-150-12	0.53	0.00	11.2	0.05	0.99	0.76	0.99	0.54
	Oloyin	0.52	0.00	11.7	0.06	0.99	0.89	0.99	0.54
DMC	IT08K-150-12	32.33	2.34	4.7	1.44	1.00	0.91	0.99	0.45
	Oloyin	32.60	1.98	4.3	1.31	0.99	0.89	0.99	0.45

Summary statistics describing cassava performance under two cowpea testers (IT08K-150-12 and Oloyin) for fresh root weight (FRWT), harvest index, and root dry matter content (DMC) in the combined analysis (2023–2024). Mn = Monoculture. Columns report predicted means, genetic variance (σ²g), coefficient of genetic variation (CVg), and expected selection gain at 10% selection intensity. System validation metrics include the genetic correlation between monoculture and intercrop performance (rg(mono)), year-to-year genetic correlation between 2023 and 2024 (rg(yr)), bivariate genetic correlation between testers (rg(testers)), and selection overlap between testers measured as the Jaccard similarity of the top 20% selected clones. These statistics assess tester equivalence, selection stability, and the reliability of intercrop evaluation for cassava breeding.

Table 3.6. Comparison of six intercrop productivity metrics for cassava fresh root weight (FRWT) across three analytical periods (2023, 2024, and combined).

Period	Metric	H^2	GMA (%)	SMA (%)	Residual	r_Pr (Pearson)	r_Pr (Spearman)	r_As (Pearson)	r_As (Spearman)
2023	Naira	0.44	16.67	0.00	83.33	0.96	0.96	-0.06	-0.08
	Zscore	0.26	7.96	0.00	92.01	0.67	0.68	0.48	0.41
	PC1	0.54	22.64	0.00	77.36	0.84	0.82	-0.77	-0.76
	PLER	0.46	15.11	0.00	82.67	0.21	0.26	0.52	0.49
	Raw	0.31	10.02	0.00	89.98	-0.25	-0.24	0.99	0.99
	Kg	0.52	21.24	0.00	78.48	1.00	1.00	-0.30	-0.29
2024	Naira	0.79	41.48	7.07	51.45	0.97	0.96	0.22	0.18
	Zscore	0.65	27.49	2.82	68.74	0.76	0.70	0.63	0.63
	PC1	0.58	8.72	16.73	74.55	-0.75	-0.73	0.58	0.57
	PLER	0.75	6.55	11.76	56.66	0.05	0.01	0.91	0.92
	Raw	0.45	6.10	10.35	83.26	0.13	0.09	0.99	0.99
	Kg	0.78	38.29	8.45	53.27	1.00	1.00	0.06	0.02
Combined	Naira	0.48	20.88	0.00	69.01	0.98	0.97	0.12	0.12
	Zscore	0.34	11.84	0.00	81.71	0.79	0.77	0.51	0.52
	PC1	0.30	10.70	0.36	73.55	0.84	0.84	-0.57	-0.49
	PLER	0.15	0.00	0.00	75.27	0.14	0.17	0.60	0.65
	Raw	0.04	1.10	0.00	82.47	0.01	0.04	0.99	0.99
	Kg	0.47	20.29	0.00	67.70	1.00	1.00	-0.07	-0.03

Comprehensive comparison of six intercrop productivity metrics for cassava fresh root weight (FRWT) across three analytical periods (2023, 2024, and combined). H^2, broad-sense heritability; GMA (%), SMA (%), Residual (%), percentage of total phenotypic variance attributable to general mixing ability, specific mixing ability, and residual error, respectively.

Table 3.7. Likelihood ratio tests for significance of random effects.

Trait	Period	Model	Effect	LRT	p	sig
FRWT	Combined	GMA	Clone	7.832	0.0026	**
	Combined	Producer	Clone	16.115	0.0000	***
	Combined	Associate	Clone	0.140	0.3542	ns
	Combined	GMA	Cowpea	0.498	0.2401	ns
	Combined	Producer	Cowpea	0.012	0.4566	ns
	Combined	Associate	Cowpea	0.000	0.4933	ns
	Combined	GMA	Clone:Cowpea	0.000	0.5000	ns
	Combined	Producer	Clone:Cowpea	0.001	0.4903	ns
	Combined	Associate	Clone:Cowpea	0.000	0.5000	ns
	Combined	GMA	YearF:Clone	1.458	0.1136	ns
	Combined	Producer	YearF:Clone	3.965	0.0232	*
	Combined	Associate	YearF:Clone	4.924	0.0132	*
	Combined	GMA	YearF:Cowpea	0.000	0.5000	ns
	Combined	Producer	YearF:Cowpea	0.001	0.4871	ns
	Combined	Associate	YearF:Cowpea	0.000	0.4937	ns
	Combined	GMA	YearF:Clone:Cowpea	0.005	0.4713	ns
	Combined	Producer	YearF:Clone:Cowpea	0.263	0.3039	ns
	Combined	Associate	YearF:Clone:Cowpea	0.354	0.2761	ns
	2023	GMA	Clone	2.950	0.0429	*
	2023	Producer	Clone	15.547	0.0000	***
	2023	Associate	Clone	5.811	0.0080	**
	2023	GMA	Cowpea	0.003	0.4795	ns
	2023	Producer	Cowpea	0.224	0.3182	ns
	2023	Associate	Cowpea	0.000	0.4977	ns

Trait	Period	Model	Effect	LRT	p	sig
	2023	GMA	Clone:Cowpea	0.000	0.4985	ns
	2023	Producer	Clone:Cowpea	0.000	0.4972	ns
	2023	Associate	Clone:Cowpea	0.000	0.4981	ns
	2024	GMA	Clone	10.126	0.0007	***
	2024	Producer	Clone	13.467	0.0001	***
	2024	Associate	Clone	0.387	0.2670	ns
	2024	GMA	Cowpea	0.643	0.2114	ns
	2024	Producer	Cowpea	0.001	0.4902	ns
	2024	Associate	Cowpea	0.030	0.4311	ns
	2024	GMA	Clone:Cowpea	0.095	0.3788	ns
	2024	Producer	Clone:Cowpea	0.803	0.1851	ns
	2024	Associate	Clone:Cowpea	1.427	0.1161	ns
	Combined	GMA	Clone	7.832	0.0026	**
	Combined	Producer	Clone	55.059	0.0000	***
	Combined	Associate	Clone	0.140	0.3542	ns
	Combined	GMA	Cowpea	0.498	0.2401	ns
	Combined	Producer	Cowpea	0.044	0.4170	ns
	Combined	Associate	Cowpea	0.000	0.4933	ns
	Combined	GMA	Clone:Cowpea	0.000	0.5000	ns
HI	Combined	Producer	Clone:Cowpea	0.000	0.5000	ns
	Combined	Associate	Clone:Cowpea	0.000	0.5000	ns
	Combined	GMA	YearF:Clone	1.458	0.1136	ns
	Combined	Producer	YearF:Clone	7.760	0.0027	**
	Combined	Associate	YearF:Clone	4.924	0.0132	*
	Combined	GMA	YearF:Cowpea	0.000	0.5000	ns
	Combined	Producer	YearF:Cowpea	0.000	0.5000	ns
	Combined	Associate	YearF:Cowpea	0.000	0.4937	ns

Trait	Period	Model	Effect	LRT	p	sig
DMC	Combined	GMA	YearF:Clone:Cowpea	0.005	0.4713	ns
	Combined	Producer	YearF:Clone:Cowpea	0.000	0.5000	ns
	Combined	Associate	YearF:Clone:Cowpea	0.354	0.2761	ns
	2023	GMA	Clone	2.950	0.0429	*
	2023	Producer	Clone	80.248	0.0000	***
	2023	Associate	Clone	5.811	0.0080	**
	2023	GMA	Cowpea	0.003	0.4795	ns
	2023	Producer	Cowpea	0.026	0.4357	ns
	2023	Associate	Cowpea	0.000	0.4977	ns
	2023	GMA	Clone:Cowpea	0.000	0.4985	ns
	2023	Producer	Clone:Cowpea	0.000	0.4985	ns
	2023	Associate	Clone:Cowpea	0.000	0.4981	ns
	2024	GMA	Clone	10.126	0.0007	***
	2024	Producer	Clone	10.649	0.0006	***
	2024	Associate	Clone	0.387	0.2670	ns
	2024	GMA	Cowpea	0.643	0.2114	ns
	2024	Producer	Cowpea	0.197	0.3284	ns
	2024	Associate	Cowpea	0.030	0.4311	ns
	2024	GMA	Clone:Cowpea	0.095	0.3788	ns
	2024	Producer	Clone:Cowpea	0.384	0.2678	ns
	2024	Associate	Clone:Cowpea	1.427	0.1161	ns
	Combined	GMA	Clone	5.996	0.0072	**
	Combined	Producer	Clone	74.587	0.0000	***
	Combined	Associate	Clone	0.106	0.3726	ns
	Combined	GMA	Cowpea	0.184	0.3338	ns
	Combined	Producer	Cowpea	0.000	0.4933	ns
	Combined	Associate	Cowpea	0.000	0.5000	ns

Trait	Period	Model	Effect	LRT	p	sig
	Combined	GMA	Clone:Cowpea	0.001	0.4903	ns
	Combined	Producer	Clone:Cowpea	0.000	0.5000	ns
	Combined	Associate	Clone:Cowpea	0.000	0.5000	ns
	Combined	GMA	YearF:Clone	1.252	0.1316	ns
	Combined	Producer	YearF:Clone	0.000	0.5000	ns
	Combined	Associate	YearF:Clone	4.248	0.0197	*
	Combined	GMA	YearF:Cowpea	0.000	0.4952	ns
	Combined	Producer	YearF:Cowpea	0.366	0.2726	ns
	Combined	Associate	YearF:Cowpea	0.000	0.5000	ns
	Combined	GMA	YearF:Clone:Cowpea	0.000	0.4946	ns
	Combined	Producer	YearF:Clone:Cowpea	3.611	0.0287	*
	Combined	Associate	YearF:Clone:Cowpea	0.319	0.2860	ns
	2023	GMA	Clone	2.950	0.0429	*
	2023	Producer	Clone	47.915	0.0000	***
	2023	Associate	Clone	5.811	0.0080	**
	2023	GMA	Cowpea	0.003	0.4795	ns
	2023	Producer	Cowpea	0.000	0.5000	ns
	2023	Associate	Cowpea	0.000	0.4977	ns
	2023	GMA	Clone:Cowpea	0.000	0.4985	ns
	2023	Producer	Clone:Cowpea	2.984	0.0420	*
	2023	Associate	Clone:Cowpea	0.000	0.4981	ns
	2024	GMA	Clone	8.813	0.0015	**
	2024	Producer	Clone	28.448	0.0000	***
	2024	Associate	Clone	0.091	0.3814	ns
	2024	GMA	Cowpea	0.126	0.3614	ns

Trait	Period	Model	Effect	LRT	p	sig
	2024	Producer	Cowpea	2.967	0.0425	*
	2024	Associate	Cowpea	0.000	0.4997	ns
	2024	GMA	Clone:Cowpea	0.000	0.4959	ns
	2024	Producer	Clone:Cowpea	1.062	0.1513	ns
	2024	Associate	Clone:Cowpea	1.755	0.0926	ns

Variance components were estimated from mixed models fitted to total intercrop yield (GMA/SMA model), cassava producer effect, and cowpea associate effect (GrainYld_z) for frsh root weight, dry matter content and harvest index. For combined-year analyses, models included clone, cowpea, clone × cowpea (SMA), and their interactions with year. Per-year models exclude year interaction terms. Significance of each variance component was assessed using likelihood ratio tests with a 50:50 mixture of χ^2_0 and χ^2_1 distributions to account for boundary constraints. Reported values include variance estimates, LRT statistics, associated p-values, and significance codes (*** $p < 0.001$; ** $p < 0.01$; * $p < 0.05$; NS $p \geq 0.05$).

Table 3.8. Broad-sense heritability estimates across mixture and monocrop models, traits, and periods.

Trait	Period	n	H2_PS	H2_GMA	H2_Pr	H2_As
	Combined	120	0.585	0.341	0.471	0.046
FRWT	2023	120	0.324	0.148	0.358	0.196
	2024	118	0.723	0.476	0.634	0.276
	Combined	120	0.811	0.341	0.717	0.046
HI	2023	120	0.670	0.148	0.697	0.196
	2024	118	0.750	0.476	0.595	0.276
	Combined	120	0.715	0.309	0.745	0.042
DMC	2023	120	0.568	0.148	0.685	0.196
	2024	115	0.802	0.400	0.799	0.292

Table 3.9. Multi-group SEM LRT, Fresh root weight (kg) pathway.

Period	χ²_config	df_config	χ²_const	df_const	Delta_χ²	Delta_df	p_value	CFI_config	RMSEA_config	SRMR_config
Combined	129.51	38	137.09	52	7.58	14	0.91	0.919	0.142	0.110
2023	69.48	38	80.97	52	11.48	14	0.64	0.966	0.083	0.069
2024	163.79	38	180.92	52	17.13	14	0.24	0.873	0.167	0.120

SEM = structural equation modeling; LRT = likelihood ratio test; χ²_config = chi square statistic for the configural model; df_config = degrees of freedom for the configural model; χ²_const = chi square statistic for the constrained model; df_const = degrees of freedom for the constrained model; Δχ² = difference in chi square between the constrained and configural models; Δdf = difference in degrees of freedom; CFI = comparative fit index; RMSEA = root mean square error of approximation; SRMR = standardized root mean square residual. In the configural model, regression paths were freely estimated for each cropping system. In the constrained model, all regression paths were specified as equal across cropping systems. A significant Δχ² test at $p < 0.05$ indicates that the pathways differ between monoculture and intercrop. A nonsignificant result indicates insufficient evidence that the pathways differ.

Chapter 4 Genetic Architecture of Root Traits Linked to Ecosystem Services and Genomic Prediction of an Ecosystem Service Index in Dual-Purpose White Lupin

Abstract

Agricultural systems in the southeastern United States are constrained by nutrient losses during winter fallow periods that contribute to downstream water quality degradation, and by strong soil phosphorus fixation that reduces plant-available phosphorus. Cover crops can mitigate these losses, but adoption remains limited due to the absence of direct economic returns. White lupin (Lupinus albus L.) offers a unique dual-purpose solution: it delivers ecosystem services as a cover crop through cluster root-mediated phosphorus mobilization and nitrogen fixation while providing marketable grain and forage. However, the genetic basis of root traits driving these ecosystem functions remains poorly understood.

232 white lupin (WL) accessions were evaluated across two field seasons using shovelomics and the RhizoVision Explorer imaging system to quantify root crown traits, coupled with genome-wide association studies (GWAS) using 174,284 SNPs. An Alabama Ecosystem Service Index (AESI) was developed to integrate root traits and grain yield into a unified selection framework.

Root traits showed moderate heritability but pronounced year-to-year instability, indicating strong environmental sensitivity in root system expression. Genetic correlations revealed a consistent trade-off between root exploration traits relevant to ecosystem service delivery and yield traits, such that the traits most valuable for

phosphorus mobilization were also those most negatively associated with yield. GWAS detected no genome-wide significant loci for AESI in either year, consistent with a polygenic architecture in which no single locus exerts a detectable major effect. Genomic prediction accuracy for AESI using the full marker panel was low (r = 0.18), indicating that current sample size and marker density are insufficient to fully capture this distributed genetic architecture. However, AESI rankings were stable across weighting perturbations and identified genotypes combining ecosystem service potential with competitive yield, demonstrating that selection need not treat root exploration and grain production as mutually exclusive breeding objectives.

These results support index-based selection as a practical near-term strategy for dual-purpose white lupin breeding, with genomic selection offering a longer-term path for capturing distributed genetic architecture as training populations expand.

4.1 Introduction

Agriculture is a major source of nonpoint-source pollution, with nitrogen and phosphorus losses driving eutrophication, algal blooms, and water quality impairment in approximately 40% of water bodies (Daniel et al., 1994; USEPA, 2002; Omernik et al., 2016; Prasad & Chakraborty, 2024). Also, in Alabama, highly weathered Ultisols with low organic matter and strong phosphorus fixation produce soils rich in total phosphorus but deficient in plant-available forms (Shaw et al., 2002; Ye et al., 2020; Waldrip et al., 2023). Within the USDA–NRCS "avoid, control, and trap" framework (Osmond et al., 2015), well-rooted cover crops offer a practical strategy to trap nutrients in biomass, reduce runoff, and improve soil structure.

Despite cover crops' capacity to deliver critically needed ecosystem services, such as erosion and nonpoint-source pollution reduction, adoption remains limited due to economic constraints, as they incur costs without direct market returns (Roesch-McNally et al., 2018; Gamble, 2020; Griffiths et al., 2022; SARE/CTIC, 2023). This highlights the need for finding cash cover crops that provide both economic and ecological benefits.

Winter-type white lupin (WL; Lupinus albus L., 2n = 50, 451Mb; Zhang et al., 2020) addresses this gap as a dual-purpose annual legume that delivers both ecosystem services and economic return. Unlike conventional cover crops, it produces a high-value grain (28–44% protein, 8–14% oil, 30–40% fiber) for food, feed, and nutraceutical uses (Sujak et al., 2006) and high-quality forage comparable with alfalfa (Bhardwaj et al., 2010). It also fixes atmospheric nitrogen via Bradyrhizobium symbiosis reducing fertilizer requirements (Lambers et al., 2013). WL is the only widely cultivated annual grain legume with a demonstrated capacity to form cluster (proteoid) roots that mobilize otherwise unavailable soil phosphorus (Lambers et al., 2013; Zhang et al., 2020). This capacity is uniquely valuable in Alabama's phosphorus-fixing soils and can enhance phosphorus availability to neighboring crops, extending its ecological benefit beyond the immediate season (Hori et al., 2015; Cu et al., 2005).

Variation in root system architecture directly links plant phenotypes to ecosystem functioning by regulating nutrients and carbon cycling and contributing to the formation and stabilization of soil structure (Prieto et al., 2012; Dignac et al., 2017; Freschet et al., 2017; Freschet et al., 2021). Because ecosystem functions such as phosphorus mobilization, leaching reduction, and erosion control are not easily measured directly at

field breeding scale, root morphological traits can serve as practical proxies for selection toward these outcomes (Henneron et al., 2020; Freschet et al., 2021). Freschet et al. (2021) proposed that establishing causal hierarchies among root traits provides a hypothesis-driven framework to identify parsimonious trait sets linking genotypes to plant and ecosystem function; accordingly, guided by ecosystem service needs in Alabama, this study evaluated root crown traits using RhizoVision Explorer and derived metrics to define a minimal set of traits for selecting WL genotypes with enhanced ecosystem service function. However, how trait combinations collectively determine ecosystem service potential, and efficient selection strategies, remains a challenge in breeding contexts where traits may be antagonistic or functionally redundant (Griffiths et al., 2021; Griffin et al., 2025).

Phenotyping root systems at breeding scale has historically been a bottleneck. Shovelomics is a high-throughput field phenotyping method that characterizes root architectural traits by excavating, washing, and analyzing root crowns (Trachsel et al., 2011). Combined with automated image analysis platforms, shovelomics is enabling scalable characterization of root system architecture across large germplasm collections (Trachsel et al., 2011; Burridge et al., 2016). The RhizoVision Explorer platform improves throughput and reproducibility by enabling automated extraction of quantitative root traits from large image datasets, with demonstrated utility in genetic mapping and breeding (Seethepalli et al., 2020; Seethepalli et al., 2021; Martin et al., 2022). Despite this progress, the heritability, genetic correlations with yield, and genomic architecture of root traits in WL remain uncharacterized, limiting selection for

varieties with root morphology enhanced for ecosystem service delivery (Griffiths et al., 2021; Brummer et al., 2021; Bagale et al., 2025).

Breeding for dual-purpose white lupin requires simultaneous improvement of grain/forage yield and belowground traits linked to ecosystem service delivery. The use of selection indices (Céron-Rojas & Crossa, 2022) offers a quantitative framework for integrating correlated traits into a unified selection criterion, and have been proposed as a route to operationalize ecosystem service breeding objectives in cover crops, where direct measurement of ecosystem function at field scale is impractical (Freschet et al., 2021; Griffiths et al., 2022). Here, the Alabama Ecosystem Service Index (AESI) was developed to quantify the combined genetic merit of WL genotypes for root traits associated with key ecosystem services in Alabama alongside grain yield. Assessing the performance of the AESI, and its agreement with phenotypic and genomic data, is critical to establish its utility for dual-purpose breeding.

Genome-wide association studies (GWAS) have identified loci for root traits, including deep root mass and root length (Shen et al., 2001; Steele et al., 2006) in rice. These architectural root traits usually involve the collective action of many genes governing cell division, elongation, branching, and response to soil heterogeneity (Bray & Topp, 2018), and are expected to show a polygenic architecture in which individual loci contribute small, often undetectable effects (Boyle et al., 2017). Composite traits that integrate multiple correlated root and yield components, such as the AESI, are likely to compound this polygenicity, since the genetic signal underlying the index reflects the combined architecture of its component traits rather than a small number of major loci.

This study addressed the identified gaps discussed above by integrating high-through-put phenotyping (HTP) and genomic analysis of root crown trait variation in WL under Alabama field conditions. The objectives of this study were to: (1) evaluate the shovelomics–RhizoVision Explorer pipeline and estimate broad-sense heritability of root and yield traits; (2) quantify phenotypic and genetic correlations between root traits and yield components; (3) identify genomic regions associated with root traits, yield components, and AESI using GWAS and (4) develop and evaluate the AESI as an integrated selection criterion for dual-purpose WL improvement.

4. 2 Materials and Methods

4.2.1 Experimental sites and design

Field experiments were conducted during two consecutive growing seasons (2023 to 2024 and 2024 to 2025) at the Alabama Agricultural Experiment Station E.V. Smith Research Center, Plant Breeding Unit (PBU), Tallassee Alabama (32.49°N, 85.89°W) on a Wickham sandy loam soil. In both years, experiments were arranged in a row-column design with two replications laid out in a 20 × 20 row-column grid. Each plot consisted of two rows, 15 feet (4.57 m) long on raised ridges. Daily weather data was retrieved from NASA POWER using the EnvRtype R package and summarized by growing season (Figure 5.1).

4.2.2 Genetic materials and panel development

A total of 441 WL accessions, comprising advanced breeding lines from the Auburn University program and plant introductions from the USDA National Plant Germplasm System (NPGS), were planted in fall 2022 at the E.V. Smith Research

Station's Plant Breeding Subunit (PBU) in Tallassee, Alabama. 354 accessions survived winter freeze and were genotyped. These 354 accessions represented the AU germplasm and were reported to describe the population structure of the entire germplasm. Based on field performance, a subset of 200 accessions was selected for evaluation in the 2023–2024 field trial (Year 1), and a subsequent selection of 200 accessions was advanced to the 2024–2025 trial (Year 2). Across both years, 168 accessions were common to both trials and 32 were unique to each year, hence a total of 232 unique accessions were evaluated for the two-year experiment. Population structure analyses used the full set of 354 genotyped accessions, while GWAS, and all phenotype-based analyses were conducted on the 232-accession subset.

4.2.3 Agronomic traits

Alkaloid content was assessed at flowering using a Dragendorff spot test (Raffauf, 1962) where fresh flower tissue sap was spotted onto filter paper, and development of a reddish-orange color indicated alkaloid presence, scored as a binary variable (1 = present, 0 = absent) from five independent tests per plot. At maturity, grain yield was harvested using an Almaco R1 plot combine and expressed in kg ha^{-1}. Hundred-seed weight (HSW) was subsequently determined from a random subsample of 100 seeds using a seed counter and analytical balance.

4.2.4 Root crown traits

Root crowns were excavated at pod maturity from five plants per plot, using the shovelomics protocol (Trachsel et al., 2011; Burridge et al., 2016), cleaned, and imaged using a custom RhizoBox system equipped with five synchronized monochrome cameras capturing multi-angle silhouettes under controlled LED illumination (Figure

5.2). Images were processed using RhizoVision Explorer (RVE) version 2.0.3 (Seethepalli et al., 2021) with standardized batch parameters applied consistently across both years (Table 5.1). Plot-level trait values were computed by statistical aggregation across the five camera angles following Seethepalli et al. (2024). To complement primary RVE metrics, additional traits identified in the literature as relevant to root ecosystem service function, summarizing depth allocation, foraging geometry, branching, diameter structure and efficiency, were computed from RVE outputs. Full trait names, formulas, and definitions are provided in Table 5.2.

4.2.5 Variance component and heritability

Variance components, heritability, BLUPs and BLUEs were estimated for all traits using ASReml-R version 4.2 (Butler et al., 2017). Analyses were conducted both across years (combined-year) and within each year (per-year). The following mixed-model was fitted for each trait:

$$y_{ijkl} = \mu + f(cov) + Y_j + R_{k(j)} + G_i + (GY)_{ij} + s_{jl} + \varepsilon_{ijkl} \quad (5.1)$$

where $y_{ijkl}$is the observed phenotype; μ is the intercept; $f(cov)$is a fixed covariate for the number of harvested plants per plot applied only to grain yield; $Y_j$is the fixed effect of year; $R_{k(j)}$is the random effect of replication nested within year; $G_i$is the genotype (accession) effect; $(GY)_{ij}$ is the genotype-by-year interaction; s_{jl}represents spatial variation modeled as separable first-order autoregressive structure AR1(row) × AR1(column) within year; and $\varepsilon_{ijkl}$is the residual error. For per-year analyses, $Y_j$and $(GY)_{ij}$were excluded.

Genotype was modeled as a random effect for estimation of variance components, heritability, and to obtain BLUPs used for AESI selection index construction, and as a

fixed effect for estimation of genotype means (BLUEs), while retaining the same model structure and spatial correction.

Eight root traits exhibiting right-skewed distributions were log-transformed prior to analysis. Summary statistics are reported on the original scale. Alkaloid content was analyzed as a binary trait using a generalized linear mixed model with a logit link, with residual variance fixed at $\pi^2/3$ and heritability interpreted on the latent scale.

Broad-sense heritability was estimated on an entry-mean basis as:

$$H^2 = \frac{\sigma_G^2}{\sigma_G^2 + \frac{\sigma_{GY}^2}{Y} + \frac{\sigma_E^2}{YR}} \quad (5.2)$$

where $Y = 2$ years and $R = 2$ replicates. For per-year analyses, the genotype-by-year component was excluded. Cullis heritability was computed from the mean prediction error variance of BLUP differences (Cullis et al., 2006), and Piepho heritability from the variance of genotype BLUEs and their associated standard errors (Piepho & Möhring, 2007).

Variance component significance was assessed using likelihood ratio tests comparing full and reduced models. Standard errors for heritability estimates were obtained from 200 bootstrap resamples stratified within year-by-replication, with models refitted for each resample. Genomic heritability was estimated by replacing the identity matrix with a genomic relationship matrix following VanRaden (2008), while retaining the same model structure. BLUEs from the fixed-effect model were used in all downstream analyses.

4.2.6 Phenotypic and genetic correlation

Phenotypic correlations between agronomic and root crown traits were computed as Pearson correlations on combined-year BLUEs across all traits.

Genetic correlations (rG) were estimated using bivariate linear mixed models:

$$[y(A)ijk, y(R)ijk]T = \mu + f(cov) + Yj + Rk(j) + Gi + (GY)ij + sj + \varepsilon ijk \quad 5.3$$

where y(A) and y(R) are the agronomic and root crown traits, respectively, and all other terms are as defined in Section 4.2.4.1. A plant-stand covariate was included for trait pairs involving grain yield. Genetic correlation was modeled as an unstructured matrix (corgh (accession)). Significance of rG was assessed by likelihood ratio tests against an idh (accession) baseline, with p-values adjusted by the Benjamini–Hochberg procedure at a false discovery rate of 0.05 (Benjamini & Hochberg, 1995).

4.2.7 Genotyping and SNP Data

Genomic DNA from 354 white lupin accessions, comprising the 232 accessions phenotyped in this study and an additional 122 germplasm accessions assembled for broader diversity characterization, was sequenced at the Hudson Alpha Institute for Biotechnology using low-pass whole-genome sequencing (~3× coverage). Reads were aligned to the reference genome of Hufnagel et al. (2020), and SNPs were called and imputed using the KHUFU platform (Korani et al., 2021). After quality control (MAF ≥ 0.05, heterozygosity ≤ 0.15, missingness ≤ 0.10), 174,284 high-quality SNPs were retained. Population structure analyses used the full 354-accession panel to enable characterization of all accessions in the germplasm, while GWAS and downstream genomic analyses used the same SNP set restricted to the 232 phenotyped accessions.

4.2.8 Population structure, genetic relationships, and phenotypic structure

Population structure was inferred from the 354-accession panel using ADMIXTURE v1.3.0 (Alexander et al., 2009). Markers were LD-pruned in PLINK (window = 50, step = 10, $r^2 = 0.1$) prior to analysis, and ADMIXTURE was run for K = 2 to 10 with 10-fold cross-validation; K = 5 minimized CV error. Genetic relationships were visualized as a midpoint-rooted neighbor-joining tree of pairwise Euclidean distances on standardized genotypes, with tips colored by continent of origin, improvement level, and source (Auburn University vs. NPGS). Phenotypic structure was independently assessed by principal component analysis (prcomp, centered and scaled) on combined-year and per-year BLUEs of the 22 traits for the 232 phenotyped accessions.

4.2.9 Genome-wide association analysis

Genome-wide association analysis was performed using the GAPIT3 package in R (Wang and Zhang, 2021), applying three models: mixed linear model (MLM), FarmCPU, and BLINK, to all traits across three analytical scopes: combined-year BLUEs (2023–2024), 2023, and 2024. Analyses used the SNP dataset described above. Significance thresholds were derived from SNP count: a Bonferroni threshold of $p < 0.05/n$, where n is the number of SNPs tested. The genomic inflation factor (λ) was computed per trait–model combination, and Benjamini–Hochberg FDR correction was applied within each trait–model at a false discovery rate of 0.05. Significant loci were retained for downstream annotation.

4.2.10 Alabama Ecosystem Service Index (AESI): construction and genomic prediction

The AESI was constructed from combined-year scaled and centered BLUPs of 11 traits retained from the 22 phenotyped traits after heritability filtering ($H2 \geq 0.10$; grain

yield (GY_KgHa) was retained a priori as the primary economic driver of dual-purpose adoption despite falling marginally below threshold; four traits with zero genetic variance were excluded) and Ward's clustering on (1 − |r|) cut at 0.30 was applied to remove redundancy among collinear traits. Retained traits were assigned to four ecosystem services with literature-grounded a priori weights summing to unity (P mobilization 0.35; erosion control 0.25; soil organic matter 0.20; dual-purpose yield 0.20; Table 5.3); economic weights were not applied because WL lacks established commercial production in the southeastern United States and several index components (e.g., soil retention, P mobilization) lack defensible market prices. Within services, traits were equally weighted to avoid arbitrary differentiation among collinear root metrics; Alkaloid and median_diameter were treated as penalty traits via sign inversion after standardization (Table 5.3), reflecting penalty direction. AESI was computed for the 168 accessions overlapping both years as: $AESI = \sum_{s=1}^{4} w_s \cdot \bar{z}^*_{ts}$ where z^*_{ts} denotes the direction-corrected z-scored BLUPs of trait t within service s and ws is the service weight. A dual-purpose composite, Final Index = 0.6 · z(GY_KgHa) + 0.4 · AESI, ranked elite candidates, and median splits on (AESI, GY_KgHa) classified accessions into four ideotype quadrants. Robustness of AESI rankings was validated by ±20% per-service weight perturbations (stability defined as Spearman $r \geq 0.90$ relative to the base ranking) and by 2023 versus 2024 rank stability, benchmarked against per-trait stability of the 11 components.

AESI was further treated as a phenotype and analyzed through the GAPIT described in Sections 4.2.9. Genomic prediction of AESI was evaluated using GBLUP implemented via the rrBLUP R package, with the genomic relationship matrix computed

following VanRaden (2008) using 174,284 markers. Two prediction frameworks were applied. First, temporal cross-validation assessed breeding-scenario accuracy: GBLUP was trained on 2023 AESI and used to predict 2024 AESI (forward), and vice versa (backward), for accessions with phenotypes in both years (n = 168). Second, combined-year cross-validation assessed within-dataset prediction accuracy on combined-year AESI BLUEs using 5-fold CV (20 repetitions). Selection concordance was quantified as the proportion of genomically selected accessions (top and bottom 5-30%) that matched observed rankings in the prediction year.

4.3 Results

4.3.1 Phenotypic variation, heritability, and genomic capture of trait variance

The shovelomics–RhizoVision pipeline detected substantial phenotypic variation among the tested WL accessions for root crown traits across both years (Table 5.4). Mean root architectural traits differed between years, with Average_hole_size decreasing from 22.78 in 2023 to 10.02 in 2024 and network_area decreasing from 2,523.72 to 1,614.99 mm², while avg_orientation increased from 42.06° to 46.72°. Grain yield ranged from 79.14 to 1,841.55 kg ha^{-1} in 2023 and from 308.53 to 3,130.78 kg ha^{-1} in 2024, with higher mean yield in 2024 (1,301.05 vs. 702.43 kg ha^{-1}).

Hundred-seed weight (HSW_g) showed the strongest genetic control, with a large proportion of genetic variance in both years (VG% = 80.5% in 2023 and 68.9% in 2024; LRT $p < 0.001$) and high heritability (H^2_Piepho = 0.90 and 0.86, respectively; Table 5.4). Grain yield exhibited significant genetic variance in 2023 (VG% = 26.3%; $H^2 = 0.43$; LRT $p < 0.001$) but not in 2024 (VG% = 0.0%; $H^2 = 0.00$; LRT ns; Table 5.4).

Significant genetic variance was detected for 12 root crown traits (RCT) in 2023, but only four in 2024 (median_roots, median_diameter, Depth_Dominance, and shallow_freq), with residual variance (VE%) exceeding 85% for most traits in 2024. Significant genotype × year interaction was observed for Branching_Intensity, Depth_Dominance, and avg_hole_size in the combined analysis. Genomic heritability (H^2_SNP) was highest for HSW_g (0.78–0.91 across analytical scopes), closely matching phenotypic estimates (Table 5.4). Grain yield H^2_SNP was low (0.20 in 2023 and 0.00 in 2024). Across root traits, H^2_SNP ranged from 0.00 to 0.32 and was consistently lower than H^2_Piepho (Table 5.4). The largest discrepancies were observed for avg_hole_size (0.65 vs. 0.21), Gap_Index (0.66 vs. 0.18), and Branching_Intensity (0.62 vs. 0.32) in 2023 (Table 5.4).

4.3.2 Genetic correlations between root trait classes and agronomic traits

For the combined years data, bivariate genetic correlations between grain yield and root crown traits were predominantly negative (Figure 5.3). Total root length showed a significant negative association with grain yield ($rG = -0.64$; $p = 0.024$; Figure 5.3), while network area showed a strong negative correlation approaching significance ($rG = -0.99$; $p = 0.05$; Figure 5.3). For 100-seed weight, diameter traits such as median diameter ($rG = 0.89$; $p < 0.001$) and solidity ($rG = 0.74$; $p < 0.001$), as well as coarse fraction length ($rG = 0.42$; $p = 0.01$), were positively associated. In contrast, branching and exploration traits, including average hole size ($rG = -0.99$; $p < 0.001$), gap index ($rG = -0.84$; $p < 0.001$), median root number ($rG = -0.743$; $p < 0.001$), and total length ($rG = -0.38$; $p = 0.019$), were negatively associated. Orientation traits were also negatively associated, while shallow frequency showed a positive association ($rG = 0.46$; $p =$

0.0012), and depth-related traits were not significantly associated ($p \geq 0.93$). Alkaloid status showed similar patterns with 100-seed weigh. Genetic correlations among root traits revealed two dominant and opposing trait clusters (Figure 5.3). Branching and exploration traits, including root tips, total length, and width:depth ratio, were tightly coupled, with near-perfect positive correlations ($rG \approx 0.99$; $p \leq 0.01$), and were positively associated with median root number ($rG = 0.80–0.95$; $p \leq 0.0038$). Diameter and structural traits formed a second cluster, with strong positive associations among median diameter, solidity, and coarseness index ($rG = 0.72–0.99$; $p \leq 0.021$). These traits were negatively correlated with branching traits, including median root number ($rG = -0.92$; $p < 0.001$), total length ($rG = -0.85$; $p = 0.0127$), and width:depth ratio ($rG = -0.87$; $p = 0.017$).

Year-specific analyses revealed consistent negative genetic correlations between grain yield and branching and exploration traits across both years. In 2023, root tips ($rG = -0.63$), total root length ($rG = -0.62$), and network area ($rG = -0.61$) were significantly associated with yield, while in 2024, root tips and total root length remained strongly negative ($rG = -0.99$), with network area also negative but marginal ($P = 0.097$). These patterns were directionally consistent with the combined analysis, although only total root length remained significant when years were merged ($rG = -0.64$) (Figure 5.4).

4.3.3 Multivariate organization of root architecture and its consistency across years

For the PCA from the combined analysis (Figure 5.5), the PC1 separated more highly branched and extensive root systems (root tips, total length, width:depth ratio, median roots, gap index) from coarser root systems, while PC2 separated larger systems from more steeply oriented root systems (Figure 5.5). In 2023, PC1 separated

root systems with greater lateral spread and branching (higher gap index, width:depth ratio, total length, and median roots) from systems with thicker, more coarse roots (higher coarseness index, median diameter, and coarse fraction length). PC2 separated larger root systems (higher total length and network area) from more steeply oriented and deeper-distributed systems (higher steep frequency and depth dominance). All improvement groups were distributed across both lateral–branched and coarse root types, as well as across larger and more vertically oriented systems. In 2024, PC1 separated root systems with greater lateral spread (gap index, width:depth ratio) from larger, more extensive systems (total length, network area, root tips), while root orientation (average orientation, steep frequency) varied primarily along PC2. PC2 further separated finer root systems (higher surface area to volume ratio and fine fraction length) from coarser root systems (higher coarseness index and coarse fraction length). All groups were distributed across fine, coarse, and differently oriented root systems. All improvement levels overlapped across these root system types, with no consistent differentiation in root size, branching, depth, or thickness. The PCA-biplot by continent (not shown) showed North American accessions were consistently positioned in the positive PC1 region, associated with greater lateral spread and branching in 2023 and combined data scope.

4.3.4 SNP data, Population structure and genetic relationships

Following quality control, 174,284 SNPs were retained from 256,652 raw markers after removing 48,142 SNPs with heterozygosity ≥15% (18.8%) and 34,226 with MAF <0.05 (13.3%), achieving complete coverage of all 25 chromosomes at an average inter-marker spacing of ~2.5 kb and a genotyping rate of 100% across 354 accessions

(Figure 5.6). LD half-decay distance was 40 kb, corresponding to a spacing-to-decay ratio of 1:16, with 76.1% of pairwise SNP comparisons below $r^2 = 0.2$ (Figure 5.6).

Population structure at K = 5 revealed both discrete clustering and extensive admixture across the panel (Figure 5.7). The kinship heatmap (Figure 5.7A) showed two broad blocks of genetic similarity with internal sub-structure, consistent with partial differentiation rather than sharply separated groups. This pattern was reflected in the PCA (Figure 5.7B), where individuals formed overlapping clusters along PC1 (17.17%) and PC2 (1.89%), indicating modest genetic structure with substantial shared variation. The ADMIXTURE bar plot (Figure 5.7C) confirmed this pattern: while some individuals exhibited near-complete assignment to a single ancestry component, a large proportion showed mixed ancestry across multiple populations, demonstrating widespread admixture. This was consistent across the full panel (n = 354), with no clear boundaries separating genetic groups. At the continental level (Figure 5.7D), all five ancestry components were present across regions, although their relative proportions varied. No continent was associated with a unique ancestry component. Mean ancestry per population ranged from 0.122 to 0.320, indicating variable genetic distinctness among inferred groups.

4.3.5 Genome-wide association study for yield and root crown traits

Genome-wide association analysis detected significant marker–trait associations (MTAs) in the combined-year analysis for the following traits: median diameter was associated with Chr16 (5.34 Mb) (Figure 5.8), and coarseness index with Chr03 (12.05 Mb) (Figure 5.9). Gap index showed the strongest signal at Chr22 (10.89 Mb), detected across all models and reached Bonferroni significance in FarmCPU and BLINK (Figure

5.10). In 2024 (not shown), shallow frequency showed a consistent signal on Chr02 (11.28 Mb), detected across MLM, FarmCPU, and BLINK. Root depth was associated with a locus on Chr08 (3.04 Mb), identified by both FarmCPU and BLINK. Coarse fraction length mapped to Chr21 (0.52 Mb) across FarmCPU and BLINK, while average hole size showed a BLINK-specific signal on Chr01 (1.48 Mb).

4.3.6 Annotation of candidate loci associated with root architectural traits

Candidate loci were classified into three tiers based on the strength and consistency of evidence across analytical methods (Table 5.5). Two Tier 1 loci showed strong, biologically consistent associations: Chr16_5502603 was linked to multiple structural traits and annotated for cell wall and carbohydrate metabolism, while Chr19_2764944 was associated with shallow root frequency and annotated for auxin signaling and transport. Tier 2 loci included multi-trait regions such as Chr19_18016413 and additional loci associated with structural and architectural traits, with annotations related to metabolic activity, cytoskeletal organization, and signaling. Tier 3 loci showed weaker or single-trait associations, and several lacked functional annotations.

4.3.7 Alabama Ecosystem Service Index (AESI)

The Alabama Ecosystem Service Index (AESI) was constructed from 11 traits retained after heritability filtering and redundancy pruning (Table 5.6). AESI rankings were highly robust to weighting perturbations (Spearman r = 0.993–0.997 across ±20% service-weight adjustments (Table 5.7). Across years, AESI showed consistency, with a subset of genotypes maintaining above-median performance in both 2023 and 2024, while others exhibited substantial re-ranking (Figure 5.11). When evaluated jointly with grain yield, AESI differentiated WL accessions into four ideotype classes (Figure 5.12).

A distinct subset of accessions combined high AESI and high yield, defining dual-purpose ideotypes, while other genotypes exhibited trade-offs between ecosystem service provision and grain production (Figure 5.12). GWAS of AESI identified no loci exceeding Bonferroni significance threshold at p = 0.05 (Figure 5.13).

4.3.8 Genomic and prediction accuracy for AESI

Genomic prediction accuracy for AESI (Figure 5.14), using the full marker set was low (r = 0.18). Under temporal validation (Figure 5.15), prediction accuracy showed directional asymmetry. In the forward scenario (2023 trained to predict 2024), accuracy increased from r = 0.25, while in the backward scenario (2024 trained to predict 2023), showed prediction accuracy of r = 0.36

4.4 Discussion

4.4.1 Shovelomics phenotyping reveals heritable root trait variation

The shovelomics pipeline coupled with RhizoVision Explorer detected substantial phenotypic variation in root crown architecture among 232 white lupin accessions evaluated under Alabama field conditions, confirming the feasibility of high-throughput root phenotyping at breeding scale for this species (Trachsel et al., 2011; Burridge et al., 2016; Seethepalli et al., 2021). Year-to-year instability in heritability observed for some traits is consistent with the broader literature on field-measured root traits, which are subject to strong environmental modulation of root plasticity (Griffiths et al., 2022; Griffin et al., 2025). The growing season of 2024 differed from 2023 in rainfall distribution and temperature profiles, and such environmental variation is known to differentially affect root trait expression (Freschet et al., 2021).

4.4.2 Genetic control, environmental sensitivity, and genomic capture of root and agronomic traits

Hundred-seed weight exhibited the strongest and most stable genetic control across both years, which aligns with its well-documented high heritability in grain legumes (Annicchiarico et al., 2023, 2025). Grain yield showed significant genetic variance in 2023 but collapsed in 2024, likely reflecting the strong genotype-by-environment interaction that characterizes yield in white lupin under southeastern US conditions, where terminal drought and heat stress during reproductive stages can override genetic differences among lines. This pattern is consistent with Pecetti et al. (2023), who reported environment-specific yield QTLs under drought versus moisture-favorable conditions and emphasized the importance of multi-environment evaluation for yield improvement in WL. Large gaps between phenotypic and genomic heritability were observed for several traits, possibly reflecting non-additive effects, structural variants missed by biallelic SNPs, or rare alleles below the MAF threshold (0.05). Similar gaps have been reported elsewhere for field-measured root traits (Bagale et al., 2025).

4.4.3 Trade-off between root exploration and grain yield traits constrain dual-purpose breeding

Genetic correlations revealed two opposing root trait clusters: a branching and exploration cluster (root tips, total length, width:depth ratio, median roots) and a diameter and structural cluster (median diameter, solidity, coarseness index), reflecting a fundamental architectural tradeoff between investing in extensive, finely branched roots for soil exploration versus compact, thick roots for structural anchorage. This pattern is consistent with the root economics spectrum described by Freschet et al. (2021), that

suggest a “conservatism-to-acquisitiveness” gradient in root functional strategies. It also agrees with the root phene-based ideotypes proposed by (Lynch, 2011, 2019), in which topsoil foraging phenes that enhance phosphorus acquisition through extensive branching and exploration shows a trade off against the architectural and anatomical phenes driving deeper, more metabolically economical root systems (Lynch, 2013).

Critically, grain yield was negatively correlated with exploration traits, while hundred-seed weight was positively associated with diameter traits. These correlations were directionally consistent across both years, suggesting a stable genetic antagonism between root exploration investment and grain production. From an ecosystem service perspective, these trade-offs have significant consequences: the root traits most valuable for phosphorus mobilization are those negatively correlated with yield traits. This pattern agrees with a general observation well documented in the root biology literature that traits conferring an advantage under resource limitation can impose a metabolic or carbon cost that reduces yield when that limitation is absent. Lynch (2013, 2019) has described this as an inherent property of soil-foraging ideotypes: phenes that enhance acquisition of a scarce resource are not always beneficial, and the same architectural structures that improves performance under stress can become a net carbon cost under non-limiting conditions. Likewise, Tardieu and Tuberosa (2010) and Tardieu et al., (2018) reported that for drought-adaptive root traits, the effect of a given trait or allele on yield is scenario-dependent rather than fixed, such that root traits selected for their benefit under stress can carry a yield penalty when the corresponding stress does not materialize. This context-dependency offers one plausible physiological explanation for the negative yield-exploration correlation observed, and underscores why selection indices such as AESI,

which explicitly balance ecosystem service potential against yield rather than maximizing either independently, may be more robust selection tools than single-trait selection under variable field conditions.

The AESI framework was developed to navigate this trade-off by identifying genotypes that achieve acceptable levels of both ecosystem service delivery with root traits that prioritize shallow soil exploration and grain production, rather than maximizing either in isolation.

Prior GWAS studies in WL and narrow leaf lupin have focused on anthracnose resistance (Alkemade et al., 2022; Schwertfirm et al., 2024), seed quality (Annicchiarico et al., 2025), flowering time (Rychel-Bielska et al., 2024), drought tolerance (Pecetti et al., 2023), and frost resistance (Nazzicari et al., 2025), none of which examined root system architecture. The negative yield-root exploration correlation reported here should be considered in future white lupin breeding programs that aim to improve both aboveground and belowground performance. The AESI trait selection demonstrated that although there is a negative correlation between yield and root traits it is still possible to select cultivars with high yields and root traits that can help specific ecosystems services such as P mobilization.

4.4.4 Polygenic architecture of root traits revealed by GWAS

Despite deploying 174,284 SNPs, approximately four-fold denser than any previously published white lupin GWAS (Alkemade et al., 2022, 4,611 SNPs; Annicchiarico et al., 2025, 41,116 SNPs), few loci reached genome-wide significance. This outcome is consistent with the polygenic architectures reported across all prior

white lupin GWAS for traits ranging from anthracnose resistance (distributed across 14 to 17 of 25 chromosomes; Schwertfirm et al., 2024), frost tolerance (Nazzicari et al., 2025) to grain yield under drought (Pecetti et al., 2023). In all cases, many small-effect loci were implicated, and significant SNPs were often inconsistent across environments. The difficulty of detecting associations in white lupin is compounded by rapid linkage disequilibrium decay. Schwertfirm et al. (2024) reported genome-wide LD declining below $r^2 = 0.1$ within 1 kb in a panel of 255 accessions and found that their initial GBS marker set failed to detect the well-characterized pauper alkaloid locus on Chr18 until targeted SNP enrichment increased local density from 1 SNP/12.2 kb to 1 SNP/753 bp. In the present study, LD half-decay was longer (40 kb), likely reflecting the narrower genetic base of the Auburn breeding panel, but average inter-marker spacing of 2.5 kb still exceeds the resolution needed to tag all causal variants in a genome where LD erodes rapidly (Seck et al., 2020). Root architectural traits, which integrate the collective action of hundreds of genes governing cell division, elongation, branching, and response to soil heterogeneity, are expected to exhibit similarly distributed genetic architectures (Bray et al., 2018; Seck et al., 2020).

The strongest and most consistent signals emerged for branching-related traits. Gap index showed significant association on Chr22 (10.89 Mb) detected across all three GAPIT models in the combined analysis, and shallow frequency was associated with a cross-model locus on Chr02 (11.28 Mb) in 2024. These loci represent candidate regions for future fine-mapping and functional annotation. The recurrence of suggestive signals on Chr03 (coarseness index, SA_to_V), Chr05 (network area, root tips), and Chr16 (gap index, median diameter) across traits and years suggests the presence of pleiotropic

regions influencing root architectural variation, although none reached formal significance in the combined analysis.

The limited number of high-confidence loci and the predominance of trait-specific associations indicate that root architecture in white lupin is controlled by a distributed, polygenic architecture rather than a few major-effect genes. This pattern is consistent with theoretical and empirical evidence showing that complex quantitative traits are typically governed by many loci of small effect (Bernardo, 2008; Boyle et al., 2017). The functional annotations of key loci, particularly those related to cell wall metabolism and auxin signaling, support known biological mechanisms underlying root development and soil spatial distribution.

From a breeding perspective, this architecture suggests that selection strategies based on a limited number of loci are unlikely to be effective, whereas genomic selection approaches that capture genome-wide effects provide a more suitable framework (Heffner et al., 2009). The loci identified in this study nonetheless offer biologically relevant targets for validation and improved interpretation of selection responses.

4.4.5 The Alabama Ecosystem Service Index: a selection framework for dual-purpose white lupin

The AESI represents a composite selection index constructed explicitly for ecosystem service breeding. Its design was motivated by two practical realities: first, ecosystem functions such as phosphorus mobilization, erosion control, and soil organic matter contribution cannot be measured directly at field breeding scale, necessitating the

use of root morphological proxies (Freschet et al., 2021; Griffiths et al., 2022); second, individual root traits are often collinear and antagonistically correlated with yield, making single-trait selection inefficient or counterproductive (Fletcher et al., 2015; Freschet et al., 2021; Griffiths et al., 2022). By grouping 11 heritable, non-redundant traits into four ecosystem service categories with literature-grounded weights reflecting Alabama's agricultural priorities, the AESI provides a framework that balances ecological function against economic viability.

The numerical stability of AESI rankings under ±20% weight perturbation (Spearman r = 0.993 to 0.997) indicates that the index is not sensitive to precise weight specification, which addresses a common concern with expert-weighted selection indices (Céron-Rojas & Crossa, 2022). The dual-purpose composite identified a subset of accessions that combined above-median ecosystem service potential with competitive grain yield, defining a dual-purpose ideotype class that could serve as parental material for future crosses. Partial year-to-year rank stability was observed, with a subset of genotypes maintaining high AESI performance across both seasons, though substantial re-ranking also occurred, reflecting the environmental sensitivity of root trait expression documented in Section 4.3.1.

The decision to weight phosphorus mobilization most heavily (0.35) reflects the specific edaphic context of Alabama's Ultisols, where strong phosphorus fixation renders 70 to 90% of soil phosphorus unavailable to plants despite high total phosphorus pools (Shaw et al., 2002; Ye et al., 2020; Waldrip et al., 2023). WL’s unique capacity for cluster root formation and carboxylate exudation (Lambers et al., 2013; Zhang et al., 2020) makes phosphorus mobilization the ecosystem service most uniquely attributable to this

species and least substitutable by alternative management practices. The explicit exclusion of nitrogen fixation from the index, despite its agronomic importance, reflects the fact that nodulation was not measured in the current study, and inclusion would have required unverifiable assumptions. This decision, while limiting, ensures that every index component traces to a directly measured phenotype.

4.4.6 Genetic architecture underlying ecosystem service potential and the case for genomic selection

GWAS of AESI identified no genome-wide significant loci in either year, consistent with a polygenic architecture in which no single locus exerts a detectable major effect (Spindel et al., 2016). From a breeding perspective, this indicates that selection strategies based on a limited number of loci, such as marker-assisted selection (MAS), are unlikely to be effective for AESI, whereas genomic selection provides a more effective framework for capturing cumulative small-effect variation (Hazel 1943; Bernardo, 2008; Heffner et al., 2009). Genomic selection, which uses genome-wide markers rather than individually significant loci, is therefore better suited to capturing this distributed architecture (Meuwissen et al., 2001; de los Campos et al., 2013). The observed predictive ability of AESI supports the use of genomic selection as a practical first-pass strategy for ranking candidates on composite ecosystem service merit, where direct phenotyping of all underlying traits at scale is impractical. Breeders could use AESI-based genomic predictions to advance a shortlist of top-ranked cultivars into targeted field evaluation, where the individual component traits underlying the index could be directly phenotyped to confirm realized ecosystem service performance prior to release.

4.4.7 Limitations and future directions

This study has several limitations worth mentioning. First, the study was conducted at a single location across two years, this limits generalizability of AESI weights and accessions rankings to other environments; therefore, multi-environment validation across contrasting soils and climates is needed. Second, the panel size (232 accessions) limits power to detect small-effect loci, and truncation selection via selection-based advancement between years may have further reduced phenotypic variance and allele frequency dispersion. Finally, AESI is built on root morphological proxies rather than direct measurements of phosphorus mobilization, erosion control, or carbon sequestration.

Future work should increase sample size, validate AESI across environments and years, link index scores to measured ecosystem functions, and integrate the framework into genomic prediction pipelines for breeding applications.

4.5 Conclusion

This study makes four contributions to white lupin breeding research. First, it validates shovelomics and RhizoVision Explorer pipeline for root crown phenotyping in white lupin, demonstrating the feasibility of root phenotyping at breeding scale for this species (Trachsel et al., 2011; Seethepalli et al., 2021; Burridge et al., 2016). Second, bivariate genetic correlation analysis revealed a previously undocumented architectural trade off in white lupin between root exploration traits associated with ecosystem service delivery and grain yield, providing new quantitative genetic evidence relevant to dual-purpose breeding objectives. Third, this study provides the first genome-wide

association analysis of root architectural variation in white lupin, extending prior GWAS work in the species, which has focused exclusively on aboveground traits such as disease resistance, phenology, and seed quality (Alkemade et al., 2022; ; Annicchiarico et al., 2023; Pecetti et al., 2023; Schwertfirm et al., 2024; Rychel-Bielska et al., 2024; Nazzicari et al., 2025; Annicchiarico et al., 2025), to belowground traits and confirming a polygenic genetic architecture consistent with patterns reported for other complex root traits. Fourth, the development of the Alabama Ecosystem Service Index (AESI) provides a quantitative framework for selecting genotypes based on root-derived ecosystem service potential alongside grain yield. AESI rankings were robust to weighting perturbations and identified genotypes combining ecosystem service potential with competitive yield, although genomic prediction accuracy for the index using the full marker panel was low, indicating that current sample size and marker density are insufficient to fully capture its underlying genetic architecture.

While developed in white lupin, the AESI framework is applicable to other dual-purpose and cover crop systems where root traits serve as proxies for ecosystem functions. As breeding programs increasingly target environmental co-benefits alongside productivity (Brummer et al., 2011), index-based approaches such as AESI offer a practical bridge between ecological objectives and yield selection.

References

Alexander, D. H., Novembre, J., & Lange, K. (2009). Fast model-based estimation of ancestry in unrelated individuals. Genome Research, 19(9), 1655–1664. https://doi.org/10.1101/gr.094052.109

Alkemade, J. A., Messmer, M. M., Voegele, R. T., Finckh, M. R., & Hohmann, P. (2022). Genome-wide association study reveals white lupin candidate gene involved in anthracnose resistance. Theoretical and Applied Genetics, 135(3), 1011–1024. https://doi.org/10.1007/s00122-021-04014-7

Annicchiarico, P., de Buck, A. J., Vlachostergios, D. N., Heupink, D., Koskosidis, A., Nazzicari, N., & Crosta, M. (2023). White lupin adaptation to moderately calcareous soils: Phenotypic variation and genome-enabled prediction. Plants, 12(5), 1139. https://doi.org/10.3390/plants12051139

Annicchiarico, P., Osorio, C., Nazzicari, N., Ferrari, B., Barzaghi, S., Biazzi, E., Tava, A., Pecetti, L., Notario, T., Romani, M., & Crosta, M. (2025). Genetic variation and genome-enabled selection of white lupin for key seed quality traits. BMC Genomics, 26, 922. https://doi.org/10.1186/s12864-025-12048-0

Baets, S.D., Poesen, J., Knapen, A. and Galindo, P. (2007), Impact of root architecture on the erosion-reducing potential of roots during concentrated flow. Earth Surf. Process. Landforms, 32: 1323-1345. https://doi.org/10.1002/esp.1470

Bagale, S., Enesi, R. O., & Gorim, L. Y. (2025). An overview of root traits and ideotypes for improving crop productivity and addressing agronomic challenges. Rhizosphere, 28, 101105. https://doi.org/10.1016/j.rhisph.2025.101105

Benjamini, Y., & Hochberg, Y. (1995). Controlling the false discovery rate: A practical and powerful approach to multiple testing. Journal of the Royal Statistical Society: Series B (Methodological), 57(1), 289–300. https://doi.org/10.1111/j.2517-6161.1995.tb02031.x

Bernardo, R. (2008), Molecular Markers and Selection for Complex Traits in Plants: Learning from the Last 20 Years. Crop Sci., 48: 1649-1664. https://doi.org/10.2135/cropsci2008.03.0131

Bhardwaj, H.L., Starner, D.E., and E. van Santen. 2010. Preliminary evaluation of white lupin (Lupinus albus L.) as a forage crop in the mid-Atlantic region of the United States of America. J. of Agricultural Science 2(4):13-17.

Boyle, E. A., Li, Y. I., & Pritchard, J. K. (2017). An expanded view of complex traits: from polygenic to omnigenic. Cell, 169(7), 1177–1186. https://doi.org/10.1016/j.cell.2017.05.038

Bray, A. L., & Topp, C. N. (2018). The quantitative genetic control of root architecture in maize. Plant and Cell Physiology, 59(10), 1919–1930. https://doi.org/10.1093/pcp/pcy141

Brummer, E. C., Barber, W. T., Collier, S. M., Cox, T. S., Johnson, R., Murray, S. C., Olsen, R. T., Pratt, R. C., & Thro, A. M. (2011). Plant breeding for harmony between agriculture and the environment. Frontiers in Ecology and the Environment, 9(10), 561–568. https://doi.org/10.1890/100225

Burridge, J., Jochua, C. N., Bucksch, A., & Lynch, J. P. (2016). Legume shovelomics: High-throughput phenotyping of common bean (Phaseolus vulgaris L.) and

cowpea (Vigna unguiculata subsp. unguiculata) root architecture in the field. Field Crops Research, 192, 21–32. https://doi.org/10.1016/j.fcr.2016.04.008

Butler, D. G., Cullis, B. R., Gilmour, A. R., Gogel, B. J., & Thompson, R. (2017). ASReml-R reference manual version 4. VSN International Ltd.

Céron-Rojas, J. J., & Crossa, J. (2022). The statistical theory of linear selection indices from phenotypic to genomic selection. Crop Science, 62(2), 537–563. https://doi.org/10.1002/csc2.20676

Crossa, J., Pérez-Rodríguez, P., Cuevas, J., et al. (2017). Genomic selection in plant breeding: methods, models, and perspectives. Trends in Plant Science, 22(11), 961–975. https://doi.org/10.1016/j.tplants.2017.08.011

Cu, S. T., Hutson, J., & Schuller, K. A. (2005). Mixed culture of wheat (Triticum aestivum L.) with white lupin (Lupinus albus L.) improves the growth and phosphorus nutrition of the wheat. Plant and Soil, 272(1–2), 143–151. https://doi.org/10.1007/s11104-004-4336-8

Cullis, B. R., Smith, A. B., & Coombes, N. E. (2006). On the design of early generation variety trials with correlated data. Journal of Agricultural, Biological, and Environmental Statistics, 11(4), 381–393. https://doi.org/10.1198/108571106X154443

Daniel, T. C., Sharpley, A. N., Edwards, D. R., Wedepohl, R., & Lemunyon, J. L. (1994). Minimizing surface water eutrophication from agriculture by phosphorous management. Journal of Soil and Water Conservation, 49(2), 30–38.

de los Campos, G., Hickey, J. M., Pong-Wong, R., Daetwyler, H. D., & Calus, M. P. L. (2013).
Whole-genome regression and prediction methods applied to plant and animal breeding.
Genetics, 193(2), 327–345. https://doi.org/10.1534/genetics.112.143313

Dignac, M.-F., Derrien, D., Barré, P., Barot, S., Cécillon, L., Chenu, C., ... & Basile-Doelsch, I. (2017). Increasing soil carbon storage: Mechanisms, effects of agricultural practices and proxies. A review. Agronomy for Sustainable Development, 37, 14. https://doi.org/10.1007/s13593-017-0421-2

Fletcher, R. S., Mullen, J. L., Heiliger, A., & McKay, J. K. (2015). QTL analysis of root morphology, flowering time, and yield reveals trade-offs in response to drought in Brassica napus. Journal of Experimental Botany, 66(1), 245–256. https://doi.org/10.1093/jxb/eru423

Freschet, G. T., & Roumet, C. (2017). Sampling roots to capture plant and soil functions. Functional Ecology, 31, 1506–1518. https://doi.org/10.1111/1365-2435.12883

Freschet, G. T., Violle, C., Roumet, C., & Garnier, E. (2018). Interactions between soil and vegetation: Structure of plant communities and soil functioning. In P. Lemanceau & M. Blouin (Eds.), Soils within the critical zone: Ecology (pp. 83–104). ISTE Editions.

Freschet, G. T., Roumet, C., Comas, L. H., Weemstra, M., Bengough, A. G., Rewald, B., et al. (2021). Root traits as drivers of plant and ecosystem functioning: Current

understanding, pitfalls and future research needs. New Phytologist, 232(3), 1123–1158. https://doi.org/10.1111/nph.17072

Gamble, A. (2020, February 28). Cover crops play vital role in soil conservation. Southeast AgNET. https://southeastagnet.com/2020/02/28/cover-crops-play-vital-role-soil-conservation/

Griffin, T. S., Jungers, J. M., Samac, D. A., & Kinane, J. (2025). Root phenotyping and plant breeding of crops for enhanced ecosystem services. Crop Science, 65(1), e21315. https://doi.org/10.1002/csc2.21315

Griffiths, M., Delory, B. M., Jawahir, V., Wong, K. M., Bagnall, G. C., Dowd, T. G., Nusinow, D. A., Miller, A. J., & Topp, C. N. (2022). Optimisation of root traits to provide enhanced ecosystem services in agricultural systems: A focus on cover crops. Plant, Cell & Environment, 45(3), 751–770. https://doi.org/10.1111/pce.14247

Habier, D., Fernando, R. L., & Dekkers, J. C. M. (2007). The impact of genetic relationship information on genome-assisted breeding values. Genetics, 177(4), 2389–2397. https://doi.org/10.1534/genetics.107.081190

Hazel, L. N. (1943). The genetic basis for constructing selection indexes. Genetics, 28(6), 476–490. https://doi.org/10.1093/genetics/28.6.476

Heffner, E. L., Sorrells, M. E., & Jannink, J. L. (2009). Genomic selection for crop improvement. Crop Science, 49(1), 1–12. https://doi.org/10.2135/cropsci2008.08.0512

Henneron, L., Cros, C., Picon-Cochard, C., Rahimian, V., & Fontaine, S. (2020). Plant economic strategies of grassland species control soil carbon dynamics through rhizodeposition. Journal of Ecology, 108, 528–545. https://doi.org/10.1111/1365-2745.13276

Hori, T. S., Himelblau, E., & Kimberley, M. O. (2015). Interspecific facilitation of P acquisition in intercropping of maize with white lupin in two contrasting soils as influenced by different rates and forms of P supply. Plant and Soil, 394(1–2), 223–236. https://doi.org/10.1007/s11104-015-2392-x

Hufnagel, B., Marques, A., Soriano, A., Marquès, L., Divol, F., Doumas, P., et al. (2020). High-quality genome sequence of white lupin provides insight into soil exploration and seed quality. Nature Communications, 11, 492. https://doi.org/10.1038/s41467-019-14197-9

Hufnagel, B., Soriano, A., Taylor, J., Divol, F., Kroc, M., Sanders, H., Yeheyis, L., Nelson, M., & Péret, B. (2021). Pangenome of white lupin provides insights into the diversity of the species. Plant Biotechnology Journal, 19(12), 2532–2543. https://doi.org/10.1111/pbi.13678

Korani, W., O'Connor, D., Chu, Y., Chavarro, C., Ballen, C., Guo, B., Ozias-Akins, P., Wright, G., & Clevenger, J. (2021). De novo QTL-seq identifies loci linked to blanchability in peanut (Arachis hypogaea) and refines previously identified QTL with low coverage sequence. Agronomy, 11(11), 2201. https://doi.org/10.3390/agronomy11112201

Lambers, H., Clements, J. C., & Nelson, M. N. (2013). How a phosphorus-acquisition strategy based on carboxylate exudation powers the success and agronomic potential of lupines (Lupinus, Fabaceae). American Journal of Botany, 100(2), 263–288. https://doi.org/10.3732/ajb.1200474

Lynch, J. P. (2011). Root phenes for enhanced soil exploration and phosphorus acquisition: Tools for future crops. Plant Physiology, 156(3), 1041–1049. https://doi.org/10.1104/pp.111.175414

Lynch, J. P. (2013). Steep, cheap and deep: An ideotype to optimize water and N acquisition by maize root systems. Annals of Botany, 112(2), 347–357. https://doi.org/10.1093/aob/mcs293

Lynch, J. P. (2019). Root phenotypes for improved nutrient capture: An underexploited opportunity for global agriculture. New Phytologist, 223(2), 548–564. https://doi.org/10.1111/nph.15738

Martin, K. A., Brennan, F. P., Schmidt, O., & Tracy, S. (2022). Comparison of two image analysis software for root trait analysis of single and mixed species grasslands. The Plant Phenome Journal, 5, e20034. https://doi.org/10.1002/ppj2.20034

Meuwissen, T. H. E., Hayes, B. J., & Goddard, M. E. (2001). Prediction of total genetic value using genome-wide dense marker maps. Genetics, 157(4), 1819–1829. https://doi.org/10.1093/genetics/157.4.1819

Nazzicari, N., Crosta, M., Notario, T., Ferrari, B., Pecetti, L., & Annicchiarico, P. (2025). Genetic variation and genome-enabled prediction of white lupin frost resistance

in different reference populations. International Journal of Molecular Sciences, 26(20), 10224. https://doi.org/10.3390/ijms262010224

Omernik, J. M., Griffith, G. E., Hughes, R. M., Glover, J. B., & Weber, M. H. (2016). How to make better use of ecoregions for assessing aquatic ecosystem health. In M. T. Barbour, J. R. Yoder, & J. A. Rex (Eds.), Assessing the ecological integrity of running waters (pp. 55–71). Springer.

Osmond, D., Cabrera, M., Gilliam, J., Harmel, R., Jennings, G., Line, D., ... & Rhoades, E. (2015). Water quality in the southeastern United States: Nutrient, pesticide, and sediment issues. Journal of Soil and Water Conservation, 70(6), 127A–136A.

Pecetti, L., Annicchiarico, P., Crosta, M., Notario, T., Ferrari, B., & Nazzicari, N. (2023). White lupin drought tolerance: Genetic variation, trait genetic architecture, and genome-enabled prediction. International Journal of Molecular Sciences, 24(3), 2351. https://doi.org/10.3390/ijms24032351

Piepho, H.-P., & Möhring, J. (2007). Computing heritability and selection response from unbalanced plant breeding trials. Genetics, 177(3), 1881–1888. https://doi.org/10.1534/genetics.107.074229

Prasad, R., & Chakraborty, D. (2024). Is cover crop a solution or a problem for Alabama water quality, and are there any remediation strategies? Auburn University College of Agriculture. https://agriculture.auburn.edu/feature/agricultural-grants-address-problems-on-alabama-farms/

Prieto, I., Armas, C., & Pugnaire, F. I. (2012). Water release through plant roots: New insights into its consequences at the plant and ecosystem level. New Phytologist, 193, 830–841. https://doi.org/10.1111/j.1469-8137.2011.04039.x

Raffauf, R. F. (1962). A simple field test for alkaloid-containing plants. Economic Botany, 16, 171–172. https://doi.org/10.1007/BF02860035

Roesch-McNally, G. E., Arbuckle, J. G., & Tyndall, J. C. (2018). The trouble with cover crops: Farmers' experiences with overcoming barriers to adoption. Renewable Agriculture and Food Systems, 33(4), 322–333. https://doi.org/10.1017/S1742170517000096

Rychel-Bielska, S., Bielski, W., Surma, A., Annicchiarico, P., Belter, J., Kozak, B., Galek, R., Harzic, N., & Książkiewicz, M. (2024). A GWAS study highlights significant associations between a series of indels in a FLOWERING LOCUS T gene promoter and flowering time in white lupin (Lupinus albus L.). BMC Plant Biology, 24, 696. https://doi.org/10.1186/s12870-024-05438-1

SARE/CTIC. (2023). National cover crop survey report 2022–2023. Sustainable Agriculture Research & Education and Conservation Technology Information Center. https://www.sare.org/wp-content/uploads/2022-2023-National-Cover-Crop-Survey-Report.pdf

Schwertfirm, G., Schneider, M., Haase, F. et al. Genome-wide association study revealed significant SNPs for anthracnose resistance, seed alkaloids and protein content in white lupin. Theor Appl Genet 137, 155 (2024). https://doi.org/10.1007/s00122-024-04665-2

Seck W, Torkamaneh D and Belzile F (2020) Comprehensive Genome-Wide Association Analysis Reveals the Genetic Basis of Root System Architecture in Soybean. Front. Plant Sci. 11:590740. doi: 10.3389/fpls.2020.590740

Seethepalli, A., Dhakal, K., Griffiths, M., Guo, H., Freschet, G. T., & York, L. M. (2021). RhizoVision Explorer: Open-source software for root image analysis and measurement standardization. AoB Plants, 13(6), plab056. https://doi.org/10.1093/aobpla/plab056

Seethepalli, A., Guo, H., Liu, X., Griffiths, M., Almtarfi, H., Li, Z., Liu, S., Zare, A., Fritschi, F. B., Blancaflor, E. B., Ma, X.-F., & York, L. M. (2020). RhizoVision Crown: An integrated hardware and software platform for root crown phenotyping. Plant Phenomics, 2020, 3074916. https://doi.org/10.34133/2020/3074916

Shaw, J. N., Truman, C. C., & Reeves, D. W. (2002). Mineralogy of eroded sediments derived from highly weathered Ultisols of central Alabama. Soil and Tillage Research, 68(1), 59–69. https://doi.org/10.1016/S0167-1987(02)00081-3

Shen, L., Courtois, B., McNally, K. L., & Robin, S. (2001). Evaluation of near-isogenic lines of rice introgressed with QTLs for root depth through marker-aided selection. Theoretical and Applied Genetics, 103, 75–83. https://doi.org/10.1007/s001220100538

Smith, H. F. (1936). A discriminant function for plant selection. Annals of Eugenics, 7(3), 240–250. https://doi.org/10.1111/j.1469-1809.1936.tb02143.x

Spindel, J. E., Begum, H., Akdemir, D., Collard, B., Redoña, E., Jannink, J.-L., & McCouch, S. (2016). Genome-wide prediction models that incorporate de novo GWAS are a powerful new tool for tropical rice improvement. Heredity, 116(4), 395–408. https://doi.org/10.1038/hdy.2015.113

Steele, K. A., Price, A. H., Shashidhar, H. E., & Witcombe, J. R. (2006). Marker-assisted selection to introgress rice QTLs controlling root traits into an Indian upland rice variety. Theoretical and Applied Genetics, 112, 208–221. https://doi.org/10.1007/s00122-005-0110-4

Sujak, A., Kotlarz, A., & Strobel, W. (2006). Compositional and nutritional evaluation of several lupin species. Food Chemistry, 98(4), 711–719. https://doi.org/10.1016/j.foodchem.2005.06.036

Tardieu, F., & Tuberosa, R. (2010). Dissection and modelling of abiotic stress tolerance in plants. Current Opinion in Plant Biology, 13(2), 206–212. https://doi.org/10.1016/j.pbi.2009.12.012

Tardieu, F., Simonneau, T., & Muller, B. (2018). The physiological basis of drought tolerance in crop plants: A scenario-dependent probabilistic approach. Annual Review of Plant Biology, 69, 733–759. https://doi.org/10.1146/annurev-arplant-042817-040218

Trachsel, S., Kaeppler, S. M., Brown, K. M., & Lynch, J. P. (2011). Shovelomics: High-throughput phenotyping of maize (Zea mays L.) root architecture in the field. Plant and Soil, 341(1–2), 75–87. https://doi.org/10.1007/s11104-010-0623-8

USEPA. (2002). National water quality inventory report (EPA-841-R-02-001). http://nepis.epa.gov

VanRaden, P. M. (2008). Efficient methods to compute genomic predictions. Journal of Dairy Science, 91(11), 4414–4423. https://doi.org/10.3168/jds.2007-0980

Waldrip, H. M., Campbell, T. N., Koziel, J. A., Watts, D. B., & Torbert, H. A. (2023). Legacy phosphorus in Alabama Hartsells soil after long-term amendment with broiler litter. Journal of Environmental Quality, 52, 897–906. https://doi.org/10.1002/jeq2.20462

Wang, J., & Zhang, Z. (2021). GAPIT version 3: Boosting power and accuracy for genomic association and prediction. Genomics, Proteomics & Bioinformatics, 19(4), 629–640. https://doi.org/10.1016/j.gpb.2021.08.005

Ye, R., Parajuli, B., Ducey, T. F., Novak, J. M., Bauer, P. J., & Szogi, A. A. (2020). Cover cropping increased phosphorus stocks in surface sandy Ultisols under long-term conservation and conventional tillage. Agronomy Journal, 112, 3163–3173. https://doi.org/10.1002/agj2.20227

Zhang, S., Bai, C., Fan, F., Song, D., & Liao, H. (2020). The genome evolution and low-phosphorus adaptation in white lupin. Nature Communications, 11(1), 1069. https://doi.org/10.1038/s41467-020-14891-z

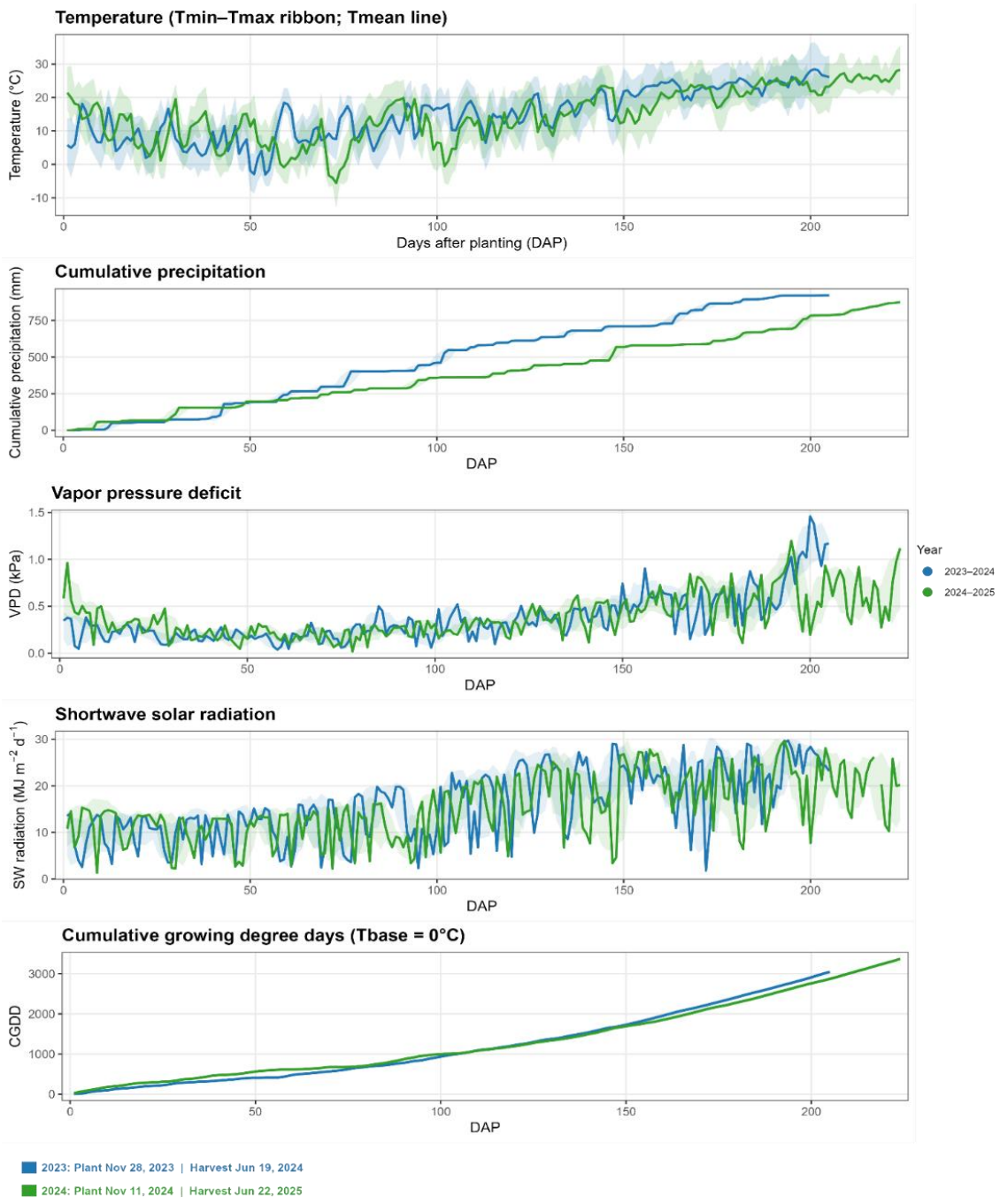

Figure 4.1. Environmental conditions during the 2023–2024 and 2024–2025 white lupin growing seasons at E.V. Smith Plant Breeding Unit, Tallassee, Alabama.

Daily temperature (A), cumulative precipitation (B), vapor pressure deficit (C), shortwave solar radiation (D), and cumulative growing degree days (E) are shown as a function of days after planting (DAP).

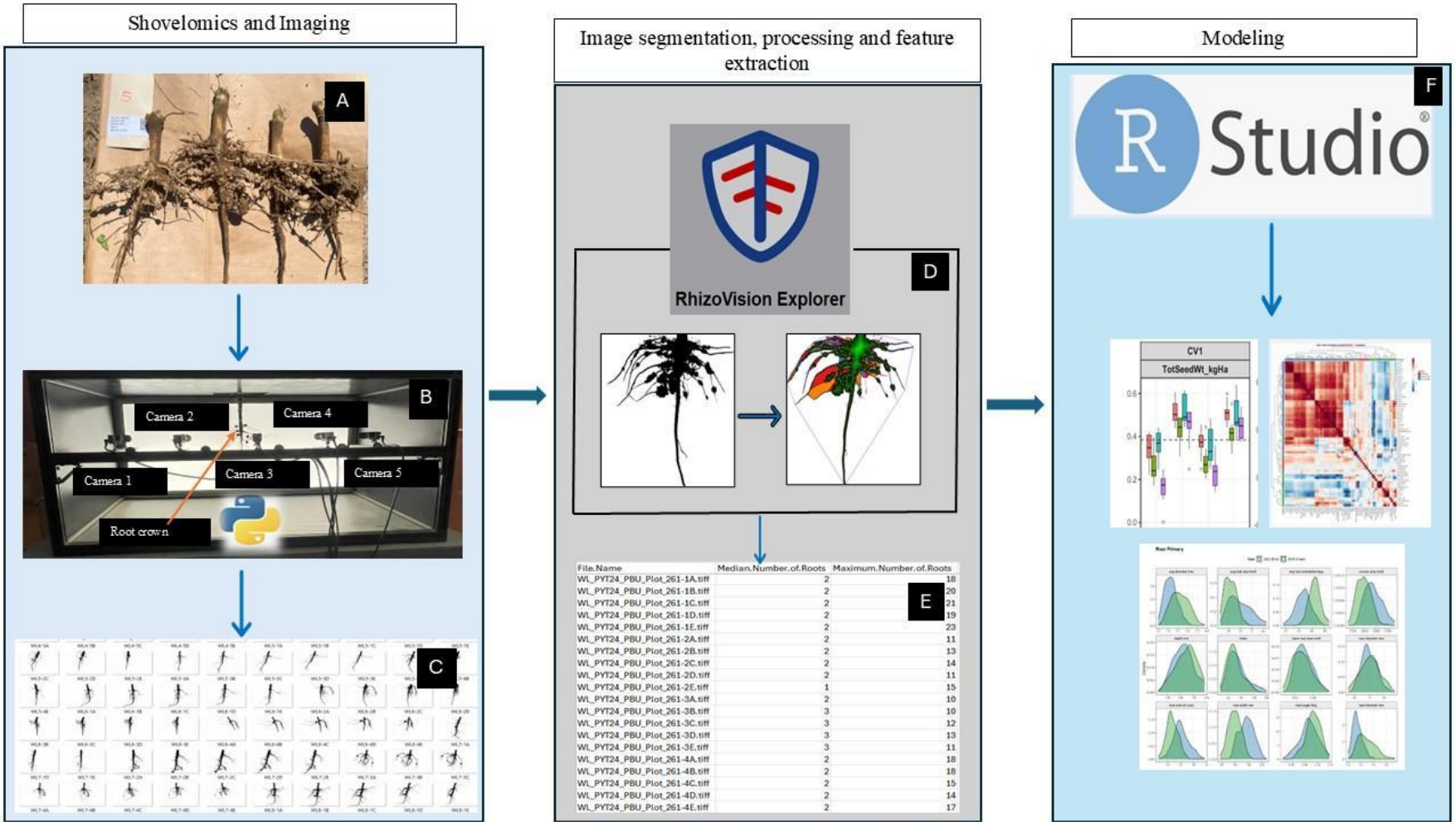

Figure 4.2. Root phenotyping pipeline for white lupin shovelomics and image analysis.

(A)Root crowns excavated using the shovelomics. (B) Imaging in a custom RhizoBox system (C) Multi-angle images from of root crown (D) RhizoVision Explorer v2.0.3 (E) Extracted root traits (F) Downstream statistical modeling

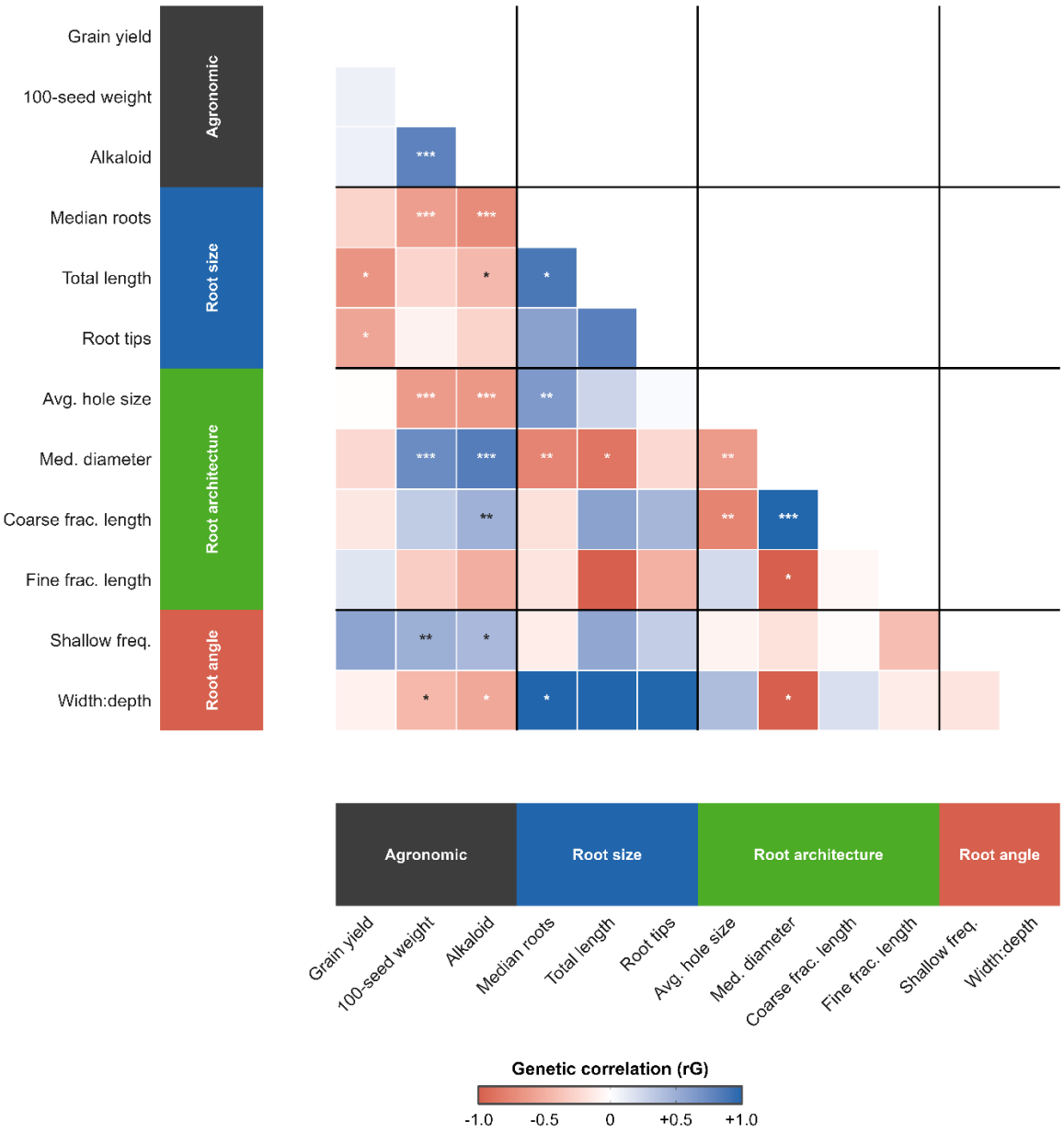

Figure 4.3. Genetic correlations among root architecture and agronomic traits in white lupin for combined-year data.

Genetic correlations were evaluated among grain yield, 100-seed weight, alkaloid content, and selected root traits. Strong positive relationships occurred among root-size traits and between median root diameter and coarse-root fraction, whereas fine-root fraction was negatively associated with several root-size and architecture traits. Several root traits also showed significant correlations with 100-seed weight and alkaloid content.

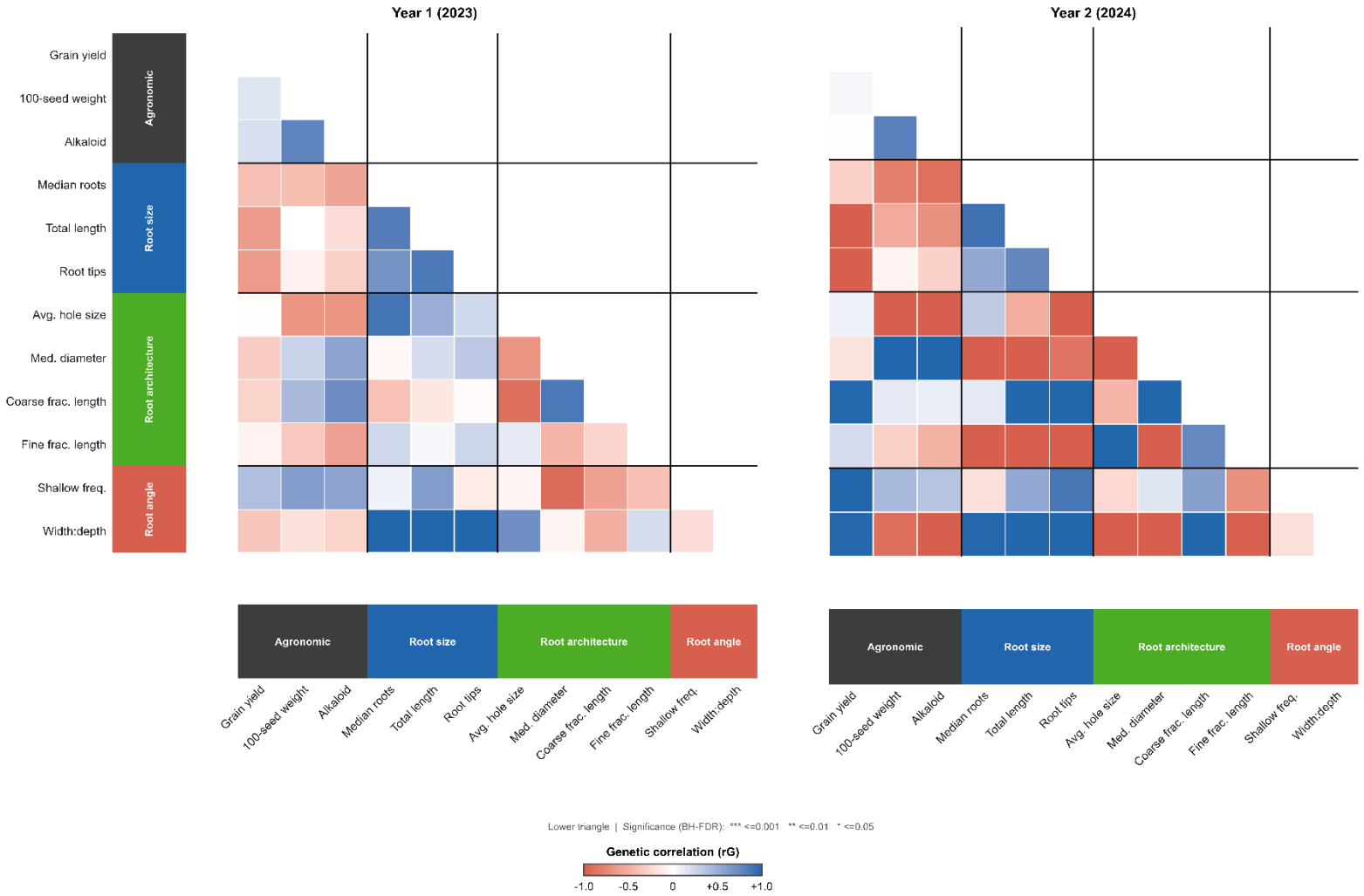

Figure 4.4. Genetic correlations among root architecture and agronomic traits in white lupin per year.

Genetic correlations among grain yield, 100-seed weight, alkaloid content, and selected root traits are shown separately for 2023 and 2024. Relationships among root-size, root-architecture, and root-angle traits were more pronounced in 2024, indicating substantial year-to-year variation in the genetic associations among traits.

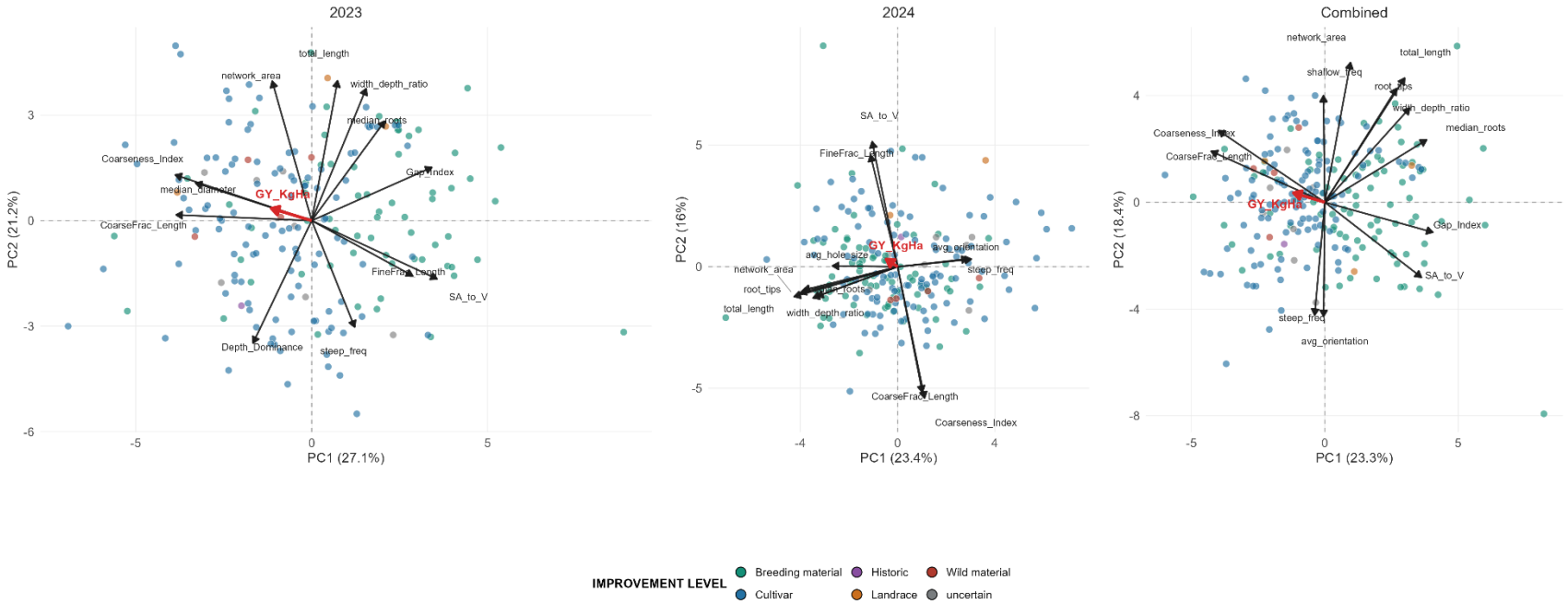

Figure 4.5. Principal component analysis of root architecture and agronomic traits in white lupin across improvement levels.

PCA biplots summarize relationships among root crown traits, grain yield, and white lupin improvement levels for 2023, 2024, and combined-year BLUEs. Arrows represent trait loadings, and point colors distinguish cultivars, breeding materials, landraces, historic accessions, wild materials, and uncertain groups. Improvement levels showed considerable overlap, indicating limited multivariate separation.

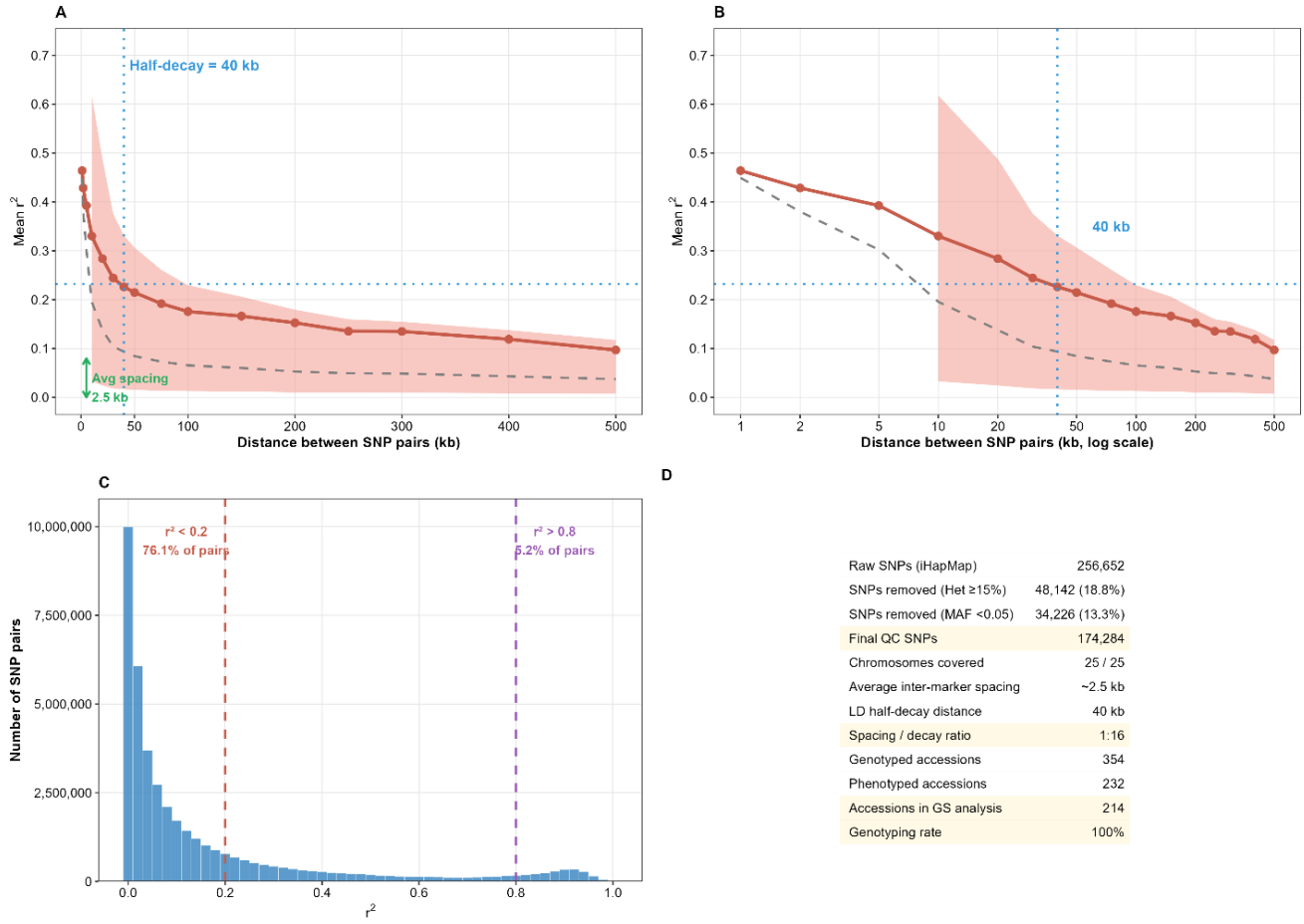

Figure 4.6. Linkage disequilibrium decay and SNP marker panel summary for white lupin.

(A) Mean r² (solid line) with 95% confidence interval (shaded ribbon) decays to half its initial value at approximately 40 kb (vertical dashed line). Average inter-marker spacing of 2.5 kb (green arrow) is well below the LD half-decay distance, indicating adequate marker density for association mapping. (B) LD decay on a logarithmic distance scale, highlighting rapid decay within the first 10 kb. (C) Distribution of pairwise r² values across all SNP pairs; 76.1% of pairs exhibit r² < 0.2 (low LD), while only 5.2% show r² > 0.8 (high LD), indicating sufficient independence among markers. (D) Summary of SNP filtering and panel characteristics.

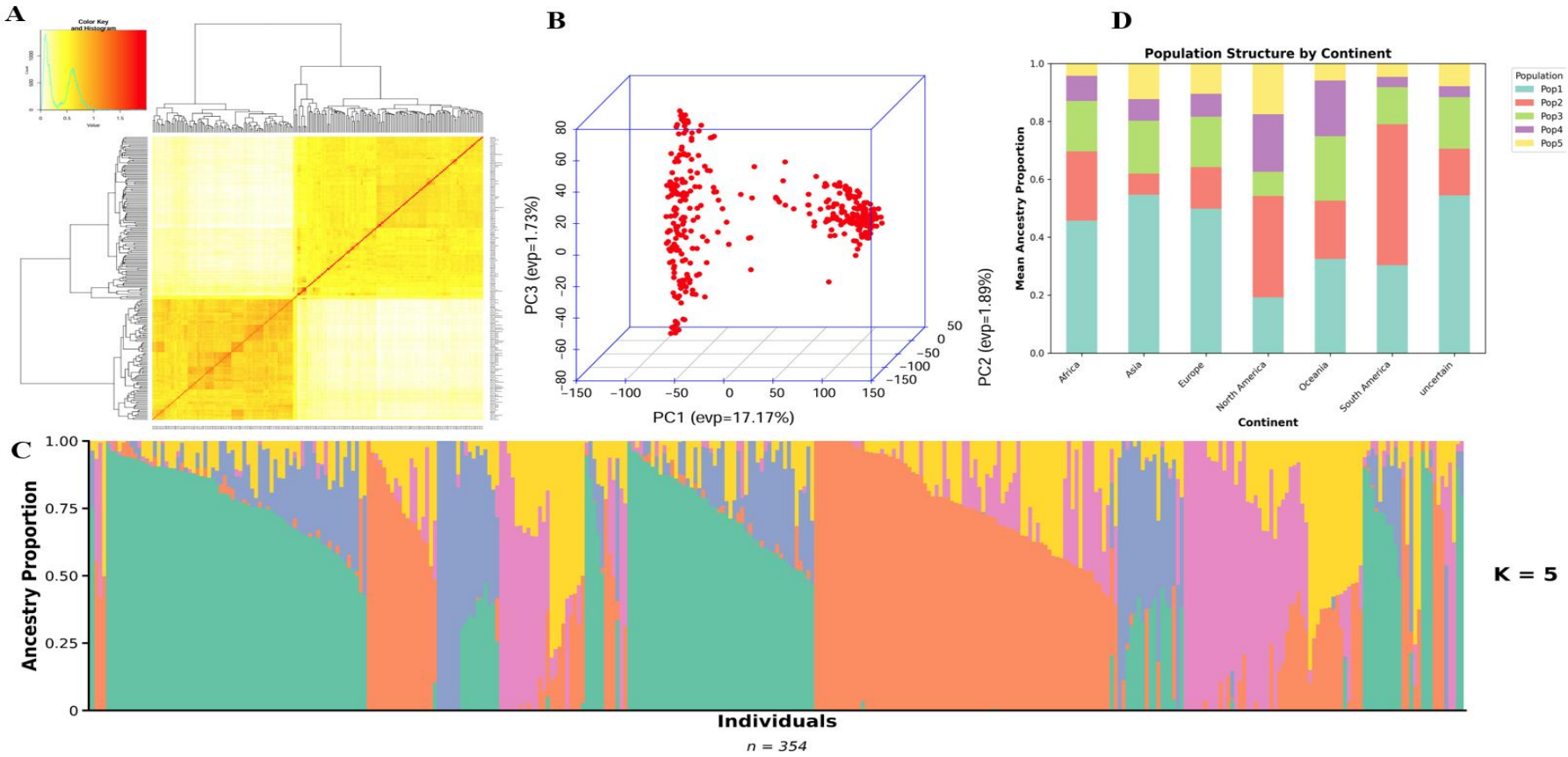

Figure 4.7. Population structure analysis of 354 white lupin accessions.

(A) Kinship heatmap and hierarchical clustering show two broad relatedness groups with internal structure. (B) Three-dimensional PCA explains 17.17%, 1.89%, and 1.73% of genetic variation across PC1–PC3 and shows overlapping clusters. (C) ADMIXTURE at K = 5 indicates extensive mixed ancestry among 354 accessions. (D) All five ancestry components occur across continents, although their relative proportions differ.

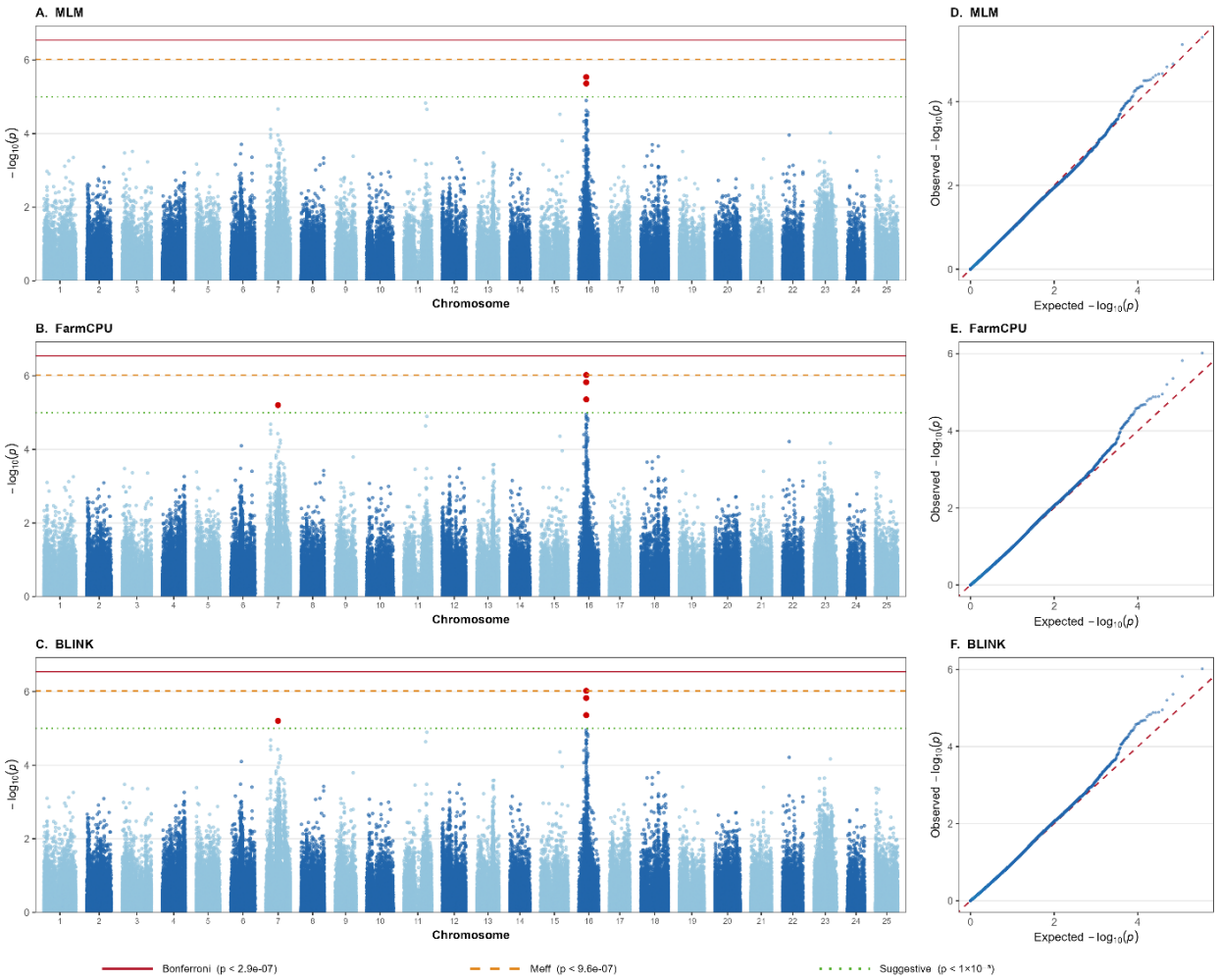

Figure 4.8. Genome-wide association analysis for median root diameter in white lupin using combined-year data.Manhattan plots

(A–C) and quantile-quantile (Q-Q) plots (D–F) for median root diameter (MLM; A, D), FarmCPU (B, E), and BLINK (C, F). In Manhattan plots, the y-axis shows $-\log_{10}(P)$ and the x-axis indicates chromosomal position. Horizontal lines denote significance thresholds: Bonferroni-corrected genome-wide significance ($P < 2.9 \times 10^{-7}$; solid red)

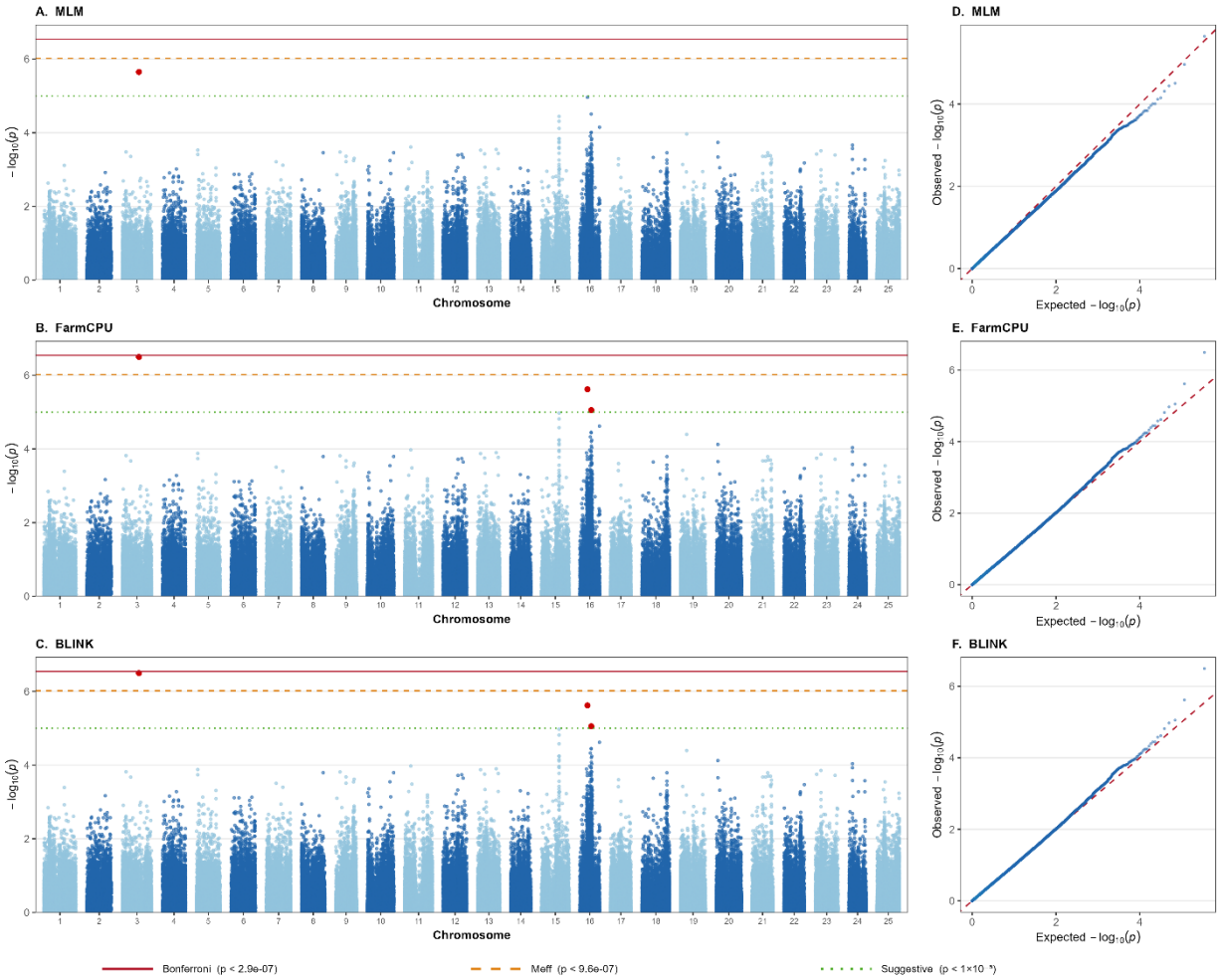

Figure 4.9. Genome-wide association analysis for root coarseness index in white lupin using combined-year data.

Manhattan plots (A–C) and quantile-quantile (Q-Q) plots (D–F) (MLM; A, D), FarmCPU (B, E), and BLINK (C, F). Manhattan plots, the y-axis shows $-\log_{10}(P)$ and the x-axis indicates chromosomal position. Horizontal lines denote significance thresholds: Bonferroni-corrected genome-wide significance ($P < 2.9 \times 10^{-7}$; solid red).

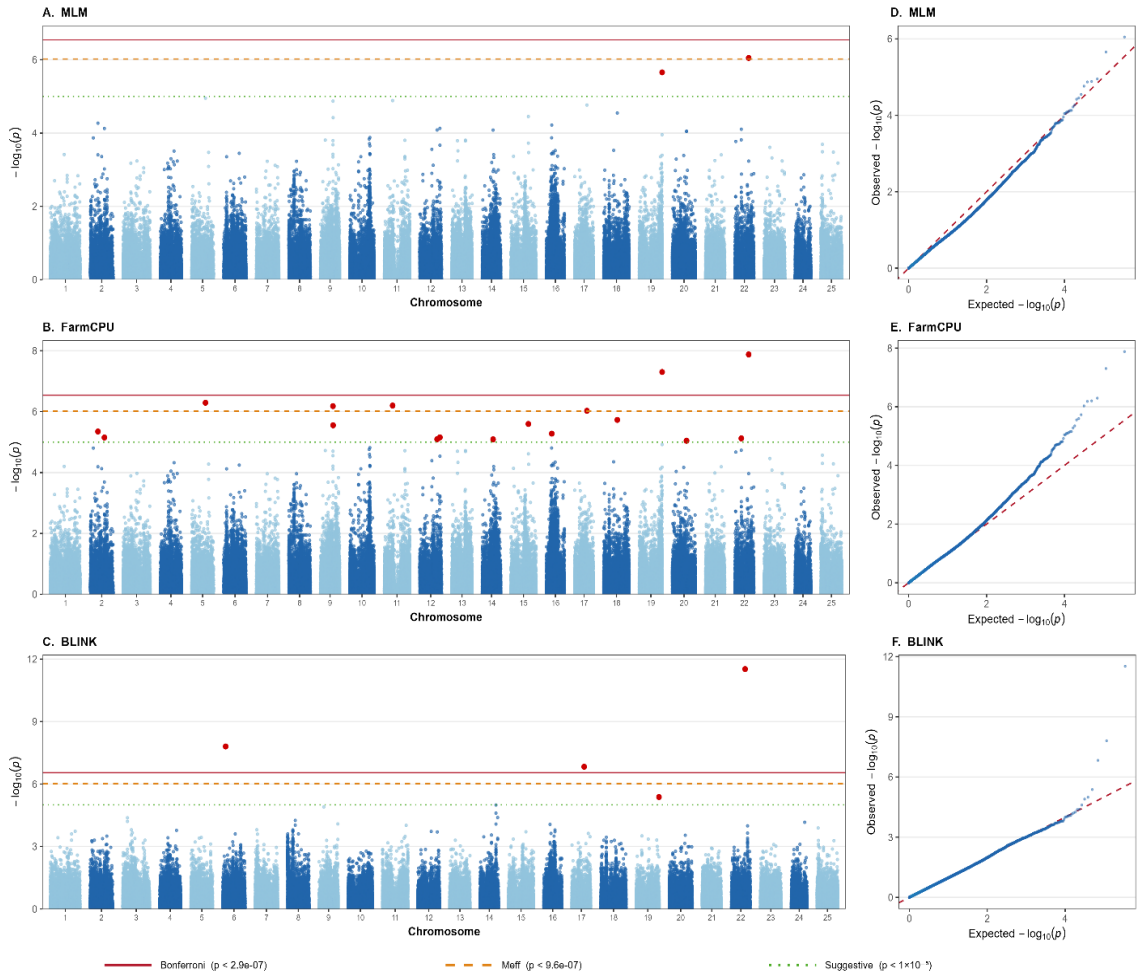

Figure 4.10. Genome-wide association analysis for root gap index in white lupin using combined-year data.

Manhattan plots (A–C) and quantile-quantile (Q-Q) plots (D–F) (MLM; A, D), FarmCPU (B, E), and BLINK (C, F). Manhattan plots, the y-axis shows $-\log_{10}(P)$ and the x-axis indicates chromosomal position. Horizontal lines denote significance thresholds: Bonferroni-corrected genome-wide significance ($P < 2.9 \times 10^{-7}$; solid red).

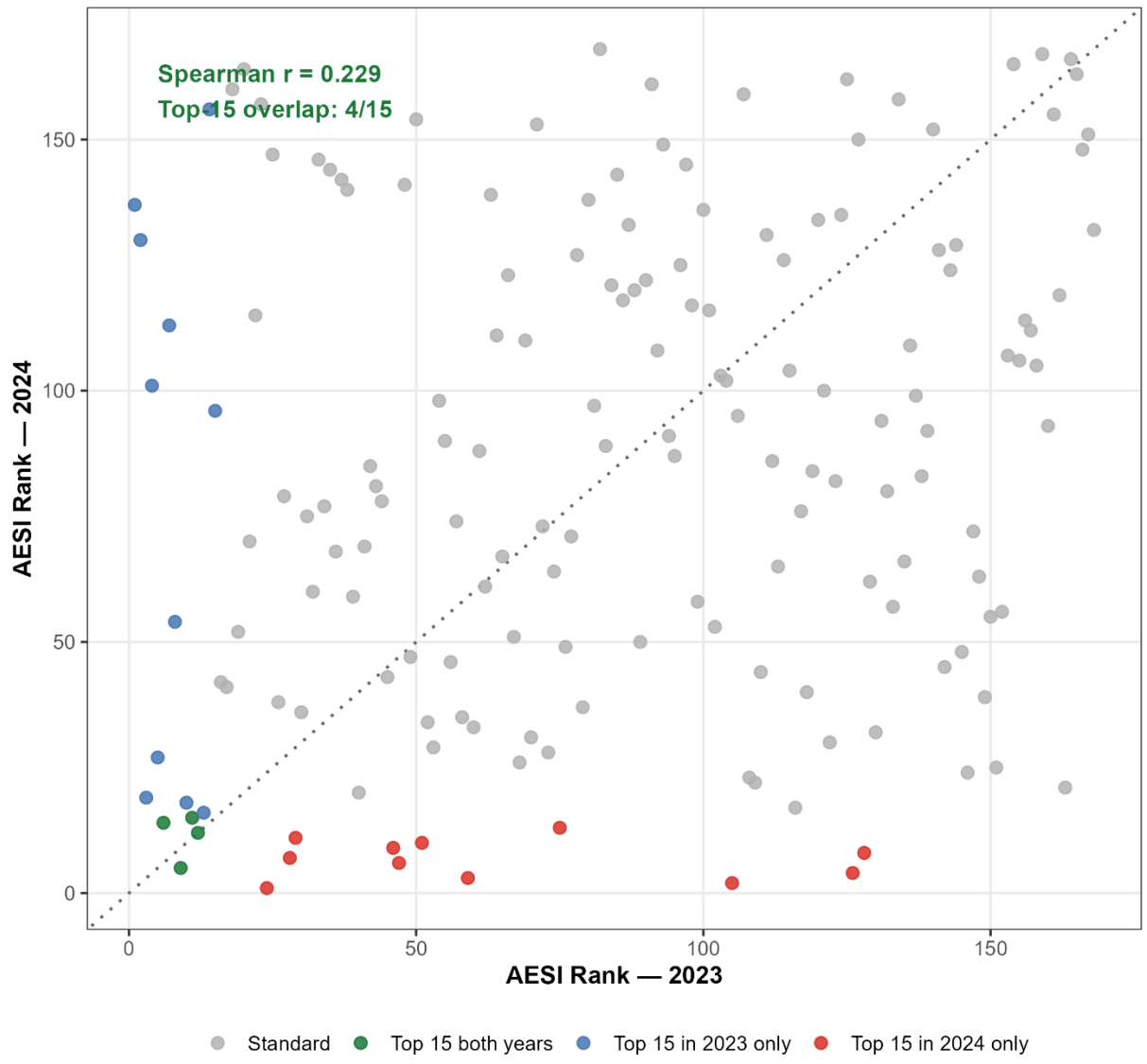

Figure 4.11. Year-to-year stability of Alabama Ecosystem Service Index (AESI) rankings in white lupin.

Scatter plot comparing AESI rank of 168 accessions common to both field seasons (2023 vs 2024). The diagonal dotted line represents perfect rank agreement

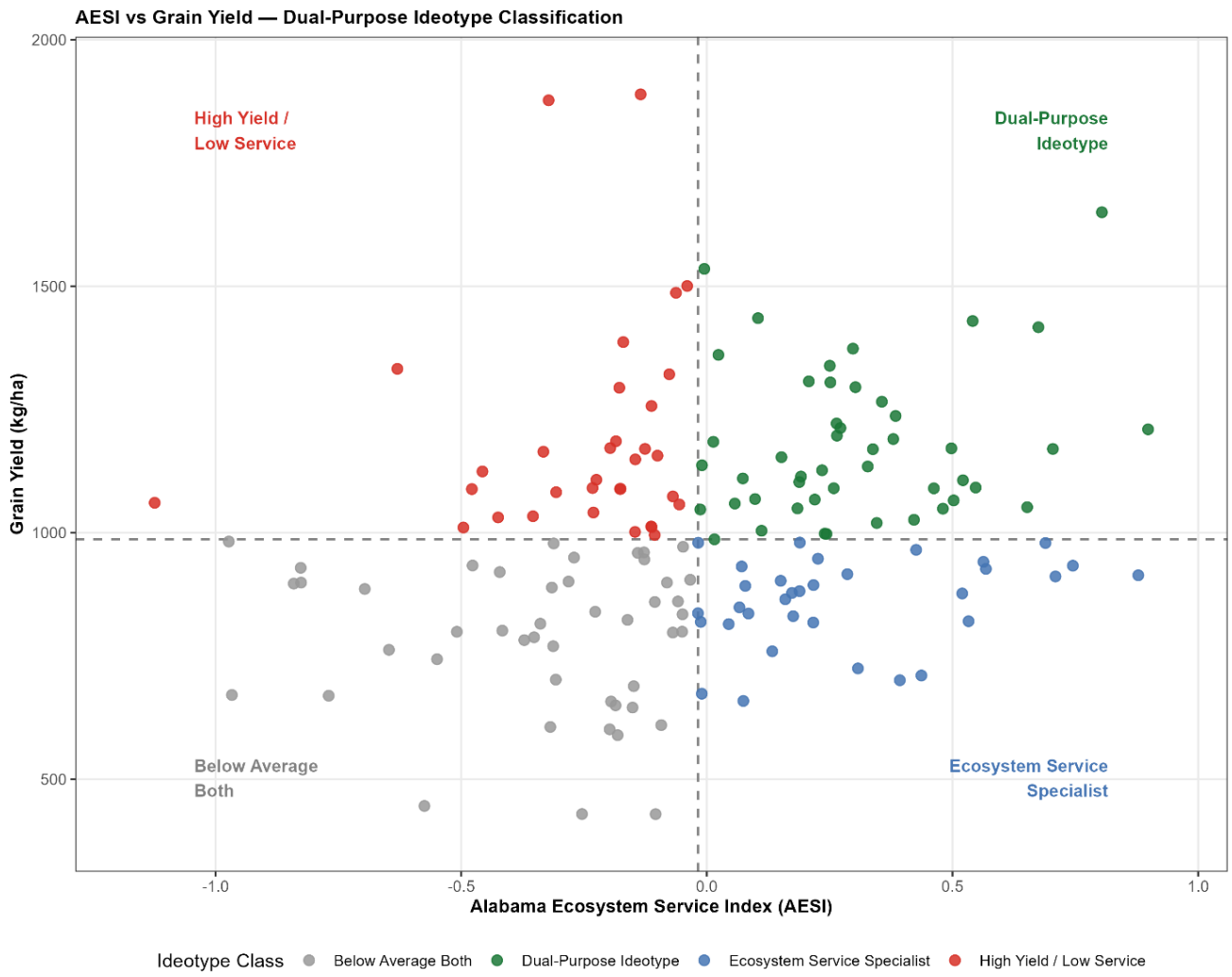

Figure 4.12. Relationship between Alabama Ecosystem Service Index (AESI) and grain yield illustrating dual-purpose ideotype classification in white lupin.

The figure shows classification of white lupin accessions using grain yield and the Alabama Ecosystem Service Index. Accessions with above-average values for both traits were identified as dual-purpose ideotypes, while the remaining groups represented yield specialists, ecosystem-service specialists, or below-average accessions.

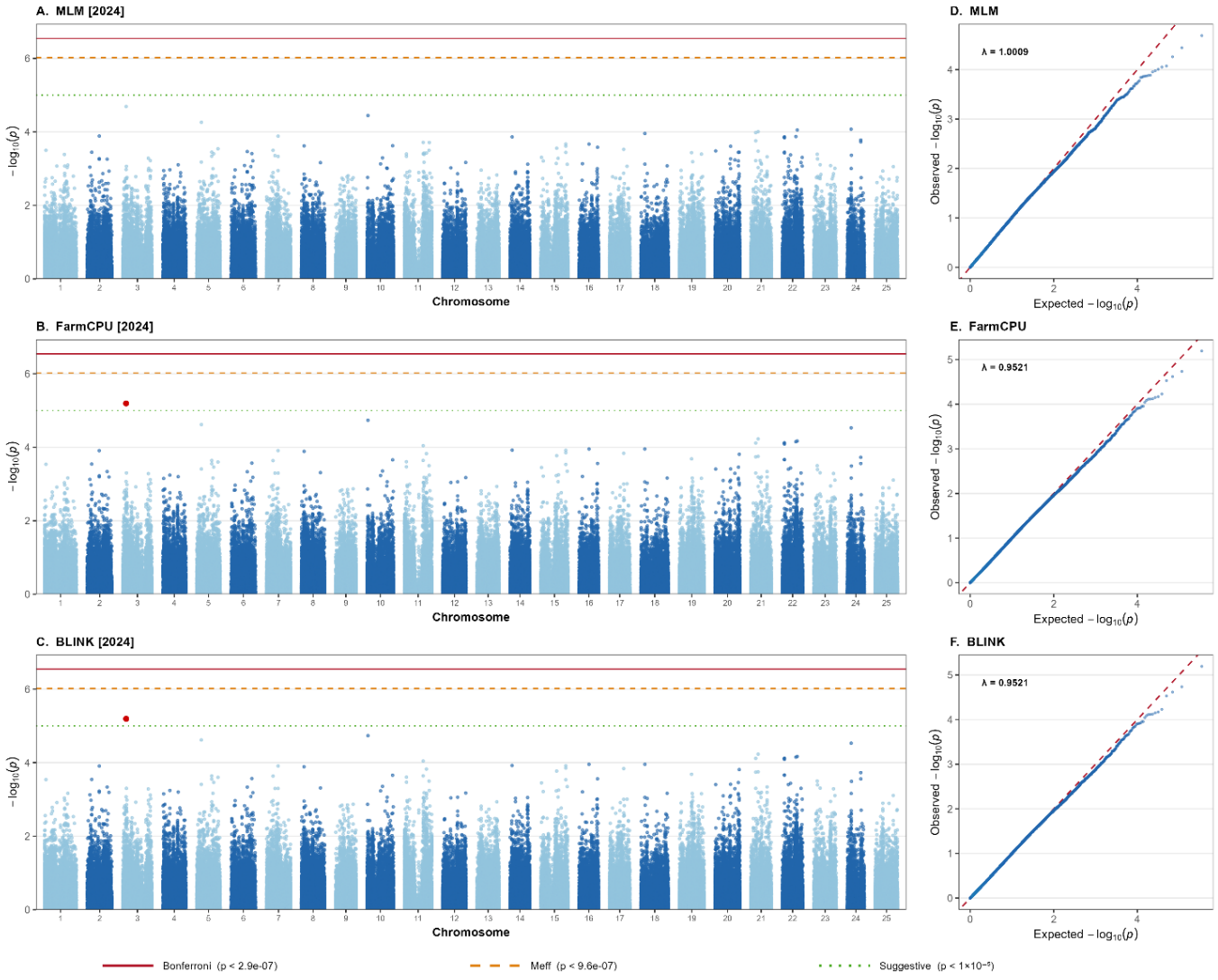

Figure 4.13. Genome-wide association analysis for the Alabama Ecosystem Service Index (AESI) in white lupin using 2024 field season data.

Manhattan plots (A–C) and quantile-quantile (Q-Q) plots (D–F) for AESI using three GWAS models: mixed linear model (MLM; A, D), FarmCPU (B, E), and BLINK (C, F). In Manhattan plots, the y-axis shows $-\log_{10}(P)$ and the x-axis indicates chromosomal position. Horizontal lines denote significance thresholds: Bonferroni-corrected genome-wide significance ($P < 2.9 \times 10^{-7}$; solid red).

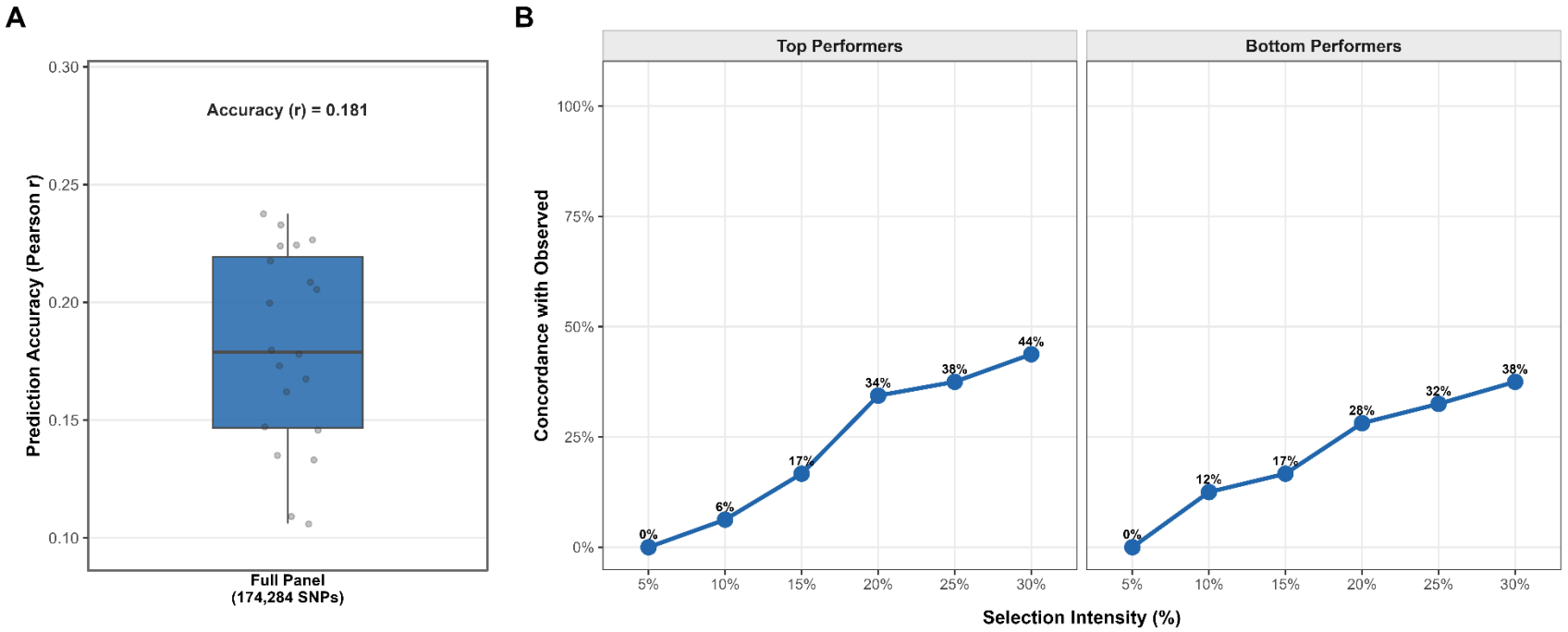

Figure 4.14. Genomic prediction accuracy and selection concordance for the Alabama Ecosystem Service Index (AESI) in WL.

(A) Boxplot comparing GBLUP prediction accuracy (Pearson r) with Full Panel (174,284 SNPs; blue) using 5 x 20 cross-validation. (B) Selection concordance between genomic estimated breeding values (GEBVs) and observed AESI values across selection intensities (5–30%) for top performers (left) and bottom performers (right). Concordance represents the percentage of individuals correctly identified by genomic prediction at each selection threshold.

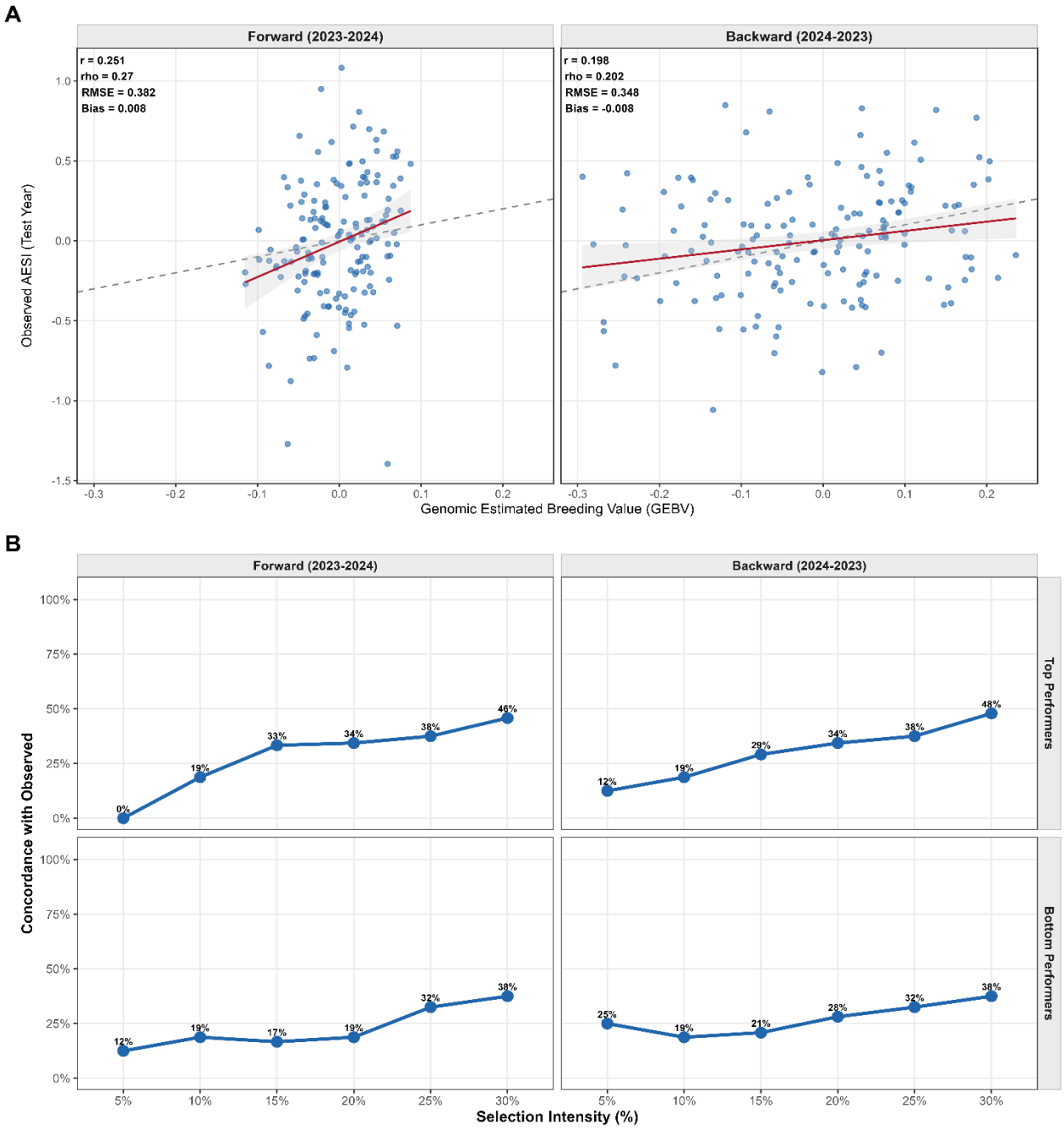

Figure 4.15. Temporal cross-validation of genomic prediction for the Alabama Ecosystem Service Index (AESI) in white lupin.

(A) Scatter plots of genomic estimated breeding values (GEBVs) versus observed AESI under two temporal validation schemes: Left panel is the forward prediction (train 2023 to predict 2024; bottom row) and right panel is the backward prediction (train 2024 to predict 2023; top row). (B) Selection concordance between GEBVs and observed AESI across selection intensities (5–30%) for forward (left) and backward (right) prediction, stratified by top performers (upper row) and bottom performers (lower row)

Table 4.1. Meta data setting for Rhizovision setting.

Parameter	Setting	
RhizoVision Explorer Version	2.0.3	
Root type	Whole root	
Image Thresholding Level	200	
Invert images	false	
Keep largest component	true	
Filter noisy components on background	false	
Maximum background noisy component size	0	
Filter noisy components on foreground	false	
Maximum foreground noisy component size	0	
Enable edge smoothing	true	
Edge smoothing threshold	4	
Enable root pruning	true	
Root pruning threshold	5	
Convert pixels to physical units	true	
Number of Pixels per mm	15	
Pixel to millimeter conversion factor	0.0666667	
Diameter Range 1	0	0.03
Diameter Range 2	0.03	0.5
Diameter Range 3	0.5	2
Diameter Range 4	2	5
Diameter Range 5	5	above
Save segmented images	true	
Segmented image file name suffix	_seg	
Save processed feature images	true	
Processed image file name suffix	_features	

Table 4.2. Agronomic, Rhizo vision and Derived traits; units, formular and description.

Category	Trait	Unit	Formula / Method	Description
RVE-traits	median_roots	count	Direct RhizoVision output	Median number of roots
	root_tips	count	Direct output	Number of root tips
	total_length	mm	Direct output	Total root length
	depth	mm	Direct output	Maximum rooting depth
	width_depth_ratio	–	width / depth	Root system spread vs depth
	network_area	mm²	Direct output	Root system 2D area
	solidity	–	network_area / convex_area	Root packing efficiency
	median_diameter	mm	Direct output	Median diameter
	avg_hole_size	mm²	Direct output	Average hole size
	avg_orientation	degrees	Direct output	Average angle of roots
	shallow_freq	count	Direct output	Number shallow-angled roots
	steep_freq	count	Direct output	Number steep-angled roots
Derived root traits	Depth_Dominance	–	depth / (depth + width)	Allocation to depth vs width (0 = spread, 1 = depth)

Category	Trait	Unit	Formula / Method	Description
		tips		
	Branching_Intensity	mm^{-1}	root_tips / total_length	Number of tips per unit length
	Gap_Index	–	(num_holes × avg_hole_size) / network_area	Measure of discontinuities in crown
	FineFrac_Length	–	(length_d1 + length_d2) / total_length	Fraction of length in fine roots
	CoarseFrac_Length	–	(length_d4 + length_d5) / total_length	Fraction of length in coarse roots
		mm^2		
	Coarseness_Index	mm^{-1}	volume / total_length	Thickness of roots per unit length
	SA_to_V	mm^{-1}	surface_area / volume	Root surface efficiency

Table 4.3. Alabama Ecosystem Service Index (AESI) weight structure for 11 root crown and agronomic traits in white lupin.

Ecosystem service	Service weight	Trait	Trait weight†	Direction‡	Functional justification
P mobilization	0.35	SA_to_V	0.117	+	Root surface area-to-volume ratio; proxy for cluster root P absorption capacity (Lambers et al., 2013)
		total_length	0.117	+	Primary determinant of soil volume explored for P foraging (Lynch, 2019)
		shallow_freq	0.117	+	Topsoil foraging accesses legacy P in Alabama Ultisols (Lynch, 2019)
Erosion control	0.25	width_depth_ratio	0.083	+	Root system width-to-depth ratio; lateral spread anchors topsoil horizontally (Ola et al., 2015)
		FineFrac_Length	0.083	+	Fine root mat physically binds soil particles (Baets et al., 2007)

Ecosystem service	Service weight	Trait	Trait weight†	Direction‡	Functional justification
		median_diameter	0.083	–	Smaller diameter increases root surface density per unit biomass (Baets et al., 2007)
Soil organic matter	0.20	solidity	0.100	+	Denser networks contribute greater belowground C inputs (Griffiths et al., 2022)
		median_roots	0.100	+	Larger root systems increase rhizodeposition and senescence C (Rasse et al., 2005)
Dual-purpose yield	0.20	GY_KgHa	0.067	+	Grain yield; primary economic return justifying farmer adoption (SARE/CTIC, 2023)
		HSW_g	0.067	+	Grain size determines market grade and end-use quality (Annicchiarico et al., 2025)
		Alkaloid	0.067	–	High alkaloids disqualify from food, feed, and nutraceutical markets (Schwertfirm et al., 2024)

Abbreviations: SA_to_V = surface area to volume ratio, total_length = total root length, shallow_freq = shallow root frequency, width_depth_ratio = width-to-depth ratio of the root system, FineFrac_Length = fine root fraction length, median_diameter = median root diameter, solidity = root system solidity, median_roots = median root number, GY_KgHa

= grain yield (kg ha⁻¹), HSW_g = hundred-seed weight (g), and Alkaloid = seed alkaloid content.† Trait weight = service weight / ntraits within service. All trait weights are positive and sum to 1.00, reflecting the total allocation of the weighting budget. The direction of trait contribution to AESI is encoded separately via z-score sign reversal (see Direction column), not through negative weights in the summation.
‡ Direction indicates the favorable direction for AESI. “+” = higher trait values increase AESI; “–” = lower trait values increase AESI. For “–” traits (Alkaloid, median_diameter), z-scores are sign-reversed before within-service averaging, so that genotypes with high alkaloid content or large root diameter are penalized. The AESI formula is: AESI = Σs ws · mean(z*ts), where z* denotes the direction-corrected z-score and ws is the service weight.

Table 4.4. Heritability summary for 22 agronomic and root crown traits in white lupin evaluated across three analytical scopes (2023, 2024, and Combined).

Trait	Scope	H²_piepho[a]	H²_cullis	H²_mean	H²_SNP	VG (%)	LRT_VG	LRT_VG Y[b]
Alkaloid	2023	0.02	0.45	0.56	0.38	37.6	ns	—
	2024	0.01	0.46	0.58	0.42	41.1	ns	—
	Combined	0.02	0.64	0.82	0.73	51.5	ns	ns
avg_hole_size	2023	0.65	0.44	0.52	0.21	35.0	***	—
	2024	0.56	0.14	0.14	0.11	7.8	ns	—
	Combined	0.63	0.30	0.37	0.27	7.2	**	**
avg_orientation	2023	0.49	0.05	0.06	0.08	2.9	ns	—
	2024	0.54	0.13	0.14	0.00	7.2	ns	—
	Combined	0.56	0.20	0.26	0.10	3.7	*	ns
Branching_Intensity	2023	0.62	0.39	0.46	0.32	29.4	***	—
	2024	0.51	0.06	0.06	0.10	3.0	ns	—
	Combined	0.51	0.00	0.00	0.08	0.0	ns	*
CoarseFrac_Length	2023	0.61	0.30	0.36	0.25	20.8	**	—
	2024	0.54	0.05	0.06	0.05	2.8	ns	—
	Combined	0.55	0.19	0.24	0.18	5.9	ns	ns
Coarseness_Index	2023	0.63	0.34	0.41	0.27	23.6	**	—
	2024	0.54	0.07	0.07	0.00	3.7	ns	—
	Combined	0.56	0.22	0.28	0.14	8.5	*	ns
depth	2023	0.50	0.00	0.00	0.01	0.0	ns	—
	2024	0.48	0.00	0.00	0.00	0.0	ns	—
	Combined	0.49	0.00	0.00	0.00	0.0	ns	ns

Trait	Scope	H²_piepho[a]	H²_cullis	H²_mean	H²_SNP	VG (%)	LRT_VG	LRT_VG Y[b]
Depth_Dominance	2023	0.54	0.18	0.22	0.07	12.5	ns	—
	2024	0.56	0.24	0.25	0.12	14.5	*	—
	Combined	0.53	0.00	0.00	0.13	0.0	ns	*
FineFrac_Length	2023	0.54	0.15	0.18	0.04	9.7	ns	—
	2024	0.51	0.03	0.03	0.07	1.6	ns	—
	Combined	0.55	0.15	0.19	0.12	5.2	ns	ns
Gap_Index	2023	0.66	0.36	0.43	0.18	27.2	**	—
	2024	0.50	0.00	0.00	0.06	0.0	ns	—
	Combined	0.65	0.20	0.26	0.14	5.5	*	ns
GY_KgHa	2023	0.63	0.43	0.43	0.20	26.3	***	—
	2024	0.56	0.00	0.00	0.00	0.0	ns	—
	Combined	0.61	0.07	0.10	0.12	1.2	ns	ns
HSW_g	2023	0.90	0.89	0.89	0.86	80.5	***	—
	2024	0.86	0.83	0.83	0.78	68.9	***	—
	Combined	0.91	0.89	0.91	0.91	34.9	***	ns
median_diameter	2023	0.58	0.26	0.32	0.20	18.1	*	—
	2024	0.57	0.25	0.27	0.00	13.6	*	—
	Combined	0.57	0.20	0.25	0.21	7.3	*	ns
median_roots	2023	0.57	0.23	0.28	0.12	16.0	*	—
	2024	0.64	0.36	0.37	0.17	20.1	**	—
	Combined	0.66	0.34	0.42	0.20	12.6	**	ns
network_area	2023	0.59	0.27	0.33	0.00	19.2	*	—
	2024	0.46	0.00	0.00	0.01	0.0	ns	—

Trait	Scope	H²_piepho[a]	H²_cullis	H²_mean	H²_SNP	VG (%)	LRT_VG	LRT_VG Y[b]
	Combined	0.53	0.03	0.04	0.00	0.5	ns	ns
root_tips	2023	0.58	0.34	0.40	0.18	25.3	**	—
	2024	0.51	0.12	0.13	0.00	6.5	ns	—
	Combined	0.58	0.27	0.34	0.16	7.4	**	ns
SA_to_V	2023	0.61	0.31	0.38	0.22	21.2	**	—
	2024	0.53	0.06	0.06	0.00	3.0	ns	—
	Combined	0.55	0.22	0.28	0.12	8.2	*	ns
shallow_freq	2023	0.51	0.08	0.10	0.08	5.2	ns	—
	2024	0.55	0.21	0.23	0.03	12.7	*	—
	Combined	0.60	0.26	0.33	0.10	5.1	*	ns
solidity	2023	0.56	0.22	0.27	0.07	15.5	*	—
	2024	0.56	0.17	0.18	0.00	10.0	ns	—
	Combined	0.57	0.23	0.30	0.16	5.1	*	ns
steep_freq	2023	0.48	0.03	0.03	0.06	1.6	ns	—
	2024	0.54	0.07	0.08	0.00	4.1	ns	—
	Combined	0.55	0.14	0.19	0.07	2.6	ns	ns
total_length	2023	0.57	0.26	0.31	0.11	18.5	*	—
	2024	0.52	0.12	0.13	0.03	6.7	ns	—
	Combined	0.57	0.17	0.22	0.09	3.7	ns	ns
width_depth_ratio	2023	0.56	0.18	0.22	0.07	12.3	ns	—
	2024	0.55	0.04	0.04	0.08	2.0	ns	—
	Combined	0.58	0.16	0.21	0.11	2.5	ns	ns

a H^2_piepho, Piepho heritability ; reported as primary heritability metric consistent with BLUEs used in downstream GWAS analyses.b LRT_VGY, likelihood ratio test for genotype-by-year interaction variance; applicable to Combined scope only; indicates not applicable (per-year analyses). VG (%), percentage of total phenotypic variance attributable to the genotype effect. H^2_cullis, Cullis heritability. H^2_mean, entry-mean broad-sense heritability [σ^2_G / (σ^2_G + σ^2_GY/Y + σ^2_E/YR)]. H^2_SNP, genomic heritability estimated by substituting the identity matrix with a VanRaden (2008) genomic relationship matrix.LRT_VG, likelihood ratio test for significance of genotypic variance (H0: σ^2_G = 0). *, **, ***, significance at $p < 0.05$, $p < 0.01$, and $p < 0.001$, respectively; ns, not significant.

Table 4.5. Candidate loci and genes associated with root architecture traits in white lupin.

Tier	Locus	Associated Traits	Candidate Gene	GO Annotation	Biological Interpretation
1	Chr16_5502603	CoarseFrac_Length, Coarseness_Index, Gap_Index, SA_to_V, avg_orientation	Lalb_Chr16g0385371	GO:0004650; cell wall and carbohydrate metabolism	Structural root architecture and carbon allocation
1	Chr19_2764944	shallow_freq	Lalb_Chr19g0126691	GO:0009734, GO:0055085, GO:0060918	Shallow root proliferation and topsoil foraging
2	Chr19_18016413	Multiple root traits (7)†	Lalb_Chr19g0140181	GO:0003677, GO:0003723, GO:0046872	Multi-trait regulatory hotspot; transcriptional control
2	Chr11_6563520	CoarseFrac_Length, Coarseness_Index, Gap_Index, SA_to_V, avg_hole_size	Lalb_Chr11g0069981	GO:0004497, GO:0005506, GO:0016021, GO:0016705	Coordinated root architecture and metabolic activity
2	Chr17_5835594	CoarseFrac_Length, Coarseness_Index, Gap_Index, SA_to_V, avg_hole_size	Lalb_Chr17g0337901	GO:0008810, GO:0030245	Cell wall modification and structural remodeling
2	Chr12_7086361	avg_orientation, shallow_freq, steep_freq	Lalb_Chr12g0205521	GO:0003779, GO:0005885, GO:0030041	Directional root growth and cytoskeletal organization
2	Chr16_8255319	CoarseFrac_Length, Coarseness_Index,	Lalb_Chr16g0388041	GO:0005634, GO:0007165	Signaling-mediated regulation of root ideotype

Tier	Locus	Associated Traits	Candidate Gene	GO Annotation	Biological Interpretation
		FineFrac_Length, SA_to_V			

† Includes depth, solidity, median_diameter, avg_hole_size, CoarseFrac_Length, Coarseness_Index, and SA_to_V. Tier 1: High-confidence loci with strong statistical support across multiple methods; Tier 2: Moderate-confidence loci with consistent directional effects

Table 4.6. Heritability estimates and selection of root and agronomic traits for inclusion in the Alabama Ecosystem Service Index (AESI).

Trait	H2_mean_2023	H2_mean_2024	H2_mean_Combined	AESI_Eligible
HSW_g	0.893	0.833	0.913	TRUE
Alkaloid	0.561	0.582	0.816	TRUE
median_roots	0.276	0.375	0.418	TRUE
avg_hole_size	0.522	0.144	0.366	TRUE
root_tips	0.403	0.13	0.344	TRUE
shallow_freq	0.098	0.225	0.325	TRUE
solidity	0.27	0.185	0.298	TRUE
SA_to_V	0.376	0.06	0.28	TRUE
Coarseness_Index	0.41	0.074	0.276	TRUE
avg_orientation	0.056	0.136	0.262	TRUE
Gap_Index	0.427	0	0.26	TRUE
median_diameter	0.319	0.268	0.252	TRUE
CoarseFrac_Length	0.358	0.058	0.238	TRUE
total_length	0.313	0.13	0.225	TRUE
width_depth_ratio	0.218	0.04	0.206	TRUE
FineFrac_Length	0.183	0.033	0.188	TRUE
steep_freq	0.033	0.08	0.187	TRUE
GY_KgHa	0.432	0	0.097	FALSE
network_area	0.329	0	0.036	FALSE

Trait	H2_mean_2023	H2_mean_2024	H2_mean_Combined	AESI_Eligible
Branching_Intensity	0.463	0.063	0	FALSE
Depth_Dominance	0.223	0.254	0	FALSE
depth	0	0	0	FALSE

Table 4.7. Sensitivity of AESI genotype rankings to ±20% perturbation of ecosystem service weights.

Ecosystem service	Perturbation	Base w†	Perturbed w	Spearman r vs. base AESI
P mobilization	+20%	0.35	0.42	0.994
	–20%		0.28	0.993
Erosion control	+20%	0.25	0.30	0.996
	–20%		0.20	0.997
Soil organic matter	+20%	0.20	0.24	0.995
	–20%		0.16	0.995
Dual-purpose yield	+20%	0.20	0.24	0.997
	–20%		0.16	0.997

† Base service weights sum to 1.00. For each perturbation, the focal service weight was adjusted by ±20% and the remaining three weights were rescaled proportionally so that all four continued to sum to unity. Spearman rank correlation was computed between the base AESI ranking and the ranking under each perturbed weight set (n = 168 accessions). All perturbations yielded r ≥ 0.993, exceeding the a priori stability threshold of r ≥ 0.90.

Chapter 5 UAV-multispectral phenomics selectively improves genomic prediction of agronomic and root traits linked to ecosystem services in winter white lupin

Abstract

Agricultural systems in Alabama and the Southeastern United States face persistent sustainability challenges driven by phosphorus (P)-fixing Ultisols and legacy P accumulation, contributing to widespread non-point source pollution. Although winter cover crops reduce nutrient losses, adoption remains low due to limited profitability. Dual-purpose cover crops that deliver ecosystem services while generating income represent a critical breeding target.

White lupin (Lupinus albus L.) is uniquely suited to this role through cluster root-mediated P mobilization and high-protein grain production; however, breeding for belowground functions is constrained by limited scalable root phenotyping and predictive tools. A total of 232 accessions were evaluated over two years (2023–2024), integrating shovelomics–RhizoVision root phenotyping, UAV multispectral phenomics, and genome-wide SNP data.

Root crown traits were heritable (H^2 = 0.14–0.52). Combining genomic and phenomic information using a linear kernel outperformed either source alone for alkaloid status (r = 0.55 in 2023 and 0.59 in 2024, exceeding genomic-only prediction by 0.16–0.17); structural root traits had low prediction ability across all models. A single late-season flight outperformed temporal stacking for seven of nine root traits. In the pooled two-year population, prediction reached r = 0.53 for alkaloid status but was near zero for root architectural traits.

These results demonstrate that genomic–phenomic integration selectively improves prediction for high-heritability traits, and that flight timing matters more than flight frequency for root trait phenomics. Prediction of structural root traits remains poor across all data sources, indicating that direct phenotyping is still required for these traits in dual-purpose white lupin breeding.

5.1 Introduction

In the Southeastern United States, persistent agricultural sustainability challenges arise from highly weathered Ultisols and require targeted ecosystem services to address them. Ultisols are aluminum (Al) and iron (Fe) saturated and strongly phosphorus (P)-fixing, and decades of intensive use of poultry manure have created significant legacy phosphorus accumulation in the 0–15 cm surface horizon as Al/Fe-bound and phytate-P pools resistant to plant uptake by cash crops (Waldrip et al., 2023). These conditions have made agriculture a source of non-point source pollution in the region, with approximately 40% of Alabama's water bodies currently failing to meet designated water quality standards (USEPA, 2012). Although winter cover crops represent the most scalable non-point source management intervention available to row-crop farmers, reducing tile drain phosphorus losses by 7–58% and nitrate-N losses by 27–72% in multi-year field studies (Speir et al., 2021), only 4.7% of U.S. cropland was planted to cover crops in 2022, with profitability cited as a top barrier among non-adopters (Myers & Wilson, 2023). Within the USDA NRCS "Avoid, Control, and Trap" framework, dual purpose cover crops offer a strategic option by capturing residual N and P in harvestable biomass, providing a marketable product while reducing the risk of nutrient export to surface waters and improving runoff control through root mediated

enhancement of soil structure (Osmond et al., 2019; Christianson et al., 2021; Glaze Corcoran et al., 2023; Griffiths et al., 2022).

White lupin (Lupinus albus L.) is uniquely positioned to fulfil this role. As a winter annual legume, it can occupy the fallow season when major cash crops are absent from the field, it does not compete with summer row crops, eliminating the yield penalty that most commonly deters cover crop adoption (Knoll et al., 2022). Its 32–51% crude protein grain is nutritionally comparable to soybean, serving livestock, aquaculture, and human food markets (Prereira et al., 2022), while residue contributes approximately 143 kg N ha^{-1} to subsequent summer crops (Knoll et al., 2022). Most importantly, white lupin is uniquely adapted among major crop legumes for phosphorus acquisition in highly weathered soils. Unlike most legumes, which depend on mycorrhizal associations to access labile phosphorus, white lupin is functionally non-mycorrhizal and instead develops specialized cluster roots that release organic acids (citrate and malate). These exudates actively mobilize phosphorus from otherwise inaccessible soil pools, including forms bound to aluminum, iron, and organic compounds. As a result, white lupin can acquire substantially more phosphorus from non-labile soil fractions, up to fivefold more per unit root length than soybean (Lambers et al., 2006). This distinct physiological strategy enables white lupin to exploit legacy phosphorus in Ultisols where other legumes are largely ineffective. Phosphorus mobilized by cluster root exudation is absorbed into cover crop biomass and released to the succeeding cash crop as residues decompose, completing an agronomic P-trap cycle that directly addresses legacy-P-enriched topsoils (Damon et al., 2014). Its shallow, wide root architecture further intercepts dissolved N and P before loss to Alabama tributaries, while coarse

root biopores improve water infiltration through compacted subsoil horizons and fine root turnover drives soil organic matter formation (Rauber et al., 2024). Targeted root trait selection (Table 5.1) for these belowground functions is therefore central to developing white lupin as a dual-purpose cash cover crop for Alabama agriculture (Freschet et al., 2021).

Realizing this potential through breeding requires phenotyping root architecture at population scale, which remains the central bottleneck. Root system architecture (RSA) has been identified as a key breeding target for climate-resilient crops (Freschet et al., 2021; Griffiths et al., 2022), yet it has historically been set aside in most plant breeding programs majorly, due to difficulty of measuring root traits directly in the field (Den Herder et al., 2010; Griffin et al., 2025). Field-based methods including mini-rhizotrons, shovelomics, and core break have advanced the study of RSA and provided valuable information, but all remain constrained by population size and labor intensity (Trachsel et al., 2011; York et al., 2018). Shovelomics is high-throughput only relative to full root excavation. In absolute breeding terms it is not: each plot must be dug, each crown washed, barcoded, imaged, and segmented, and the plant is destroyed in the process, so the same genotype cannot be re-measured later in the season or in a subsequent year. Indoors root screening methods such as Paper pouch, clear pot, and rhizobox platforms have enabled genomic discoveries for seminal root traits in cereals (Alahmad et al., 2019; Robinson et al., 2016). A major limitation with these methods is that they lose field relevance: root phenotypes measured at early growth stages are poor representatives of mature field root systems and show weak to moderate associations with them (Freschet et al., 2021; Alahmad et al., 2025), which is why the

genetic control of mature root architecture under field conditions remains poorly understood. Hence, because destructive field methods are accurate but unscalable, whereas controlled environment methods are scalable but not field representative, breeding requires an indirect, nondestructive approach to obtain comparable information. Combining shovelomics with the open-source RhizoVision Explorer platform (Seethepalli et al., 2021), which extracts more than 20 architectural traits, reduces the image analysis burden and has enabled field-scale root phenotyping in breeding populations (York et al., 2019), but it does not remove the excavation step, and its deployment in a white lupin breeding program integrated with genomic prediction had not been tried prior to this work.

Remote sensing with unmanned aerial vehicles (UAV), can be an innovative solution to RSA phenotyping bottleneck. The rationale for aerial sensing of roots is that canopy signals reflect the water and nutrients delivered by roots, thereby serving as proxies for belowground function (Alahmad et al., 2025). For instance, Lopes and Reynolds (2010) demonstrated that partitioning of assimilates to deeper roots was associated with cooler canopies and higher yield under drought, and Gutierrez et al. (2010) showed that spectral reflectance indices linked to water use captured significant genetic variation for both leaf water potential and soil moisture availability under drought in wheat. Pinto et al. (2010) and Pinto and Reynolds (2015) provided additional evidence showing a common genetic basis for canopy temperature reduction under heat and drought linked to optimized root distribution. Put together, these studies reported promising correlations between crop canopy proxy traits and improved access to soil water through enhanced root architecture (Lopes and Reynolds, 2010; Pinto et

al., 2010; Pinto and Reynolds, 2015; Li et al., 2019), with the relationship mostly influenced by physiological factors such as leaf area, stomatal conductance, and root access to soil moisture (Ober et al., 2021). Furthermore, reflectance in the red-edge region near 705 to 740 nm is sensitive to chlorophyll content and therefore informative about photosynthetic capacity and nitrogen status (Li et al., 2018), and Féret et al. (2021) demonstrated that leaf protein content can be estimated from narrow shortwave infrared domains between 2100 to 2139 nm and 2160 to 2179 nm, confirming that defined spectral regions track canopy biochemical composition. Vegetative indices (VI) obtained from UAV precisely estimated sorghum leaf area and canopy cover (Potgieter et al., 2017; Zhao et al., 2021), and remote sensing enabled accurate prediction of water- and nitrogen-use efficiency and assessment of canopy temperature and stomatal conductance in cereals such as wheat and maize (Yang et al., 2020; Brewer et al., 2022). This approach is non-destructive and provides opportunity for repeatability, less susceptible to human error, and is scalable to the population sizes breeding programs require (Krause et al., 2021; Adak et al., 2021; Kaur et al., 2024). Alahmad et al. (2025) demonstrated UAV predictions in barley roots, training PLSR on UAV vegetation indices to predict root count distribution with R^2 of 0.51 to 0.75 and predicted-trait heritabilities averaging 0.71 to 0.81 across two contrasting seasons, with haplotype mapping recovering EGT2, DRO1, and RAQ1 to confirm the predictions carried real RSA biology rather than statistical artefact, although their framework stops at prediction and mapping and does not test whether spectral information adds value within a genomic prediction model.

Despite the availability of scalable root phenotyping pipelines, genomic prediction (GP) of belowground traits remains challenging. In contrast to highly heritable above-ground traits, for which prediction accuracies of 0.44–0.60 are routinely reported (Crossa et al., 2017), root architectural traits typically exhibit low to intermediate heritability. This is driven by strong genotype × environment interactions, complex polygenic control, and high phenotypic plasticity, as root systems respond dynamically to environmental variation in soil moisture, temperature, rainfall, and nutrient availability (Alahmad et al., 2025). In wheat, root traits exhibit very low heritability (≈0.03–0.06), with genomic prediction accuracies typically limited to ~0.26–0.33, substantially lower than for above-ground traits (Guo et al., 2020). Similarly, genomic prediction accuracies for root traits range from 0.08 to 0.23 in intermediate wheatgrass (Griffin et al., 2025), remain consistently lower than above-ground traits in maize (Zuffo et al., 2022). These limitations motivate the use of complementary data sources to improve prediction.

To address these gaps, a two-year field study (2023–2024) was conducted with 232 white lupin accessions in central Alabama. The objectives were to: (i) evaluate whether a shovelomics and RhizoVision pipeline produces heritable root crown traits relevant for ecosystem-service breeding, (ii) assess the prediction accuracy and selection concordance of UAV-derived phenomic models across individual and combined flight dates, (iii) determine whether integrating genomic and phenomic information in multi-kernel models improves prediction over either data source alone, and (iv) evaluate whether a phenomic kernel averaged across independently scaled per-year vegetation-index matrices predicts untested lines in a pooled two-year population.

5.2. Materials and Methods

5.2.1 Trial location, plant material, and experimental design

Field trials were conducted at the E.V. Smith Research Center - Plant Breeding Unit in Tallasee, Alabama (32.497°N, 85.892°W) over two consecutive growing seasons (Year 1: planted November 2023, harvested April 2024; Year 2: planted November 2024, harvested April 2025). A total of 232 white lupin accessions were evaluated: 168 were common to both years and 32 were unique to each year, reflecting the partially overlapping structure of a recurrent selection program. Trials were established as row–column designs (20 × 20 grid) with two replicates. Each plot comprised two rows 4.57 m long, with 0.91 m (36 in) row spacing, giving a plot width of 1.82 m (two rows at 0.91 m spacing). The field was prepared with ridges spaced 36 in apart. Dual and Lorox were applied pre-emergence; a shield-sprayer was passed between rows at least once per year in most seasons. No insecticide was applied; remaining weeds were controlled manually. Seasonal weather data were obtained from NASA and are summarized in Figure 5.1.

5.2.2 SNP Genotyping and marker quality control

Leaf tissue was submitted to the HudsonAlpha Institute for Biotechnology for low-coverage whole-genome sequencing (3×). Variant calling and imputation was performed by HudsonAlpha by the Khufu pipeline. An initial panel of 256,652 SNPs was filtered for minor allele frequency (≥ 0.05), and heterozygosity (≤ 0.15). This resulted in 174,284 SNPs across 25 chromosomes, restricted to the 232 phenotyped accessions used in this study.

5.2.3 Agronomic traits

Alkaloid status was assessed at flowering using the Dragendorff colorimetric paper test (Harrison and Williams, 1982) and scored as bitter/sweet (1/0). Plots were harvested using a combine harvester, and cleaned seed weight was used to calculate grain yield (kg ha^{-1}). Hundred-seed weight was determined from 100 clean, intact seeds (g).

5.2.4 Root crown phenotyping

Root crowns were excavated approximately two weeks before harvest using shovelomics (Trachsel et al., 2011). Five plants per plot were sampled, cleaned, and barcoded. Root crowns were imaged using a RhizoBox with a five-camera monochromatic array, and images were analyzed in RhizoVision Explorer (Seethepalli et al., 2021) for digital root trait extraction (Figure 5.2). Of 22 traits, 12 relevant to ecosystem services were selected for analysis (Table 5.1)

5.2.5 UAV multispectral data collection and vegetation index extraction

Multispectral imagery was acquired using a DJI Mavic 3 Multispectral UAV across seven flights in 2023 and eight in 2024 (Figure 5.3). Images were processed into georeferenced orthomosaics in Agisoft Metashape Professional v2.1.1, shapefiles and plot boundaries were created in R and validated in QGIS, and plot-level reflectance was extracted using the FIELDimageR package in R (Matias et al., 2020) with soil background removed following Adak et al. (2023). Forty-six vegetation indices were computed from Green, Red, Red-Edge, and Near-Infrared bands following DeSalvio et al. (2022) and Adak et al. (2023) (Table 5.2).

5.2.6 Variance components, heritability, and BLUPs

Variance components were estimated for each trait in ASReml-R v4.2 (Butler et al., 2017) using univariate linear mixed models with accession, accession-by-year interaction, and replicate-within-year as random effects and a separable AR1 × AR1 spatial residual structure per year. Grain yield included a within-year centred plant count covariate; alkaloid was modelled on the latent liability scale (binomial logit; residual variance fixed at $\pi^2/3$). Broad-sense heritability on a mean basis was estimated as:

$$H^2 = \sigma^2G / (\sigma^2G + \sigma^2GY/Y + \sigma^2E/(Y \times R)) \quad (1)$$

for the combined analysis and $H^2 = \sigma^2G / (\sigma^2G + \sigma^2E/R)$ within each year (Year (Y) = 2; replication (R) = 2). Standard errors were derived by the delta method (Lynch and Walsh, 1998). Cullis heritability (Cullis et al., 2006) was additionally computed, as it is more appropriate for models fitted with spatial autocorrelation in the residuals: $H^2\text{Cullis} = 1 - \text{SE}\bar{D}^2 / (2\sigma^2G)$, reported alongside the mean-basis estimates as an independent check. Accession BLUPs were de-regressed following Garrick et al. (2009); for each accession i, reliability $r_i = 1 - PEV_i / \sigma^2G$ and:

$$\hat{d}_i = \hat{u}_i / r_i \quad (2)$$

$$w_i = (1 - H^2) / [(c + (1 - r_i)/r_i) \times H^2] \quad (3)$$

where c = 0.5. De-regression with reliability weighting prevents the shrinkage applied during BLUP estimation from being conflated with true additive genetic signal in downstream genomic and phenomic prediction; the weights w_i, not de-regression alone, are what down-weight low-reliability records during model fitting (Garrick et al., 2009).

De-regression was performed separately per year and for the combined analysis. VI BLUPs used as phenomic predictors were standard non-de-regressed BLUPs.

5.2.7 Genomic and phenomic prediction models

Seven prediction models were evaluated within each scenario (Table 5.3). Identical training and test partitions were used across all seven models within each scenario and replicate, ensuring that prediction accuracies are directly comparable across models. Kernel-based models used de-regressed BLUPs with inverse-variance reliability weights in BGLR (Pérez and de los Campos, 2014; nIter = 120,000; burnIn = 20,000); PLSR and RF used unweighted BLUPs because reliability weighting is not supported; however, direct comparison with the weighted kernel models was not the objective. Linear and Gaussian phenomic kernels were constructed as:

$$W\_lin = XX^T / p \quad (4)$$

$$W\_gau(i,j) = \exp(-D^2_{ij} / h) \quad (5)$$

where D^2_{ij} is the squared Euclidean distance between scaled VI vectors and h is the median pairwise squared Euclidean distance in the training set. Multi-kernel models passed both G and W simultaneously to BGLR, estimating σ^2G and σ^2W jointly. The genomic relationship matrix (G) was constructed following VanRaden (2008) Method 1.

5.2.8 Prediction scenarios and cross-validation

Three prediction scenarios were implemented to address distinct questions about the value of phenomic information (Table 5.4). Scenarios A and B evaluated single-flight and combined-flight phenomic prediction within each year using 5-fold cross-validation

with 25 repeats. Scenario C tested whether averaging independently scaled per-year VI matrices into a single phenomic relationship matrix recovers stable phenomic signal in a pooled 232-accession population spanning both seasons, again using 5-fold cross-validation with 25 repeats. Because folds in Scenario C were drawn at random from the pooled data, both seasons are represented in the training and test sets; Scenario C therefore evaluates prediction of untested lines within a two-year training population, and is not a test of forward prediction into an unobserved season.

Cross-validation terminology in this study follows standard k-fold partitioning (Scenarios A, B, and C); the CV0/CV1/CV2 nomenclature of Jarquín et al. (2017), which denotes specific genotype-by-environment partitioning schemes, is not applied here because none of the three scenarios partition data strictly along those lines. A year-blocked genomic–phenomic model following the genotype-by-environment framework of Jarquín et al. (2014) was additionally fitted as an exploratory analysis of forward and backward prediction between seasons, training on the 168 accessions common to both years and testing on the 32 year-unique accessions in each direction.

Predictive accuracy was assessed as the Pearson correlation (r) between BLUPs and model predictions. Selection concordance at 10% and 20% selection intensity (Conc10, Conc20), the proportion of true top-k lines correctly identified, was computed as the primary measure of breeding utility. All analyses were conducted in R v4.3 with L’Ecuyer-CMRG reproducible random streams across parallel replicates.

5.3. Results

5.3.1 Variance components and broad-sense heritability

Grain yield increased from 316 kg ha^{-1} in Year 1 (2023 to 2024) to 897 kg ha^{-1} in Year 2 (2024 to 2025) (Figure 5.4). 100-seed weight increased from 23.9 g to 31.8 g, with overlapping but right-shifted distributions in Year 2. Alkaloid proportions were similar between years, with bitter accessions increasing from 44% in Year 1 to 51.5% in Year 2. Distributions of shallow root frequency, total root length, root tips, width-to-depth ratio, average hole size, and median root number were higher in Year 1, whereas coarse fraction length and median diameter were higher in Year 2 (Figure 5.5).

Cullis heritability varies substantially across traits (Table 5.6). Agronomic traits showed the highest estimates: alkaloid status (H^2 = 0.82 ± 0.02), 100-seed weight (0.78 ± 0.03), and grain yield (0.44 ± 0.09), all with significant genetic variance components (LRT, $p \leq 0.001$). Root crown traits showed consistently lower heritability (H^2: 0.14–0.52). Average Hole Size and Median Root Number had the highest root trait estimates in 2023 but showed year-dependent instability. Genotype-by-year interaction was significant only for average hole size (LRT $p = 0.01$). Cullis heritability of vegetation indices ranged from 0 to 0.35 across flight dates and growing seasons (Figure 5.6). At early-season flights (DAP 66–90), H^2 remained below 0.10 for all indices in both years. Estimates increased progressively toward late season, reaching a maximum at DAP 197 in 2023 (H^2: 0.19–0.35 across indices) and DAP 121–127 in 2024 (range: 0.11–0.13). H^2 estimates in 2024 were consistently lower than corresponding values in 2023 across all indices and flight dates.

5.3.2 Single time-point prediction accuracy of UAV-based phenomic models

Phenomic prediction accuracy varied markedly across traits, flight dates, and years (Figure 5.7). Alkaloid content and average hole size were the most predictable traits, with peak accuracies of r = 0.50 (W-Gaussian, DAP 197, 2023) and r = 0.44 (W-Gaussian, DAP 197, 2023), respectively. Prediction accuracy was strongly DAP-dependent and non-monotonic: for alkaloid, mid-season flights (DAP 136–141) outperformed early flights, but late-season DAP 197 yielded the highest accuracy across all models. W-Linear and W-Gaussian consistently matched or exceeded PLSR and Random Forest for well-predicted traits, while RF exhibited the most erratic DAP response (e.g., grain yield: r = −0.21 at DAP 174 vs. r = 0.21 at DAP 197 in 2023). Total root length, root tips, and shallow frequency were poorly predicted across all models and DAPs, with most accuracies near or below zero. The year 2024 showed systematically lower accuracy for agronomic and root traits.

5.3.3 Single versus combined UAV flight timing for phenomic prediction

Combining all UAV flight dates into a single phenomic kernel did not uniformly improve prediction accuracy over the best individual flight (Figure 5.8). Consistent gains from combining flights occurred for alkaloid content in Year 2 (Δr = +0.07 to +0.12 across all four models) and 100-seed weight in Year 1 (Δr = +0.01 to +0.05, all models), while average hole size in Year 1 benefited under three of four models (Δr = +0.04 to +0.06). Isolated improvements appeared for median root number in Year 2 (RF only, Δr = +0.06), fine fraction length in Year 2 (PLSR only, Δr = +0.04), and median diameter in Year 1 (RF only, Δr = +0.03). For seven of nine root traits, the best single flight outperformed the combined stack in both years, with accuracy losses of 0.08–0.19 upon combining. The decline was most pronounced for shallow root frequency, total root

length, root tips, and width-to-depth ratio. No model class was immune to this pattern. For root traits under the combined kernel, all four models performed comparably, with median r values below 0.20 and no systematic advantage for kernel-based over machine learning approaches.

5.3.4 Prediction accuracy of genomic, phenomic, and integrated genomic–phenomic models

The relative value of genomic, phenomic, and integrated information differed sharply across traits and years (Figure 5.9). For alkaloid status, integrating genomic and phenomic kernels (G+W-Linear) consistently outperformed both data sources used alone, ranking first in both years (r = 0.55 and 0.59) and exceeding G-BLUP (Figure 5.8a). Average hole size showed a similar integration advantage in Year 1 (G+W-Linear r = 0.46 vs. G-BLUP r = 0.19), although this advantage was minimal in Year 2 (Figure 5.9). For median root diameter and coarse fraction length in Year 1, phenomic-only models (W-Linear or W-Gaussian) ranked highest, and adding genomic information did not improve accuracy (Figure 5.9). In contrast, for grain yield and 100-seed weight, phenomic information improved prediction in Year 1 but was less reliable in Year 2, where G-BLUP ranked highest and W-Linear produced negative accuracies (Figure 5.9).

Among root architectural traits, genomic prediction alone was consistently superior for shallow root frequency, total root length, and root tips, with phenomic models often near zero or negative (Figure 5.10). Width-to-depth ratio showed no

consistent advantage for any data source. W-Linear generally matched or exceeded W-Gaussian, with no consistent benefit from nonlinear kernel structure (Figure 5.9).

5.3.5 Selection concordance of predicted and observed trait rankings under Scenario A and B

Concordance analysis revealed strong trait and year-dependence in model performance (Figure 5.11). For average hole size in Year 1, phenomic and integrated models identified 40–45% of the true top 10% and 46–50% of the top 20%, outperforming G-BLUP (19% and 29%), although this advantage was not observed in Year 2. For alkaloids, G+W-Linear achieved the highest concordance in Year 2 (Conc20 = 0.41), exceeding G-BLUP (0.09 and 0.32). Median root number showed the more stable concordance across years (G-BLUP Conc20 = 0.33–0.35).

Root architectural traits generally showed low concordance across all models. For instance, root tips and total root length were near random expectation at 10% selection intensity, indicating limited ability to correctly rank genotypes. Concordance at 20% selection intensity exceeded that at 10% for all traits and models, consistent with the difference in their respective random expectations (0.20 and 0.10). No single model class consistently outperformed others across all traits.

5.3.6 Pooled two-year prediction: averaged phenomic kernel

Predictive ability under the averaged W approach (Scenario C) was highest for alkaloid status, where G+W-Gaussian reached r = 0.53, the highest value observed across all seven models and all traits in this scenario (Figure 5.12). G-BLUP (r = 0.41), W-Gaussian (r = 0.44), and G+W-Linear (r = 0.42) also performed competitively; W-

Linear (r = 0.22) and PLSR (r = 0.15) were lowest. Avg. hole size was the second highest trait, with r ranging from 0.23 (G-BLUP) to 0.38 (W-Gaussian).

For grain yield, all models produced low predictive ability (r = −0.01 to 0.17). For 100-seed weight, r ranged from 0.006 (W-Linear) to 0.147 (RF). Among root traits, fine root length, total root length, and root tips had maximum r below 0.10 across all seven models, with multiple models negative. Shallow root angle was best predicted by G-BLUP (r = 0.21); adding phenomic kernels did not improve it. Width/depth ratio was best under W-Gaussian (r = 0.15), and coarse root length under W-Gaussian (r = 0.17). Median diameter and median root count ranged narrowly (r = 0.12–0.18 and 0.04–0.22 respectively).

5.3.7 Selection concordance under the averaged phenomic kernel

Selection concordance followed the same trait ordering as predictive ability (Table 5.6). Alkaloid status reached Conc20 = 0.37 under G+W-Gaussian. Avg. hole size ranged from 0.34 to 0.43 across models, the highest concordance observed in this scenario. Shallow root angle reached Conc20 = 0.34 under G-BLUP. For models with r ≤ 0, Conc20 values of 0.11–0.23 are at or below the random expectation of 0.20 and do not indicate meaningful elite identification.

5.3.8 Exploratory cross-year prediction

An exploratory year-blocked genomic–phenomic model was additionally fitted to assess forward and backward prediction between seasons, training on the 168 accessions common to both years and testing on the 32 year-unique accessions in each direction (Figure 5.13). Predictive ability varied substantially across traits and

directions. Grain yield showed the largest asymmetry (r = 0.36 predicting Year 2 from Year 1; r = 0.06 predicting Year 1 from Year 2), alkaloid status was moderate in both directions (r = 0.44 and 0.38), and total root length and root tips were negative in both directions (r = −0.20 and −0.16; r = −0.29 and −0.07). Because the test set contains only 32 accessions and a single model was fitted without a genomic-only baseline, these results are exploratory and are not used to support conclusions in this chapter.

5.4 Discussion

5.4.1 Agronomic traits are more heritable than root crown and UAV-derived traits

The integration of shovelomics with image-based analysis using RhizoVision Explorer (Trachsel et al., 2011; Seethepalli et al., 2021) provides a scalable framework for quantifying root crown architecture in white lupin field populations. Root traits derived from this pipeline were heritable, demonstrating that the approach captures sufficient genetic signal for population-level inference and genomic prediction. This establishes a practical benchmark for field-scale root phenotyping in white lupin, particularly given the historically low throughput and high measurement error associated with root trait evaluation at breeding scale (Lynch, 2022).

Agronomic traits exhibited higher heritability than root crown traits, with root traits showing relatively greater residual variance. The observed heritability range for root crown traits (0.14–0.52) aligns with shovelomics-based estimates reported in legumes (0.01–0.83; Burridge et al., 2016) and maize (0.24–0.49; Zuffo et al., 2022), and this low-to-moderate heritability inherently limits prediction accuracy for root architecture. These low to moderate heritabilities can be partly attributed to high phenotypic plasticity,

as root systems respond dynamically to environmental variation in soil moisture, temperature, rainfall, and nutrient availability (Griffin et al., 2025; Alahmad et al., 2025). Vegetation index heritability was low at early growth stages but increased at later stages, indicating that genetically informative spectral signal accumulates as the canopy develops toward maturity (Krause et al., 2019; Adak et al., 2023; Yusuf et al., 2025). This temporal pattern has direct implications for optimizing UAV flight timing in white lupin breeding programs.

5.4.2 Single time-point prediction accuracy of UAV-based phenomic models

Prediction accuracy varied substantially across traits and flight dates, and the temporal pattern was trait-specific and non-monotonic rather than uniformly increasing with crop maturity. This pattern indicates that phenomic signal is maximized when measurements coincide with trait-specific expression windows, consistent with previous studies showing that prediction performance depends on developmental stage and trait biology (Krause et al., 2019; Yusuf et al., 2025; Alahmad et al., 2025).

W-Linear and W-Gaussian kernels performed nearly equivalently under single flight-date cross-validations. The Gaussian kernel advantage documented in genomic prediction contexts, where non-linearity captures complex epistatic interactions across high-dimensional SNP panels (Bandeira e Sousa et al., 2017), did not hold for multispectral vegetation index data, suggesting that the low-dimensional, already-compressed nature of VI-derived relationship matrices makes the additive linear kernel structurally adequate. PLSR was consistently competitive with kernel models for well-predicted traits (Krause et al., 2019; Kaur et al., 2024), validating it as a practical,

interpretable alternative. Random Forest showed the widest dispersion and most DAP-dependent instability, particularly for grain yield, consistent with its known sensitivity to training population size (Xu et al., 2024). For small-to-moderate breeding nurseries, kernel models and PLSR are more appropriate choices.

Root architectural traits (total root length, root tips, and shallow root frequency) were poorly predicted across all models and flight dates, with accuracies near or below zero. This is not unexpected given that belowground traits are being predicted from aboveground spectral signatures, compounded by low heritability for these traits. Alahmad et al. (2025) demonstrated in barley that UAV-derived root trait prediction is feasible but is the most challenging application of above-ground spectral phenomics; the results in white lupin are fully consistent and extend this conclusion to a legume cover crop where those root traits directly govern phosphorus mobilization from Alabama Ultisols.

5.4.3 Single versus combined UAV flight timing for phenomic prediction

Combining multiple UAV flight dates into a single phenomic kernel did not consistently improve prediction accuracy and, for most root architectural traits, resulted in reduced performance relative to the best single flight, a pattern observed across all model classes and most pronounced for shallow root frequency, total root length, and root tips. These results indicate that temporal aggregation dilutes trait-specific spectral signals captured at phenologically optimal time points. This directly contrasts with the additive temporal benefit reported for yield in maize (Adak et al., 2023) and points to a fundamental difference between agronomic traits with prolonged canopy genetic

signatures and root architectural traits whose spectral footprint is transient and phenologically confined.

Modest improvements from combining flights were observed for alkaloid content in both years and 100-seed weight in 2023, suggesting that temporal integration can be beneficial when trait expression is distributed across developmental stages. However, the absence of consistent gains across traits indicates that increasing flight numbers does not guarantee improved prediction performance (Sun et al., 2019; Yusuf et al., 2025). From a breeding perspective, flight timing selection is more critical than flight number; strategic alignment of UAV data collection with key developmental stages will reduce operational costs without sacrificing prediction accuracy (Adak et al., 2023; Yusuf et al., 2025).

5.4.4 Prediction accuracy of genomic, phenomic, and integrated genomic–phenomic models

Direct cross-validation comparisons of phenomic and genomic prediction accuracy require careful interpretation. Wang et al. (2025) demonstrate that CV-derived accuracy statistics do not reliably index the accuracy parameter of the breeder's equation, and that phenomic and genomic selection tools differentially affect other parameters (selection intensity, cycle time, and cost), rendering head-to-head accuracy comparisons insufficient to advocate for one approach over the other. A further caution is that phenomic kernels derived from single-environment UAV data are susceptible to overfitting toward the spectral signal of a specific season, an endophenotype-bias-like effect described for spectral and metabolomic predictors by Adunola et al. (2023), which

limits their long-term reliability for parental selection across environments. Concordance analysis confirmed this constraint: correct identification of the true top 10% remained near random for most root traits across all models. Consistent with the deployment framework proposed by Adunola et al. (2023) for recurrent selection programs, UAV phenomics and integrated G+W models can be best positioned as early-cycle population-enrichment tools rather than replacements for direct phenotypic evaluation in final product development stages targeting root-mediated ecosystem services.

Genomic prediction for dual-purpose white lupin breeding is primarily justified by the imperative to accelerate selection for root architectural traits linked to phosphorus mobilization, traits for which traditional phenotyping is too slow, too costly, and insufficiently repeatable at population scale (Lynch, 2022). Prediction accuracy was strongly stratified by trait broad-sense heritability, consistent with the theoretical expectation that the genetic signal-to-noise ratio in the phenotypic record directly limits additive genetic variance captured by marker panels (Crossa et al., 2017). G-BLUP achieved its highest accuracy for alkaloid and was moderately predictive for 100-seed weight and avg. hole size. For root architectural traits with low heritability (total root length, root tips, shallow root frequency, and width:depth ratio), this could partly explain why G-BLUP accuracy was near or below zero in both years, worse than the GP accuracy of 0.26–0.33 reported for low-heritability root traits in wheat (Guo et al., 2020), confirming that genomic selection alone cannot drive genetic gain for the shallow-foraging root architecture traits responsible for legacy phosphorus mobilization from Ultisol topsoils.

Combining genomic and phenomic kernels (G+W-Linear) produced the highest prediction accuracy for alkaloid in both years, the strongest integrative gain in this study. This is consistent with evidence that multi-kernel models consistently outperform either source alone for heritable quality traits, attributed to complementarity between additive genetic effects from markers and canopy-expressed effects from spectral reflectance (Crain et al., 2018; Robert et al., 2022). The finding that combining genomic and phenomic information was most beneficial for the highest-H^2 trait and progressively less so for low-H^2 root traits confirms that phenomic supplementation amplifies existing genetic signals rather than creating them. For root architectural traits governing the ecosystem services that motivate this program, no consistent model advantage emerged across years, consistent with the broad conclusion that no universal model exists for complex trait-environment combinations (Crossa et al., 2017; Alemu et al., 2024).

Concordance analysis reinforced these findings with direct breeding relevance. For avg. hole size in Year 1, phenomic and integrated models substantially outperformed G-BLUP in identifying both the true top 10% and the true top 20%, demonstrating that for this key root trait linked to cluster root architecture, UAV phenomics provides actionable selection guidance. For root tips and total root length, concordance at 10% approached random expectation, confirming that these traits currently require direct phenotypic measurement for elite identification, and that expanding training population size and multi-environment phenotyping are the most tractable routes to improving their predictability.

5.4.5 Pooled-year prediction: year-blocked genomic–phenomic model

Pooled-year prediction represents a stringent test of model utility, reflecting the breeder's challenge of selecting genotypes for a season not yet observed. Using 168 overlapping lines for training and 32 year-unique lines as a fixed test set, the year-blocked genomic–phenomic model revealed strongly trait-dependent and directionally asymmetric predictive ability. Alkaloid content showed moderate accuracy in both directions, indicating reliable elite identification above random expectation and consistent with reported accuracies for high-heritability seed quality traits (Annicchiarico et al., 2025).

Grain yield exhibited pronounced directional asymmetry. This disparity reflects strong between-year variance heterogeneity rather than model failure, as environmental similarity, rather than genetic relatedness, primarily determines pooled-environment predictive ability (Rogers et al., 2022). The 2023 environment captured variance relevant to 2024 performance, whereas the reverse did not generalize. Root traits showed near-zero and often negative accuracies, confirming that their genetic expression is highly environment-specific and poorly transferable across years, consistent with suppression of root trait genetic variance under field heterogeneity (Lynch, 2022).

5.4.6 Pooled-year prediction: averaged phenomic kernel

The averaged phenomic kernel approach tested whether pooling independently scaled, year-specific phenomic relationship matrices could recover pooled-year signal without requiring year-matched data. For alkaloid content, G+W-Gaussian achieved the highest pooled -year accuracy observed in this study, demonstrating that aggregated

phenomic kernels retain stable canopy-genetic signal for highly heritable, physiologically expressed traits, and extending prior findings on multi-environment phenomic integration (Krause et al., 2019; Yusuf et al., 2025) to a pooled-year context.

This advantage did not extend to grain yield, where pooled phenomic kernels likely confounded environmentally divergent signals, limiting their ability to resolve pooled-year genetic structure (Krause et al., 2019). For root traits, both scenario C failed to produce meaningful predictions, confirming that pooled year genetic signal for root architecture remains undetectable under current phenotyping and modelling frameworks. Improving pooled-year prediction for root traits will require expanded multi-environment datasets, repeated root phenotyping, and explicit modelling of environmental covariates within true reaction norm frameworks incorporating environmental covariate data (Jarquín et al., 2014). These are essential steps to operationalize genomic selection for phosphorus-mobilizing root systems that underpin white lupin's role as a dual-purpose cash cover crop in Ultisol-dominated systems.

5.5 Conclusions, limitations, and future directions

This study establishes that root crown architecture in white lupin can be quantified at breeding scale using a shovelomics–RhizoVision pipeline, producing heritable and genetically structured traits directly linked to phosphorus mobilization and ecosystem service delivery. Across prediction frameworks, performance was strongly trait-dependent and constrained by heritability. Genomic–phenomic integration improved prediction for high-signal traits, while root architectural traits remained difficult to predict due to low heritability and strong environmental modulation. UAV phenomics

showed operational value, with single late-season flights outperforming temporal aggregation, but its ability to capture root architectural variation was limited. Pooled-year prediction for root traits was consistently unreliable, indicating that current models cannot yet support robust selection for root-mediated ecosystem services across years.

As a pilot study conducted in a single-site over two seasons, key limitations include limited environmental representation, training population size, and instability of root trait expression across years. Biomass partitioning data (above- versus below-ground) were collected in both years but were not analyzed here: data completeness was approximately 30% in Year 2 due to equipment failure during sample drying, and approximately 55% in Year 1 due to phenotyping timing relative to leaf senescence in early-maturing lines; this remains a priority for future analysis given its potential relevance to drought tolerance. Ongoing expansion to multiple environments, repeated root phenotyping with additional methods and root imaging platforms, and explicit modeling of environmental covariates will be essential to improve prediction. Multi-trait genomic approaches leveraging high-heritability, low-cost traits such as alkaloid status provide a practical pathway to enhance prediction of difficult root traits and accelerate breeding of dual-purpose white lupin for phosphorus-mobilizing systems in the Southeastern United States.

References

Adak, A.; Murray, S.C.; Božinović, S.; Lindsey, R.; Nakasagga, S.; Chatterjee, S.; Anderson, S.L., II; Wilde, S. Temporal Vegetation Indices and Plant Height from Remotely Sensed Imagery Can Predict Grain Yield and Flowering Time Breeding Value in Maize via Machine Learning Regression. Remote Sens. 2021, 13, 2141. https://doi.org/10.3390/rs13112141

Adak, A., Murray, S. C., & Anderson, S. L. (2023). Temporal phenomic predictions from unoccupied aerial systems can outperform genomic predictions. G3: Genes, Genomes, Genetics, 13(1), jkac294. https://doi.org/10.1093/g3journal/jkac294

Adunola, P., Tavares Flores, E., Riva-Souza, E. M., Ferrão, M. A. G., Senra, J. F. B., Comério, M., Espindula, M. C., Verdin Filho, A. C., Volpi, P. S., Fonseca, A. F. A., Ferrão, R. G., Munoz, P. R., & Ferrão, L. F. V. (2024). A comparison of genomic and phenomic selection methods for yield prediction in Coffea canephora. The Plant Phenome Journal, 7, e20109. https://doi.org/10.1002/ppj2.20109

Alahmad, S., Smith, D., Katsikis, C., Aldiss, Z., Brunner, S. M., Meer, S. V., Meijer, L., Heidariask, B., Chenu, K., Chapman, S., Potgieter, A. B., Wasson, A., Baraibar, S., Godoy, J., Moody, D., Robinson, H., & Hickey, L. T. (2025). Phenotyping the hidden half: combining UAV phenotyping and machine learning to predict barley root traits in the field. Journal of Experimental Botany, 76(17), 5161–5178. https://doi.org/10.1093/jxb/eraf268

Alahmad, S., El Hassouni, K., Bassi, F. M., Dinglasan, E., Youssef, C., Quarry, G., Aksoy, A., Mazzucotelli, E., Juhász, A., Able, J. A., Christopher, J., Voss-Fels, K.

P., & Hickey, L. T. (2019). A major root architecture QTL responding to water limitation in durum wheat. Frontiers in Plant Science, 10, Article 436. https://doi.org/10.3389/fpls.2019.00436

Alemu, A., Åstrand, J., Montesinos-López, O. A., Isidro y Sánchez, J., Fernández-Gónzalez, J., Tadesse, W., Vetukuri, R. R., Carlsson, A. S., Ceplitis, A., Crossa, J., Ortiz, R., & Chawade, A. (2024). Genomic selection in plant breeding: Key factors shaping two decades of progress. Molecular Plant, 17(4), 552–578. https://doi.org/10.1016/j.molp.2024.03.007

Annicchiarico, P., Osorio, C., Nazzicari, N., Ferrari, B., Barzaghi, S., Biazzi, E., Tava, A., Pecetti, L., Notario, T., Romani, M., & Crosta, M. (2025). Genetic variation and genome-enabled selection of white lupin for key seed quality traits. BMC Genomics, 26, Article 922. https://doi.org/10.1186/s12864-025-12048-0

Araus, J. L., & Cairns, J. E. (2014). Field high-throughput phenotyping: the new crop breeding frontier. Trends in Plant Science, 19(1), 52–61. https://doi.org/10.1016/j.tplants.2013.09.008

Bandeira e Sousa, M., Cuevas, J., de Oliveira Couto, E. G., Pérez-Rodríguez, P., Jarquín, D., Fritsche-Neto, R., Burgueño, J., & Crossa, J. (2017). Genomic-enabled prediction in maize using kernel models with genotype × environment interaction. G3: Genes, Genomes, Genetics, 7(6), 1995–2014. https://doi.org/10.1534/g3.117.042341

Benjamini, Y., & Hochberg, Y. (1995). Controlling the false discovery rate: A practical and powerful approach to multiple testing. Journal of the Royal Statistical

Society: Series B (Methodological), 57(1), 289–300. https://doi.org/10.1111/j.2517-6161.1995.tb02031.x

Burgueño, J., de los Campos, G., Weigel, K., & Crossa, J. (2012). Genomic prediction of breeding values when modeling genotype × environment interaction using pedigree and dense molecular markers. Crop Science, 52(2), 707–719. https://doi.org/10.2135/cropsci2011.06.0299

Burridge, J., Jochua, C. N., Bucksch, A., & Lynch, J. P. (2016). Legume shovelomics: High-throughput phenotyping of common bean (Phaseolus vulgaris L.) and cowpea (Vigna unguiculata subsp. unguiculata) root architecture in the field. Field Crops Research, 192, 21–32. https://doi.org/10.1016/j.fcr.2016.04.008

Butler, D. G., Cullis, B. R., Gilmour, A. R., Gogel, B. J., & Thompson, R. (2017). ASReml-R reference manual version 4. VSN International Ltd. https://asreml.kb.vsni.co.uk/wp-content/uploads/sites/3/ASReml-R-Reference-Manual-4.pdf

Brewer, K., Clulow, A., Sibanda, M., Gokool, S., Odindi, J., Mutanga, O., Naiken, V., Chimonyo, V. G. P., & Mabhaudhi, T. (2022). Estimation of maize foliar temperature and stomatal conductance as indicators of water stress based on optical and thermal imagery acquired using an unmanned aerial vehicle (UAV) platform. Drones, 6(7), Article 169. https://doi.org/10.3390/drones6070169.

Christianson, R., Fox, J., Law, N., & Wong, C. (2021). Effectiveness of cover crops for water pollutant reduction from agricultural areas. Transactions of the ASABE, 64(4), 1007–1017. https://doi.org/10.13031/trans.14028

Crain, J., Mondal, S., Rutkoski, J., Singh, R. P., & Poland, J. (2018). Combining high-throughput phenotyping and genomic information to increase prediction and selection accuracy in wheat breeding. The Plant Genome, 11(1), Article 170043. https://doi.org/10.3835/plantgenome2017.05.0043

Crossa, J., Pérez-Rodríguez, P., Cuevas, J., Montesinos-López, O., Jarquín, D., de los Campos, G., Burgueño, J., González-Camacho, J. M., Pérez-Elizalde, S., Beyene, Y., Dreisigacker, S., Singh, R., Zhang, X., Gowda, M., Roorkiwal, M., Rutkoski, J., & Varshney, R. K. (2017). Genomic selection in plant breeding: methods, models, and perspectives. Trends in Plant Science, 22(11), 961–975. https://doi.org/10.1016/j.tplants.2017.08.011

Cullis, B. R., Smith, A. B., & Coombes, N. E. (2006). On the design of early generation variety trials with correlated data. Journal of Agricultural, Biological and Environmental Statistics, 11(4), 381–393. https://doi.org/10.1198/108571106X154443

Damon, P. M., Bowden, B., Rose, T., & Rengel, Z. (2014). Crop residue contributions to phosphorus pools in agricultural soils: a review. Soil Biology and Biochemistry, 74, 127–137. https://doi.org/10.1016/j.soilbio.2014.03.003

Den Herder, G., Van Isterdael, G., Beeckman, T., & De Smet, I. (2010). The roots of a new green revolution. Trends in Plant Science, 15, 600–607.

DeSalvio, A. J., Adak, A., Murray, S. C., & Rajan, N. (2022). Corn yield prediction using hyperspectral imagery and temporal fusion of diverse UAV multispectral data. Frontiers in Remote Sensing, 3, 796077.

https://doi.org/10.3389/frsen.2022.796077 [FLAG: verify this is the correct DeSalvio et al. 2022 paper used for VI list]

Falconer, D. S., & Mackay, T. F. C. (1996). Introduction to quantitative genetics (4th ed.). Longman.

Féret, J.-B., Berger, K., de Boissieu, F., & Malenovský, Z. (2021). PROSPECT-PRO for estimating content of nitrogen-containing leaf proteins and other carbon-based constituents. Remote Sensing of Environment, 252, Article 112173. https://doi.org/10.1016/j.rse.2020.112173

Fiorani, F., & Schurr, U. (2013). Future scenarios for plant phenotyping. Annual Review of Plant Biology, 64, 267–291. https://doi.org/10.1146/annurev-arplant-050312-120137

Freschet, G. T., Roumet, C., Comas, L. H., Weemstra, M., Bengough, A. G., Rewald, B., Bardgett, R. D., De Deyn, G. B., Johnson, D., Klimešová, J., Lukac, M., McCormack, M. L., Meier, I. C., Pagès, L., Poorter, H., Prieto, I., Wurzburger, N., Zadworny, M., Bagniewska-Zadworna, A., … Stokes, A. (2021). Root traits as drivers of plant and ecosystem functioning: Current understanding, pitfalls and future research needs. New Phytologist, 232(3), 1123–1158. https://doi.org/10.1111/nph.17072

Frick, K. M., Kamphuis, L. G., Siddique, K. H. M., Singh, K. B., & Foley, R. C. (2017). Quinolizidine alkaloid biosynthesis in lupins and prospects for grain quality improvement. Frontiers in Plant Science, 8, 87. https://doi.org/10.3389/fpls.2017.00087

Garrick, D. J., Taylor, J. F., & Fernando, R. L. (2009). Deregressing estimated breeding values and weighting information for genomic regression analyses. Genetics Selection Evolution, 41(1), 55. https://doi.org/10.1186/1297-9686-41-55

Glaze-Corcoran, S., Smychcovich, A., & Hashemi, M. (2023). Dual-purpose rye, wheat, and triticale cover crops offer increased forage production and nutrient management but demonstrate nitrogen immobilization dynamics. Agronomy, 13(6), Article 1517. https://doi.org/10.3390/agronomy13061517

Glenn, E. P., Huete, A. R., Nagler, P. L., & Nelson, S. G. (2008). Relationship between remotely sensed vegetation indices, canopy attributes and plant physiological processes: What vegetation indices can and cannot tell us about the landscape. Sensors, 8(4), 2136–2160. https://doi.org/10.3390/s8042136

Griffin, A. J., Jungers, J. M., & Bajgain, P. (2025). Root phenotyping and plant breeding of crops for enhanced ecosystem services. Crop Science, 65(1), e21315. https://doi.org/10.1002/csc2.21315

Griffiths, M., Delory, B. M., Jawahir, V., Wong, K. M., Bagnall, G. C., Dowd, T. G., Chamberlain, A., Meldrum, K., Schaefer, A. L., Kaeppler, H. F., Lynch, J. P., Kaeppler, S. M., & York, L. M. (2022). Optimization of root traits to provide enhanced ecosystem services in agricultural systems: A focus on cover crops. Plant, Cell & Environment, 45(3), 751–770. https://doi.org/10.1111/pce.14247

Guo, X., Svane, S. F., Füchtbauer, W. S., Andersen, J. R., Jensen, J., & Thorup-Kristensen, K. (2020). Genomic prediction of yield and root development in wheat under changing water availability. Plant Methods, 16, Article 90. https://doi.org/10.1186/s13007-020-00634-0

Harrison, J. E. M., & Williams, W. (1982). Genetical control of alkaloids in Lupinus albus. Euphytica, 31(2), 357–364. https://doi.org/10.1007/BF00021651

Ho, M. D., Rosas, J. C., Brown, K. M., & Lynch, J. P. (2005). Root architectural tradeoffs for water and phosphorus acquisition. Functional Plant Biology, 32(8), 737–748. https://doi.org/10.1071/FP05043

Hufnagel, B., Marques, A., Soriano, A., Marquès, L., Divol, F., Doumas, P., Sallet, E., Mancinotti, D., Carrere, S., Marande, W., Arribat, S., Keller, J., Huneau, C., Blein, T., Aimé, D., Laguerre, M., Taylor, J., Schubert, V., Nelson, M., … Péret, B. (2020). High-quality genome sequence of white lupin provides insight into soil exploration and seed quality. Nature Communications, 11, Article 492. https://doi.org/10.1038/s41467-019-14197-9

Jarquín, D., Crossa, J., Lacaze, X., Du Cheyron, P., Daucourt, J., Lorgeou, J., Piraux, F., Guerreiro, L., Pérez, P., Calus, M., Burgueño, J., & de los Campos, G. (2014). A reaction norm model for genomic selection using high-dimensional genomic and environmental data. Theoretical and Applied Genetics, 127(3), 595–607. https://doi.org/10.1007/s00122-013-2243-1

Kaur, S., Kakani, V. G., Carver, B., Jarquín, D., & Singh, A. (2024). Hyperspectral imaging combined with machine learning for high-throughput phenotyping in winter wheat. The Plant Phenome Journal, 7(1), e20111. https://doi.org/10.1002/ppj2.20111

Knoll, J. E., Perkins, N., Scully, B. T., Hawkins, G. L., & Lee, R. D. (2022). Winter legume cover effects on yields of biomass-sorghum and cotton in Georgia. Agronomy Journal, 114(3), 1817–1830. https://doi.org/10.1002/agj2.21018

Krause, M. R., González-Pérez, L., Crossa, J., Pérez-Rodríguez, P., Montesinos-López, O., Singh, R. P., Dreisigacker, S., Poland, J., Rutkoski, J., Sorrells, M., Gore, M. A., & Mondal, S. (2019). Hyperspectral reflectance-derived relationship matrices for genomic prediction of grain yield in wheat. G3: Genes, Genomes, Genetics, 9(4), 1231–1247. https://doi.org/10.1534/g3.118.200856

Lambers, H., Shane, M. W., Cramer, M. D., Pearse, S. J., & Veneklaas, E. J. (2006). Root structure and functioning for efficient acquisition of phosphorus: matching morphological and physiological traits. Annals of Botany, 98(4), 693–713. https://doi.org/10.1093/aob/mcl114

Li, J., Shi, Y., Veeranampalayam-Sivakumar, A.-N., & Schachtman, D. P. (2018). Elucidating sorghum biomass, nitrogen, and chlorophyll contents with spectral and morphological traits derived from an unmanned aircraft system. Frontiers in Plant Science, 9, 1406.

Li, L., Xu, Y., Ren, Y., Guo, Z., Li, J., Tong, Y., Lin, T., & Cui, D. (2019). Comparative proteomic analysis provides insights into the regulatory mechanisms of wheat primary root growth. Scientific Reports, 9, 11741.

Liaw, A., & Wiener, M. (2002). Classification and regression by randomForest. R News, 2(3), 18–22. https://CRAN.R-project.org/doc/Rnews/

Lopes, M. S., & Reynolds, M. P. (2010). Partitioning of assimilates to deeper roots is associated with cooler canopies and increased yield under drought in wheat. Functional Plant Biology, 37(2), 147–156. https://doi.org/10.1071/FP09121

López-Cruz, M., Crossa, J., Bonnett, D., Dreisigacker, S., Poland, J., Jannink, J. L., Singh, R. P., Autrique, E., & de los Campos, G. (2015). Increased prediction

accuracy in wheat breeding trials using a marker × environment interaction genomic selection model. G3: Genes, Genomes, Genetics, 5(4), 569–582. https://doi.org/10.1534/g3.114.016097

Lynch, J. P. (2013). Steep, cheap and deep: an ideotype to optimize water and N acquisition by maize root systems. Annals of Botany, 112(2), 347–357. https://doi.org/10.1093/aob/mcs293

Lynch, J. P. (2015). Root phenes that reduce the metabolic costs of soil exploration: opportunities for 21st century agriculture. Plant, Cell & Environment, 38(9), 1775–1784. https://doi.org/10.1111/pce.12451

Lynch, J. P. (2022). Harnessing root architecture to address global challenges. The Plant Journal, 109(2), 415–431. https://doi.org/10.1111/tpj.15557

Lynch, M., & Walsh, B. (1998). Genetics and analysis of quantitative traits. Sinauer Associates.

Matias, F. I., Caraza-Harter, M. V., & Endelman, J. B. (2020). FIELDimageR: an R package to analyze orthoimages from agricultural field trials. The Plant Phenome Journal, 3(1), e20005. https://doi.org/10.1002/ppj2.20005

Mevik, B.-H., & Wehrens, R. (2007). The pls package: principal component and partial least squares regression in R. Journal of Statistical Software, 18(2), 1–23. https://doi.org/10.18637/jss.v018.i02

Myers, R. L., & Wilson, K. R. (2023). Farmer perspectives about cover crops by non-adopters. Frontiers in Sustainable Food Systems, 7, 1011201. https://doi.org/10.3389/fsufs.2023.1011201

Ober, E. S., Alahmad, S., Cockram, J., Forestan, C., Hickey, L. T., Kant, J., Maccaferri, M., Marr, E., Milner, M., Pinto, F., Rambla, C., Reynolds, M., Salvi, S., Sciara, G., Snowdon, R. J., Thomelin, P., Tuberosa, R., Uauy, C., Voss-Fels, K. P., . . . Watt, M. (2021). Wheat root systems as a breeding target for climate resilience. Theoretical and Applied Genetics, 134(6), 1645–1662. https://doi.org/10.1007/s00122-021-03819-w

Osmond, D., Cabrera, M., Grabow, G., Hansard, R., Harris, J., Hatten, J., Havlin, J., King, K., Kleinman, P., Leytem, A., Mikkelsen, R., Moore, P., Nelson, N., Shober, A., Sharpley, A., Smeal, D., Smith, D., Toor, G., & Weld, J. (2015). Water quality in the southeastern United States: nutrient, pesticide, and sediment issues. Journal of Soil and Water Conservation, 70(6), 127A–136A. https://doi.org/10.2489/jswc.70.6.127A

Pauli, D., Chapman, S. C., Bart, R., Topp, C. N., Lawrence-Dill, C. J., Poland, J., & Gore, M. A. (2016). The quest for understanding phenotypic variation via integrated approaches in the field environment. Plant Physiology, 172(2), 622–634. https://doi.org/10.1104/pp.16.00592

Pérez, P., & de los Campos, G. (2014). Genome-wide regression and prediction with the BGLR statistical package. Genetics, 198(2), 483–495. https://doi.org/10.1534/genetics.114.164442

Pinto, R. S., & Reynolds, M. P. (2015). Common genetic basis for canopy temperature depression under heat and drought stress associated with optimized root distribution in bread wheat. Theoretical and Applied Genetics, 128(4), 575–585. https://doi.org/10.1007/s00122-015-2453-9

Pinto, R. S., Reynolds, M. P., Mathews, K. L., McIntyre, C. L., Olivares-Villegas, J.-J., & Chapman, S. C. (2010). Heat and drought adaptive QTL in a wheat population designed to minimize confounding agronomic effects. Theoretical and Applied Genetics, 121(6), 1001–1021. https://doi.org/10.1007/s00122-010-1351-4

Potgieter, A. B., George-Jaeggli, B., Chapman, S. C., Laws, K., Suárez Cadavid, L. A., Wixted, J., Watson, J., Eldridge, M., Jordan, D. R., & Hammer, G. L. (2017). Multi-spectral imaging from an unmanned aerial vehicle enables the assessment of seasonal leaf area dynamics of sorghum breeding lines. Frontiers in Plant Science, 8, Article 1532. https://doi.org/10.3389/fpls.2017.01532

Pereira, A.; Ramos, F.; Sanches Silva, A. Lupin (Lupinus albus L.) Seeds: Balancing the Good and the Bad and Addressing Future Challenges. Molecules 2022, 27, 8557. https://doi.org/10.3390/molecules27238557

Rauber, L. R., Reinert, D. J., Gubiani, P. I., & Loss, A. (2025). Structure and water infiltration in an Ultisol affected by cover crops and seasonality. Soil and Tillage Research, 247, Article 106366. https://doi.org/10.1016/j.still.2024.106366

Rincent, R., Charpentier, J. P., Faivre-Rampant, P., Paux, E., Le Gouis, J., Bastien, C., & Segura, V. (2018). Phenomic selection is a low-cost and high-throughput method based on indirect predictions: proof of concept on wheat and poplar. G3: Genes, Genomes, Genetics, 8(12), 3961–3972. https://doi.org/10.1534/g3.118.200760

Robert, P., Auzanneau, J., Goudemand, E., Oury, F. X., Rolland, B., Heumez, E., Laurent, B., Le Gouis, J., & Rincent, R. (2022). Phenomic selection in wheat breeding: identification and optimisation of factors influencing prediction accuracy

and comparison to genomic selection. Theoretical and Applied Genetics, 135(3), 895–914. https://doi.org/10.1007/s00122-021-04005-8

Rogers, A. R., Dunne, J. C., Romay, C., Bohn, M., Buckler, E. S., Ciampitti, I. A., Edwards, J., Ertl, D., Flint-Garcia, S., Gore, M. A., Graham, C., Hirsch, C. N., Holland, J. B., Hooker, D., Knoll, J., Lee, E. C., Lorenz, A., Lynch, J. P., Moose, S. P., … de Leon, N. (2022). Environment-specific genomic prediction ability in maize using environmental covariates depends on environmental similarity to training data. G3: Genes, Genomes, Genetics, 12(2), jkab440. https://doi.org/10.1093/g3journal/jkab440

Robinson, H., Hickey, L., Richard, C., Mace, E., Kelly, A., Borrell, A., Franckowiak, J., & Fox, G. (2016). Genomic regions influencing seminal root traits in barley. The Plant Genome, 9(1), Article plantgenome2015.03.0012. https://doi.org/10.3835/plantgenome2015.03.0012

Seethepalli, A., Guo, H., Liu, X., Griffiths, M., Almtarfi, H., Li, Z., Liu, S., Zare, A., Fritschi, F. B., Blancaflor, E. B., & York, L. M. (2021). RhizoVision Explorer: open-source software for root image analysis and measurement standardization. AoB Plants, 13(6), plab056. https://doi.org/10.1093/aobpla/plab056

Speir, S. L., Tank, J. L., Trentman, M. T., Mahl, U. H., Sethna, L. R., Hanrahan, B. R., & Royer, T. V. (2022). Cover crops control nitrogen and phosphorus transport from two agricultural watersheds at multiple measurement scales. Agriculture, Ecosystems & Environment, 326, Article 107765. https://doi.org/10.1016/j.agee.2021.107765

Sukumaran, S., Jarquín, D., Crossa, J., & Reynolds, M. (2018). Genomic-enabled prediction accuracies increased by modeling genotype × environment interaction in durum wheat. The Plant Genome, 11(2), 170112. https://doi.org/10.3835/plantgenome2017.12.0112

Sun, J., Poland, J., Mondal, S., Crossa, J., Juliana, P., Singh, R. P., Rutkoski, J. E., Jannink, J. L., Crespo-Herrera, L., Velu, G., Huerta-Espino, J., & Sorrells, M. E. (2019). High-throughput phenotyping platforms enhance genomic selection for wheat grain yield across populations and cycles in early stage. Theoretical and Applied Genetics, 132(6), 1705–1720. https://doi.org/10.1007/s00122-019-03309-0

Trachsel, S., Kaeppler, S. M., Brown, K. M., & Lynch, J. P. (2011). Shovelomics: High throughput phenotyping of maize (Zea mays L.) root architecture in the field. Plant and Soil, 341(1–2), 75–87. https://doi.org/10.1007/s11104-010-0623-8

USEPA. (2012). National water quality inventory: report to Congress (EPA 841-R-02-001). U.S. Environmental Protection Agency. https://www.epa.gov/waterdata/national-water-quality-inventory-report-congress

VanRaden, P. M. (2008). Efficient methods to compute genomic predictions. Journal of Dairy Science, 91(11), 4414–4423. https://doi.org/10.3168/jds.2007-0980

Waldrip, H. M., Campbell, T. N., Koziel, J. A., Watts, D. B., & Torbert, H. A. (2023). Legacy phosphorus in Alabama Hartsells soil after long-term amendment with broiler litter. Journal of Environmental Quality, 52(4), 897–906. https://doi.org/10.1002/jeq2.20462

Wang, F., Feldmann, M. J., & Runcie, D. E. (2025). Do not benchmark phenomic prediction against genomic prediction accuracy. The Plant Phenome Journal, 8, e70029. https://doi.org/10.1002/ppj2.70029

Xu, X. B., Teng, C., Zhu, H. C., Feng, H. K., Zhao, Y., & Li, Z. H. (2024). Comparison of three models for winter wheat yield prediction based on UAV hyperspectral images. International Journal of Agricultural and Biological Engineering, 17(2), 260–267. https://doi.org/10.25165/j.ijabe.20241702.5869

Yang, M., Hassan, M. A., Xu, K., Zheng, C., Rasheed, A., Zhang, Y., Jin, X., Xia, X., Xiao, Y., & He, Z. (2020). Assessment of water and nitrogen use efficiencies through UAV-based multispectral phenotyping in winter wheat. Frontiers in Plant Science, 11, Article 927. https://doi.org/10.3389/fpls.2020.00927

York, L. M., Galindo-Castañeda, T., Schussler, J. R., & Lynch, J. P. (2019). Digital imaging to evaluate root system architectural changes associated with soil biotic factors. Phytobiomes Journal, 3(2), 119–128. https://doi.org/10.1094/PBIOMES-12-18-0062-R

Yusuf, M., Meng, X., Stefaniak, T. R., Montesinos-López, O. A., & Shannon, L. M. (2025). Leveraging unmanned aerial vehicle-derived multispectral data for improved genomic prediction in potato (Solanum tuberosum). The Plant Genome, 18(3), e70082. https://doi.org/10.1002/tpg2.70082

Zhao, Y., Zheng, B., Chapman, S. C., Laws, K., George-Jaeggli, B., Hammer, G. L., Jordan, D. R., & Potgieter, A. B. (2021). Detecting sorghum plant and head features from multispectral UAV imagery. Plant Phenomics, 2021, Article 9874650. https://doi.org/10.34133/2021/9874650

Zuffo, L. T., DeLima, R. O., & Lübberstedt, T. (2022). Combining datasets for maize root seedling traits increases the power of GWAS and genomic prediction accuracies. Journal of Experimental Botany, 73(16), 5460–5473. https://doi.org/10.1093/jxb/erac236

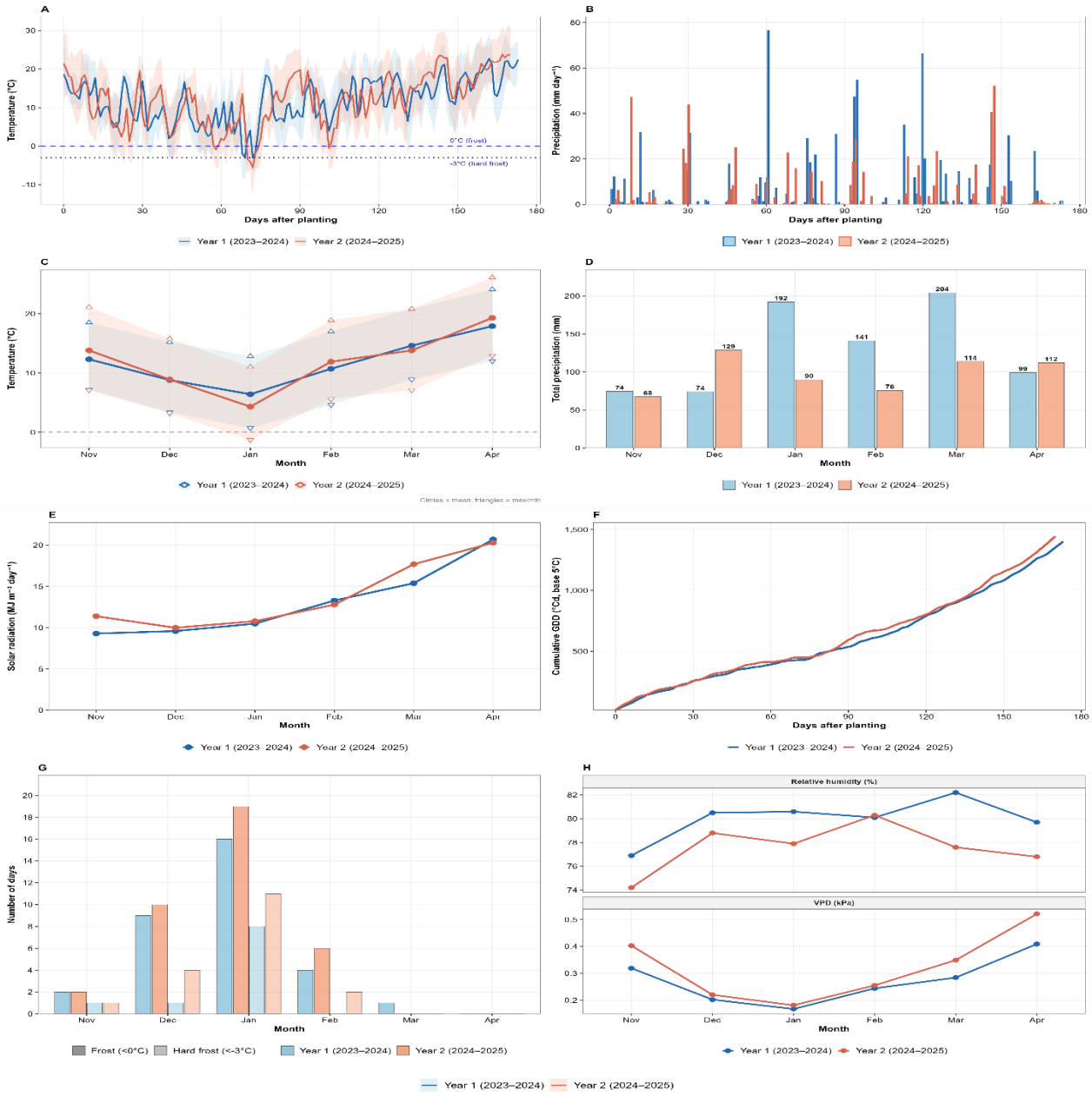

Figure 5.1. Environmental conditions at the E.V. Smith Research Center, Tallassee, AL (32.50°N, 85.89°W) during the 2023–2024 (Year 1) and 2024–2025 (Year 2) white lupin growing seasons (November–April).

(A) Daily mean temperature with shaded min–max range; dashed and dotted lines indicate frost (0°C) and hard frost (−3°C) thresholds. (B) Daily precipitation. (C) Monthly mean temperature (circles) with max/min (triangles) and shaded range. (D) Monthly total precipitation. (E) Monthly mean solar radiation. (F) Cumulative growing degree-days (base 5°C). (G) Monthly frost (<0°C) and hard frost (<−3°C) days. (H) Monthly mean relative humidity (top) and vapor pressure deficit (bottom). Meteorological data retrieved from NASA POWER (NASA, 2024).

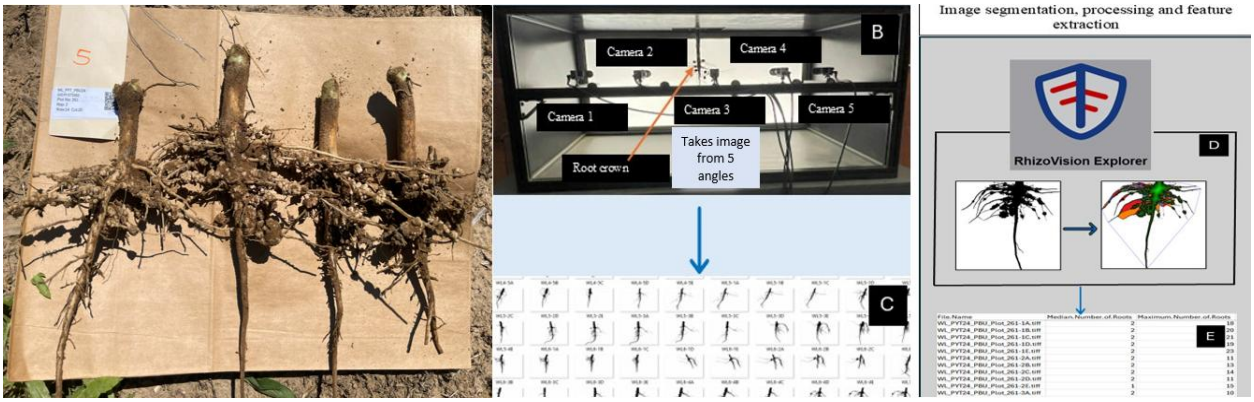

Figure 5.2. Root crown phenotyping pipeline used in this study.

(A) white lupin root crown excavated by shovelomics at physiological maturity, individually barcoded and cleaned prior to imaging. (B) Custom five-camera monochromatic imaging array used to capture root crown images in batch mode, with the root crown positioned centrally for simultaneous multi-angle acquisition. (C) Representative batch of segmented root crown images generated from a single plot across five camera positions. (D) RhizoVision Explorer interface showing automated root crown segmentation and colorimetric classification of architectural features. (E) Representative output data table.

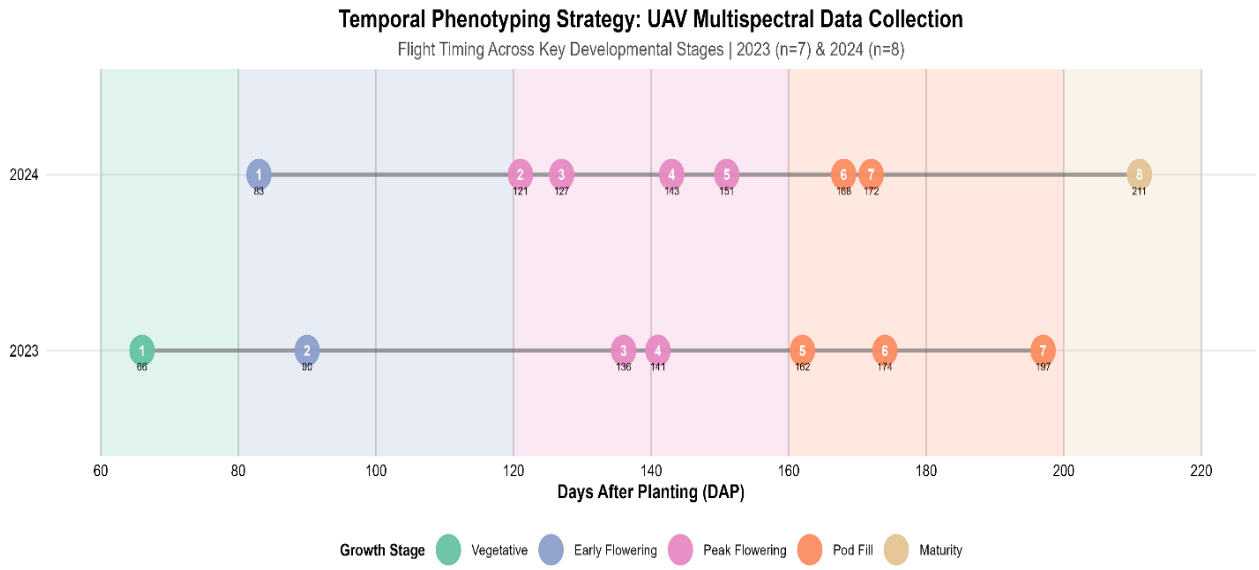

Figure 5.3. UAV multispectral flight schedule across two growing seasons in white lupin.

Timeline of UAV data collection flights in 2023 (n = 7) and 2024 (n = 8) plotted against days after planting (DAP). Each numbered marker indicates a single flight event, colour-coded by crop growth stage: vegetative (DAP 66), early flowering (DAP 90 in 2023; DAP 83 in 2024), peak flowering (DAP 136–141 in 2023; DAP 121–127 in 2024), pod fill (DAP 162–174 in 2023; DAP 143–172 in 2024), and maturity (DAP 197 in 2023; DAP 211 in 2024). Flights spanned the full crop development cycle from early vegetative growth through physiological maturity. Forty-six vegetation indices were extracted from each flight for use as phenomic predictors in genomic and phenomic prediction models.

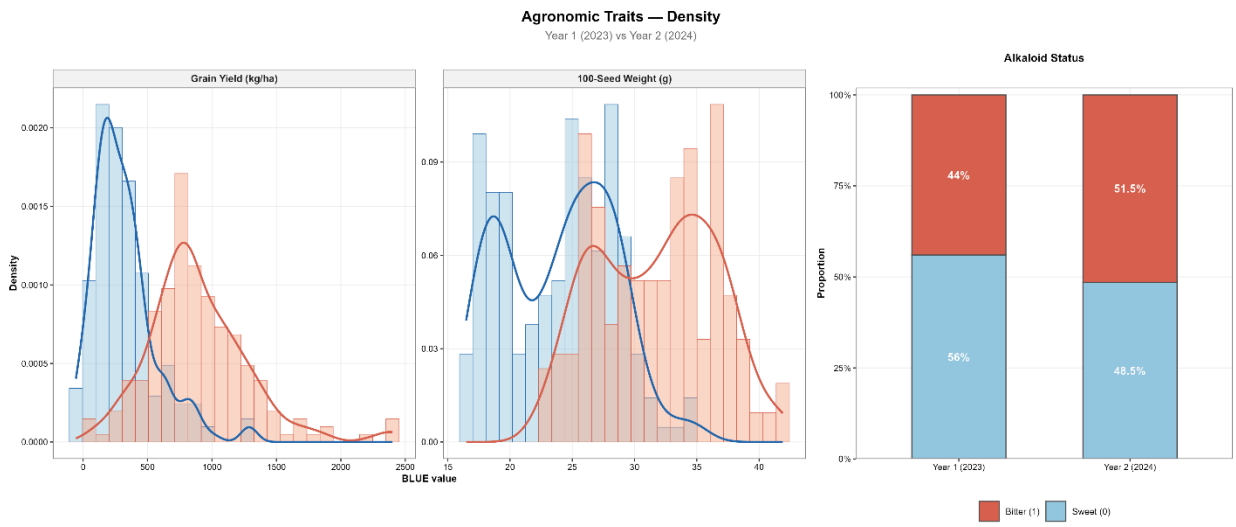

Figure 5.4. Phenotypic distributions of agronomic traits across two growing seasons.

Frequency distributions of best linear unbiased estimates (BLUEs) for grain yield (kg ha^{-1}) and 100-seed weight (g), and alkaloid class frequency, are shown for Year 1 (2023, blue) and Year 2 (2024, red). Continuous traits are presented as overlaid histograms with kernel density estimates; alkaloid content, scored as a binary trait (sweet = 0; bitter = 1) using the Dragendorff colorimetric test, is presented as stacked proportion bars. BLUEs for continuous traits were clipped to the 1st–99th percentile prior to plotting. The bimodal distribution of 100-seed weight reflects the co-evaluation of determinate and indeterminate plant types within the panel.

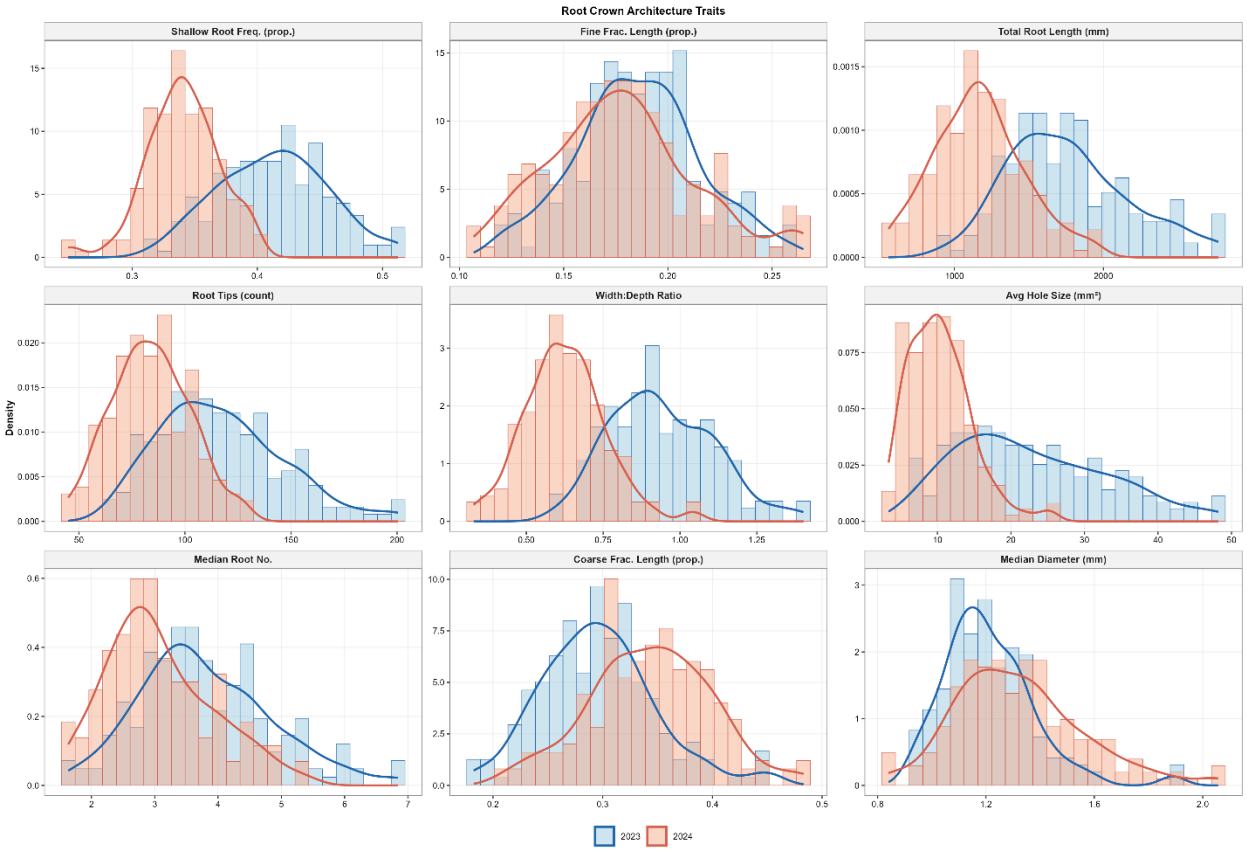

Figure 5.5. Phenotypic distributions of priority root crown architectural traits across two growing seasons.

Frequency distributions of best linear unbiased estimates (BLUEs) for nine root crown traits are shown for Year 1 (2023, blue) and Year 2 (2024, red), presented as overlaid histograms with kernel density estimates. Traits were measured from root crown images captured using the shovelomics protocol and processed in RhizoVision Explorer (Seethepalli et al., 2021). Log-transformed traits are presented on their analysis scale. BLUEs were clipped to the 1st–99th percentile prior to plotting. Year-to-year shifts in distribution location and spread reflect the combined effects of genetic differences among accessions evaluated in each year and environmental variation between seasons.

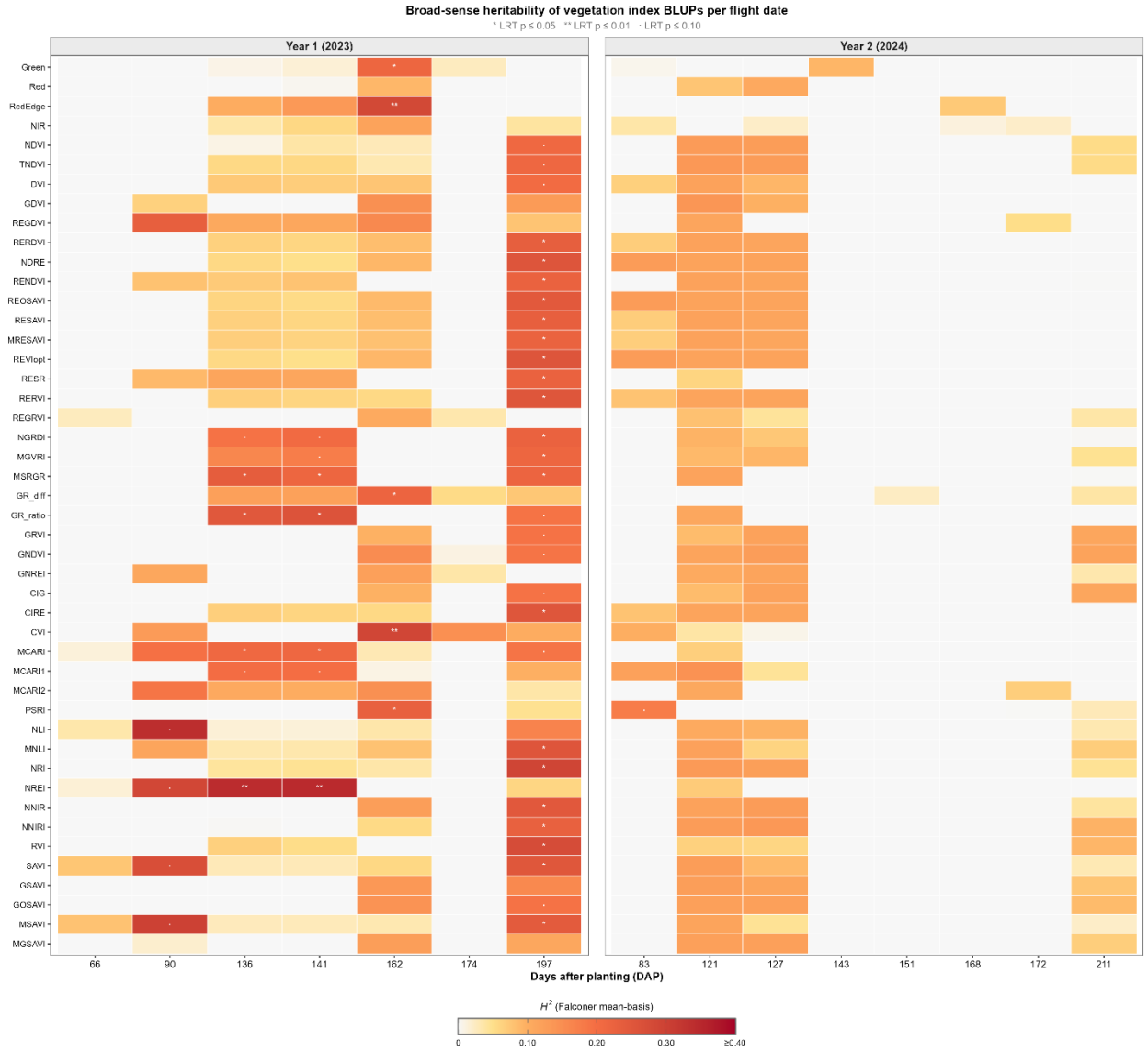

Figure 5.6. Cullis heritability (H^2) of best linear unbiased predictor (BLUP) values for 46 vegetation indices across UAV multispectral flight dates.

Heatmaps compare heritability of 46 vegetation indices across UAV flight dates in 2023 and 2024. Darker cells indicate higher heritability, and symbols mark significant likelihood-ratio tests. Heritability was stronger and more frequent in 2023, particularly at 136–141 and 197 days after planting.

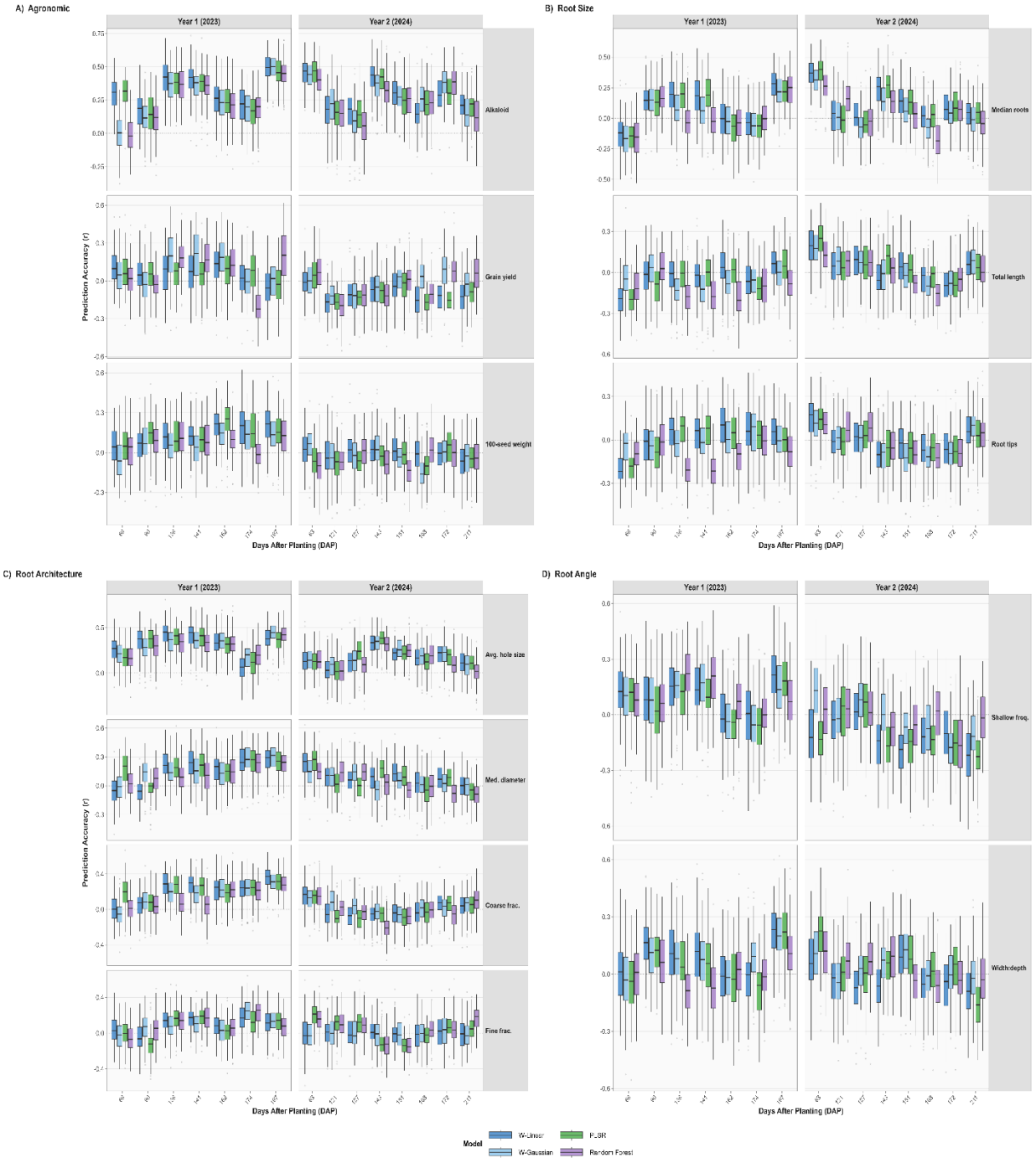

Figure 5.7. Single-flight phenomic prediction accuracy across UAV flight dates for agronomic and root traits in white lupin.

Prediction accuracy is shown for (A) agronomic traits, (B) root-size traits, (C) root-architecture traits, and (D) root-angle traits across UAV flight dates in 2023 and 2024. Boxplots represent cross-validation results for W-linear, W-Gaussian, PLSR, and Random Forest models. Accuracy varied by trait, year, flight timing, and model, with alkaloid content generally predicted more accurately than grain yield and most root traits.

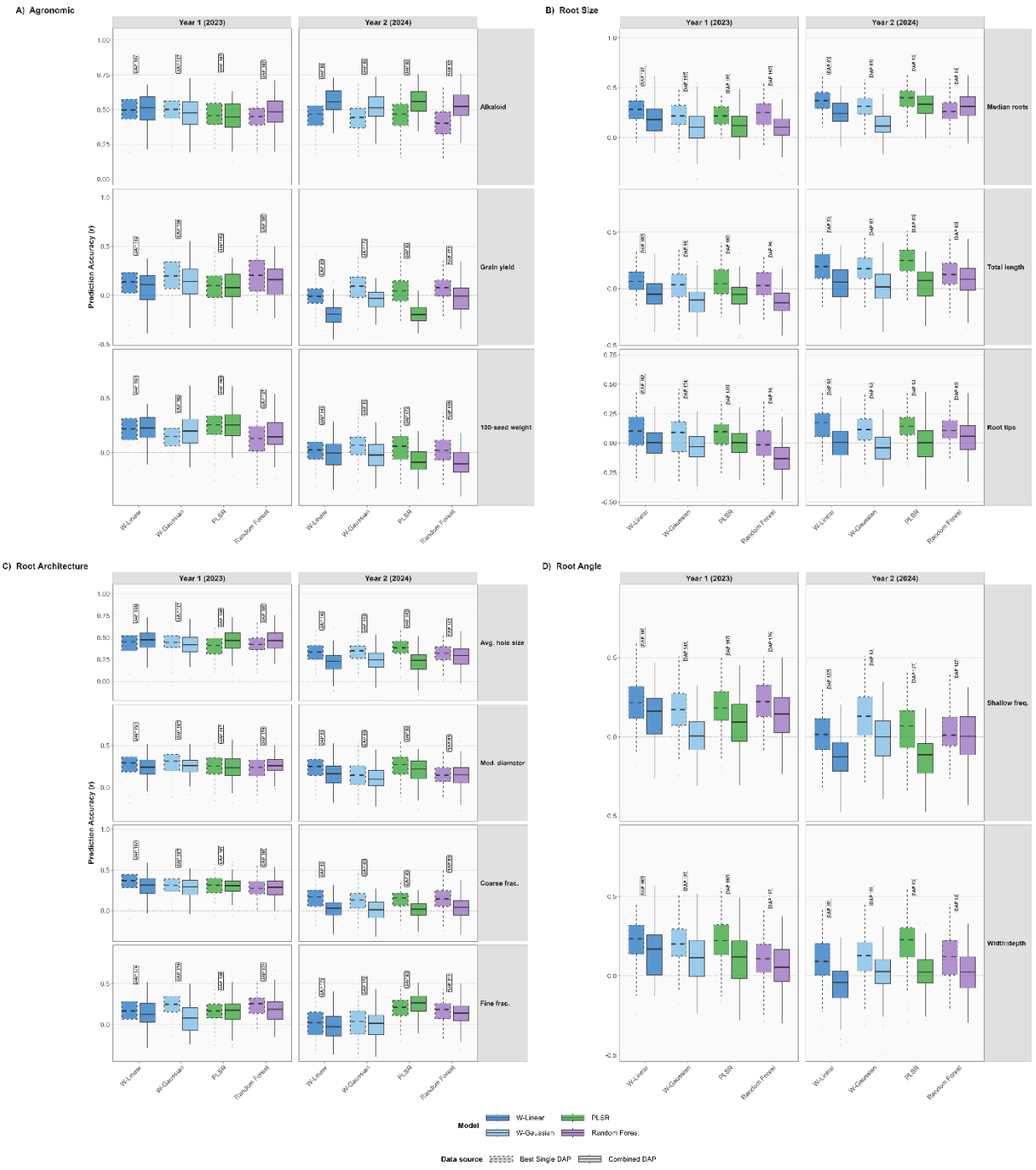

Figure 5.8. Best single flight versus combined flight phenomic prediction accuracy for agronomic and root traits in white lupin.

Prediction accuracy from the best single flight and combined flights is compared for (A) agronomic traits, (B) root-size traits, (C) root-architecture traits, and (D) root-angle traits across two years and four models. Alkaloid content and average hole size were predicted most consistently, whereas grain yield and several root traits showed lower or negative accuracies. Combining flights provided limited and inconsistent improvement over the best single flight.

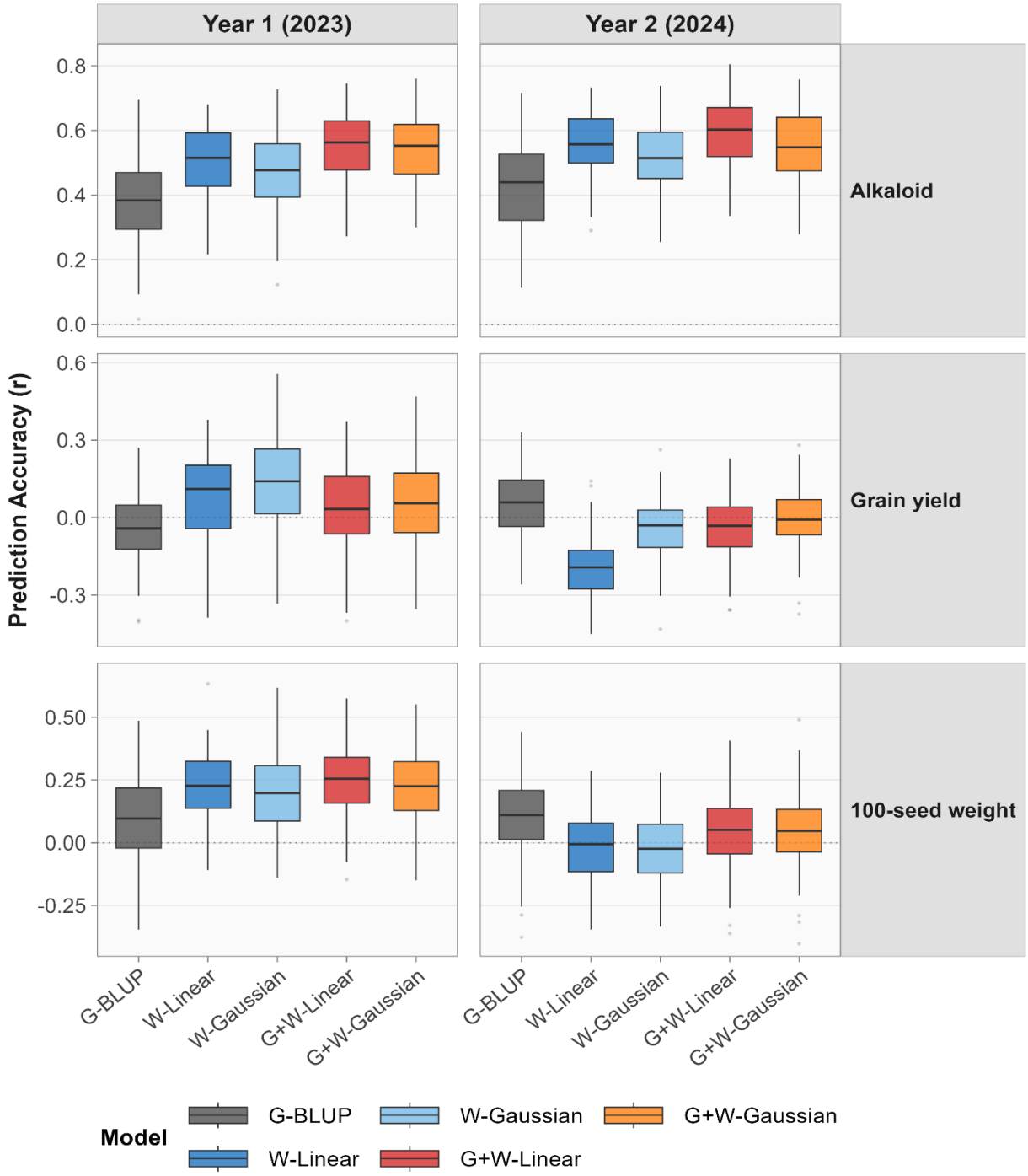

Figure 5.9. Genomic, phenomic, and integrated genomic–phenomic prediction accuracy for agronomic traits in white lupin.

Prediction accuracy is shown for agronomic traits. Alkaloid was predicted best across both years, especially by phenomic and integrated models. Grain yield had generally low accuracy, with several models near or below zero, particularly in 2024. Prediction of 100 seed weight was moderate in 2023 but declined to near-zero or only slightly positive values in 2024.

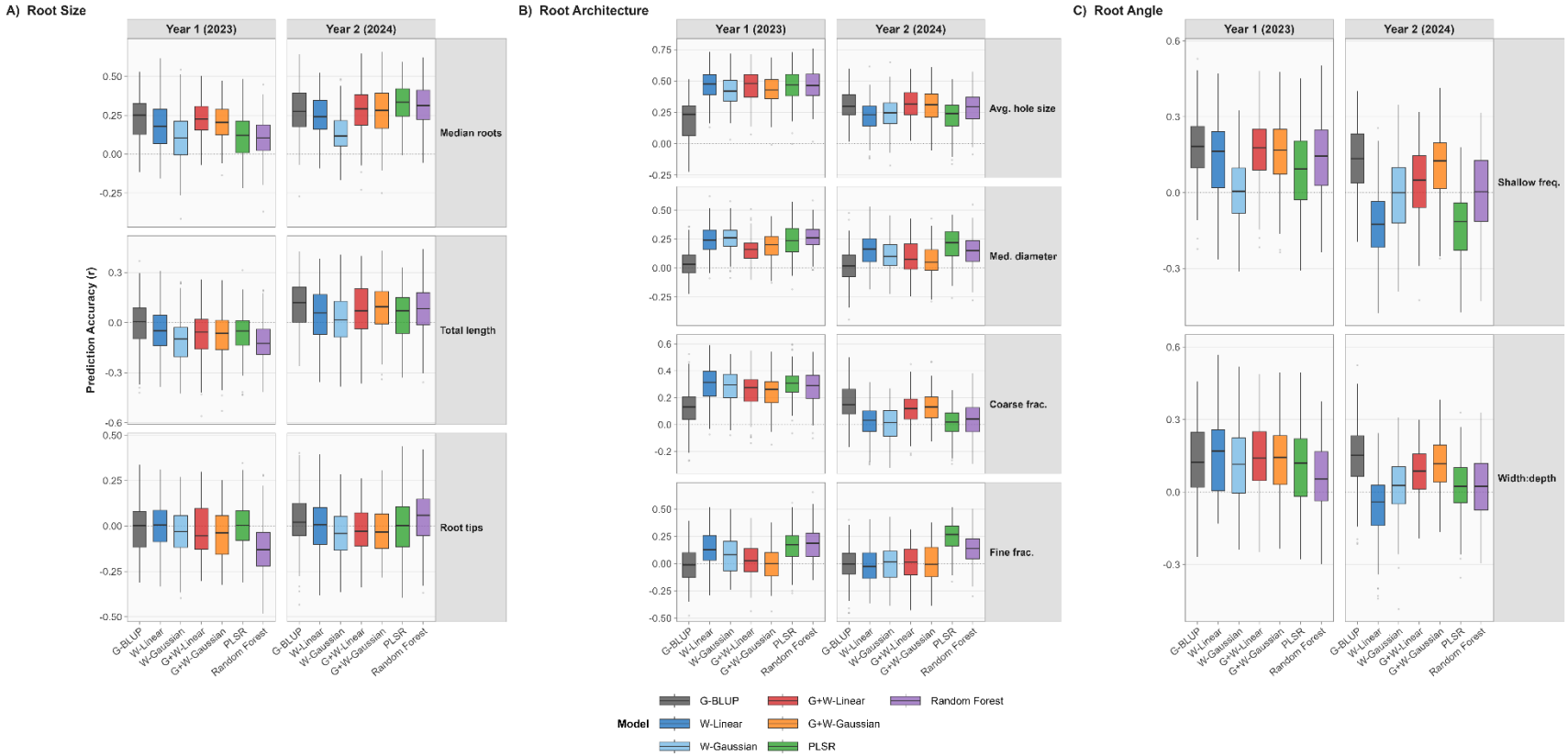

Figure 5.10. Genomic, phenomic, and integration of genomic-phenomic prediction accuracy for RSA traits in white lupin.

Prediction accuracy is compared among G-BLUP, W-Linear, W-Gaussian, G+W-Linear, G+W-Gaussian, PLSR, and Random Forest for RSA traits in white lupin. In panel A, median roots and total length are predicted more accurately in 2024 than in 2023, while root tips remain low across models. In panel B, root architecture traits, especially average hole size, median diameter, and the coarse and fine fractions, show the strongest and most consistently positive accuracies. In panel C, root angle traits have lower and less stable prediction accuracy, with several models near zero or negative, particularly in 2024.

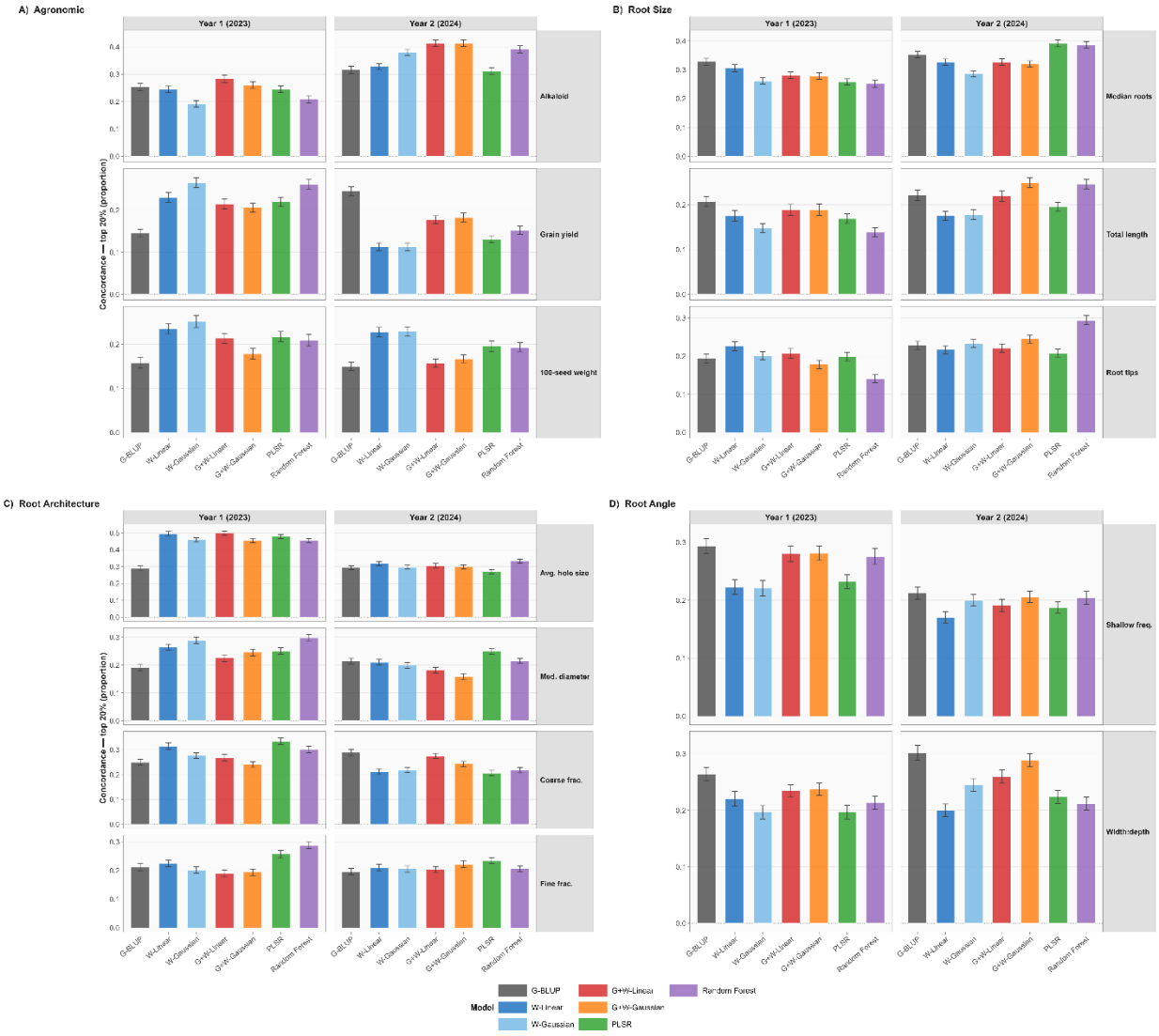

Figure 5.11. Selection concordance at 20% selection intensity for agronomic and root traits under within-year prediction in white lupin

Selection concordance is shown for (A) agronomic traits, (B) root-size traits, (C) root-architecture traits, and (D) root-angle traits across two years and seven prediction models. Concordance was trait and year dependent, with higher values for alkaloid and several root architecture traits, while grain yield and some root angle traits showed lower agreement between predicted and observed selections.

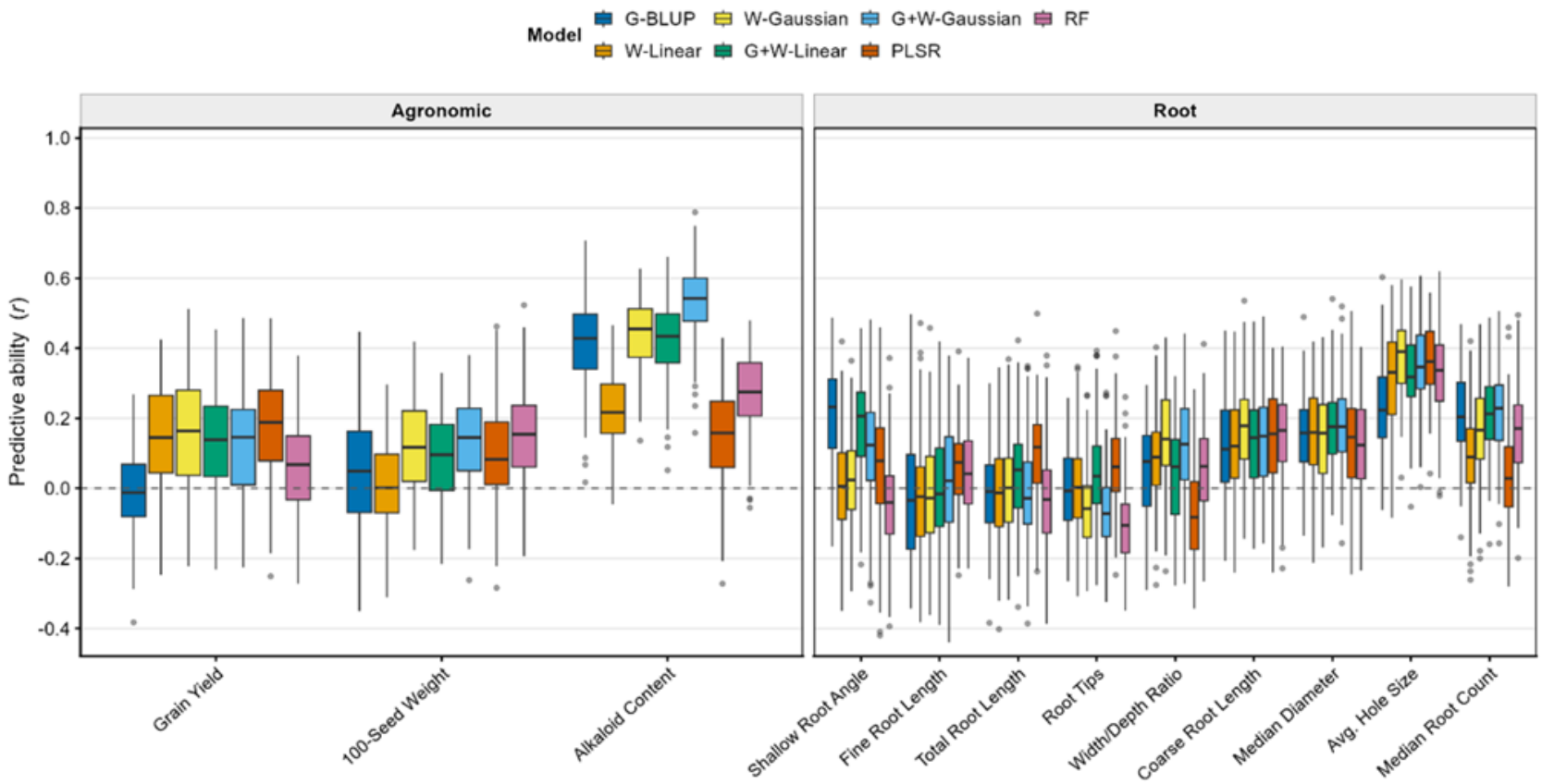

Figure 5.12. Predictive ability of seven prediction models under the averaged W kernel approach for agronomic and root traits in a pooled two-year population of white lupin.

Predictive ability is shown for agronomic traits and nine root traits using the averaged phenomic kernel across both years. Alkaloid content was predicted most accurately among agronomic traits, whereas grain yield and 100-seed weight showed lower accuracy. Among root traits, average hole size performed best, followed by median diameter and coarse root length, while several root-size traits had low or inconsistent prediction.

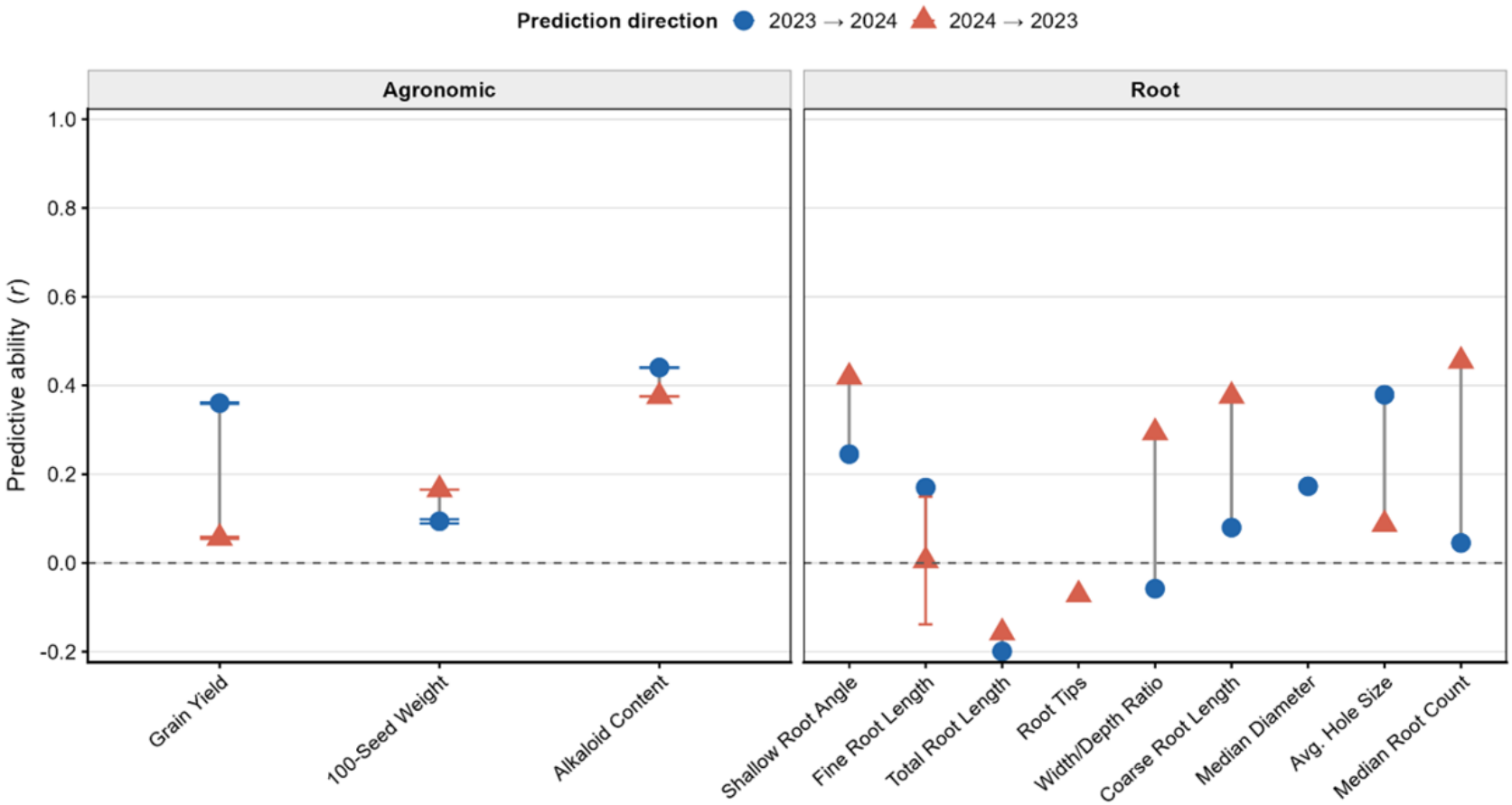

Figure 5.13. Exploratory cross-year predictive ability of a year-blocked genomic–phenomic model for agronomic and root traits in white lupin.

Cross-year predictive ability (r) of the G+WE year-blocked genomic–phenomic model across two growing seasons (2023 and 2024) for twelve traits: three agronomic (left panel) and nine root architectural (right panel).

Table 5.1. Target traits for dual-purpose white lupin (Lupinus albus L.) breeding in Alabama, with the ecosystem service each trait delivers and its mechanistic basis.

Trait code	Full name	Ecosystem service(s)	Role and mechanistic basis	Key reference(s)
A. Agronomic / cash crop traits — dual-purpose system economic and food safety drivers				
GY_KgHa	Grain yield (kg ha^{-1})	Cash crop viability; N cycling	Primary determinant of economic return in the dual-purpose system. High-yielding lines provide grain protein for food/feed while residue N credits reduce synthetic N demand in subsequent crops. Auburn field trials recorded ~30 bu ac^{-1} in white lupin, matching soybean N-fixation credits.	Reeves (USDA ARS, 1995); Sulas et al. (2015)
HSW_g	100-seed weight (g)	Grain quality; marketability	Seed weight is a proxy for protein content and market grade in lupin grain. Heavier seeds correlate with higher protein per unit weight, determining feed and food value. Essential for breeding towards industry protein thresholds (32–38% protein in L. albus).	Bhardwaj et al. (1998); Pereira et al. (2022)
Alkaloid	Seed alkaloid content	Food/feed safety; pest resistance; N partitioning	Quinolizidine alkaloids (QAs) must remain ≤0.02% in grain for food/feed markets (industry threshold). Breeding for low-QA grain while retaining vegetative QA preserves insect resistance. QA content is also negatively correlated with nodulation intensity, linking alkaloid selection to symbiotic N fixation capacity.	Frick et al. (2017); Cowling et al. (1998); Pereira et al. (2022)
B. Root architecture traits — Alabama ecosystem service delivery				

Trait code	Full name	Ecosystem service(s)	Role and mechanistic basis	Key reference(s)
shallow_freq	Shallow root angle frequency	Topsoil P mobilisation; NPS pollution control	Frequency of roots growing at <30° from horizontal (topsoil foraging). In Alabama Ultisols, legacy P from 3.6 × 10^9 lb yr^{-1} poultry litter is stratified in the 0–15 cm horizon. Shallow root growth maximises lateral surface coverage in the P-enriched horizon and intercepts dissolved P in surface runoff before it reaches Alabama River basin tributaries (Mulberry, Catoma watersheds — hypertrophic).	Lynch & Brown (2001); Lambers et al. (2006); Waldrip et al. (2023)
FineFrac_Length	Fine root fraction of total root length	P mobilisation; soil C input	Proportional length of fine roots (diameter <1.7 mm in RhizoVision classification), which in white lupin are the cluster (proteoid) root structures. Cluster roots exude citrate and malate to dissolve Al/Fe-bound and phytate-P in poultry-litter-enriched Ultisol topsoils. Fine root turnover is the dominant pathway for soil organic matter formation in Alabama Ultisols.	Neumann & Martinoia (2002); Lambers et al. (2006); Heckman et al. (2021)
total_length	Total root system length	P mobilisation; N interception; NPS pollution control	Master determinant of P acquisition efficiency across soil depths. Root length density is linearly correlated with ^{15}N uptake at all soil depths across cover crop species, establishing total_length as the key variable for intercepting mobile NO_3^- leaching from poultry litter N through Hartsells sandy loam soils under Alabama's 1,377 mm yr^{-1} rainfall.	Vance et al. (2003); Kristensen & Thorup-Kristensen (2004)
root_tips	Root tip count	P mobilisation;	Root tips are initiation sites for cluster root primordia under P deficiency and for rhizobium	[CITATION NEEDED]; Rojas-

Trait code	Full name	Ecosystem service(s)	Role and mechanistic basis	Key reference(s)
		N fixation; NPS pollution control	infection threads for nodulation. Root tip count captures both P mobilisation capacity and N fixation substrate. Active root tips release organic acids and phosphatases creating P-immobilisation microsites in the rhizosphere, reducing dissolved P available for runoff from poultry litter zones.	Tapias et al. (2021)
width_depth_ratio	Root system width-to-depth ratio	Topsoil P foraging; water infiltration; soil structure	Single architectural summary of topsoil vs subsoil foraging strategy. High ratio = wide, shallow architecture = topsoil P-specialist ideotype aligned with Alabama's surface-stratified legacy P constraint. Lateral root biopores created by wide-spreading roots persist 1–2 seasons, improving water infiltration through compacted Ultisol argillic (Bt) horizons and reducing surface runoff carrying dissolved P to Alabama River tributaries.	Lynch (2022); Ho et al. (2005); Rauber et al. (2025)
CoarseFrac_Length	Coarse root fraction of total root length	Soil structure; biopore creation; water infiltration	Coarse roots (diameter >3.41 mm) form the primary structural framework anchoring the root system and creating persistent biopores in compacted Ultisol Bt horizons. Biopores from coarse root channels improve water infiltration, reduce surface runoff, and provide conduits for fine root and mycorrhizal hyphal access into subsoil P pools.	Lambers et al. (2006); Rauber et al. (2025)
median_diameter	Median root diameter	P acquisition efficiency; metabolic	Root diameter is negatively correlated with P acquisition efficiency under low P: thinner roots have higher specific root length, covering more	Lambers et al. (2006); Postma & Lynch (2011)

Trait code	Full name	Ecosystem service(s)	Role and mechanistic basis	Key reference(s)
		cost of root system	soil volume per unit of C invested. Decreased average diameter under P deficiency is a documented adaptive response. In white lupin, smaller median diameter reflects greater investment in fine cluster roots relative to coarse structural roots.	
avg_hole_size	Average hole size (root crown image)	Root system branching architecture index	Computed from root crown images as the average size of internal void regions (disconnected components in the inverted binary image) within the root crown silhouette. Larger avg_hole_size reflects sparser internal branching density and wider spacing between roots, an indicator of topsoil foraging architecture. Defined and standardised in the RhizoVision root image analysis platform.	Seethepalli et al. (2021); York et al. (2019)
median_roots	Median root number	Root system density; N and P interception capacity	Median number of roots recorded at horizontal cross-sections through the root crown image, indexing root branching density and lateral root proliferation. Higher median root number reflects greater root tip and lateral root production, increasing both P mobilisation site density and N interception capacity in the soil profile. Root number and angle are documented as the primary drivers of RSA variation under P stress.	Lynch (2022); Trachsel et al. (2013)

Table 5.2. Vegetation indices (VIs) computed from UAV multispectral imagery.

Code	Full Name	Formula (N=NIR, R=Red, G=Green, RE=Red-Edge)
Green	Green reflectance band	G
Red	Red reflectance band	R
RedEdge	Red-Edge reflectance band	RE
NIR	Near-Infrared reflectance band	N
CIG	Chlorophyll Index Green	N/G − 1
CIRE	Chlorophyll Index Red-Edge	N/RE − 1
CVI	Chlorophyll Vegetation Index	(N × R) / G²
DVI	Difference Vegetation Index	N − RE
GDVI	Green Difference Vegetation Index	N − G
GNDVI	Green Normalized Difference Vegetation Index	(N − G) / (N + G)
GNREI	Green Normalized Red-Edge Index	(RE − G) / (RE + G)
GOSAVI	Green Optimised Soil-Adjusted VI	(1 + 0.16)(N − G) / (N + G + 0.16)
GRVI	Green Ratio Vegetation Index	N / G
GSAVI	Green Soil-Adjusted Vegetation Index	1.5 × (N − G) / (N + G + 0.5)
MCARI	Modified Chlorophyll Absorption Ratio Index	((RE − R) − 0.2 × (RE − G)) × (RE / R)
MCARI1	Modified Chlorophyll Absorption Ratio Index 1	[(N − RE) − 0.2 × (N − G)] × (N / RE)
MCARI2	Modified Chlorophyll Absorption Ratio Index 2	(1.5(N−RE) − 1.3(N−G)) / sqrt((2N+1)² − (6N − 5√RE) − 0.5)
MGSAVI	Modified Green SAVI	0.5 × [2N + 1 − sqrt((2N+1)² − 8(N − G))]
MNLI	Modified Non-Linear Index	1.5 × (N² − R) / (N² + R + 0.5)
MRESAVI	Modified Red-Edge SAVI	0.5 × [2N + 1 − sqrt((2N+1)² − 8(N − RE))]
MSAVI	Modified Soil-Adjusted Vegetation Index	0.5 × [2N + 1 − sqrt((2N+1)² − 8(N − R))]
MSRGR	Modified Simple Ratio Green-Red	sqrt(G / R)
NDRE	Normalized Difference Red-Edge Index	(N − RE) / (N + RE)
NDVI	Normalized Difference Vegetation Index	(N − R) / (N + R)
NLI	Non-Linear Index	(N² − R) / (N² + R)
NNIR	Normalized NIR Index	N / (N + RE + G)
NNIRI	Normalized NIR-to-Red-Edge Index	N / (N + RE + R)
NREI	Normalized Red-Edge Index	RE / (N + RE + G)

Code	Full Name	Formula (N=NIR, R=Red, G=Green, RE=Red-Edge)
NRI	Normalized Red Index	R / (N + RE + R)
PSRI	Plant Senescence Reflectance Index	(R − G) / RE
REGDVI	Red-Edge Green Difference VI	RE − G
REGRVI	Red-Edge Green Ratio VI	RE / G
RENDVI	Red-Edge Normalized Difference VI	(RE − R) / (RE + R)
REOSAVI	Red-Edge Optimised SAVI	(1 + 0.16)(N − RE) / (N + RE + 0.16)
RERDVI	Renormalized Difference Red-Edge VI	(N − RE) / sqrt(N + RE)
RERVI	Red-Edge Ratio Vegetation Index	N / RE
RESAVI	Red-Edge Soil-Adjusted VI	1.5 × (N − RE) / (N + RE + 0.5)
RESR	Red-Edge Simple Ratio	RE / R
REVIopt	Optimised Red-Edge Vegetation Index	100 × (ln(N) − ln(RE))
RVI	Ratio Vegetation Index	N / R
SAVI	Soil-Adjusted Vegetation Index	1.5 × (N − R) / (N + R + 0.5)
TNDVI	Transformed Normalized Difference VI	sqrt((N − R)/(N + R) + 0.5)
GR_diff	Green-Red Difference	G − R
GR_ratio	Green-Red Ratio	G / R
NGRDI	Normalized Green-Red Difference Index	(G − R) / (G + R)
MGVRI	Modified Green-Red Vegetation Index	$(G^2 - R^2) / (G^2 + R^2)$

Table 5.3. Prediction models evaluated within each scenario.

Model	Formal name	Information source	Kernel or algorithm	Scenarios	Fitting details
G-BLUP	Genomic BLUP	Genomic only	$G = ZZ^T / [2\Sigma p_j(1-p_j)]$; VanRaden (2008) Method 1; 174,284 SNPs; missing genotypes imputed by Binomial(2, p)	A, B, C	BGLR RKHS; nIter = 120,000; burnIn = 20,000; NA masking for test prediction
W-Linear	Phenomic linear kernel	Phenomic only	$W = XX^T/p$; X = VI matrix scaled per year; full n×n W with NA masking	A, B, C	BGLR RKHS; nIter = 120,000; burnIn = 20,000; NA masking
W-Gaussian	Phenomic Gaussian kernel	Phenomic only	$K(i,j) = \exp(-D^2_{ij}/h)$; h = median pairwise squared Euclidean distance; full n×n kernel with NA masking	A, B, C	BGLR RKHS; nIter = 120,000; burnIn = 20,000; NA masking
G+W-Linear	Integrated linear	Genomic + Phenomic	Dual-kernel RKHS: G + W_lin; σ^2G and σ^2W estimated jointly; NA masking on both kernels	A, B, C	BGLR RKHS; nIter = 120,000; burnIn = 20,000; NA masking
G+W-Gaussian	Integrated Gaussian	Genomic + Phenomic	Dual-kernel RKHS: G + W_gau; σ^2G and σ^2W estimated jointly; NA masking on both kernels	A, B, C	BGLR RKHS; nIter = 120,000; burnIn = 20,000; NA masking
PLSR	Partial least squares regression	Phenomic only (ML)	Regression on VI columns directly; ncomp selected by LOO-CV on training set (max 10); no kernel	A, B, C	R pls package (Mevik & Wehrens, 2007); no MCMC; standard BLUPs as response; no weights
RF	Random Forest	Phenomic only (ML)	Regression on VI columns directly; ntree = 500; mtry tuned by OOB error (grid: p/3, $\sqrt{p}$, p/2); no kernel	A, B, C	R randomForest package (Liaw & Wiener, 2002); no MCMC;

Model	Formal name	Information source	Kernel or algorithm	Scenarios	Fitting details
					standard BLUPs as response; no weights

Table 5.4. Prediction scenarios evaluated for genomic and phenomic selection in white lupin (Lupinus albus L.).

Code	Formal name	CV scheme	Train / test years	No. models	W-kernel construction
A	Per-DAP Within-Year	5-fold × 25 reps	2023 (separate); 2024 (separate)	7	$W = ZZ^T/p$; Z = 46 VI BLUPs at a single UAV flight (one DAP per run); extracted per DAP via ASReml-R with AR1×AR1 spatial correction
B	Combined-DAP Within-Year	5-fold × 25 reps	2023 (separate); 2024 (separate)	7	$W = ZZ^T/p\_total$; Z = all DAP flights stacked within one year (2023: 7 flightd; 2024: 8 flights)
C	Averaged W Pooled Prediction	5-fold × 25 reps	Pooled 2023 + 2024 (232 unique accessions)	7	Z scaled per year independently; $Z\_avg = (Z^*\_2023 + Z^*\_2024)/2$ for 168 overlap lines; year-unique lines retain single-year Z; $W = Z\_avg\ Z\_avg^T / p$

All Bayesian kernel models used de-regressed BLUPs (Garrick et al., 2009) as response variables with reliability weights. The genomic relationship matrix (G) was constructed from 174,284 SNP markers following VanRaden (2008). Phenomic W matrices were derived from BLUPs of 46 vegetation indices from UAV multispectral imagery (2023: 7 flights; 2024: 8 flights). MCMC settings: nIter = 120,000; burnIn = 20,000. CV, cross-validation; DAP, days after planting; VI, vegetation index.

Table 5.5. Variance components and broad-sense heritability estimates for agronomic and root crown architectural traits.

Trait	Year	VG	VGY	VE	VTotal	VG (%)	VGY (%)	VE (%)	H^2F	H^2C	χ^2G	PG	χ^2GY	PGY
ALk	Combined	3.65	2.00E-06	3.29	6.94	52.56	0.00	47.44	0.82	0.64	0.00	0.50	0.00	0.50
	2023	2.10	NA	3.29	5.39	38.99	NA	61.01	0.56	0.45	NA	NA	NA	NA
	2024	2.29	NA	3.29	5.58	41.07	NA	58.93	0.58	0.46	NA	NA	NA	NA
GY	Combined	25644.32	4946.95	122884.78	153476.04	16.71	3.22	80.07	0.44	0.33	10.21	0.00	0.23	0.31
	2023	16735.16	NA	89928.65	106663.81	15.69	NA	84.31	0.27	0.27	NA	NA	NA	NA
	2024	42536.12	NA	171682.29	214218.41	19.86	NA	80.14	0.33	0.26	NA	NA	NA	NA
HSW_g	Combined	6.51	0.69	6.09	13.29	49.01	5.19	45.80	0.78	0.73	78.50	0.00	2.45	0.06
	2023	7.64	NA	4.49	12.13	62.99	NA	37.01	0.77	0.77	NA	NA	NA	NA
	2024	6.38	NA	7.70	14.07	45.31	NA	54.69	0.62	0.62	NA	NA	NA	NA
CF_L	Combined	0.00	0.0014	0.04	0.05	7.46	2.85	89.69	0.24	0.19	2.67	0.05	0.18	0.34
	2023	0.01	NA	0.03	0.04	21.82	NA	78.18	0.36	0.30	NA	NA	NA	NA
	2024	0.00	NA	0.05	0.05	3.00	NA	97.00	0.06	0.05	NA	NA	NA	NA
FF_L	Combined	0.00	0.00	0.00	0.00	5.49	0.00	94.51	0.19	0.15	1.68	0.10	0.00	0.50
	2023	0.00	NA	0.00	0.00	10.08	NA	89.92	0.18	0.15	NA	NA	NA	NA
	2024	0.00	NA	0.00	0.00	1.66	NA	98.34	0.03	0.03	NA	NA	NA	NA
AHS	Combined	11.41	12.20	54.50	78.10	14.61	15.62	69.77	0.37	0.30	7.93	0.00	6.13	0.01
	2023	47.32	NA	86.71	134.03	35.31	NA	64.69	0.52	0.44	NA	NA	NA	NA
	2024	2.40	NA	28.42	30.82	7.78	NA	92.22	0.14	0.14	NA	NA	NA	NA
MD	Combined	0.00	0.0031	0.03	0.04	8.39	7.77	83.84	0.25	0.20	2.89	0.04	1.43	0.12
	2023	0.00	NA	0.02	0.03	18.98	NA	81.02	0.32	0.26	NA	NA	NA	NA
	2024	0.01	NA	0.04	0.05	15.45	NA	84.55	0.27	0.25	NA	NA	NA	NA
MR	Combined	0.21	0.053	1.06	1.32	15.81	4.02	80.17	0.42	0.34	9.28	0.00	0.40	0.26
	2023	0.26	NA	1.36	1.62	16.01	NA	83.99	0.28	0.23	NA	NA	NA	NA
	2024	0.24	NA	0.82	1.06	23.04	NA	76.96	0.37	0.36	NA	NA	NA	NA

Trait	Year	VG	VGY	VE	VTotal	VG (%)	VGY (%)	VE (%)	H^2F	H^2C	χ^2G	PG	χ^2GY	PGY
RT	Combined	0.01	0.0020	0.08	0.10	11.82	2.08	86.10	0.34	0.27	5.88	0.01	0.11	0.37
	2023	0.02	NA	0.07	0.09	25.25	NA	74.75	0.40	0.34	NA	NA	NA	NA
	2024	0.01	NA	0.10	0.10	6.93	NA	93.07	0.13	0.12	NA	NA	NA	NA
SF	Combined	0.00	0.00	0.01	0.02	10.75	0.00	89.25	0.33	0.26	5.22	0.01	0.00	0.50
	2023	0.00	NA	0.02	0.02	5.16	NA	94.84	0.10	0.08	NA	NA	NA	NA
	2024	0.00	NA	0.01	0.01	12.68	NA	87.32	0.23	0.21	NA	NA	NA	NA
TL	Combined	0.01	0.0033	0.10	0.11	6.96	3.00	90.03	0.22	0.17	1.95	0.08	0.19	0.33
	2023	0.01	NA	0.06	0.08	18.55	NA	81.45	0.31	0.26	NA	NA	NA	NA
	2024	0.01	NA	0.13	0.13	6.93	NA	93.07	0.13	0.12	NA	NA	NA	NA
WDR	Combined	0.00	0.00	0.06	0.06	6.09	0.00	93.91	0.21	0.16	1.83	0.09	0.00	0.50
	2023	0.01	NA	0.04	0.05	12.25	NA	87.75	0.22	0.18	NA	NA	NA	NA
	2024	0.00	NA	0.07	0.07	2.02	NA	97.98	0.04	0.04	NA	NA	NA	NA

VG, genetic variance; VGY, genotype-by-year interaction variance; VE, residual variance; VTotal, total phenotypic variance; VG (%), VGY (%), and VE (%), percentage contribution to VTotal. H^2F, mean-basis broad-sense heritability following Falconer and Mackay (1996); H^2C, design-based reliability estimator following Cullis et al. (2006); both derived from REML variance components. χ2G and PG, likelihood ratio test statistic and P-value for VG; χ2GY and PGY, likelihood ratio test statistic and P-value for VGY; each test used a χ2 distribution on 1 degree of freedom. Combined estimates are from the two-year joint analysis; per-year estimates are from single-year models, for which the interaction and LRT columns are not applicable (NA). Trait abbreviations: ALk, alkaloid status; GY, grain yield (kg ha^{-1}); HSW_g, 100-seed weight (g); CF_L, coarse fraction root length; FF_L, fine fraction root length; AHS, average hole size (mm^2); MD, median root diameter (mm); MR, median root number; RT, root tips; SF, shallow root angle frequency; TL, total root length (mm); WDR, width-to-depth ratio. Alkaloid status was scored as a binary trait (sweet = 0; bitter = 1) and modelled on the latent liability scale with residual variance fixed at π2/3.

Table 5.6. Pooled-environment concordance, across seven prediction models under the averaged W kernel approach.

Trait group	Trait	Model	Conc20
Agronomic	Grain Yield	G-BLUP	0.19
		W-Linear	0.26
		W-Gaussian	0.26
		G+W-Linear	0.24
		G+W-Gaussian	0.23
		PLSR	0.33
		RF	0.26
Agronomic	100-Seed Weight	G-BLUP	0.19
		W-Linear	0.18
		W-Gaussian	0.21
		G+W-Linear	0.18
		G+W-Gaussian	0.19
		PLSR	0.22
		RF	0.21
Agronomic	Alkaloid Content	G-BLUP	0.32
		W-Linear	0.26
		W-Gaussian	0.28
		G+W-Linear	0.36
		G+W-Gaussian	0.37
		PLSR	0.23
		RF	0.25
Root	Shallow Root Angle	G-BLUP	0.34
		W-Linear	0.18
		W-Gaussian	0.25
		G+W-Linear	0.31
		G+W-Gaussian	0.30
		PLSR	0.21
		RF	0.18
Root	Fine Root Length	G-BLUP	0.20
		W-Linear	0.19
		W-Gaussian	0.20
		G+W-Linear	0.20
		G+W-Gaussian	0.21
		PLSR	0.22
		RF	0.22
Root	Total Root Length	G-BLUP	0.19
		W-Linear	0.17

Trait group	Trait	Model	Conc20
		W-Gaussian	0.19
		G+W-Linear	0.17
		G+W-Gaussian	0.17
		PLSR	0.22
		RF	0.20
Root	Root Tips	G-BLUP	0.23
		W-Linear	0.16
		W-Gaussian	0.14
		G+W-Linear	0.17
		G+W-Gaussian	0.14
		PLSR	0.17
		RF	0.11
Root	Width/Depth Ratio	G-BLUP	0.20
		W-Linear	0.21
		W-Gaussian	0.25
		G+W-Linear	0.19
		G+W-Gaussian	0.23
		PLSR	0.18
		RF	0.20
Root	Coarse Root Length	G-BLUP	0.27
		W-Linear	0.28
		W-Gaussian	0.29
		G+W-Linear	0.27
		G+W-Gaussian	0.28
		PLSR	0.27
		RF	0.23
Root	Median Diameter	G-BLUP	0.20
		W-Linear	0.31
		W-Gaussian	0.29
		G+W-Linear	0.22
		G+W-Gaussian	0.22
		PLSR	0.26
		RF	0.25
Root	Avg. Hole Size	G-BLUP	0.30
		W-Linear	0.42
		W-Gaussian	0.40
		G+W-Linear	0.43
		G+W-Gaussian	0.42
		PLSR	0.42

Trait group	Trait	Model	Conc20
		RF	0.34
Root	Median Root Count	G-BLUP	0.27
		W-Linear	0.29
		W-Gaussian	0.30
		G+W-Linear	0.28
		G+W-Gaussian	0.28
		PLSR	0.25
		RF	0.32

Predictive ability (r) is the Pearson correlation between observed deregressed BLUPs and model predictions, summarised as the mean across 125 cross-validation replicates (5-fold × 25 repetitions); 95% CI computed as mean ± 1.96 × SE across replicates. RMSE is in phenotype units and is not comparable across traits. Conc20 is the proportion of the true top 20% of genotypes correctly captured among the model's top 20% nominations. H2 is broad-sense heritability estimated on a mean basis from the combined two-year ASReml-R analysis: H2 = VG / (VG + VGY/Y + VE/YR), where VG is accession variance, VGY is genotype-by-year interaction variance, VE is residual variance, Y = 2 years, R = 2 replicates. The pooled population comprised up to 232 unique genotypes per trait depending on phenotypic data availability. All values are rounded to two decimal place.

Chapter 6 General discussion, synthesis, and future directions

6.1 Overview

The research reported here addressed a central problem in applied plant breeding. Cultivars are usually selected for agronomic yield under conventional monoculture evaluation. Still, their value increasingly depends on traits that those systems do not measure, such as superior performance in species mixtures (intercrops) and improved provision of the ecosystem services expected from cover crops (Annicchiarico et al., 2019, 2021; Freschet et al., 2021; Moore et al., 2022; Wolfe et al., 2021; Griffiths et al., 2022). This mismatch arises from three obstacles: (i) the combinatorial scale of evaluating mixtures, (ii) the limited quantitative-genetic foundation for the target traits, and (iii) the phenotyping bottlenecks that cap how many candidates can be screened each cycle. Four research chapters addressed that problem in three breeding scenarios: crimson clover and oat mixtures in the southeastern United States (Chapters 2), cassava and cowpea intercrops in sub-Saharan Africa (Chapter 3), and dual-purpose white lupin for Alabama Ultisols (Chapters 4 and 5). This chapter brings the findings together into an operational synthesis of how breeding programs can use genomic data, high-throughput phenotyping and phenomic (spectral) information, tester designs for intercrop evaluation, calibration strategies, and selection indices to increase the rate of genetic gains. It then identifies the major limitations of the work and outlines the future research priorities that follow.

6.2 Phenomic information supports selection when genomic relatedness is weak

Where family structure is shallow, or the target trait is highly polygenic, a well-timed UAV flight can supply selection signals that markers cannot yet provide, with genomic information layered in later as recurrent selection makes the between-family relatedness stronger. In white lupin (Chapter 5), genomic prediction (G-BLUP) could not recover the low-heritability root architectural traits, where heritabilities fell below 0.30; phenomic kernels built from UAV vegetation indices recovered the signal the genomic kernel could not, and the joint genomic-plus-phenomic (G+W) model matched or exceeded the phenomic-only model without underperforming it. The clover and oat section (Chapters 2) pointed the same way: with high to moderate UAV phenomic prediction of species-specific and total biomass.

The reason is consistent across both systems. Phenomic kernels are built from the realized phenotypic expression of the current cycle, including environment variation, so they explain how the population actually performed, which is what selection needs. However, this must be handled with caution: phenomic kernels absorb non-heritable plot-to-plot covariance, which inflates cross-validation accuracy relative to genomic prediction, so genomic (G) and phenomic (W) sources cannot be compared head-to-head as though they estimated the same quantity (Wang et al., 2025). The G+W model is valuable for exactly this reason: by estimating genomic and phenomic variance components separately, it assigns heritable additive variation to the correct source and leaves the genomic kernel positioned to contribute more as pedigree depth accumulates.

A crucial factor was trait heritability. Phenomic advantage was not general; it depended on whether the target trait contained enough repeatable genetic signal for

prediction to exploit. In white lupin, the G+W benefit was clearest for the high-heritability trait, but limited for the low-heritability root traits. This does not mean that low-heritability traits are unsuitable for genomic or phenomic prediction. Rather, it shows that such traits require larger training populations, stronger multi-environment replication, improved phenotyping protocols, or better timed phenomic measurements before prediction can reliably support selection. Phenomics can extend the reach of selection, but it cannot fully compensate for weak trait repeatability on its own.

6.3 General mixing ability dominates, reducing tester requirements

When general mixing ability (GMA) dominates specific mixing ability (SMA), a breeder does not need to evaluate every genotype against every partner. A small, representative set of companion testers captures a focal genotype's mixing value, which makes intercrop evaluation affordable and lets it be added to an existing monoculture program rather than replacing it, and further reducing the combinatorial problem significantly (Wright, 1985; Annicchiarico et al., 2019; Sampoux et al., 2020; Haug et al., 2023).

Both intercrop systems showed the same variance structure. In cassava and cowpea (Chapter 3), SMA was negligible for all three traits, producer effects explained 20 to 47% of intercrop variance, and two cowpea testers of deliberately contrasting growth habit ranked the cassava clones almost identically.

The breeding consequences are therefore clear: because clover GMA is carried almost entirely by producer effects, the operational recommendation is direct selection on clover fraction yield in the mixed plots, a quantity the breeder can measure, rather than on an associate effect that is both weak and difficult to phenotype. In cassava-

cowpea intercrop, selecting on the mean of monoculture and intercrop performance captured more than half of the gain from direct intercrop selection, in line with theoretical expectation for systems with weak producer-associate trade-offs (Sampoux et al., 2020); the observed producer-associate correlation for cassava fresh root weight was far less limiting than values reported for pea and barley. This justifies a staged pipeline for cassava: monoculture selection through the early generations, with single-tester intercrop evaluation introduced only at the advanced yield trial stage, a structure that is both genetically defensible and operationally feasible within the IITA program. The same logic supports the sparse incomplete-factorial design used in clover and oat, where a modest set of oat testers spread across the clover families sampled tester space well enough to estimate clover GMA without observing every combination.

6.4 UAV-phenomic efficiency depends on flight timing and calibration depth

The value of UAV phenotyping is determined by when the imagery is captured and how many plots are ground-truthed, not by the sophistication of the prediction model. A breeder can cut the most expensive part of mixture and cover-crop phenotyping, the destructive harvest, by half or more without losing meaningful genetic gain.

Two chapters agreed on this. In the clover and oat mixtures (Chapter 2), predictive ability for total biomass reached 95% of the full-data baseline when only 25% of plots (150 of 600) were destructively harvested for calibration, and expected response to selection stabilized at 50% calibration, implying a 50 to 75% reduction in destructive phenotyping labor for less than 10% loss in genetic gain. A regularized linear model (Elastic Net) reached near-optimal accuracy at a fraction of the computational

cost of kernel or ensemble methods, which matters for routine deployment. In white lupin (Chapter 5), a single well-timed late-season flight outperformed stacking imagery from the whole season for seven of nine root traits, with accuracy losses of 0.08 to 0.19 when all flights were combined, because the canopy signal coupled to root expression is transient and phenologically timed, so averaging across the season dilutes it rather than enriching it.

For a breeding program, this provides a simple and repeatable protocol: acquire one flight at the right phenological window, ground-truth a quarter to a half of the plots chosen to span the spectral range, and predict the remainder with a regularized linear model. The labor saved is not marginal; destructive species separation and root excavation are the dominant per-plot costs in these programs and halving them directly relaxes the constraint on how many families a breeder can carry each cycle.

6.5 Dual-purpose breeding requires index selection when objectives conflict

When two breeding goals are genetically opposed, selecting on either one alone moves the program backward on the other. A defensible dual-purpose program must select on an explicit index that weights the competing objectives, not on yield with ecosystem function treated as an afterthought. The white lupin analyses revealed this antagonism most clearly (Chapters 5 and 6). The root-exploration traits that drive phosphorus mobilization were negatively correlated with grain yield, consistent with the root economics spectrum (Freschet et al., 2021). Selecting on yield alone would therefore erode ecosystem-service delivery, and selecting on root exploration alone would erode profitability. The AESI, which combines root and yield traits under literature-grounded ecosystem-service weights, gave a stable selection criterion and identified a

set of accessions pairing above-median ecosystem-service potential with competitive yield, that is, a deployable dual-purpose ideotype.

The genetic architecture of the index reinforces how it should be used. The association analysis of the AESI returned a polygenic profile with no individual locus surviving genome-wide correction, which means marker-assisted selection on a few large-effect loci is not a credible route for these composite traits; whole-genome prediction, which spreads selection across many small effects, is the appropriate tool. The wider lesson is applicable beyond white lupin: in any dual-purpose or intercrop program where agronomic performance and ecological function are genetically antagonistic, index selection is the mechanism that makes simultaneous progress possible.

6.6 Limitations

Four limitations apply across the dissertation. First, the temporal scope is one to two years per system, so multi-cycle response to selection, and in particular how the balance between phenomic and genomic information shifts as a pedigree deepens, remains to be demonstrated rather than assumed. Second, geographic scope is narrow: the clover and oat work spans two southeastern locations and the cassava work is single-location, leaving genotype-by-environment interaction across wider environments untested. Third, species-specific biomass in the clover and oat program was inferred from a single composite orthomosaic, in which spectral values were extracted at the plot level rather than resolved to each species. The reflectance signal therefore integrated both canopies, so clover and oat contributions were not spectrally separated at the pixel level. This limitation is compounded by vertical occlusion: because oat overtops the

shorter clover, a nadir UAV view captures the upper oat canopy preferentially and conceals the clover beneath it, biasing the integrated signal toward the dominant species. Species-aware spectral segmentation, and sensing geometries or platforms that mitigate occlusion of the understory, will be needed before species-specific biomass can be estimated directly rather than inferred. Fourth, the white lupin root traits were measured destructively at a single growth stage, and ecosystem function was represented by root architectural proxies rather than by direct measurement of phosphorus exudation or erosion reduction, so the AESI remains a proxy-based criterion that is yet to be functionally validated.

6.7 Future research priorities

Four priorities follow directly from these limitations. First, resolving the species-mixture phenotyping problem by moving from composite plot-level orthomosaics to species-aware spectral segmentation, together with sensing geometries or platforms that reduces occlusion of oats over the clovers, so that each species biomass can be estimated directly rather than inferred. Second, evaluate the white lupin root traits and the AESI across five or more site-years spanning Alabama's soil diversity, and further validate the index against direct measurements of phosphorus mobilization and erosion reduction in contrasting Ultisol. Third, extend the cassava-cowpea intercrop evaluation to multiple locations across IITA's agroecological zones. Fourth, run the joint genomic-plus-phenomic framework across three to five cycles of recurrent selection in the Auburn clover and oat program, tracking cycle by cycle how the contributions of phenomic and genomic information to selection accuracy change, which is the empirical test of the layering strategy proposed in Section 6.2.

6.8 Conclusions

Collectively, this research shows that UAV phenomics provides usable selection guidance in breeding populations where genomic information is still developing, and that the joint genomic-plus-phenomic model, demonstrated in white lupin, is the sound default where both sources are available, because it uses each without forcing a choice between them. General mixing ability dominated specific mixing ability in both intercrop systems examined, which validates minimal-tester designs and staged pipelines that add intercrop evaluation to existing monoculture programs rather than rebuilding them. Calibrating on a quarter to a half of plots and acquiring a single well-timed flight preserves most of the genetic gain available from exhaustive phenotyping while removing the harvest bottleneck that limits population size in mixture and cover-crop breeding. Where breeding objectives are genetically antagonistic, as ecosystem service and yield are in dual-purpose white lupin, index selection is the mechanism that keeps both moving, and whole-genome prediction suits the polygenic composite traits involved better than marker-assisted selection. Taken together, the work shows that the tools needed to breed for agroecological function, namely genomic prediction, UAV phenomics, sparse factorial designs, and selection indices, are available now and can be combined into working breeding programs with real gains in efficiency, accuracy, and ecological value.

References

Annicchiarico, P., Collins, R. P., De Ron, A. M., Firmat, C., Litrico, I., and Hauggaard-Nielsen, H. (2019). Do we need specific breeding for legume-based mixtures? Advances in Agronomy, 157, 141–215. https://doi.org/10.1016/bs.agron.2019.04.001

Annicchiarico, P., Nazzicari, N., Notario, T., Monterrubio Martin, C., Romani, M., Ferrari, B., and Pecetti, L. (2021). Pea breeding for intercropping with cereals: Variation for competitive ability and associated traits, and assessment of phenotypic and genomic selection strategies. Frontiers in Plant Science, 12, 731949. https://doi.org/10.3389/fpls.2021.731949

Freschet, G. T., Roumet, C., Comas, L. H., Weemstra, M., Bengough, A. G., Rewald, B., and Stokes, A. (2021). Root traits as drivers of plant and ecosystem functioning: Current understanding, pitfalls and future research needs. New Phytologist, 232(3), 1123–1158. https://doi.org/10.1111/nph.17072

Griffiths, M., Delory, B. M., Jawahir, V., Wong, K. M., Bagnall, G. C., Dowd, T. G., Chamberlain, A., Meldrum, K., Schaefer, A. L., Kaeppler, H. F., Lynch, J. P., Kaeppler, S. M., and York, L. M. (2022). Optimization of root traits to provide enhanced ecosystem services in agricultural systems: a focus on cover crops. Plant, Cell and Environment, 45(3), 751–770. https://doi.org/10.1111/pce.14247

Haug, B., Messmer, M. M., Enjalbert, J., Goldringer, I., Flutre, T., Mary-Huard, T., and Hohmann, P. (2023). New insights towards breeding for mixed cropping of spring pea and barley to increase yield and yield stability. Field Crops Research, 297, 108923. https://doi.org/10.1016/j.fcr.2023.108923

Moore, V. M., Schlautman, B., Fei, S.-Z., Roberts, L. M., Wolfe, M., Ryan, M. R., Wells, S., and Lorenz, A. J. (2022). Plant breeding for intercropping in temperate field crop systems: A review. Frontiers in Plant Science, 13, 843065. https://doi.org/10.3389/fpls.2022.843065

Sampoux, J.-P., Giraud, H., and Litrico, I. (2020). Which recurrent selection scheme to improve mixtures of crop species? Theoretical expectations. G3: Genes, Genomes, Genetics, 10(1), 89–107. https://doi.org/10.1534/g3.119.400809

Wang, F., Feldmann, M. J., and Runcie, D. E. (2025). Do not benchmark phenomic prediction against genomic prediction accuracy. The Plant Phenome Journal, 8(1), e70029. https://doi.org/10.1002/ppj2.70029

Wolfe, M. D., Jannink, J.-L., Kantar, M. B., and Santantonio, N. (2021). Multi-species genomics-enabled selection for improving agroecosystems across space and time. Frontiers in Plant Science, 12, 665349. https://doi.org/10.3389/fpls.2021.665349

Wright, A. J. (1985). Selection for improved yield in inter-specific mixtures or intercrops. Theoretical and Applied Genetics, 69(4), 399–407. https://doi.org/10.1007/BF00263967.